The HKIE Geotechnical Division 38th Annual Seminar 2018

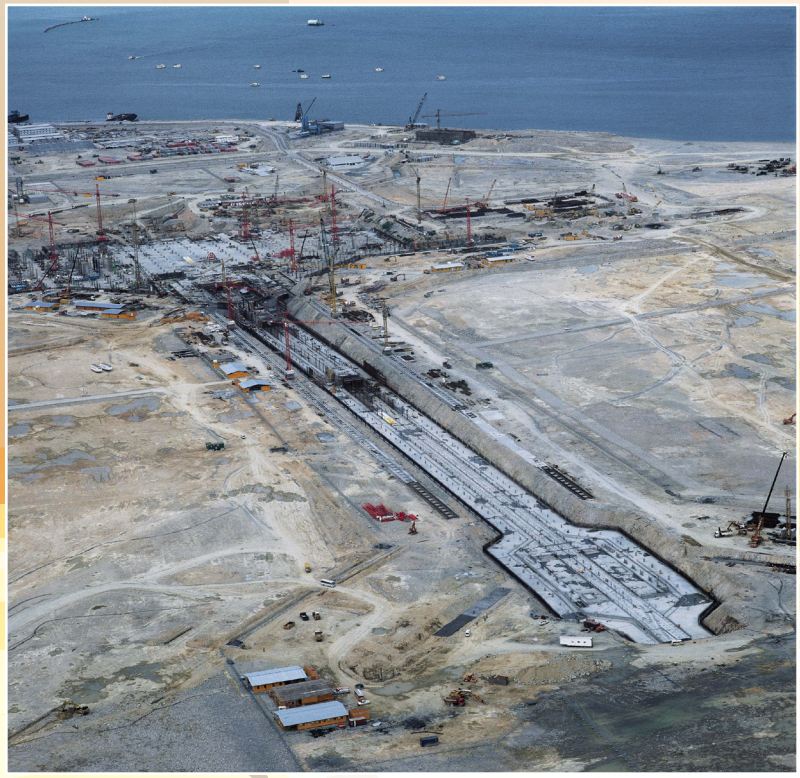

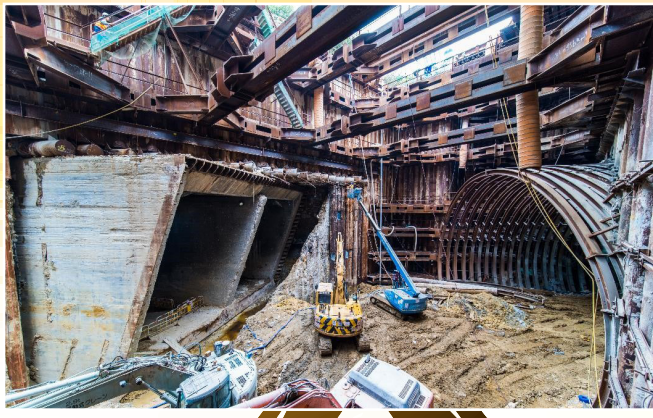

Geotechnical Engineering for

INFRASTRUCTURE DEVELOPMENT

THE HONG KONG INSTITUTION OF ENGINEERS 香港工程師學會
Geotechnical Division 岩土分部

Co-organiser

HKGES 香港岩土工程學會 Since 2003

Supporting Organisations

THE HONG KONG INSTITUTION OF ENGINEERS 香港工程師學會 Civil Division 土木分部

THE HONG KONG INSTITUTION OF ENGINEERS 香港工程師學會 Structural Division 結構分部

AECOM Imagine it. Delivered.

INFRASTRUCTURE THAT TRANSFORMS THE FUTURE

As a premier and fully integrated global infrastructure firm, we design, build, finance, operate and manage projects and programs that unlock opportunities, protect our environment and improve people's lives.

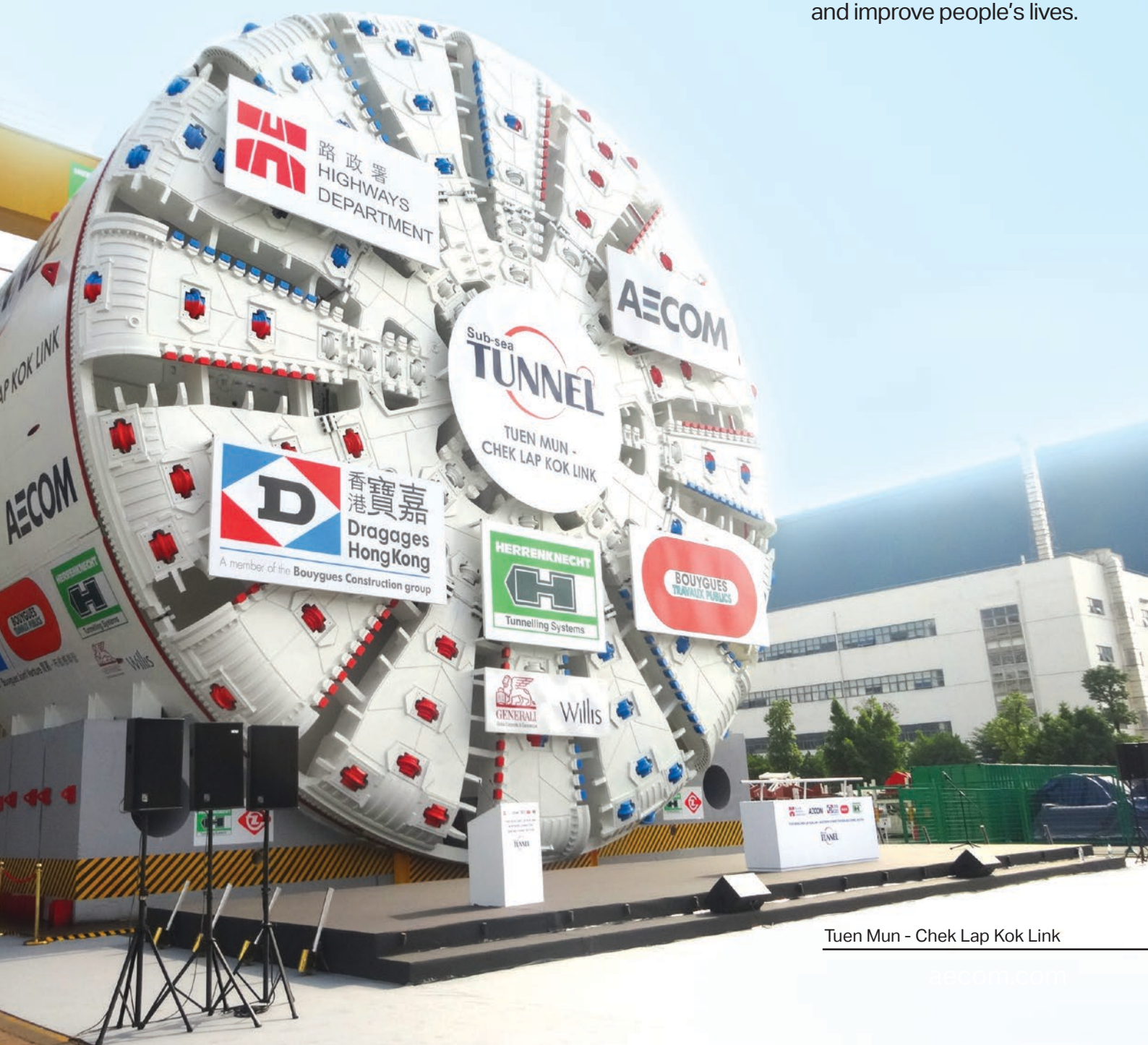

Tuen Mun - Chek Lap Kok Link

aecom.com

我們的主要業務包括：
Our Business includes:

- 基礎工程
  Foundation Works
- 斜坡及擋土牆長遠防治山泥傾瀉工程
  Construction of Landslip Preventive and Mitigation Works to Slopes and Retaining Walls
- 道路及渠務工程
  Roads and Drainage
- 水務工程
  Waterworks
- 地盤平整工程
  Site Formation

中国地质工程集团公司
CHINA GEO-ENGINEERING CORPORATION

香港灣仔港灣道 30 號新鴻基中心 24 樓 2421-25 室
Rm. 2421-25, 24/F., Sun Hung Kai Centre, 30 Harbour Road, Wanchai, Hong Kong
Tel: (852) 2511 9001 Fax: (852) 2580 0697

Anderson Road Underpass

Lam Tin – TKO Tunnel

MTRC XRL 825
Mai Po to Ngau Tam Mei Tunnel

High-Performance Ground Engineering Systems

Dextra is a global leader in the manufacturing, and delivery of engineered construction products to help complete your next building challenge.

Over the past 15 years we have developed a unique range of ground engineering soultions composed of both steel and composite material (FRP), suitable for a variety of applications in soil retention and stabilization, tunneling and mining, and the installation of deep foundations.

Dextra

Dextra Pacific Ltd.
Tel: +852-2511 8236

Suite 1901, Tung Wai Commercial Building,
109 Gloucester Road, Wan Chai, Hong Kong

www.dextragroup.com

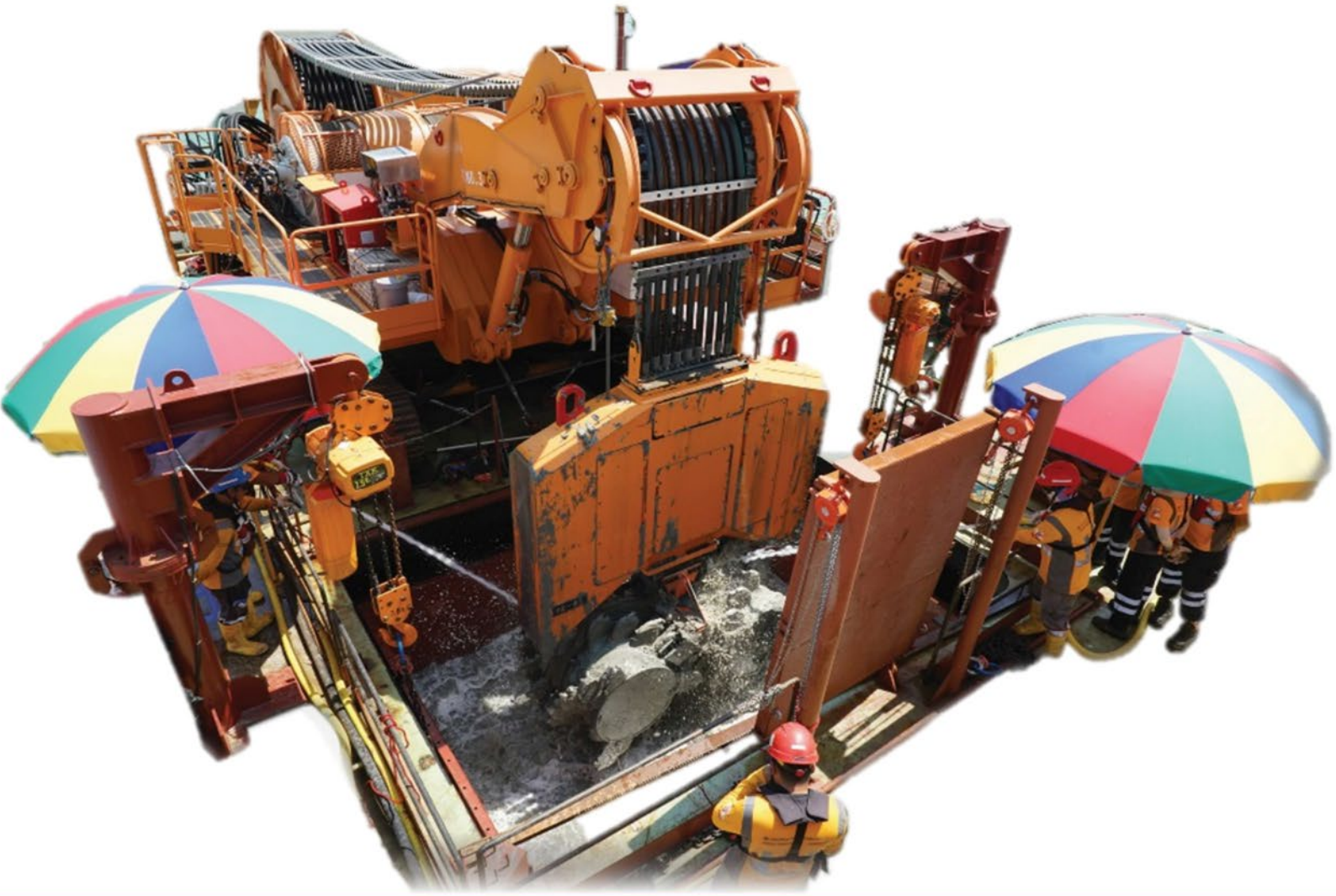

Low Headroom Cutter Soil Mixing

Build on us

Hong Kong International Airport Three Runway System Project
Deep Cement Mixing Works (Low Headroom)

www.bachy-soletanche.com.hk

bsg@soletanche-bachy.com

A subsidiary of SOLETANCHE BACHY

BACHY SOLETANCHE
法國地基建築公司

Geomil equipment

www.geomil.com

World's first manufacturer of CPT equipment

Tailored CPT solutions for any requirement

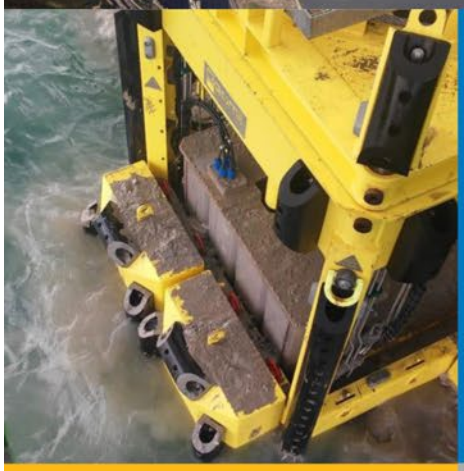

Grizzly-200

Truck mounted CPT system

Manta-200

Sea bed CPT system

Geotechnical Sensor Network (GSN)

The new standard for CPT

Our products are tailor made in the Netherlands and locally supported to make your Cone Penetration Testing project a success

歐美大地
EARTH PRODUCTS CHINA LTD
(852) 2392 8698
info@epc.com.hk
www.epc.com.hk

C M WONG & ASSOCIATES LTD
黃志明建築工程師有限公司

11/F Universal Trade Centre
3-5A Arbuthnot Road, Hong Kong
Tel: (852)2522-1068
Fax: (852)2526-3111
www.cmwal.com
cmwal@cmwal.com

C M Wong & Associates Ltd is a Hong Kong based consulting engineer in providing a full range of professional services including feasibility studies, planning, design and supervision in relation to building and infrastructure projects. Our clients include various Hong Kong Government departments, institutions and major developers.

We adopt a flexible approach to suit clients' needs. We are also renowned for providing innovative engineering solutions for challenging projects especially for those with difficult ground conditions.

ISO 9001 : 2008
Certificate No.: CC 801

ISO 14001 : 2004
Certificate No.: CC 5408

OHSAS 18001 : 2007
Certificate No.: CC 5409

BOSA

BOSA TECHNOLOGY (HONG KONG) LTD

SUPPLIER AND MANUFACTURER OF MECHANICAL COUPLERS AND REBAR THREADING SYSTEMS

UNIT 02, 23/F, 9 CHONG YIP STREET, KWUN TONG, KOWLOON

Email : bosa.technology@gmail.com

TEL : (852) 2505-5568 MOB : (852) 6218-3537

GROUND ENGINEERING SPECIALIST

Intrafor performs a wide range of activities for buildings and civil infrastructure – including geotechnical investigation, ground improvement and the construction of special foundations such as deep diaphragm walls.

Intrafor Hong Kong Ltd.
20/F Eight Commercial Tower
8 Sun Yip Street, Chai Wan, Hong Kong
Tel. 2590 2288 - www.intrafor.com

INTRAFOR

ARCADIS Design & Consultancy for natural and built assets

SMART
INNOVATIVE
SUSTAINABLE

Delivering smart engineering solutions

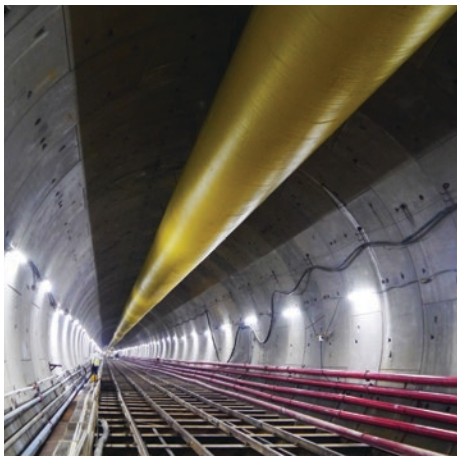

Arcadis is the leading global Design & Consultancy firm for natural and built assets. From tall buildings to the busy airports; from tunnels to iconic bridges, we combine our global best practice with local knowledge to deliver exceptional and sustainable outcomes for our clients in Asia. We can call upon the skills and resources of over 27,000 professionals active in 70 countries of whom 5,000 are based in the Asian region.

For more information please contact:
T: (852) 2911 2233
E: ArcadisDE-HK@arcadis.com
www.arcadis.com

OPTIMISE CONSTRUCTION PROCESSES, REDUCE RISK *AND* *ENHANCE* PROJECT PERFORMANCE

To find out more

AskFugro.com

China Harbour Engineering Company Limited (CHEC) *founded its local representative, namely Zhen Hua Engineering Company Limited (ZHEC) and started its operation in Hong Kong in 1989. Over the past 30 years, CHEC has persisted in its pursuit of excellence and carved out for itself a solid market share in the local construction industry. Being one of the leading contractors in Hong Kong in the field of Road & Bridge, Marine Engineering, Infrastructures & Site Formation, and Environmental Protection & Waste Treatment, CHEC provides quality services in design, construction and project management for a variety of engineering projects in Hong Kong.*

5 years+ 商界展關懷 caringcompany
Awarded by The Hong Kong Council of Social Service 香港社會服務聯會頒發

HK 2018 Drive for Corporate Citizenship 企業公民嘉許標誌

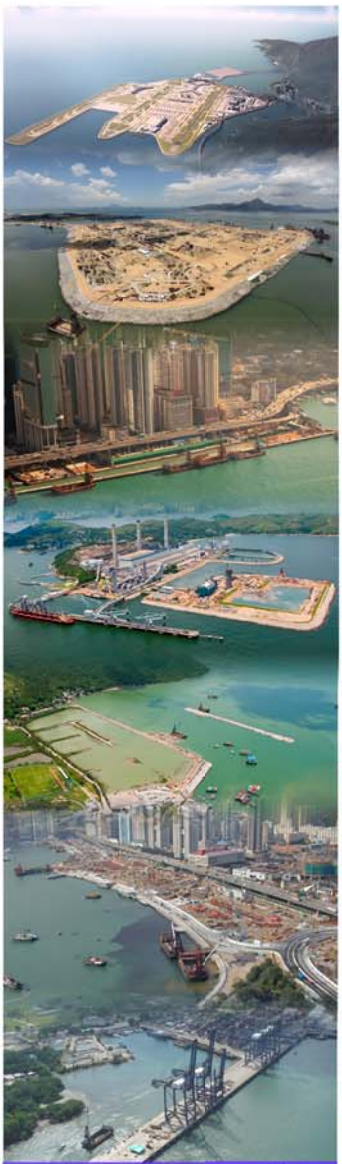

Marine Engineering

*Contract No. 3206 Hong Kong International Airport, Three Runway System Project
*HZMB - HBBCF Contract No. HY/2010/02 Reclamation Works
*Contract No. HY/2009/11 Central - Wan Chai Bypass North Point Reclamation

Road & Bridge

*Contract No. HY/2011/09 Hong Kong Link Road - Section Between Boundary and Scenic Hill
*Contract No. HY/2009/03 Design and Build of Traffic Improvements to Tuen Mun Road Town Centre Section
*Contract No. ST86/2000 Construction of Road T7 in Ma On Shan

Infrastructure & Site Formation

*HZMB - HKBCF Contract No. HY/2013/03 -Vehicle Clearance Plazas and Ancillary Building and Facilities
*HZMB - HZMB Contract No. HY/2013/02 -Infrastructure Works Stage I (Western Portion)
*Third Golf Course at Kau Sai Chau

Environmental Protection & Waste Treatment

*Shuen Wan Landfill Restoration Contract
*Urban Landfills Restoration Contract
*EP/39 Sai Tso Wan Recreation Ground
*Construction of Tai Po Sewage Treatment Works

CHEC 中國港灣工程有限責任公司 CHINA HARBOUR ENGINEERING COMPANY LTD.

China Harbour Engineering Company Limited
19/F, China Harbour Building, 370-374 King's Road, North Point, Hong Kong
Tel: (852) 2887 8118 (General Line) Fax: (852) 2512 0427
E-mail: chechk@chechk.com Websites: www.chec.bj.cn/ www.chechk.com

Q CERTIFIED COMPANY HKQAA
ISO 9001 : 2008
Certificate No.: CC 624

CERTIFIED COMPANY HKQAA
ISO 14001 : 2004
Certificate No.: CC 2666

ARUP

Underpinning world-class infrastructure

From underground space strategies to railway networks, from the airport gateway to port terminals, and from community water systems to cross-border connectivity, Arup's geotechnical expertise underpins world-class infrastructure projects that make our city a better place to live, work and do business.

Image Kwun Tong Line Extension –
Yau Ma Tei to Whampoa Tunnels & Ho Man Tin Station

We shape a better world | www.arup.com

香港 國際機場 | HONG KONG INTERNATIONAL AIRPORT

Hong Kong International Airport (HKIA) has a global network covering over 220 destinations worldwide. HKIA is one of the busiest aviation hubs in the world which handled 72.9 million passenger trips and moved over 5 million tonnes of cargo and air mail in 2017. HKIA is committed to sustainable growth and development, and aspires to be the finest in the world.

www.hongkongairport.com

泰錦建築工程有限公司

Tai Kam Construction Engineering Company Limited

Slope Stabilization & Site Formation Specialist Contractor

Director: K S LAU

BSc(Hon) MSc DIC LLB (hon)
CEng MICE MHKIE RPE(Civil) RSO RSA ASA

Address: Room 1114, 11/F,
Wealth Commercial Centre,
48 Kwong Wa Street,
Mongkok, Kowloon, HK.

Tel: 2663 1166 **Fax: 2663 9688**
E-mail: taikamsafety@hotmail.com

LAMBETH

Distinctly Different



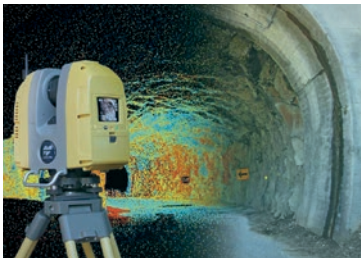

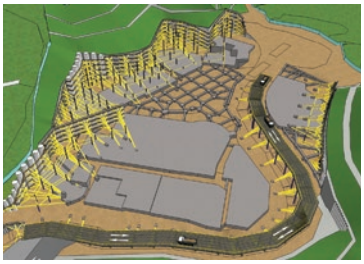

Lambeth brings together the diverse experience of operations, planning, commercial and design professionals – from within Gammon and Balfour Beatty – ensures it remains at the forefront of new techniques and new thinking. We set the standard for both innovation and technological advancement in building, civil, environmental, foundations, geotechnical and safety disciplines.

A member of the Gammon Group

28/F Devon House, Taikoo Place, 979 King's Road, Hong Kong Tel: 2516 8790 Fax: 2516 6352

GEOTECHNICAL AND STRUCTURAL MONITORING

PROVEN LONG-TERM RELIABILITY, PRECISION AND ACCURACY

- STRAIN GAGES
- CRACKMETERS
- JOINTMETERS
- EXTENSOMETERS
- PIEZOMETERS
- SETTLEMENT SENSORS
- PRESSURE CELLS
- LOAD CELLS
- INCLINOMETERS
- TILTMETERS
- TEMPERATURE SENSORS
- CUSTOM DESIGNS
- READOUTS
- DATALOGGERS
- WIRELESS SYSTEMS
- SOFTWARE

to learn more, please visit: **www.geokon.com.sg**

GEOKON®(S) PTE LTD | INNOVATION AND QUALITY **SINCE 1979**

GEOKON (S) PTE. LTD. | Singapore | phone: +65.6701.8578

Proceedings of the 38th Annual Seminar
Geotechnical Division, The Hong Kong Institution of Engineers

Geotechnical Engineering for Infrastructure Development

18 May 2018
Hong Kong

Jointly organised by:
Geotechnical Division, The Hong Kong Institution of Engineers
The Hong Kong Geotechnical Society

Supported by:
Civil & Structural Divisions, The Hong Kong Institution of Engineers

Captions of Figures on the Front Cover

Top Left to Right:
1) Hong Kong Airport (Courtesy of Gammon Construction Limited)
2) Slope Restoration and Topographical Monitoring for Heritage Preservation of Gediminas Hill and Castle Tower in Lithuania (Courtesy of the University of Hong Kong)

Middle:
3) Hong Kong Link Road – Contract HY/2011/03 (Courtesy of Ove Arup & Partners (HK) Limited)

Bottom:
4) Natural Terrain Landslide Risk Mitigation Measures at Yu Tung Road, Tung Chung (Courtesy of CEDD of HKSAR)

Soft copy of the proceedings can be downloaded from the HKIE Geotechnical Division's website http://mobile.hkieged.org/download/as/AS2018.pdf

ORGANISING COMMITTEE

Chairman
Ir Ian Askew

Members & Technical Sub-committee
Ir Dr Tony Chen
Ir Y C Lam
Ir Dr S W Lee
Ir Clifford Phung
Ir Grace Tam
Ir Martin Yip

Published by:
Geotechnical Division
The Hong Kong Institution of Engineers
9/F., Island Beverley, 1 Great George Street, Causeway Bay, Hong Kong
Tel: 2895 4446 Fax: 2577 7791

Prepared in Hong Kong

FOREWORD

I would like to welcome all distinguished guests, speakers, academics and geotechnical professionals to the HKIE Geotechnical Division Annual Seminar 2018.

This year, our Annual Seminar places the emphasis on the geotechnical engineering aspects on infrastructure developments. Infrastructural developments are essential to the success of any international world class cities, such as Hong Kong. The average daily patronage of our rail system is nearly 5 million and more than 600,000 people are crossing the border each day. Every day, we open our tap to get safe and portable water and we all take it for granted. Infrastructure development in Hong Kong has evolved to meet the changing demands of society. The 1950s-1960s focused on basic needs in water supply and public housing. Expansion of new towns and the railway network accelerated in the 1970s-1980s. The 1990s heralded the airport and port strategy, while the 2000's brought greater cross-border connectivity. 2010s brought a focus on driving enhanced economic competitiveness and improving living environments. The recent era of infrastructure development, including the Ten Major Infrastructure Projects, further enhanced Hong Kong's transport network, urban environment and the quality of life of the population.

The HKIE Geotechnical Division Annual Seminar provides a platform for engineers to share and document their experiences working on infrastructure projects in Hong Kong and overseas. The seminar is divided in four sessions on different category of infrastructural projects, each with selected presentations. We are particularly grateful to Ir Kevin Poole of delivering a keynote lecture on the airport development and Ir Neil Ng, on the construction challenges of the Sha Tin to Central Link. I wish that practitioners would find the knowledge and experiences gained from our Annual Seminar useful and insightful in their next endeavor of delivering high quality infrastructure projects.

On behalf of the Geotechnical Division, I would like to express my gratitude to the invited lecturers, authors and speakers contributing to this seminar. My special thanks also go to all members of the Organizing Committee, led by Ir Ian Askew, whom they have worked extremely hard in making this event happen. I would also like to thank the Hong Kong Geotechnical Society (HKGES) for jointly organizing this seminar, as well as the HKIE Civil Division and Structural Division for their support.

Ir Sammy Cheung
Chairman, Geotechnical Division
Hong Kong Institution of Engineers (2017/18 session)
May 2018

ACKNOWLEDGEMENTS

The Organising Committee would like to acknowledge the support of the following sponsors for their generous support of the Seminar:-

AECOM Asia Company Ltd.

Airport Authority

ARCADIS Design & Engineering Ltd.

Bachy Soletanche Group Ltd.

BOSA Technology (Hong Kong) Ltd.

C M Wong & Associates Ltd.

China Geo-Engineering Corporation

China Harbour Engineering Company Ltd.

Dextra Pacific Ltd.

Earth Products China Ltd.

Fugro Geotechnical Services Ltd.

Geokon (S) Pte. Ltd.

Intrafor Hong Kong Ltd.

Lambeth Associates Ltd.

Meinhardt Consulting Engineers

Ove Arup & Partners (HK) Ltd.

Reinforced Earth Pacific Ltd.

Tai Kam Construction Engineering Company Ltd.

TREVI Construction Company Ltd.

THE HKIE GEOTECHNICAL PAPER AWARD

2018 sees the third exercise of the HKIE Geotechnical Paper Award in its current format. At 24, the number of entries is between those in 2014 (36) and 2016 (17). With the endorsement of the Geotechnical Division Committee (GDC), a seven-member Assessment Board was formed to look for winning papers. It comprises Ir Sammy PY Cheung (Chairman), Ir Ian Askew, Ir Y C Koo, Ir Dr C K Lau, Ir Dr Eric Li, Ir Dr Victor Li, and Ir Y C Chan (Secretary). Ir Cheung and Ir Askew are ex-officio members of the Board by being Chairman and Vice-Chairman of GDC. The other five members are selected from the Assessment Board Panel taking into consideration the subject nature of the contending papers and reducing potential conflict of interest.

The Assessment Board follows the same practices as in previous exercises to ensure confidentiality of identity of participants and fair but critical judgment on the contending papers. Hence, members receive information on a need-to-know basis, and only the winning papers are made known publicly. Board members share views through a hub that remove identity tags. Deciding winners in the Assessment Board meeting is by blind voting. Members with perceived conflict of interest take part in sharing of views but not voting.

The Assessment Board has found the best two papers to be equally meritorious, and hence recommended both for the Award. The titles and the basis of the choices are as follows.

Kwan, J.S.H., Koo, R.C.H. & Ng, C.W.W. (2015) Landslide mobility analysis for design of multiple debris-resisting barriers. Canadian Geotechnical Journal, Vol 52(9), pp 1345-1359

> The paper documents development of a methodology for rational design of multiple barriers for intercepting mobile landslide debris. It started with Newtonian mechanics, took hints from physical model tests and case records, demonstrated by application to a real design case, and benchmarked against an advanced numerical model. This comprehensive and solid approach won confidence. The proposed methodology promises to fill another gap in Hong Kong's continual search for more reliable and effective design of debris flow barriers. The paper is clearly and logically written, with the support of two very helpful appendices on aspects demanding greater details to make sense of the subject matter. It should be accessible to most geotechnical practitioners with a good grasp of basic mechanics.

Ng, P.L., Polycarpe, S., Barrett, T.N.D.R., Roux, G. and Vallon, F. (2017) Development of a novel tunnel dismantling machine for the MTR West Island Line construction. HKIE Transactions, the Hong Kong Institution of Engineers, Vol. 24, No. 3, pp. 151-168

> The Tunnel Demolition Machine is a bold solution to a uniquely demanding project setting. Its success required precise ground and support modelling to guide the design of bespoke mechanical components and work cycles. The advanced technology applied would be of interest to practitioners. The paper instead takes readers through a perspective uncommon for project case papers, by providing a superb step-by-step record of how the project challenges were tackled. From it, one may appreciate the nature of innovation: persistent drive for better answers to issues, a wide and in-depth knowledge base to support creativity, and great attention to detail and rigorous preparation to ensure final success. The paper is well written with excellent figures and hence very readable.

Prize giving is in the Annual Seminar. The winners will be presented with a trophy for each paper, and a crystal plaque and a certificate to each co-author. One author of each paper will then give a brief presentation to highlight key messages from it.

There have been changes to the framework of the Award Scheme. A basic building block of the scheme is the Assessment Board Panel of eminent local geotechnical practitioners, to give views on the scheme and have members ready to form Assessment Boards. In 2017, GDC endorsed invitation of eminent practitioners to join the Panel. This increases its number from 16 to 20, and of members with tunneling experience.

At its conception, the scheme bars papers with a co-author who is an Assessment Board Panel member. In the 2016 exercise, an entry was not accepted on this basis. The engineer who entered the paper appealed. The issue was raised for discussion among Panel members after the award exercise. Views for and against relaxing this restriction were heard. In the end, we decided to suspend the restriction for two exercises, to observe implications.

This report is brief because much has already been said on the scheme in the reports of the first two exercises, especially the first one in the 2014 Annual Seminar Proceedings at http://mobile.hkieged.org/km.vbhtml. Please also visit http://mobile.hkieged.org/geopaper.vbhtml, the official site of the Award scheme, for further information.

Ir Y C Chan
Secretary, Assessment Board
The 2018 HKIE Geotechnical Paper Award
May 2018

TABLE OF CONTENTS

Extensive Ground Treatment for TBM Crossing Underneath Live MTR Tunnels

S. Auvergne, K. Kwok, & K.L. Lee
Dragages Bouygues Joint-Venture, Hong Kong

X. Heurtaux
Intrafor Bachy Soletanche Join-Venture, Hong Kong

J.F. Brewer
MTR Corporation Limited, Hong Kong

ABSTRACT

The Dragages Hong Kong Ltd. Bouygues TP Joint Venture (DBJV) was awarded MTR Shatin to Central Link (SCL) Contract 1128 – South Ventilation Building to Admiralty Tunnels, which forms part of the "North-South Corridor" of the SCL Project. This Contract comprises the construction of twin tunnels namely Eastern and Western Bored Tunnels connecting to the future Exhibition Centre Station in one of the busiest and densely urban areas of Hong Kong Island. Western Bored Tunnels alignments commence near the Hong Kong Convention and Exhibition Centre and arrive at MTR Admiralty Station Extension underneath the existing MTR Admiralty Station (ADM). These parallel tunnels were excavated by Tunnel Boring Machines (TBMs), i.e. typical slurry mix-shield through varied geology with ground cover ranging from 20 to 30m. They passed underneath several major trunk roads and bridges, underground utilities, buildings and the existing MTR Tsuen Wan line (TWL) at TWL South Ventilation Building (SVB) with minimum separation of 2.5m, and ADM. In order to overcome this challenging tunnel alignment in close proximity to the existing MTR tunnels at SVB, extensive ground treatment works was designed from the planning stage and further developed with a team of International Grouting Specialists throughout the construction stage. The successful completion of the two TBM drives in November 2017 proved that the extensive ground treatment allowed the safe TBM tunneling in close proximity to the live railway tunnels without any interruption to the train service and impact on stakeholders. This paper presents the specific ground treatment underneath the existing MTR live railway tunnels in Wan Chai District.

1 INTRODUCTION

This paper presents how a horizontal ground treatment block in old reclaimed fill at approximately 25m depth was completed, under the one of the busiest MTR line of Hong Kong without any disturbance to passengers including during the subsequent successful TBM crossing.

1.1 General Overview

Dragages Hong Kong Ltd. was awarded the MTR Contract SCL1128 to construct two twin tunnels under one of the most congested and busiest areas of Hong Kong Island North from Causeway Bay Typhoon

Shelter to the integrated Admiralty Station, on interchange for the existing Tsuen Wan Line, Island Line and recently opened South Island Line. The Eastern and Western Tunnels are connected on either side of the future Exhibition Centre Station (constructed under MTR Contract SCL1123). The challenges for the Eastern Tunnels were discussed in detail by Kwok (2017), S. Auvergne (2017), and Jacques (2017). This paper focuses on the TWL crossing which is located on the western side of the contract.

The SCL Western bored tunnel are approximately 505m long and excavated using two slurry TBMs. Around 65m away from the TBM break-in position, the machines were excavating just beneath the MTR's Tsuen Wan Line (TWL) in the vicinity of the Unit 1 of the TWL Immersed Tube Tunnel (IMT). This sensitive TBM crossing required comprehensive implementation of mitigation works in order to minimize the impact on the existing TWL structure. The major mitigation measure involved horizontal ground treatment between the TBM excavation and underneath the existing MTR TWL.

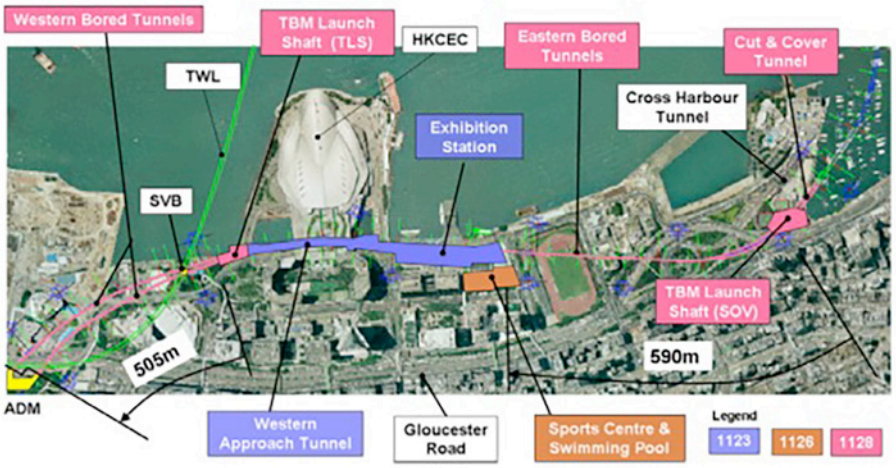

Figure 1: Overall Project Layout

1.2 Geological conditions

The two Western Tunnels are parallel to each other with the Up-track Tunnel (UT) being slightly deeper. Both tunnels are excavated within varied ground (rock, mix ground and soft ground in CDG and alluvium) with around 20 to 30m cover. Figure 2 below shows the longitudinal geological section along the Up-Track Western drive and Figure 3 shows a close up at the TWL Down-Track (DT) crossing location.

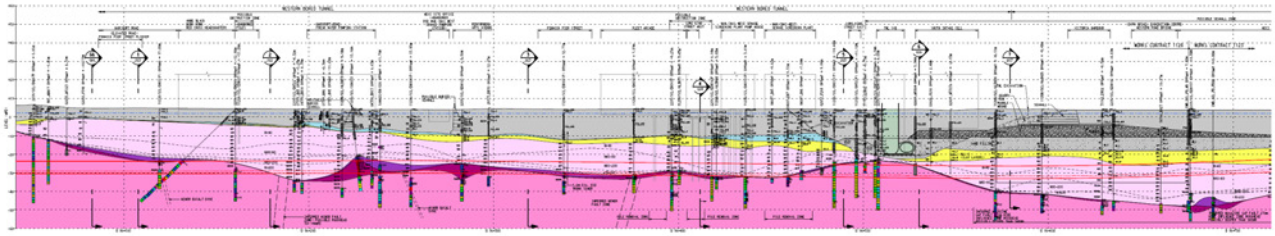

Figure 2: Longitudinal geological section along the Up Track Western drive

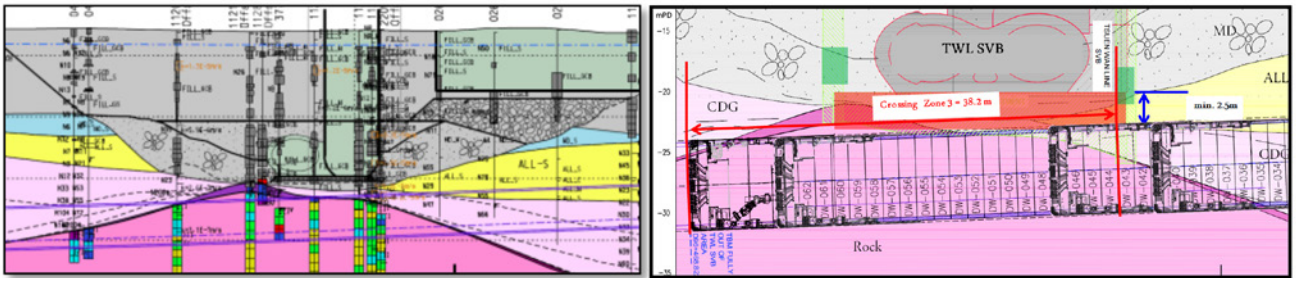

Figure 3: Longitudinal geological section along the Down-Track Western drive at the TWL Location

The crossing area had been reclaimed during 1968 & 1969, the available information suggested the sea bed level was approximately -10mPD and underlain by marine deposits, alluvium, weathered granite and granite bedrock. However, the marine deposits at this location were largely removed by the subsequent excavation for the SVB-TWL construction and replaced in the dredged trench by 'sand fill'. The alluvium layer had also been largely removed during the SVB-TWL excavation.

The aggregate layer is critical due to its location in vicinity of the Down-Track TBM crown and its high permeability. In-situ tests demonstrated its permeability to lie between 10-4m/s to 10-5m/s. To better understand this aggregate layer, additional GI was performed close to the edges of the existing TWL, using foam as a medium fluid instead of water for better recovery purpose. The additional GI demonstrated the presence of special fill comprising soft cementitious grout patches (due to grouting from inside the IMT after construction) and silt matrix at the bottom of the aggregate layer (due to deposit directly after the dredging process prior to the aggregate layer installation). Ground investigation from the inside of TWL was proposed to investigate the geological condition directly under the structure, but due to the sensitivity of the structure this was not possible. Therefore the ground conditions remained uncertain for the overall 18m distance of crossing.

Below provides a brief description of the materials encountered while boring the western drives.

Geological Formations	Brief Description	Western Drives	Color on Figure 2
FILL	Mostly composed of sand, gravels, clayey materials and man-made debris and structures	Not encountered	Grey
Aggregate Layer	Technical Fill mostly composed gravels with locally silt & sand & soft grout matrix		
Marine Deposits	Mostly sandy/silty materials in upper part and more clayey soft materials in the lower part. Thicknesses varying along the alignment (up to full face).	Not encountered	Blue
Alluvium	Widespread stratum that comprises mainly clayey to sandy materials with occasional gravels.	Downtrack and uptrack	Yellow
Kowloon Granite	Medium grained granite. Encountered in various stages of decompositions (from MDG to CDG)	Downtrack and uptrack	Pink (dark and light)
Mafic dykes	Dykes of mafic materials were encountered in the most eastern side of the drive.	Downtrack and uptrack	Not shown for clarity

Table 1: Brief description of the geological formations encountered through the western drives

Two slurry tunnel boring machines (TBMs) were used for the western tunneling works. The Up-Track and Down-Track drives were successfully completed in May and November 2017 respectively.

1.3 Existing MTR TWL conditions

According to the as-built construction drawings, MTR TWL was constructed by Spherical Graphite Iron (SGI) segment lining and Immersed Tube Tunnel (IMT) units. The connection junction between SGI lining and IMT units was located right underneath the TWL SVB structure. The SVB and IMT unit were founded on a layer of one-size gravel and gravel backfill has also been placed along both sides of the structures. This gravel fill layer has been partially grouted during TWL construction. However, there was no available ground investigation in the immediate proximity of the connection of the segmental TWL tunnel and the SVB structure. A joint inspection was conducted on 22 October 2014 and minor groundwater leakage (continuous dripping) was observed at the circle joint between Ring 41 and 42, at the connection part between the SGI segments and the IMT structure.

1.4 Crossing description

The Up-Track TBM crossed the existing TWL from 26th to 31st Mar 2017 with a minimum separation of 5.8 metres. At preliminary stage, horizontal ground treatment was expected, however additional ground

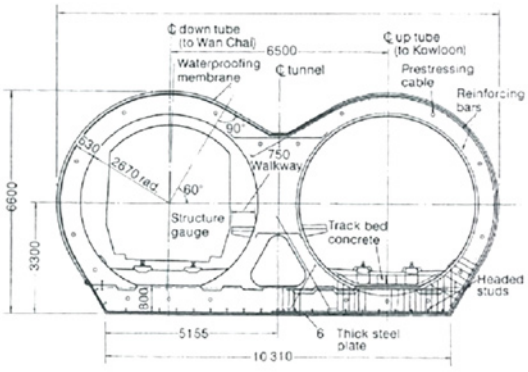

Figure 4: Typical section of the IMT

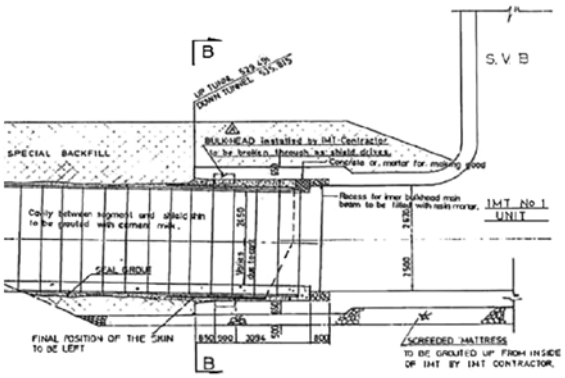

Figure 5: SGI /IMT Tunnel Construction Joint

investigation works demonstrated that the alignment was full face into rock formation and therefore no ground treatment was required.

The Down-Track TBM crossed the existing TWL from 6th to 11st Oct 2017 with a minimum separation of 2.5 metres. Due to the sensitive geology at this location, TBM excavation in mixed ground condition with alluvium layer / aggregated layer very close to the TBM crown, ground improvement was required.

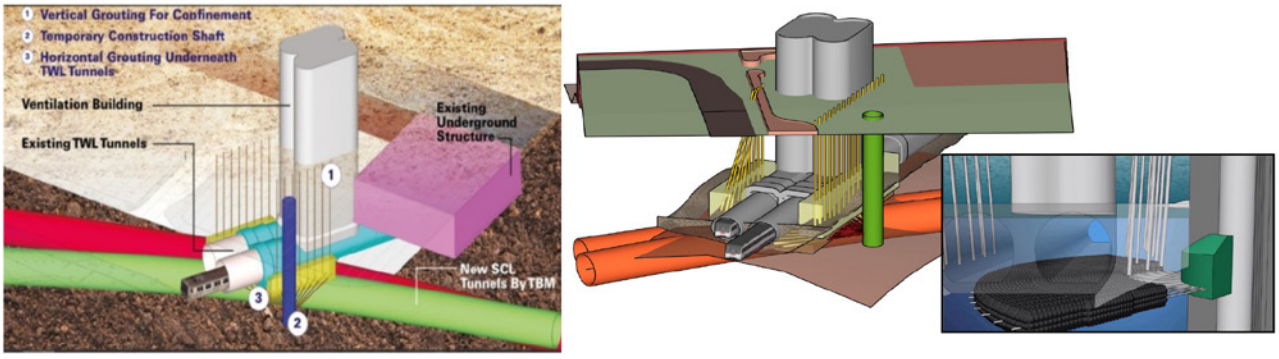

Figure 6: 3D geometry of the crossing

2 DESIGN OF THE GROUND TREATMENT WORKS

2.1 Design Principles

The future SCL DT would cross below the existing TWL at SVB, which was seated on a bed of partially grouted gravel fill. High risks of loss of slurry pressure, over-excavation, ground collapse, and excessive ground movements were anticipated due to excavation through the unconsolidated gravel. A two-stage ground treatment was designed to reduce the permeability at the gravel fill by cementing the gravel bedding adjacent to and immediately below the TWL Tunnel. This aimed to prevent the risk of slurry loss through the void between the soil particles of the gravels during TBM operation, hence to control the settlement above the TBM drive and minimize the potential disturbance to the operating TWL.

Stage 1 - Vertical Permeability Grouting with TAM

Stage 1 comprised vertical/sub-vertical TAM grouting along the two sides of SVB where it was intersected by the SCL tunnels. This would consolidate the strip of gravel along the two sides of the SVB and isolate the central portion beneath the base of the SVB. Hence, this would prevent the horizontal grout from escaping into areas where the treatment is not foreseen, and prevent grout loss outside the treatment zone.

Stage 2- Horizontal Telescopic Grouting
Stage 2 comprised horizontal grouting to fill voids in the gravel fill above the SCL tunnels and underneath the footprint of SVB and SGI/IMT interface joint. This treatment aimed to reduce the permeability to an acceptable limit of 10-5m/s and prevent slurry leaks during TBM operation.

2.2 Design Acceptance Criteria

The design permeability criterion of the aggregate layer was initially targeted at 10-7m/s with design grout strength at 2.0MPa, but was finally set at at 10-5m/s with zero design strength. This was because the key purpose of ground treatment was to stabilize the loosely filled gravel zone as soon as possible and to provide a practical condition for passage of TBM underneath the TWL. However, permeability of 10-7m/s and design strength of 2.0MPa were practically difficult to achieve, additional stages of prolonged drilling and grouting would likely be required and increased the settlement risk to the SVB structure. Since the bentonite cake formed at the excavation face would contribute to face stability and confinement control for compressed air intervention, it was considered the treated soil with permeability of 10-5m/s and zero design strength would be sufficient for passage of TBM and overall TBM excavation.

2.3 Design Grouting Volume

For the horizontal holes, the targeted treatment volumes per sections were rectangular in cross section. Unfortunately, neither the void ratio nor the parameters in determining the void ratio (such as size and shape of the rock particles, the grading and the degree of compaction) could be measured directly. This was due to the limitation in obtaining representative in-situ samples of the screed gravel. By assuming the specific gravity of the soil (Gs) to be 2.6 and fully submerged soil (Sr = 1), the void ratio to fill has been assumed as 35%. Therefore, the grouting volume was assume to be 35 % of the treated ground to fill up the void the screed gravel layer, which was filled up with underground water before ground treatment.

2.4 Mixes Design

More than 30 numbers of grout mixes had been tested and eventually a Bentonite Cement Silicate (BSC) mix was adopted. This had been defined considering mainly the gel time and setting to ensure that the grout would not be wash away nor set too early and create unnecessary issues; cost and strength were also considered.

BSC:	Bentonite	25 kg
(ID 20)	OPC Cement	400 g
	Sodium Silicate	6 kg
	Water	857 L

Table 2: BSC mix composition

2.5 Design Cut-off Criteria

- Stage 1 - Vertical Grouting
The cut-off criteria for vertical grouting are stipulated in the table below. The target grouting pressure was the total overburden pressure plus 2 bar which would be 4 bar with in addition 2 bar. Therefore the target acceptance pressure was set at 6 bars to ensure the targeted area to be filled with grout, whereas the cut-off pressure was set at 10 bars to ensure no damage would be imposed on the existing TWL. The cut-off volume considered was 35% of the treatment zone which corresponded to 2.1m diameter column around the TAM hole. It shall be noted that microfine cement (MFC) was used after reviewing stage 1 data, and it was considered not necessary for stage 2 grouting.

	Phase 1 (BCS)	Phase 2 (MFC)
Cut-off volume:	25% of ground treatment volume	10% of ground treatment volume
Cut-off pressure:	Acceptance 6 bar Maximum 10 bar reached (without head loss)	

Table 3: Cut-off criteria for Stage 1 vertical grouting

- Stage 2 – Horizontal Grouting

For each 0.5 m retraction of the drill pipe, pumping would be terminated at either a)reaching specified volume criteria in this location OR b)reaching maximum grout pressure of 8 bar at a minimum flow rate of about 1 L/min, depending on which criterion is met first. In either case, flow rate, pressure and total quantity at time of termination must be recorded. For safety reason, grouting pressure was limited to 8 bars (without head loss). It should be reminded that the acceptance criteria for horizontal grouting would be the volume criteria. This is because the primary goal of grouting was to completely fill as far as possible all the voids in the gravel layer without having a second stage of injection, hence to stabilize it and reduce its permeability. Only the grout placed can achieve this goal, whereas pumping pressure just serves as a tool to understand the actual conditions and achieve this goal. It shall be noted that bentonite cement (BC) was used prior to the injection of BCS, this was for practical reason and to avoid any blockage of the casings.

	Phase 1 (BC)	Phase 2 (BCS)
Cut-off volume:	100L for every 5m section	35% of ground treatment volume
Cut-off pressure:	Maximum 8 bar reached (without head loss)	

Table 4: Cut-off criteria for Stage 2 horizontal grouting

3 METHOD OF THE GROUND TREATMENT WORKS

To perform the horizontal grouting, first a vertical grout curtain was completed on both side of the existing TWL using TAM technique, then a vertical shaft was sunk and a cavern excavated at the bottom to fit the drilling rig. The construction sequence is briefly summarized as follows:

1. Phase 1 ground treatment of vertical grouting works using TAM grout at the eastern side of SVB.
2. Construction of Access shaft and grouting chamber at eastern side of SVB.
3. Phase 1 ground treatment of vertical grouting works using TAM grout at the western side of SVB.
4. Phase 2 ground treatment of horizontal grouting under MTR TWL and SVB.

3.1 Vertical shaft

Gaining benefit from the higher rock head level in TWL D/T, the grouting zone was optimized with only one vertical shaft being required. 9 numbers of concrete columns were constructed to allowed excavation of the bell out at the bottom of the shaft. The 2.7m diameter shaft was constructed as bored caisson using bored piling method. The casing was left in the ground and then equipped with ladder and safety equipment (CCTV etc.) to provide safety access to the shaft.

3.2 Curtain vertical grouting by TAM

Two rows of grout holes (15 nos. on eastern side and 12 nos. on western side of the SVB) formed the vertical confinement walls adjacent to the TWL tunnels. Drilling was carried out by hole hammer wash

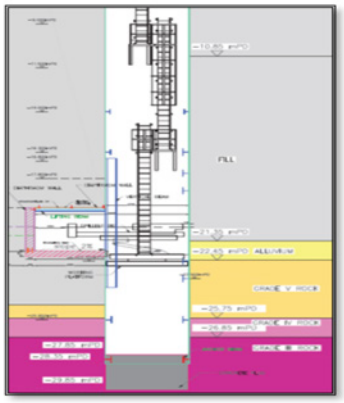

Figure 7: Vertical Shaft

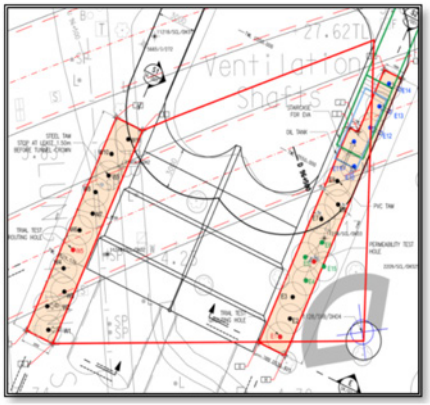

Figure 8: Vertical TAM grouting Layout

boring method using a temporary casing of diameter of 101 mm. Inclination, orientation and depth checks were carried out by inclinometer and jointly inspected by MTR team. The general layout of TAM vertical grouting are presented in Figure 8.

3.3 Telescopic horizontal grouting

Horizontal grouting utilised telescopic grouting using a drill rig mounted on a turn table for the drilling of two rows of grout holes at -20.5mPD and -21.0mPD respectively. The two rows of grout holes, which are 115mm in diameter and approximately 23 meters long at 1.5m horizontal spacing formed a fan shape under the SVB and SGI/IMT interface. There are totally 25 no. of drill holes. The grout holes treatment sequence was carefully planned, in order to satisfy the requirement of no redrilling for the same hole or drilling the adjacent hole before 48h of setting time and overcome grout hole access limitations in the drilling chamber.

The drilling started with the lower row by drilling the segment of 5m through a Blow-Out-Preventer (BOP) to ensure drillhole stability via the applied back pressure obtain using the return line for the cutting directly linked to the surface, then injecting grout directly through the casing while retracting it. After the entire fan of grout holes had been treated from 0 to 5m, it was redrilled and the hole from 5 to 10 m was then treated. Once the lower row of holes was completed, the same procedure was followed with the upper row. The deviation check was done using Reflex Gyro system for each 5m segment and provided to the MTR team.

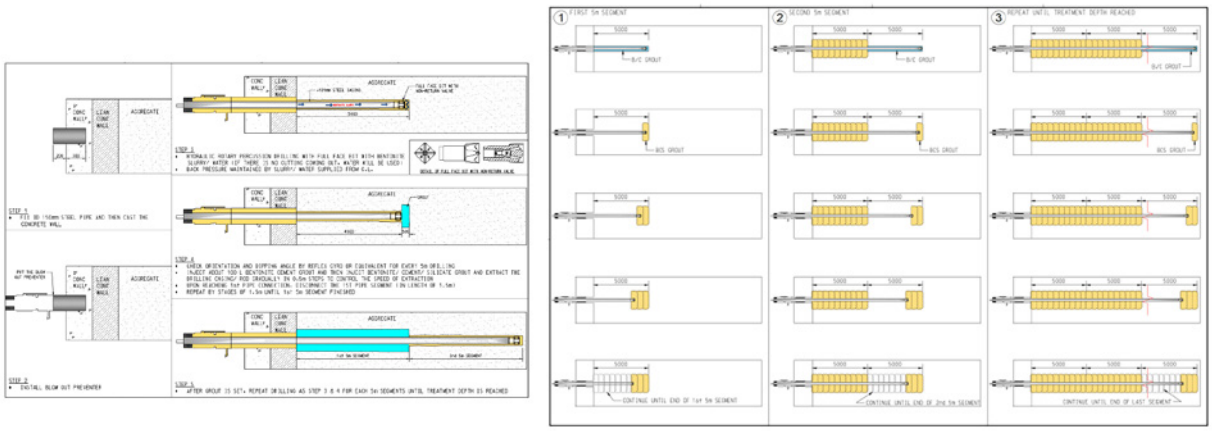

Figure 9: Horizontal grouting sequence

4 CHALLENGES FROM RAILWAY ORDINANCE (RAILWAY PROTECTION)

Due to the close proximity to the existing TWL structure, extra constraints were imposed to the ground treatment works, as all the grouting works on site need to comply with the requirements stipulated in WBTC no. 19/2002: Mass Transit Railway Protection and APP-24 Practice Note for Authorized

Persons, Registered Structural Engineers and Registered Geotechnical Engineers. Verticality control was extremely stringent to ensure the precision position of grout holes as discussed in Section 5.2. The pressure during grouting was carefully controlled to avoid any damage of the structure. The impact of 10 bar of grouting pressure at 1m plan distance from TWL was proved to be within the 20kPa pressure limit specified in PNAP APP-24. Furthermore, sensitivity tests were conducted to assess the structural settlement and structural heave of MTR TWL structure due to the drop or rise of back pressure at the horizontal grout holes. A back pressure of 1.5 bars or 10 bars was applied perpendicular to the grout pipes and the induced structural impact due to the back pressure change was considered to be minimal. Nevertheless, minimum and maximum pressure was set to control the adverse impact towards TWL.

5 ACTUAL GROUND TREATMENT WORKS

5.1 Site Set up

A concrete platform was provided at the cavern for placing drilling tools and grouting works. A steel platform was provided at -22.5 mPD to seat the drilling rig. Besides, hoisting device with 10 ton capacity was provided to load down the required materials and equipment (such as drilling rig and casings) within the shaft. Prior to the drilling work, the location and orientation of the drilling was set out. Prior to drilling work, the angle and orientation of the drilling machine and the location of the drill hole was checked, and BOP was installed to prevent any uncontrolled flow, or blowout of underground water. Slurry consumption was closely monitored during grouting and the return line was connected to the surface to ensure a back pressure slightly above the hydrostatic pressure at all times.

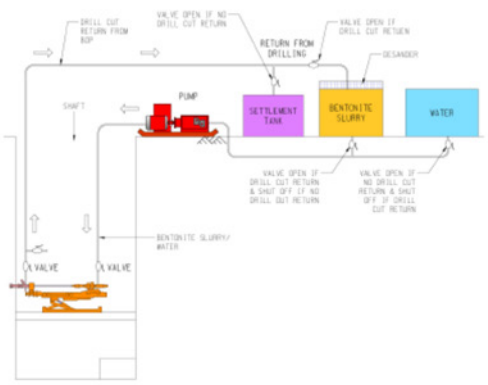

Figure 10: Circulation line of drilling fluid

Figure 11: Site photos for horizontal grouting (bentonite or water)

5.2 Quality Control

Due to the close proximity to TWL, stringent verticality control was carried out. Each measurement was required to compare with the theoretical coordinates to ensure the drilling would not affect MTR Structure. A report was also required stating the deviations and the projected horizontal distance to the SVB or TWL tunnel prior to any further drilling. At 3 m from MTR Structure, the deviations shall be kept at least 1 m away from the MTR structure. At MTR Structural level, if any significant deviations are found, the hole would require to be re-drilled.

For stage 1 vertical grouting, verticality, inclination and orientation check were performed by inclinometer in addition to the location and depth check to ensure the precise position of drill holes. Verticality check and inclination check by inclinometer were required for wash boring at 3m from MTR Structure or 1 m above the TWL tunnels whichever shallower.

For stage 2 horizontal grouting, verticality checks were required at every 5 m and the minimum distance of drill holes with at least 1 m away from the MTR Structure. Inclination and verticality checks were required at levels of MTR Structure by Reflex Gyro (directly inserted into the casing due to the

non-return value). Around 170 nos. of verticality checks were performed using the Reflex Gyro method through the drilling casings for every 5m of drilling to check orientation and dip angle, with the dip angle tolerance of 1/50 downward or 1/100 upward. Only 1 hole (A06 3rd section) was found to be out of tolerance and re-drill was carried out.

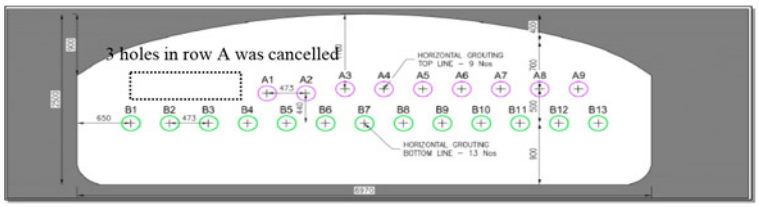

Figure 12: Section of horizontal grout holes

Figure 13: Reflex Gyro

Figure 14: Jean Luz computer

For both stages, the viscosity, gel time and density tests were carried out 3 times in a 12 hours shift during the grouting of BCS. In addition, the grout plant was equipped with a full automatic recording system known as Jean Luz for continuous monitoring of grout pressure and injected volume during grouting. The data collected were reviewed to determine if re-grouting was required prior to further drilling. The permeability of the treated ground was confirmed by in-situ test for the selected drillholes as discussed in Section 5.3.

5.3 Analysis of the grouting parameters

For vertical grouting, it was found that the injected quantities in average are similar to the target volume. It was observed large dispersion of grout intake occurred for BCS: grout volume was larger in the eastern side when compared with the western side. This was anticipated due to the different profile of special fill during the TWL construction observed in the GI findings and TWL construction as-built records. Furthermore, the southern part of both east and west side observed less grout intake when compared with the northern part. It believed this was due to some previous grouting carried out in the proximity of the junction between the IMT tunnel and the SGI tunnel.

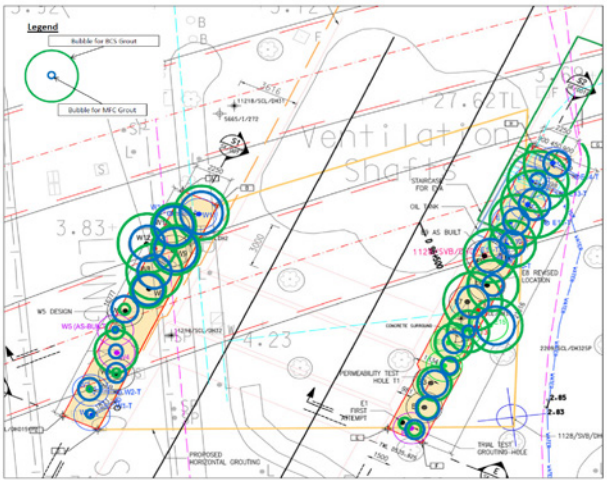

Figure 15: Grout volume intake repartition for vertical grouting

	Total	East Side (Exclude E1)	West Side
BCS (Total)	27.82% L	37.54% L	12.60% L
BCS (Horizontal zone)	31.78% L	38.44% L	18.08% L
MFC (Total)	9.28% L	10.50% L	7.37% L
MFC (Horizontal zone)	8.74% L	10.56% L	4.99% L

Table 5: Actual injected volume for vertical grouting

Row	Treated Area (m^2)	Actual Grout Intake (%)
A	365.6	6.6%
B	566.8	15.7%
Total:	932.4	12.1%

Table 6: Actual grout intake (%) for row A and B

During horizontal grouting, the total actual grout intake for row B is larger than that of row A. It was considered that the earlier grouted row B had successfully formed a confinement curtain fan at the bottom for effective row A grouting. And row B treated a larger area than expected so part of row A treatment area was injected during row B grouting works. It was observed that the injected volume for hole B13 was relatively larger. This could be due to the possibility of grout outflow from the inclined vertical grouted holes (E10 to E14) and part of the hole (from 0m to 5m) was out of the footprint of the vertical TAM curtain. The relatively larger volume along the far end perimeter of curtain (B6, B7, B8, B12) was due to the lack of vertical grout to work as grout flow barrier. This also proved the confinement formed by vertical grouting was effective, when compared with B1 to B5. Furthermore, the result shows that desirable grout volume and pressure were achieved for hole B1 to B4, despite 3 planned holes in row A above them were cancelled due to their close proximity to the TWL structure. Furthermore, the actual grout volume placed for row A only accounted for 6.6% of the targeted ground volume. This figure was less than the value for row B as expected, in addition to the final pressure recorded at each injection step, indicates that the available void in the gravel layer have been properly filled. With the overall grout volume being 12.1% of the total ground treatment volume, it also suggested the original design assumption of 35% void ratio was on the conservative side.

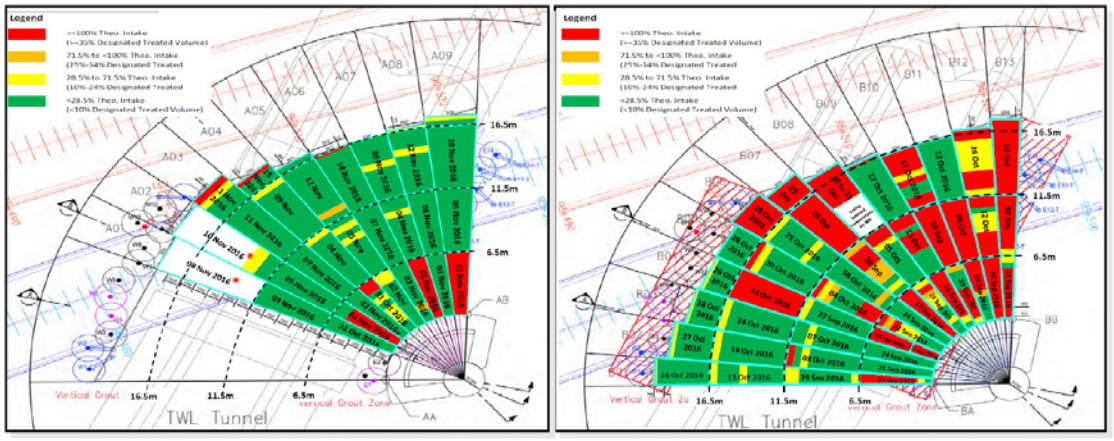

Figure 16: Actual Injected Volume for row A and B

5.3 Permeability Verification Test

Verification tests were carried out to verify the reduction in the permeability following the grouting. For vertical grouting, in-situ constant head permeability test were carried out using a GI rig. The T2 (western side) and T3 (eastern side) measurement showed satisfactory permeability of 1.43x10-7 to 7x10-8m/s and 2.15x10-6 to 7.74x10-7m/s respectively after BCS and MFC grouting.

For horizontal grouting, the drilling and ingress measurement of the pre-planned test sections started immediately after the grouting of Row A and was finished on 21 November 2016. Water ingress was measured for 1m response length as a basis for calculation of residual permeability using the Goodman (1965) formula as an indication, and verified by the designer using a seepage analysis 3D model. The poorest result out of the 5 tests shows permeability of one 20th of the allowed maximum permeability, whereas the best measurement shown permeability of one 130th of the allowed maximum. The results are therefore much better than the targeted permeability limit of 10-5 m/s.

It shall be noted that the 5 one metre long test sections representing all of the treated ground volume cannot be viewed as conclusive evidence that isolated locations with permeability higher than the specified limit remain. Minor adjustments made to the drilling and grouting pattern due to obstructions and jammed casing were considered to be appropriate and did not negatively influence the results. Nevertheless, in view of the overall grouting data, the risk of serious problems caused by TBM excavation underneath the SVB was considered to be minimal. The reduction in the permeability of the special fill layer to less than the target 10E-5m/s is shown in Table 7.

B03 (13.5m to 14.5m): 0.17 L/min	correlate to	1.32E-07 m/s
A03 (16.5m to 17.5m): < 0.1 L/min	correlate to	< 7.94E-08 m/s
B09 (14.5m to 15.5m): 0.5 L/min	correlate to	3.86E-07 m/s
A07 (12.5m to 13.5m):m 0.1 L/min	correlate to	7.71E-08 m/s
TA1 (14.5m to 15.5m): 0.59 L/min	correlate to	4.67E-07 m/s

* The correlated permeability is calculated according to Goodman Formula

Table 7: Measured water ingress from pre-determined test sections, recalculated to permeability

5.4 Instrumentation and Monitoring (I&M)

Comprehensive instrumentation monitoring was installed inside the TWL for monitoring purpose. It comprised the tilt meter and Electro Level (EL) beams, crackmeter and real-time monitoring (ADMS) prisms to monitor the tilting, gap between rings and the 3D movement respectively. Borehole instruments such as inclinometers, extensometer and piezometer were also installed as close as possible to the running tunnels and the existing TWL structure. A staged I&M plan was implemented to best suit the works. Only minor movements of around 1mm were recorded while conducting the horizontal grouting directly underneath the TWL and subsequent SCL1128 TBM crossing, and were well within the requirements stipulated in WBTC No. 19/2002.

Stages	Works involved	Monitoring equipment installed	Coverage
1	Grouting from surface	EL beams and crackmeter	Interface IMT /SSL
2	SVB shaft construction	EL beams, crackmeter and ADMS	Interface IMT /SSL
		Manual borehole inclinometer and extensometer	Ground between shaft/ cavern and TWL
3	Grouting from SVB shaft	EL beams, crackmeter and ADMS	Ten rings inside the SSL and first IMT unit
4	TBM crossings	EL beams, crackmeter and ADMS	Forty rings inside the SSL and first IMT unit

Table 8: Stage I&M plan for two stage ground treatment and TBM crossing under TWL

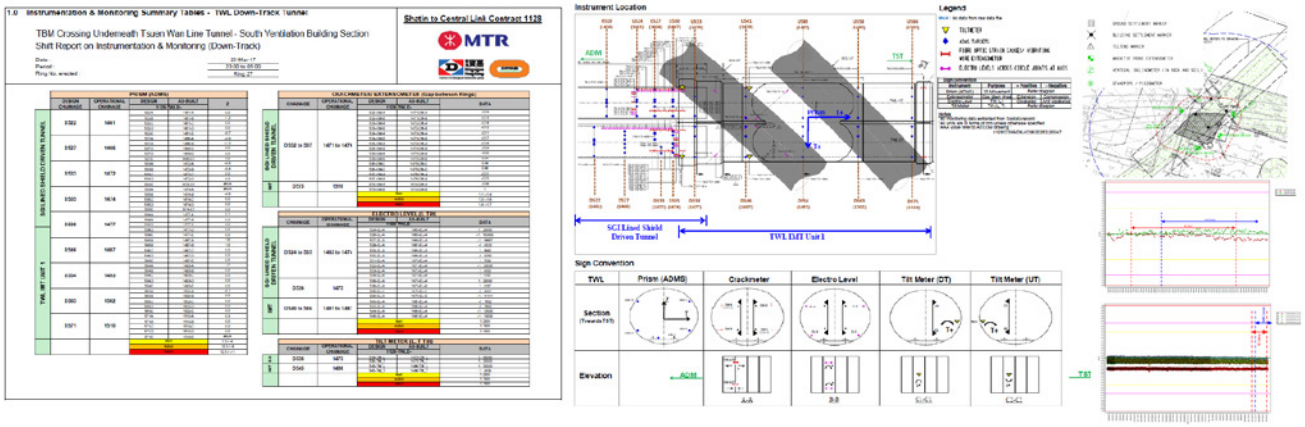

Figure 17: I&M layout plan for grouting works and its monitoring record

6 CONCLUSION

In view of the extreme proximity to the existing TWL structure (with a minimum 2.5m clear separation), the unique and technically challenging two-stage ground treatment of the gravel layer beneath the SVB was design and implemented, in order to reduce the permeability of gravel bed as well as the settlement and disturbance to the TWL operation due to the SCL TBM drive. Due to the limited available

ground information, the ground treatment was designed based on the target permeability provided by the TBM specialists. Drilling and grouting execution data were systematically reviewed during the implementation along with the test results. The results indicated that the design permeability criterion of 10-5m/s was well achieved. TBM had safely and successfully passed underneath SVB without any disturbance to TWL structure and railway operation, with around 1mm movement observed during the overall construction work including the grouting works and TBM excavation works. Hence, it was concluded that the two-stage grouting method was successfully completed and proved to be efficient in the highly permeable open ground. After the successful TBM crossing, the vertical shaft had been backfilled. The success of this ground treatment works lies on the close partnership between the client, contractor, and sub-contractor.

REFERENCES

Auvergne, Gauffre & Prost 2017a, *Extensive use of I&M to Enable Safe TBM Drive in Urban Dense Area, a Focus on SCL1128 Eastern Downtrack Drive, Proceedings of the HKIE Geotechnical Division Annual Seminar 2017, Hong Kong*.

Auvergne, Yu, Mogenier & Barrett 2017b, *Geophysical Investigations for Obstruction Detection and Mitigation for Marsh Road TBM Crossing, SCL1128, Proceedings of the HKIE Geotechnical Division Annual Seminar 2017, Hong Kong*.

Jacques, Laverret, Reilly 2017, *SCL1128 – Hong Kong's First Variable Density Tunnel Boring Machine, Proceedings of theHKIE Geotechnical Division Annual Seminar 2017, Hong Kong*.

Kwok, Bracq & Barrett 2017, *Hong Kong MTR Shatin to Central Link Contract1128 (Eastern Approach) – Tunneling in Sensitive and Congested Urban Environment, Proceedings of the HKIE Geotechnical Division Annual Seminar 2017, Hong Kong.*

Experience of Jet Grouting in Hong Kong

C. Borgatti
Trevi Construction Hong Kong Limited, Hong Kong

Victor Li
Victor Li & Associates Ltd, Hong Kong

ABSTRACT

This paper describes the experience of jet grouting in Hong Kong. The principles, practice and applications of jet grouting are briefly described. Some recommendations on design, specification and quality control of jet grouting are made.

1 INTRODUCTION

Jet grouting is a versatile method of ground improvement. In Hong Kong, it has been widely used in various applications in civil engineering projects and is becoming more common for controlling ground movement of deep excavations in private development projects. This paper discusses the experience of jet grouting in Hong Kong.

2 BASIC THEORY OF JET GROUTING

The jet grouting process involves disaggregating the soil or weak rock and mixing it with and partial replacement by a cementing agent. The disaggregation is achieved by means of high energy jet of one or more fluids, one of them being the grout mix itself. A high pressure, which may be up to 400 bars, is provided by a high pressure pump to the cement grout. The cement grout flows through high pressure hoses into the jetting rod and flows out from the nozzles in the jetting rod into the soil. In the delivery hose, the velocity head is small because the flow rate is low, but the pressure head is very high. There is a common misconception that jet grouting is dangerous because the high pressure will stay in the ground after jetting, causing the risk of ground heave. This is not the case as can be explained by the well-known Bernoulli's principle in fluid mechanics which state that:

pressure head + velocity head + potential head = constant

The potential head term can be ignored since its change is usually small compared with the other two terms. The jet grouting process involves forming an open drillhole in the ground using the drillbit connected to the jetting rod. As long as the drillhole remains unblocked, the pressure head in the drillhole will also be maintained at a low value close to the hydrostatic head. If so, the pressure head at the jetting point must be low and the velocity head of the fluid in the jet must increase to maintain a constant total head, thus forming a high velocity jet for disintegrating the soils. It is only when the drillhole is blocked that a high fluid pressure will develop in the ground. Nowadays, the jet grouting process is highly automatic and computerized. When there is any sign of blockage of the drillhole as indicated by a drop in discharge rate in the jet, increase in torque of operating the drillbit or reduced return of spoils from the drillhole, the jet grouting process will be aborted by the machine to remove the danger of ground heave.

3 TYPES OF JET GROUTING

In Hong Kong, the mono-fluid and double-fluid system are more common and the triple-fluid system is seldom used. Figure 1 shows the mono-fluid system which uses the grout mix for jetting. Figure 2 presents the double-fluid system in which compressed air is used to increase the efficiency of jet grouting. The air will reduce the viscosity of the slurry mixture of disaggregated soils and cement grout. For this reason, a jet grout column with a larger diameter can be formed using a double-fluid system.

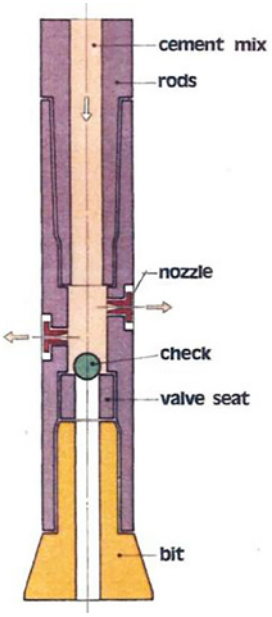

Figure 1: Mono-fluid system

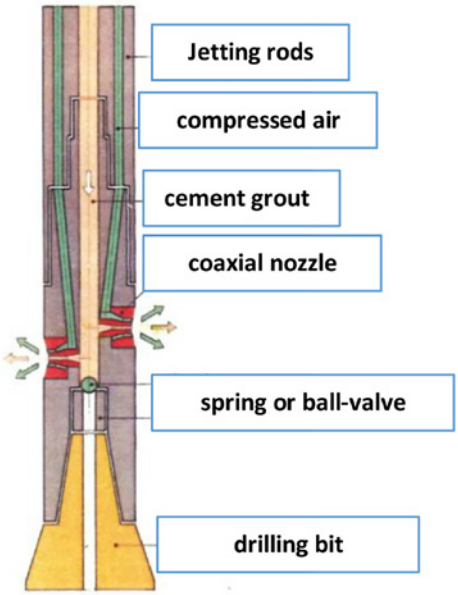

Figure 2: Double-fluid system

Although a double-fluid system is more efficient, the compressed air may leak and affect adjacent areas. The mono-fluid system is therefore more suitable when the application of jet grouting is to isolate the construction works in the site from affecting adjacent sensitive structure.

4 WORKING PROCEDURES

Figure 3 shows the procedures for forming a jet grout column (JGC). Depending on the design requirement, a JGC can be installed to specified top and bottom levels below the ground. To achieve a bigger JGC, pre-cutting with air and water is sometimes carried out before jetting with cement grout. Figure 4 presents the execution process of jet grouting.

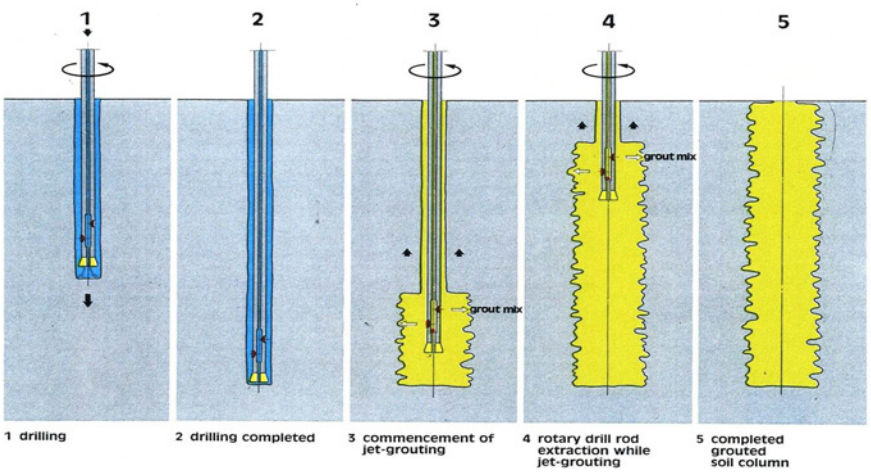

Figure 3: Construction of jet grout column

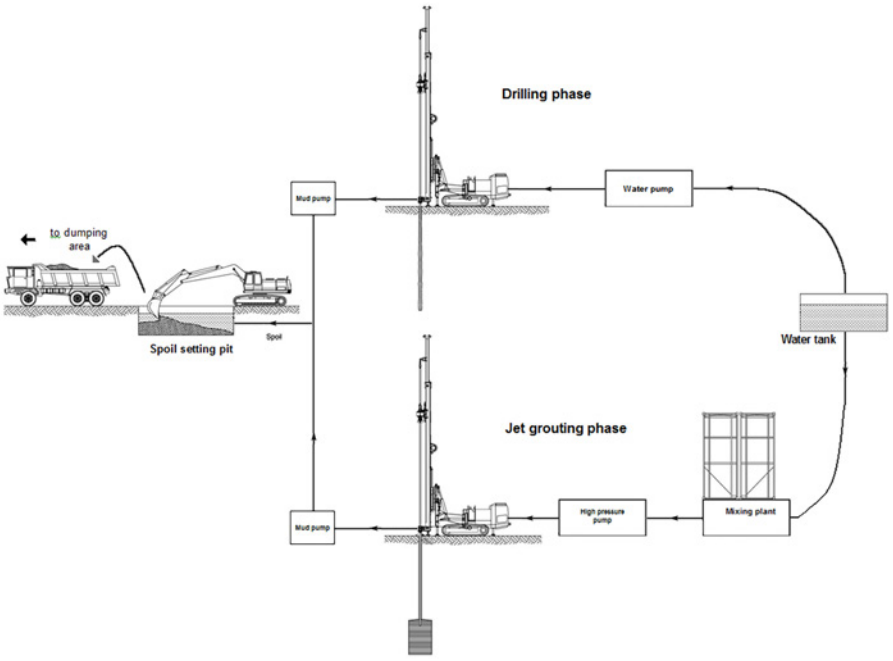

Figure 4: Execution process of jet grouting

Jet grouting requires the use of a crawler mounted, hydraulically operated rig. The rig is equipped with a computer system which records the essential parameters for monitoring the jet grouting operation. The cement grout is mixed by a high turbulence automatic plant capable of producing a grout supply of at least 20m^3/hr. Water is stored on site in tanks. Mixed grout is temporarily stored in an agitator with 3m^3 capacity and kept in constant movement until required by the high pressure pump. The grout mix is supplied by means of a high pressure pump through high pressure hose (Type AA55). Hose connectors must be capable of holding up a pressure of at least 1200 bars. The pump should be close to the jetting rig to avoid loss of pressure. The mixing plant is connected to cement silos. According to the Air Pollution Ordinance, the total volume of cement stored in silos on site is limited to 50 tonnes. This places a severe restriction on the production rate of jet grouting in Hong Kong.

5 SUITABILITY

Jet grouting is suitable for a wide range of soils as shown in Figure 4. In granular materials, there is a higher risk that the compressed air may spread. It may be cautious to use a temporary casing for forming the drillhole to create a more controlled path for the compressed air and spoils to return to the ground surface through the casing.

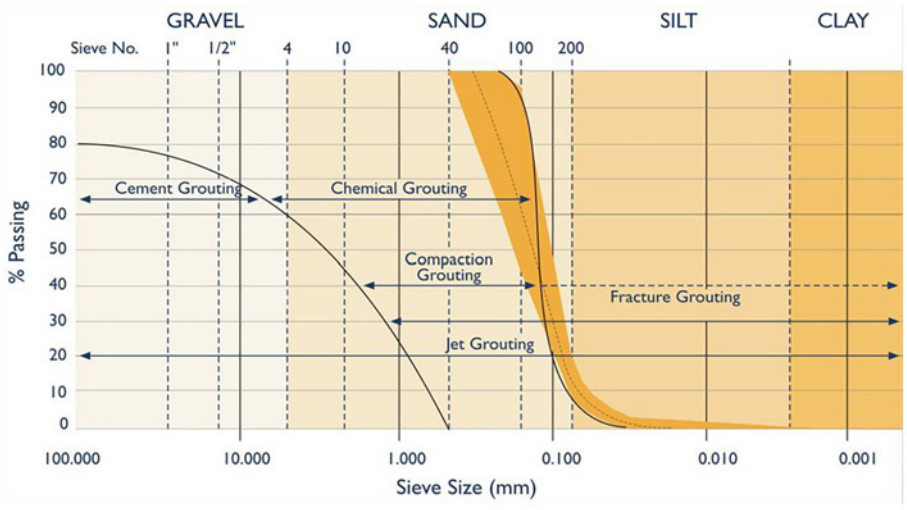

Figure 5: Soils suitable for jet grouting

6 JET GROUTING DESIGN

Figure 6 shows the typical patterns for jet grouting. The linear layout is usually used for forming a separation wall or a grout curtain. The triangular mesh is usually for forming a jet grout block. The impervious or pervious pattern can be used depending on whether it is necessary to form a completely water-tight jet grouted block.

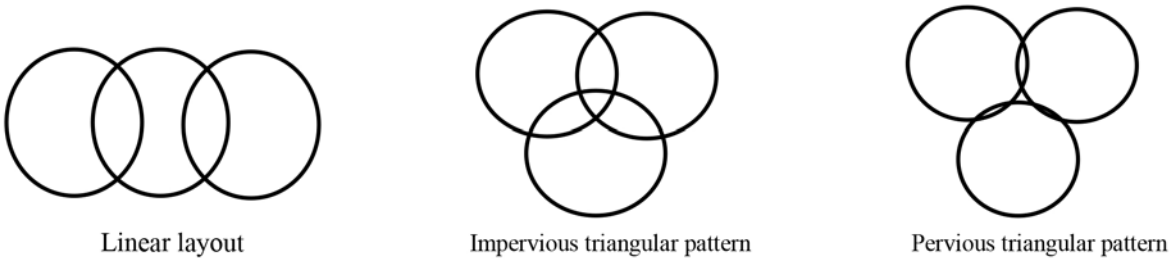

Figure 6: Jet grouting pattern

Grout mixes used for jet grouting usually has a water/cement ratio of 0.8 to 1.2 by weight. Table 1 gives some guidelines on the sizes and properties of JGC that are achievable for different types of soils based on past experience in Hong Kong.

Table 1: Achievable properties of jet grout columns

		Mono-fluid system	Double-fluid system	Achievable lower bound results		
Description of soil	**SPT**	**diameter achievable**	**diameter achievable**	**UCS**	**E**	**k**
				(MPa)	(MPa)	(m/sec)
Marine deposit	<<10	from 800mm to 1200mm	up to 3000mm	1.2	150	10^{-7}
	from 11 to 40	from 600mm to 800mm	up to 2000mm			
Alluvium sand	from 11 to 40	from 600mm to 800mm	up to 2400mm	2	200	10^{-7}
	from 50 to 80	up to 600	up to 2200mm			
	from 80 to 100	up to 600	up to 1800mm			
Alluvium clay	up to 20	up to 800	up to 2400mm	1.2	150	10^{-7}
	from 20 to 40	up to 600	up to 2000mm			
	from 40 to 60	up to 600	up to 1800mm			
Completely decomposed granite	up to 20	up to 800	up to 2400mm	1.5	200	10^{-7}
	from 20 to 40	up to 600	up to 2000mm			
	from 40 to 60	up to 600	up to 1800mm			
Gravel/granular fill		from 800mm to 1000mm	up to 2400mm	3	300	10^{-7}
Rockfill with fines		up to 600	up to 1600mm	3	300	10^{-7}
UCS = unconfined compressive strength; E = Young's modulus and k = permeability						

The results for UCS and E shown in the above table are the likely achievable lower bound results and the quoted permeability k, which is the same for all soil types, is the expected upper bound value. For sandy soils, the jetting process is more effective in producing a more thorough mixture of soils and cement mix and a permeability of 10^{-7} m/s or lower should be achievable. For clay soils, the jetting process may be less effective in achieving a thorough mixture. As the permeability of clay itself is likely to have a permeability lower than 10^{-7} m/s, the mass permeability of JGC containing clay lumps is still expected to be 10^{-7} m/s or lower.

In Hong Kong, design engineers sometimes specify the strength properties of JGC in terms of effective cohesion and angle of shearing resistance. At present, there is no commercial laboratory which has the facility to measure these properties of JGC. It is unreasonable to require the contractor to verify these design parameters when there is no available facility for performing the relevant tests. From a design point of view, it will be much simpler and more practical for the designer to ignore the friction component of strength and model JGC as a $\phi = 0$ material with a high shear strength S equal to half of the unconfined compressive strength. In this case, the contractor can easily verify the required strength by unconfined compression tests.

7 TESTING AND ACCEPTANCE CRITERIA

The acceptance criteria are usually related to the permeability, deformation modulus and strength properties depending on the function of the JGC. The insitu permeability of JGC can be measured using field permeability tests such as constant or falling head permeability test. The strength of JGC can be assessed using unconfined compression tests of a core sample. Deformation modulus can be inferred from the stress-strain curve measured in an unconfined compression test. It can also be assessed using pressuremeter tests. Sometimes, a total core recovery (TCR) criterion is specified. This parameter may be useful as a rough indicator of the homogeneity of JGC, but should not be used as rigid acceptance criterion. As long as the overall TCR of all the JGCs or grout block meets the target value, the presence of some local weak spots with lower TCR should not normally affect the performance of the jet grouting.

8 QUALITY CONTROL

The end product of jet grouting is cement-stabilized soil and not the hardened grout itself. Designers in Hong Kong often incorrectly and unnecessarily apply the quality control measures for the cement grout used in foundation construction (such as unconfined compression test of cube samples) to the grout mix for jet grouting. The grout mix for jet grouting has a much lower water/cement ratio than that of the thicker, non-shrink grout used for foundation works. As a result, bleeding is expected to be significant for the grout mix used for jet grouting. It is not suitable or meaningful to prepare cube sample for the grout mix for unconfined compression because a cubic specimen cannot be formed as a result of bleeding and sedimentation of cement inside the mould. Even if a confined compression test can be carried out on a non-standard test cube, the strength of cement grout gives no indication of the strength of JGC in the ground.

It is recommended that quality control of grout mix based on the density and viscosity only will be sufficient for jet grouting. The density of grout mix can be measured using the Baroid mud balance and the theoretical range of grout density is 1.43 to 1.59 tonne/m^3 for water/cement ratio between 0.8 to 1.2. The viscosity can be measured using the flow cone and the recommended range of Marsh cone viscosity is 30 to 40 seconds.

Other quality control measures during construction include the control of alignment of grout rod, pump pressure, grout flow and etc. Equipment used by specialist contractors for jet grouting in Hong Kong are usually equipped with computer controlled devices to fulfil these quality control requirements.

Jet grouting is a soil improvement technique. Designers cannot expect to have uniform jet grout columns similar to what is achieved by the tremie concrete in pile foundations or diaphragm walls. Even when the jetting parameters are monitored and recorded by electronic instruments, the diameter of and cement content in jet grout columns will be affected by variations of soil properties and hence not uniform. The final strength can vary along the jet grout column.

A jet grout column is not as strong as concrete. Coring can sometimes damage the core samples,

giving a wrong impression that the quality of JGC is poor. Even if the coring is properly executed, the presence of hard materials such as gravel, boulders and in general obstructions can damage or affect the integrity of the core during the course of coring. Under such circumstances, televiewer can be used as an alternative to verify the integrity of the JGC in question by visual inspection.

9 APPLICAITONS

Jet grouting has a wide range of applications. The common applications in Hong Kong are discussed below.

Plate 1: JGC for enhancing stability of temporary cut slope

a. JGC can be used as stabilizing piles to enhance the stability of slopes. Plate 1 shows the large diameter JGC installed for enhancing the temporary slopes formed during excavation within a large cofferdam for the project of West Kowloon Terminus Station North.

b. Construction of a block of strong and impermeable material to support the construction of cross passages between tunnels or excavation by tunnel boring machine at the break-out point at the launching shaft and the break-in point at the receiving shaft.

c. Ground improvement works to increase the strength and stiffness of soils to reduce the ground movement during excavation of cofferdams. JGC can be installed behind the embedded wall to reduce the active earth pressure or within the cofferdam to enhance the passive resistance of soils or both. A jet grout slab can also be formed as a pre-installed strut before excavation, although it is not common in Hong Kong.

d. Jet grouting is also useful in sealing up utility windows. The JGC will basically act as an embedded wall for supporting the excavation beneath the utilities. Plate 2 shows such an example for the project of Central Reclamation Phase III.

e. Jet grouting can be used for sealing gaps or openings in the embedded wall. For instance, jet grouting can be used to form a strong and robust grout curtain behind pipe pile wall. In doing so, it may no longer be necessary to install lagging wall. For excavations in areas with high rockhead profile and when excavation needs to be carried deep below the rockhead levels, jet grouting can be used seal the toe of sheetpile wall or pipe pile wall founding at the rockhead to prevent water inflow at the soil/rock interface. Plate 3 shows an example of jet grouting used for project of Shatin to Central Link – Diamond Hill to Kai Tak Tunnels for sealing gaps between pipe piles.

Plate 2: Jet grouting for sealing up utility windows

Plate 3: JGC for sealing gaps between pipe piles

f. JGC can be installed using mono-fluid system to form a separation wall to mitigate the effect of construction works on sensitive structures. Plate 4 shows an example in which JGC was installed to mitigate the potential effect of building settlement of old buildings before trench excavation for construction of diaphragm wall.

Plate 4: Jet grouting for protecting old building

10 CONCLUSION

Jet grouting is a versatile method of ground improvement. Some of the common applications of jet grouting in Hong Kong are discussed in this paper. With proper control during installation, buildup of pressure in the ground will not occur, particularly when using the mono-fluid system. It should be borne in mind that the end product of jet grouting is the cement-stabilized soil and not the cement grout itself. Quality control should be focused more on the JGC and not the grout mix. Many of the quality control measures commonly used for the denser cement grout for foundation works are not applicable to the grout mix with a high water/cement ratio used for jet grouting. Depending on the application, the quality control of JGCs can be carried out by means of field permeability tests, unconfined compression tests

for measurement of strength or unconfined compression test/pressuremeter tests for measurement of stiffness. There is at present no commercial laboratory in Hong Kong which provides the services for measurements of the effective stress parameters of core samples of JGCs, such as triaxial tests. From a design point of view, it will be simpler to model the jet grouted soils as $\phi = 0$ material with a target shear strength equal to half of the design unconfined compressive strength. In doing so, verification of strength parameters of JGC can be effected simply by means of unconfined compression tests. The jet grouted zone is commonly designed as a block with uniform properties mainly for convenience of analysis. This explains why the impervious triangular pattern of JGC is often specified by the designer. A uniform grout block may not be necessary for some geotechnical applications because the performance of geotechnical works, e.g. shoring system, is largely controlled by the average mass properties of grouted block and not the weakest spot in the stabilized soils. The use of pervious triangular pattern or perhaps non-overlapping JGCs at much reduced costs may often be sufficient to meet the design requirement.

TBM Bored Tunnels in Marble

Eric Chan
MTR Corporation Limited, Hong Kong

Derek Kwok
MTR Corporation Limited, Hong Kong

ABSTRACT

The Guangzhou – Shenzhen – Hong Kong Express Rail Link (XRL) is a committed cross boundary transport infrastructure project, which will provide high speed rail services between Hong Kong and Guangzhou, and a connection to the national high speed passenger rail network serving major mainland cities outside of Guangdong province. The XRL, a dedicated corridor, comprises about 26 km tunnels from boundary to a terminus at West Kowloon.

XRL Contract 826 involved construction of tunnels by Tunnel Boring Machine (TBM) from Mai Po area and cross the boundary to a new high speed rail station at Futian that was constructed by mainland China. The tunnels were expected to be bored within marble and associated cavities in Mai Po area in the design stage and therefore the challenging geological conditions posed risk of unstable ground, loss of face support pressure and slurry blow out to the TBM tunneling. Special design and construction considerations including extensive ground investigation and geophysics were given for the TBM tunneling. Comprehensive mitigations measures and monitoring system were implemented in order to mitigate the geotechnical risks.

1 INTRODUCTION

1.1 Scope of Works

The northern section of XRL project extends from Huanggang to north of Pat Heung Ventilation Building. It comprises tunnels from Huanggang to Tse Uk Tsuen, Stabling Sidings and Emergency Rescue Siding at Shek Kong, Emergency Access Point at Tai Kong Po and ventilation buildings at Mai Po and Ngau Tam Mei. The layout of XRL Tunnels and Associated Works is shown on Figure 1.1.

XRL Contract 826 comprised twin bored tunnels of 9.3 m diameter from a launching shaft at Huanggang in mainland China to ventilation building at Mai Po (VB1). The length of each tunnel is about 1.9 km from Huanggang to Hong Kong Border and 1.5 km from Hong Kong Border to VB1.

At the north of the Hong Kong Border, the tunnels in the Shenzhen Special Economic Zone (SEZ) run beneath existing highway corridors to the Shenzhen River, the boundary between the Shenzhen SEZ and the HKSAR. Once across the river, the alignment passes beneath the Mai Po Marshes.

1.2 Site Condition

The site area consists of marshland and numerous fish ponds, much of which lies within the environmentally important Mai Po Marshes Ramsar reserve and the adjacent conservation area. Low density low rise residential and light industrial / commercial development are adjacent to the site.

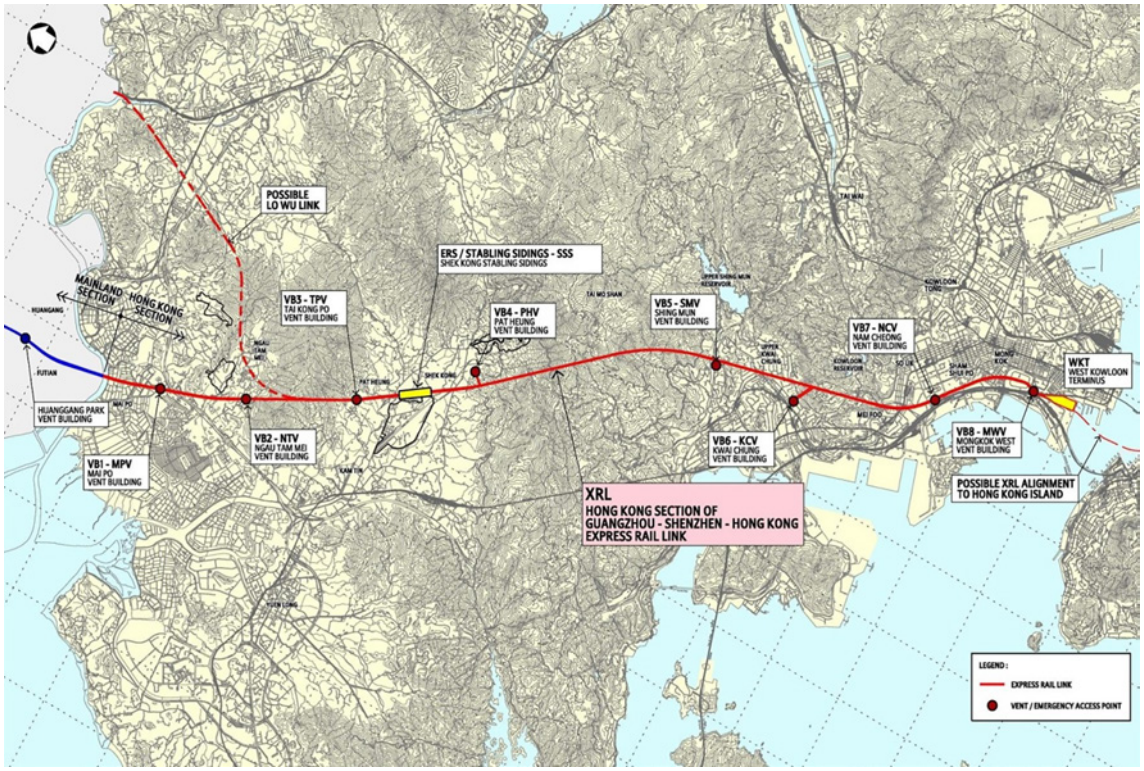

Figure 1.1: XRL Alignment

Plate 2.1: General View of the Fish Ponds in Mai Po

1.3 TBMs Details

TBM machines adopted in the Contract were two slurry shield TBMs manufactured by Herrenknecht. Outer and inner diameters of the TBMs are 9.96m and 8.7m respectively. Tunnel lining thickness of 450mm was designed to suit site condition.

2 GEOLOGICAL CONDITIONS

2.1 Geological Setting

The 1:20,000 and 1:100,000 scale geological maps of Hong Kong published by the Geotechnical Engineering Office (GEO) (Strange and Shaw (1994) and Sewell et al. (2000)) indicate that the entire alignment of the tunnel is within metasiltstone and metasandstone under Lok Ma Chau Formation. Typically the metasiltstone/metasandstone exhibits a classic weathering profile with completely (Grade V) and highly decomposed (Grade IV) metasiltstone/metasandstone. Slightly decomposed marble (Grade II) and minor granitic intrusion (Grade III to V) also occur within the tunnel profile. From project-specific borehole information and as-constructed record, it is revealed that cavities within that 200-meter long Marble zone along the tunnel alignment were identified. Cavities vary from 0.5m up to 5.4m in height.

Superficial soils occurring above the weathered metasiltstone/metasandstone comprise some Fill, Lacustrine Deposits, Marine Deposits and Alluvium Deposits of variable thickness.

North-east and north-west trending photolineaments are identified along the Tuen Mun-Lo Wu Fault Zone. The site was subjected to folding, intense faulting and metamorphism sequentially with dominant north-east trending fault and overthrust.

Solid Geology Map from Geotechnical Baseline Report (Arup (2009c)) was extracted in Figure 2.1 below.

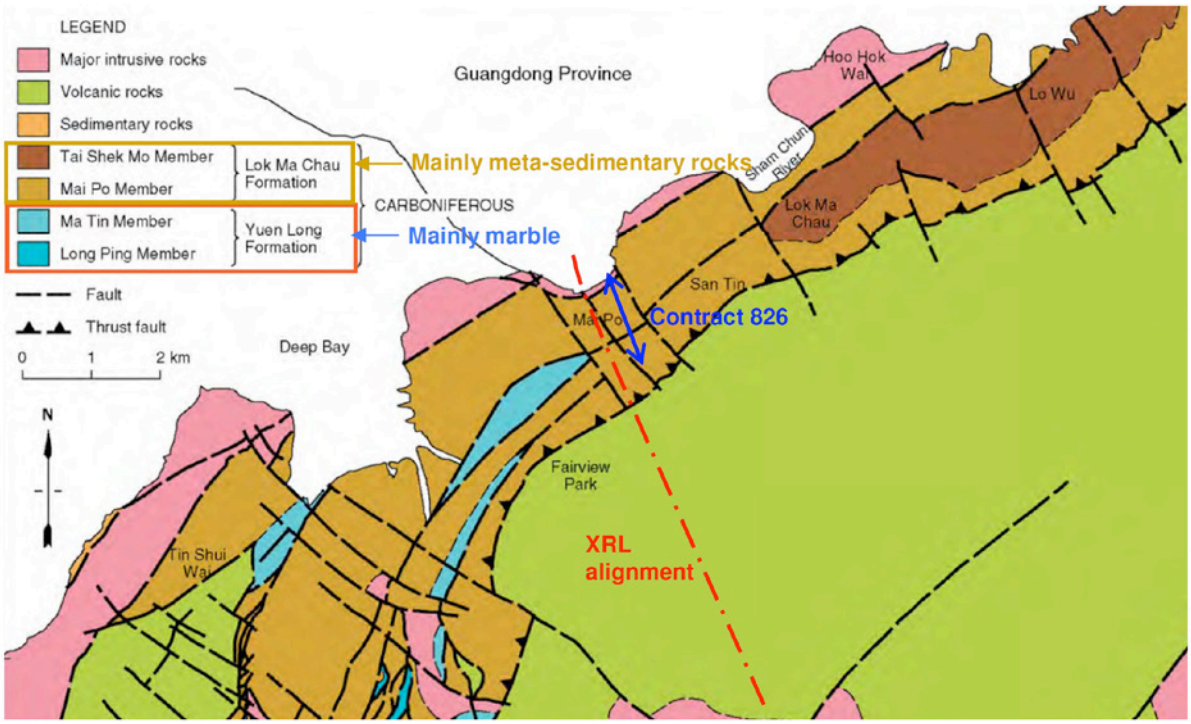

Figure 2.1: Solid Geology in the North-western New Territories (Arup, 2009c)

2.2 Project Specific Ground Investigation

Apart from archival ground investigation records from GIU of the CEDD Library, site specific ground investigations were conducted during Preliminary Project Feasibility Study in mid-2007 and Detailed Design Stage Ground Investigation in 2009. Project specific ground investigation data revealed that the anticipated ground at the tunnel alignment comprises alluvium (clay and sand) underlain by weathered metasiltstone/metasandstone (Grade III, IV and V), granite (Grade IV to V) and marble (Grade II). Marble was encountered at both downtrack and uptrack for approximate 200m in length each. Karst deposit and cavity were observed. The largest cavity observed was approximately 5.4m in height at drillholes no. 2108/XRL/A001a between -35.2mPD and -40.66mPD. It is 7.5m below tunnel axis level. Drill string lost in torque for 0.8m followed by drop of drill string. It is believed that the cavity was partially infilled.

Numerous small and possibly interconnecting cavities range from 0.5m to 2m in height were also evident. Ground investigation layout and geological section was presented in Figure 2.2 below.

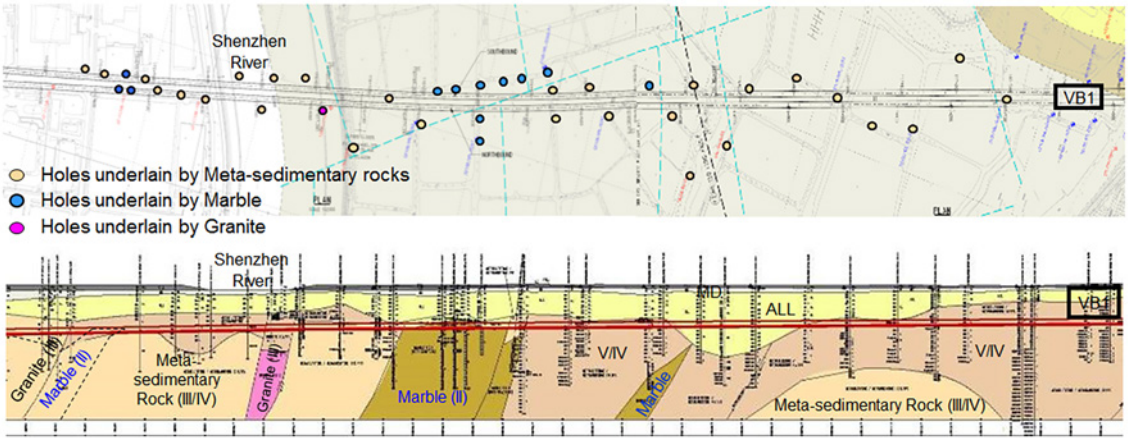

Figure 2.2: General Layout of Ground Investigation Drillholes and Geological Section (Arup, 2009c)

2.3 Project Specific Microgravity Investigation

Due to site constrains and objection from the fish pond operators, ground investigation drillholes could only be sunk along the earth bunds. Localized drillhole locations gave limitation on ground model interpretation. In addition, large cavities are believed to be found more commonly along hydrogeological fissures and marble/non-marble contact boundary. In order to mitigate TBM tunneling risks (to be discussed in detail in section 3 below) induced by the presence of cavity within marble subcrop, microgravity survey was undertaken to give comprehensive review on geological constraint of the site. Possible cavity along major dissolution trends within or in close relationship with marble subcrop was identified. In this survey, a total number of 224 gravity stations were applied along the earth bund in 5m to 10m intervals. It revealed that marble was found at 25m to 30m in depth and 200m in length in east-west direction. The findings were generally aligned with previous drillhole data with slight adjustment on the extent of marble subcrop (Figure 2.3). There was no extensive solution channel and void detected from this survey.

Supplemented with the findings of microgravity investigation, ground model was further refined and identified possible risk of solution channels and void in the proximity of the faulted Marble boundary where marble is fractured. See detail from the interpreted ground model in Figure 2.4 below.

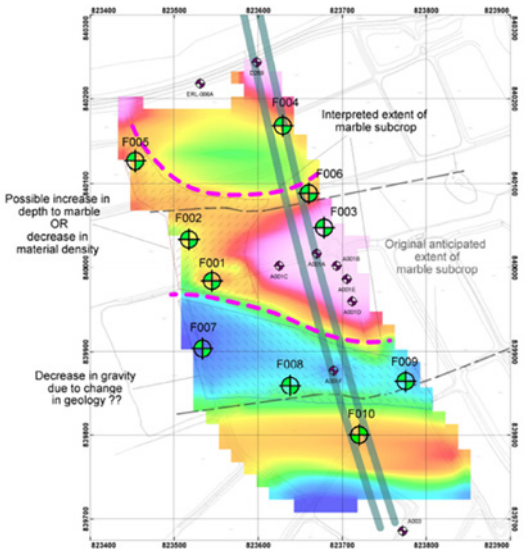

Figure 2.3: Microgravity Investigation Report (Fugro, 2009)

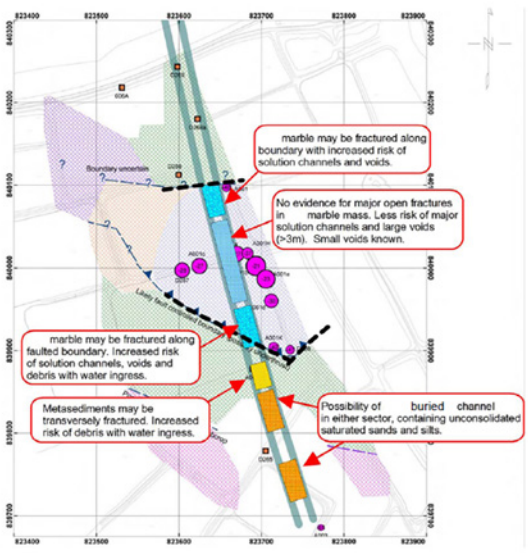

Figure 2.4: Interpreted Ground Model from Microgravity Report (Arup, 2009a)

3 TBM TUNNELLING RISK IN MARBLE

3.1 Tunnel Collapse

When a TBM is passing through marble zone with cavities underneath, possible tunnel collapse may be induced by the weight of moving TBM. When cavities are present at the tunnel invert, excessive tilting or settlement of the TBM may be induced by displacement of water or soft infilling material. Furthermore, strong marble is commonly associated with sharp weathering front of contrast between strong rock and soft weathered materials infilled cavity. It affects TBM performance and stability when soft materials are preferentially excavated.

3.2 Loss of Face Support Pressures

Presence of cavities directly above, below or in front of the TBM may induce sudden drop in face support pressure during excavation. Displacement of soft infilling materials or groundwater within the void may lead to loss of slurry. Loss of face support pressure could result in collapse of tunnel face followed by excessive settlement on the surface.

3.3 Slurry Blow Out and Air Leakage

Besides presence of cavity at tunnel crown, it is also possible to induce air leakage during compressed air intervention. Compressed air intervention is inevitable for maintenance and obstacle removal. Compress air loss may occur when cavity is present at the location of compressed air intervention. When air is lost through interconnected cavities or untreated fissures connecting to surface, it will result in a blow-out incident. Furthermore, risk of over pressure during tunneling should be mitigated to avoid slurry blow-out at uneven ground profile of the fish ponds. Confinement pressure should be optimized at all time and minimized when possible.

4 MITIGATION MEASURES FOR TBM TUNNELLING RISK IN MARBLE

4.1 Probing Works

4.1.1 TBM Specification

Since ground investigation data revealed possible cavities along the tunnel alignment, Particular Specification (PS) of this Contract detailed the requirements of TBM to detect voids ahead of the excavation face and in its vicinity. As stipulated in PS, the TBMs adopted in this Contract could conduct 360º probing and grouting ahead of the shield (Figure 4.1 and 4.2). There were a total of 22 inclined ports and 3 drilling rigs with two mounted on a ring carrier. The inclined ports were located strategically

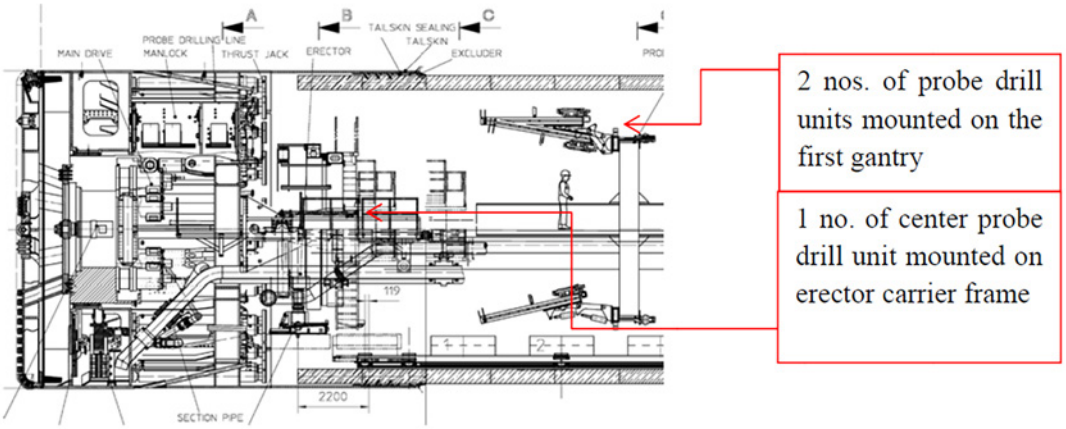

Figure 4.1: Probe Drill Units of TBM (CRCC-HC-CR15G JV, 2015)

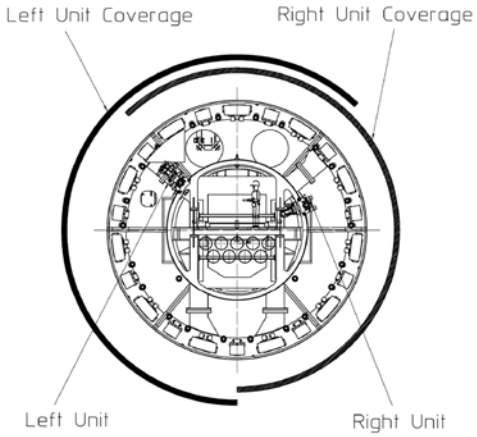

Figure 4.2: Full circumference probing and drilling unit at TBM shield (CRCC-HC-CR15G JV, 2015)

around the circumference of the shield body reaching a distance of 10 to 50 meters in front of the machine. TBM design provision was made such that, as a minimum, the zone to be probed shall be two tunnel diameters in width and one and a half tunnel diameters in depth, measured from the TBM axis. The location of the ports allowed the use of blow out preventers when drilling. The probe drilling rig contained suitable data logging equipment to record the drilling parameters such as torque, drilling speed, etc.

4.1.2 Probing for Detecting Marble Zone

As stipulated in approved method statement for probing works in this Contract, the Contractor conducted no less than five probe holes at every probing chainage prior to entering marble zone. In other words, probing was commenced 23m ahead from the predefined marble zone. Probe holes were drilled at 13° from horizontal at tunnel invert with a drill length of 23m and an overlapping length of 10m to the previous one. Since probing at this stage was predominately within alluvium soil, probing was suspended when the slurry loss through the excavation chamber in front of the TBM has exceeded $15m^3$ per hour. This is to minimize the risk of disturbing the ground while probing in this soft ground stratum. According to the probing result, actual location of marble zone was generally aligned with interpreted ground model.

4.1.3 Probing for Partial Marble Zone

After marble was detected partially on excavation footprint, probe hole numbers increased from 5 to 10. Probe holes were drilled 13° from horizontal with a drill length of 23m and an overlapping length of 10m to the previous one. Probe holes were conducted from tunnel invert or tunnel crown subject to actual site condition. According to the probing result, there was no cavity detected in the close proximity of the tunnel within partial marble zone.

4.1.4 Probing for Full-face Marble Zone

After full-face marble was detected, probing was conducted from invert towards tunnel axis at 10-meter interval or approximately every 5 rings (Figure 4.3). From the lesson learnt in past air loss and slurry loss incidents, probe hole drilling above axis was eliminated to avoid potential disturbance to the alluvium layer and fish ponds above. In additional to inclined probing, horizontal probing at tunnel face was also conducted to detect cavity right at excavation face. Horizontal probing was conducted at 40m in length with an overlapping length of 5m to the previous one. If extensive cavity was detected, additional horizontal probe holes would be conducted at 5° to horizontal to detect actual extent of the cavity. According to the probing result, there was no cavity detected in the close proximity of the tunnel within full-face marble zone.

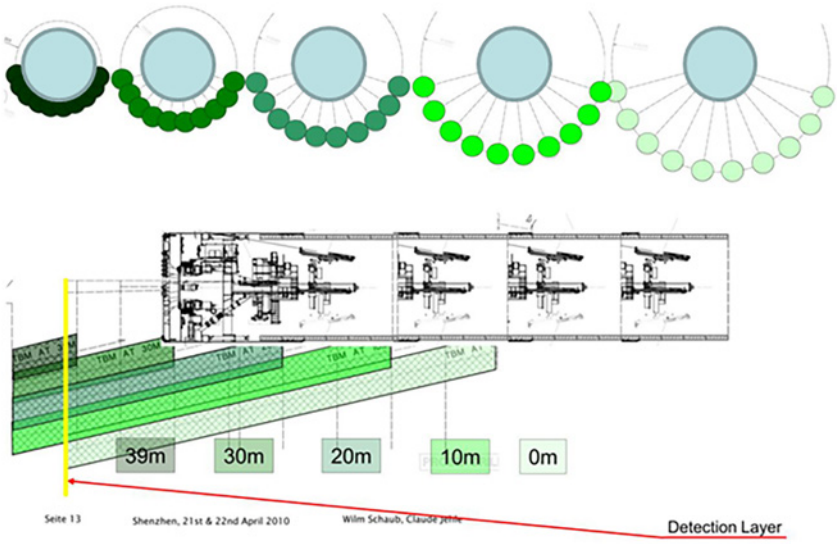

Figure 4.3: Probing Arrangement within Marble Zone (CRCC-HC-CR15G JV, 2015)

4.2 Grouting Works

4.2.1 General

In general scenario, detected cavities from probing would be treated by grouting. The grouting pressure was controlled within 1.0 to 1.5 MPa. Probe hole drilling stopped once cavity is detected. Probing resumed after cavity was treated by grouting with the aid of inflatable packers. All detected cavities were properly filled with cementitious grout (Ordinary Portland Cement was applied in this Contract) prior to TBM arrival. Grouting performance was checked according to radial probing works with no cavity detected in the upcoming excavation locations.

4.2.2 Cavity at Tunnel Crown or above

When face pressure drops below a pre-set value induced by cavity at tunnel crown, Auxiliary Face Support system (AFS) will automatically inject bentonite into the crown of the excavation chamber. Given the application of AFS, probing at/above tunnel crown to detect cavity above tunnel became unnecessary. It enhanced site progress by removing redundant probing works. AFS was also served as a contingency measures in case of sudden loss of face support during excavation. Since there was no cavity at tunnel crown or above detected from probing, probe holes were backfilled by grout injected through the locations of probe holes.

4.2.3 Cavity at Tunnel Invert or below

To avoid tunnel collapse and excessive TBM tilting when TBM passes through cavity at tunnel invert level, detection drilling pattern should concentrate on the lower portion of the TBM (Section 4.1.4). The cavities would then be treated by filling them with grout at low pressure. Since there was no cavity at tunnel invert or below detected from probing, probe holes were backfilled by grout injected through the locations of probe holes.

4.2.4 Inter-connecting Cavity

Inter-connecting cavity gives massive loss of grout with a possibility of grout reaching ground surface. If grout is pumped without achieving reasonable pressure, accelerator should be added to limit spreading distance of grout. Furthermore, abundant fresh slurry supply with total capacity of 3,000m^3 was ready on-site at all times. According to probing result, there was no inter-connecting cavity to be treated in this Contract.

4.2.5 Cavity affecting Tunnel Stability in Long Term

When cavity is evident underneath tunnel alignment, it may give potential risk to tunnel in service when cavities enlarged after construction. After TBM driving through cavities, therefore, proof drilling with remedial grout was injected through grout ports within each segment. Tunnel lining was grouted in full circumference. After grouting of all detected cavities, another round of proof drilling was conducted to verify the effectiveness of grouting. Since there was no cavity detected from probing, no post-tunneling grouting was required.

4.3 Rock Pilar Stability Analysis

Apart from conventional probing and grouting works, site specific Rock Pilar Stability Analysis was conducted for this Project to justify minimum pillar thickness required for safe TBM tunneling. Discontinuum and continuum analyses were conducted to simulate failure at jointed rock and intact rock respectively.

Discontinuum analyses were carried out at pillar thicknesses ranging from 2 to 6m with joint friction angles of 30 and 25. Continuum analyses were carried out for the same pillar thickness range and for GSI values of 55 and 40. Critical load case was considering the cutterhead weight transversely across the 10m span void.

Discontinuum analyses revealed that plastic failure was initiated when the pillar was reduced to 3m and complete collapse occurred when the pillar reduced to 2m (Figure 4.4). Continuum analyses revealed that failure was observed when the pillar was reduced to 1m and 2m with GSI =40 and GSI=55 respectively (Figure 4.5).

2m pillar, $\phi = 30^{\circ}$

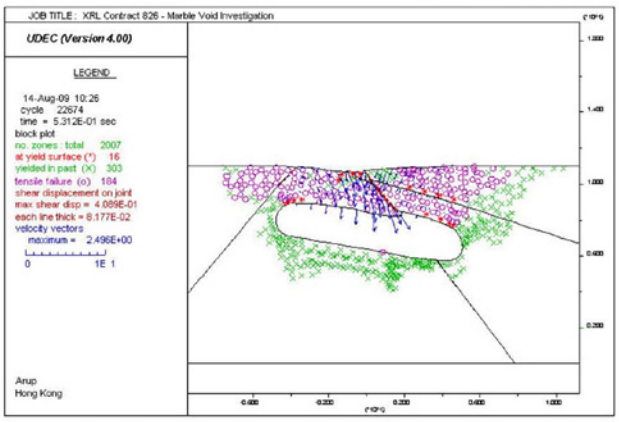

Figure 4.4: Failure Scenario of Discontinuum Analyses (Arup, 2009b)

1m pillar, GSI=55

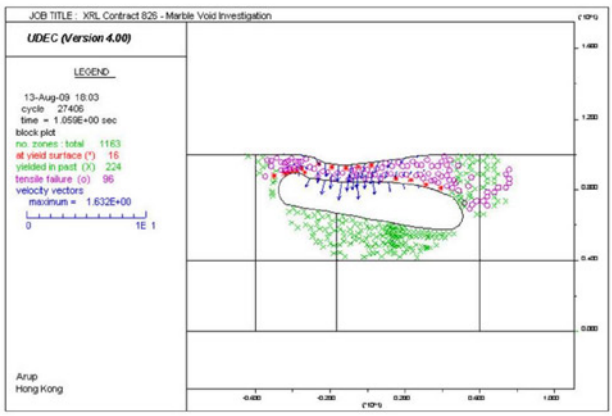

2m pillar, GSI=40

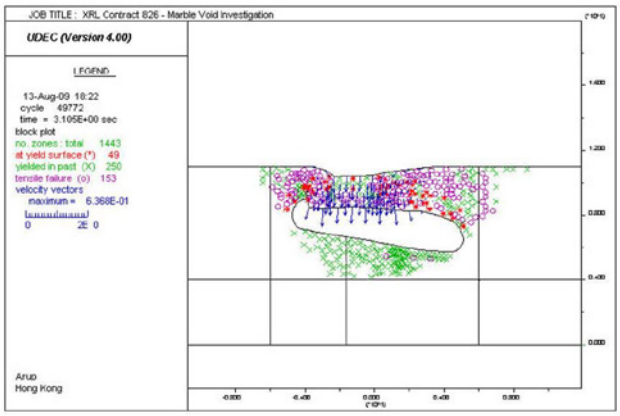

Figure 4.5: Failure Scenario of Continuum Analyses with GSI 55 (Arup, 2009b)

In this study, factor of safety was also assessed by taking formation of plastic yield points as an indication of failure. For a 5-meter thick pillar, it fails when GSI reduced to 35. Hence, a 5-meter thick pillar with GSI=55, it gives a FOS of 1.6.

Given the findings from above, it was considered that rock pillar with a minimum 5-meter thick is safe for TBM traverses. Compare to a 10-meter thick rock pillar was required to achieve the desired Factor of Safety in Reference Design, this finding successfully optimized required probing length from 40m to 23m.

5 CONCLUSION

Two slurry TBMs deployed in Contract 826 successfully bored through 200m zone of marble in both uptrack and downtrack. It eventually took 9-month to complete this 400m zone of high potential risk. A majority of effort and time was consumed in marble probing works. Probing method applied to detect rock level and cavity in marble zone was proven to be effective. It gave accurate prediction on ground condition ahead. There was no large cavity identified during the probing and hence no significant grouting works were required. Both actual ground movement and measured volume loss within the marble zone were less than the predicted values. Hence, it can be concluded that TBM tunneling risk in marble was well managed.

REFERENCES

Arup. 2009a. *Consultancy Agreement No. C803 – Working Paper no. 10 Risk of Tunnelling Through Marble at Mai Po (Revision A) Contract 826: Huanggang to Mai Po.*

Arup. 2009b. *Consultancy Agreement No. C803 – Working Paper no. 10 Marble Pillar Stability Calculations for TBM Tunnels (Supplementary Report) Contract 826: Huanggang to Mai Po.*

Arup. 2009c. *Consultancy Agreement No. C803 – Geotechnical Baseline Report (Revision C) Contract 826: Huanggang to Mai Po.*

CRCC-HC-CR15G JV. 2015. *Express Rail Link Contract 826 – Huanggang to Mai Po Tunnels: Method Statement for Probing and Grouting for TBM through Marble Zone.*

CRCC-HC-CR15G JV. 2016. *Express Rail Link Contract 826 – Huanggang to Mai Po Tunnels: TBM Performance Review Report.*

Fugro Aperio. 2009. *Express Rail Link Mai Po – Microgravity Investigation.*

MTRC. 2016. *Contract 826 – Huanggang to Mai Po Tunnels Bored Tunnel Report.*

MTRC. 2017. *Review of TBM works and Performance of WIL, XRL and SCL*

The Scenic Hill Jacked Box Tunnel Under The Hong Kong Airport Express Line

R.B. Cook
Aecom, Hong Kong (formerly Benaim)

I. Tsaparas
Benaim, Hong Kong

Ch. Venetz
VSL / Intrafor, Hong Kong

ABSTRACT

The Hong Kong Link Road, which connects the Hong Kong Zhuhai Macao Bridge with the Hong Kong Boundary Crossing Facilities, passes beneath the Airport Express Line (AEL) within the Hong Kong International Airport reclamation near Scenic Hill. The up to 89m long dual tunnel sections beneath the AEL were constructed using box jack techniques to prevent disruption to railway operations. It is the first time this method has been employed in Hong Kong. This paper presents the technical solutions developed to minimise settlement, overcome difficult ground conditions and cope with the high friction forces and space constraints. After extensive ground treatment by permeation grouting and installation of a pipe canopy roofing system, the two tunnels T001 and T002 were jacked into place in segments, whilst at the same time the soil was excavated and removed through the rear. Each segment was jacked using a 'pulling' jack system followed by a 'pushing' jack system between each segment. This was a cyclical operation, where the jacks between different segments were loaded sequentially to advance the boxes. The box jacking technique allowed safe construction of the works, whilst also delivering the boxes to their final position without disrupting AEL operations.

1 INTRODUCTION

1.1 General

The Section of the Hong Kong Link Road (HKLR) between Scenic Hill and the Hong Kong Boundary Crossing Facilities (HKBCF) was constructed under Contract HY/2011/03. The project comprises a 1.0km long dual 3-lane tunnel, a 1.6km dual 3-lane at-grade road and a number of slip roads. These together connect the HKBCF with the Hong Kong International Airport (HKIA). An up to 89m section of the dual tunnel designated T001 and T002 beneath the Airport Express Line (AEL) at Scenic Hill (see Figure 1) was built using box jacking techniques to install the segmented tunnel box sections. The ground under the AEL was treated by permeation grouting and horizontal steel pipes, forming a canopy roof, were installed between the launch and reception shafts. The tunnel boxes were precast in the launch shaft adjacent to the AEL before being jacked into their required positions beneath the operating railway. This construction method allowed the AEL to continue to operate undisrupted during the course of the works.

Figure 1: Site Location Plan

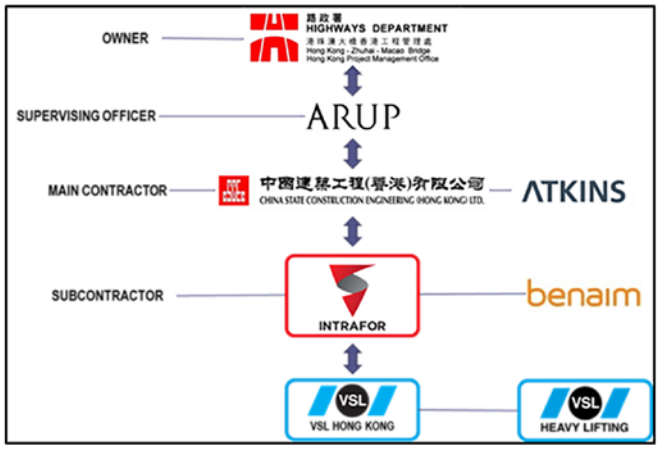

Figure 2: Main Parties Involved In The Project

VSL and Intrafor Hong Kong Ltd executed the box jacking works as the Specialist Subcontractor to the Main Contractor, China State Construction Engineering Hong Kong (CSCE). VSL/Intrafor's scope of works included the ground treatment under the AEL, the directional steel pipe installation to form the protective canopy roofing system, the box jacking works and the underground excavation and face stabilisation works. VSL/Intrafor teamed up with consultant Benaim, due to the latter's previous international experience in the detailed design of box jacking works, and because of their recent work together on the award winning Brisbane Airport Link jacked tunnels at Toombul in Australia. The main parties involved in the project are presented in Figure 2.

1.2 Overview Construction Concept

The geometric characteristics of the two jacked boxes T001 and T002 are shown in Table 1. In order to facilitate their construction, two temporary shafts were constructed (see Figures 3 and 4). The eastern shaft being the casting and launch shaft and the western shaft being the receiving shaft. The two shafts were approximately 26m deep and were formed by steel pipe piles toed into rock, supported mainly by a traditional braced steelwork excavation and lateral support system, but with soil nails at the headwall/jacked box interface.

A grout curtain was provided down to rock around the perimeter of the two shafts which was integrated with other grout curtains along the northern and southern external sides of the two boxes future alignment to form a groundwater cut-off. These were reinforced with steel tubes to aid the front face excavation stability on the inside face of the grout curtains. The grout curtains were supplemented by a mass grouting array within the intervening ground mass, extending from the launch shaft to the receiving shaft, to improve the excavation face stability and stabilise any residual water bearing ground. The mass grouting displaced the groundwater from the grouted mass, which dewatering was then checked by horizontal probing from the shafts before headwall removal.

The excavation face of the tunnel roof zone was protected from collapsing and from excessive deformations by pipe canopy roofing under the AEL. The canopy was formed using 800mm diameter steel tubes,infilled with grout and extended from the launch shaft to the reception shaft. The canopy also acted as an anti-drag system isolating the embankment over the boxes from horizontal displacement effects. Excavation of the ground was then carried out in 1.0m steps under the canopy, followed by the jacking of the tunnel boxes.

The boxes were oversized from their original curved alignment to allow their jacking along a horizontal plane and on a straight line. As no waterproofing could be applied to the boxes, they were designed to a strict crack width criteria of 0.2mm at the external concrete face, in accordance with the Hong Kong Structures Design Manual for Highways (HKSDM). In lieu of a waterproofing membrane a C50/20 concrete mix including a hydrophobic waterproofing additive was adopted for the permanent reinforced concrete structure. In addition to the above a sacrificial cover of 35mm beyond durability requirements was provided for the protection of the permanent structures from abrasion by the ground during the jacking works.

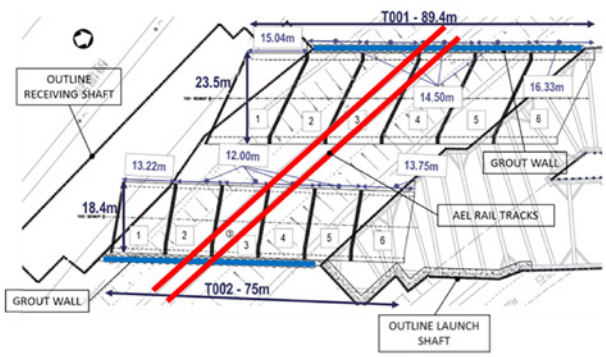

Figure 3: General Layout Longitudinal Section

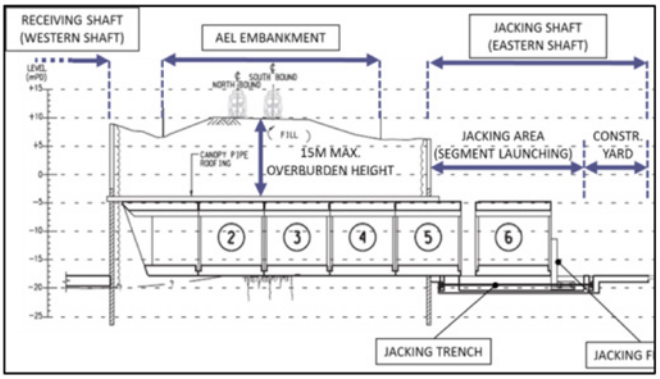

Figure 4: General Layout Plan

The skew geometry of the tunnel boxes was developed to minimise the extent of the shaft length and the number of segments. This influenced the skew shape of the T001 and T002 segments which are different.

The relatively large overburden depth of approximately 15m (Figure 4) from the AEL track level,when considered as a whole, would result in large friction along the boxes subsequently leading to large jacking loads. Therefore, each of the jacked box tunnels was divided into six segments to reduce jack loads (see Figures 3 and 4). The length of each segment (see Table 1) was optimised to lower friction forces to manageable levels, minimise the number of joints in the tunnel, and address spatial constraints which required the newly cast segment to be jacked while the following segment was under construction. A key design criteria was establishing the minimum length of the leading segment and its sloping nose so as to maintain stability when entering the ground at a skew angle. Each segment was precast inside the launch shaft, which ensured a higher quality of works compared to casting the tunnel in-situ beneath the AEL. The segments were then jacked forward off the casting bed using strand jacks located in trenches below the segments (Figures 9 and 17) 'pulling' against vertical jacking frames mounted at the back of each segment. After the jacking frames reached the jacking trenches limit, intermediate 'pushing' jack stations (IJS), housed between the segments base slabs and lower part of the walls, were activated in a cyclical manner between each segment by the distance of the available jack stroke, creating a caterpillar motion.

Table 1: Geometric Characteristics of the Jacked Tunnel Boxes T001 & T002

Box	Total Jacking Length	No. of Segments	Segment Length (m)	External Dimensions (w x h)	Roof slab thickness	Base Slab thickness	Wall thickness
T001	89.4m	6	14.50m to 16.33m	23.53m x 14.24m	2.20m	2.20m	1.80m
T002	75.0m	6	12.00m to 13.75m	18.47m x 13.06m	1.50m	1.80m	1.20m

An extensive instrumentation and monitoring plan was set up by CSCE. This included an automatic data monitoring system (ADMS,) with "Alert", "Alarm" and "Action" limits for the AEL rails tracks. Vertical track movement (settlement and heaving), horizontal movement, differential settlement between rails, as well as vibration were recorded. Various contingency measures were put in place and the AP/RSE/RGE and the MTRC representative were kept informed automatically whenever any of the response limits were exceeded. In a few limited cases the construction works was halted and re-tamping of the rail tracks provided, which mitigation was carried out by MTRC at night during non-operational hours, without affecting the regular AEL operations.

2 GROUND CONDITIONS & GROUND IMPROVEMENT WORKS

A major challenge of the scheme was the complex ground conditions beneath the embankment of the AEL. The embankment fill comprises 5m to 25m thick, Type A/B mixed sized rock fill (cobbles, boulders

and gravel) with occasional sand fill layers. Mixed ground of completely decomposed granite (CDG), alluvium sand (Figure 6) and traces of alluvium clays and marine deposits underlay the fill. Granite rock, Grade III or higher, lies beneath the CDG. The rock head falls from the northeast towards the southwest (see Figure 6). The rock head level on the northeast side of the project area lies above the top of box T001, however on the southwest side the rock head level was below the base slab of T002.

The ground improvement scheme comprised two external grout walls, 5m thick, two internal grout walls, 2m thick, and a grout block formed between the grout walls (Figure 6). The grout block was extended to rockhead or up to 2m below the excavation level, whichever was higher, while the grout walls were extended to rockhead. The drill diameters were specified to suit the ground material, 102mm diameter for soil and rock-fill and 45mm diameter in rock. The spacing of the drilling holes are shown in Figure 5.

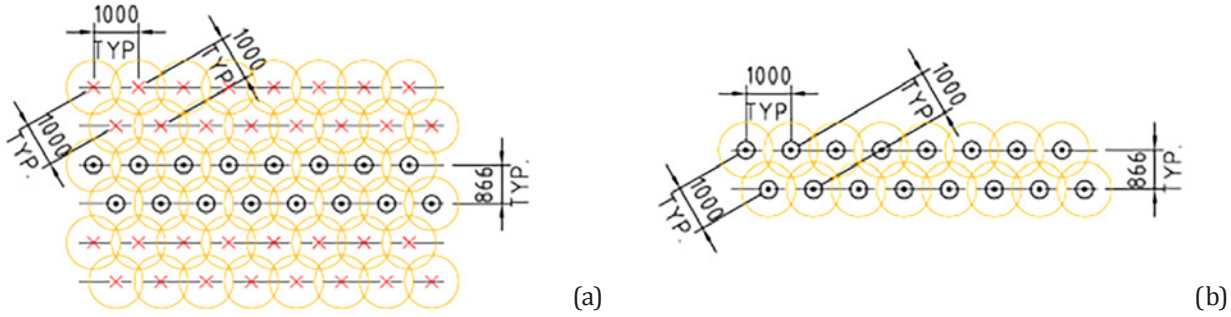

Figure 5: Grout Holes pattern used for (a) Grout walls and (b) Grout block (with secondary holes where required)

Ground improvement was implemented by permeation grouting utilising tubes-à-manchettes (TAM) methods. The controlled injection of grout was undertaken in multiple stages for each formation to suit the porosity and permeability of the formation type. Primary grouting was undertaken using bentonite-cement mix followed by micro-fine cement grout for rockfill and by chemical grouting with sodium silicate for CDG and alluviums. Approximately 67,000m length of TAM was installed from up to 2,600 No. injection points, which represents a record in Hong Kong. Grout was introduced by drilling from the launching and the receival shafts to form a fan-shaped layout, so ensuring that ground improvement covered the entire area underneath the AEL. The ground improvement extended from 5m above the top slabs of the boxes to 2m below the boxes base slab soffit or to the rock head level, whichever was higher. Automatic drilling parameter recorders were deployed which mapped the treatment and selected the most appropriate grout mix, which was then prepared in an automated mixing plant. The automatic data measuring system was used to locate weak clay zones, which were then strengthened by chemical grouting to prevent potential settlement and disruption of the AEL. The automatic grouting recorders monitored the effectiveness of the ground treatment throughout the injection works. This allowed tracking of the grout take and the grout pressure termination criteria for the different materials. Upon completion of the grouting, vertical and inclined verification holes were drilled across the treated zone to enable pressuremeter and permeability tests to be carried out at each drillhole location.

Table 2 presents the target improved ground properties of each formation that were adopted at the design stage. The ground improvement works, utilising approximately 17,000m3 of injected grout, enhanced the in-situ properties not only of the rock fill, the alluvium sands and the CDG but also the clay formation. Figure 6b shows representative ground conditions on the excavation face that were encountered during the jacking works of T002 with uniformly grouted non-cohesive formations. This shows where chemical grout penetrated the clayey formation, despite original expectations that the clay formations maybe “untreatable” without fracturing methods being adopted. In order to address approval authorities’ requirements for increased safety in relation to the AEL operations, additional measures (see Section 3 below) were undertaken in order to further enhance the stability and the stiffness of the grout block.

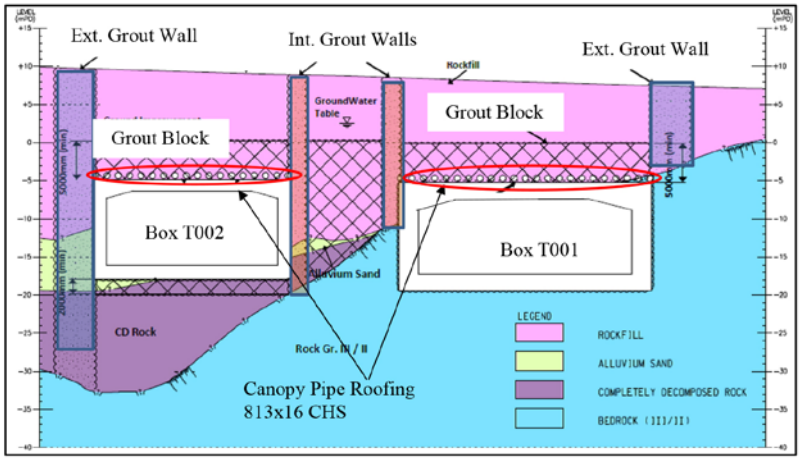

Figure 6: (a) Geotechnical Cross Section of T001 & T002 Tunnels

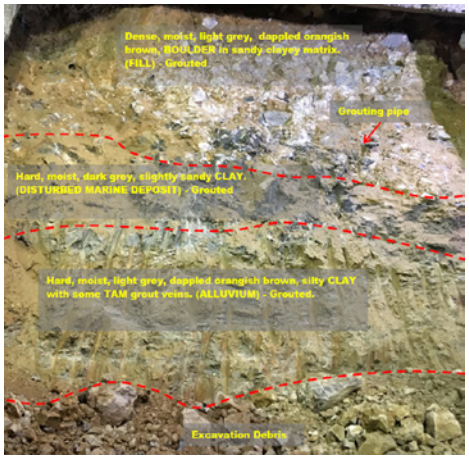

(b) Grouted Ground Formations During The Excavation Works For T002

Table 2: Target Ground Properties After Ground Improvement Works

Soil Material	Unit Weight (kN/m^3)	c' (kPa)	φ' (deg.)	E' (MPa)	v'
Grouted Rock Fill	22	100	40	150	0.3
Grouted Alluvium Sand	22	70	33	50	0.3
Grouted CDG	22	60	35	75	0.3

3 EXCAVATION WORKS AND STABILITY

An open face shield was adopted for the boxes after taking into consideration the improved ground conditions expected after the completion of ground improvement and the dewatering. The excavation face was retained at 70° to the horizontal and advanced 1.0m ahead of the leading segment without the shield being pushed into the ground (Figure 12). The sloping nose of the leading segment was constructed of reinforced concrete including embedded couplers to allow future stitching to the adjacent cut & cover sections. A 500mm long steel hood was mounted in front of the box shield to enhance safety for the site personnel and equipment during the excavation works, whilst improving excavation access.

As noted above the excavation roof face of each tunnel was protected from collapsing and from excessive deformations by pipe canopy roofing, comprising 44 No. 813mm diameter steel tubes, 16mm thick, spaced at 950mm centres, which were grout infilled after installation (see Figures 7 and 8). The target clearance between the canopy tubes and the box roof slabs was 75mm to allow for construction tolerances during the canopy installation. However, during the box jacking, shoes were attached to the canopy tubes at regular centres that allowed only 10mm clearance between the shoe and the roof slab to control the amount of settlement at the ground surface. The steel tubes spanned the gap between the front of the box and the ground mass and skidded on top of the box as it moved forward. The friction along the sliding interface above the boxes generated horizontal forces in the canopy, which were resisted by a steel frame in the west receiving shaft and initially by the friction under the canopy remote from the boxes. Thus the canopy served as an anti-drag system (ADS) isolating the jacked box from the embankment above, preventing the embankment being displaced laterally.

The target physical gap (overcut) between the excavated ground and the tunnel walls as well as the tunnel bottom slab was 75mm, but was in practice over 100mm where rockfill was excavated. The overcut at the base slab excavation face ahead of the leading segment was filled with gravel to prevent the segment dropping.

The excavation stability analysis was carried out on geotechnical design sections that addressed the most adverse stability criteria where maximum overburden pressures combined with critical ground profiles (e.g. localized clayey material layers). Face stability analysis adopted a minimum global factor of safety (FoS) equal to 1.4 in line with the Hong Kong GEO Manual for Slopes (1984) requirements

Figure 7(a): Installed Canopies from Launch Shaft to Receival Shaft

(b): Canopy Tubes Supported By Tunnel Box

Figure 8: Breakthrough of Canopy Tube with Bohrtec Front Steer System

where high risk to life as well as high economic risks occur. Additional stability analysis checks were also undertaken by adopting partial safety factors in line with HK GEO Rep. 298 (2014). Analysis was carried out using both finite element methods (FEM) by PLAXIS as well as using Morgenstern-Price limit equilibrium methods (LEM) by SLOPE/W.

Initially 2D FEM soil-structure interaction analysis (SSIA) was undertaken, replicating the staged excavation process assuming 1m excavation ahead of the tunnel box face, taking into account the beneficial action of the canopy tubes. The SSIA modelled the redistribution, at each excavation stage, of the overburden pressures above the unsupported length of the canopy (Figure 11). Face stability was assessed using a shear strength reduction procedure. A conventional LEM analysis produced comparable results taking into account the canopy roofing as a horizontal restraint equivalent to the friction along the interface between the canopy and the underlying ground ahead of the excavation. Considering both global FoS and partial factor methods enabled a sensitivity check to be carried out, which gave comfort that the excavation works underneath the AEL could be safely executed. Nevertheless the FEM analysis was recognised as the more realistic method, as controlling parameters such as the ground stress-strain relationship, soil structure interaction and soil arching were able to be modelled. Finally, an additional 3-D Plaxis analysis was undertaken to assess the stability of the vertical excavation side walls and provide final verification of the 2-D assessments. This 3-D analysis allowed consideration of the side face arching effects, where steel pipe reinforced grout curtains had been provided to enable side excavation stability.

As discussed in the previous section, clayey formations were anticipated during the excavation works. The stability of these formations during the excavation works was considered a primary concern. For robustness the following additional measures were implemented ahead of the excavation works in clay zones:

A. Installation of drainage holes through the clay formations to ensure pore-water dissipation within the clay mass - Piezometers were installed at various locations and depths within the clay formation to measure pore pressure development with time. Additional stability analyses were then undertaken adopting the measured pore-water pressure profiles to further demonstrate stability during excavation.

B. GFRP soil nails installation - At particular clay formation locations to enhance stability and limit ground movements.

4 JACKING METHODOLOGY

4.1 General

The approximately 26m deep launch shaft housed all of the equipment needed to jack the boxes forward beneath the AEL and provided the casting area for the segments (Figure 9). The planning of the jacking works was done in coordination with all other planned construction activities (e.g. excavation and lateral support) to ensure that there would be no clashes when components were lifted by crane in and out of the shafts.

The jacking process consisted of two main jacking operations:-

A. The 'Pull System' with strand jacks located in trenches below the jacking slab at the rear of the box;

B. The 'Push System' with solid ram jacks located between the bottom slab and the lower part of the walls of two adjacent box segments.

Effectively, the segments were jacked horizontally into the ground in a continuous cyclical caterpillar motion.

4.2 Jacking Slab

The jacking slab provided the reaction restraint required to enable the pushing of the box sections forward as well as to provide alignment guides. Tunnel boxes T001 and T002 were jacked along a horizontal and straight plane. The slab extended to the faces of the launch shaft walls enclosing the excavation (Figure 9). However, this slab was structurally isolated with movement joints around its perimeter, separating the jacking slab structure from the cofferdam's excavation and lateral support (ELS) system.

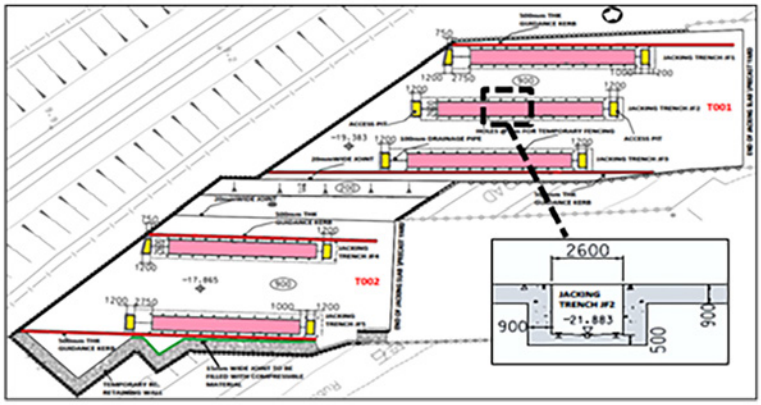

Figure 9: Jacking Slab - General Layout

Figure 10: Tunnel Excavation

To enable the 'Pull System', 3 No. trenches for T001 and 2 No. trenches for T002 were constructed below the jacking slab's top level with nominal dimensions of 2.5m deep by 2.6m wide (Figure 17). Each trench was designed to house two rows of three strand jacks. The strands were anchored at both ends of the trench in specially designed reinforced concrete anchor blocks. For the purposes of installation and maintenance of the strand jacking system, access pits were provided behind each anchor block. The front anchor block (i.e. adjacent to the headwall) transferred the load from the jacking strands into the sidewalls of the jacking trench, and subsequently into the jacking slab and finally into the ground. The jacking slab and the jacking trenches were constructed so as to interlock directly into the grade III granite rock, with no blinding layer in between. The mechanical interlock/bond or friction between the

concrete jacking slab and the granite rock provided the required restraint to resist the applied jacking loads from the anchor blocks.

Concrete alignment guide kerbs were cast on top of the slab on each side of the box segments to constrain the box segments within a small lateral positional tolerance during the trench jacking operations. This tolerance distance allowed sufficient space to accommodate the construction tolerances needed as the boxes moved along the jacking slab. In order for the guide kerbs to perform their function, it was important that the line of the kerbs were set out to a high degree of accuracy. The kerbs were as small as practicable to minimise access issues, but still provided sufficient capacity to resist any unforeseen out of balance shear and torsional earth loads which occurred prior to full embedment of the segment into the embankment. A vertical steel plate bearing runner was fixed to the inner face of the guide kerbs and to a horizontal strip of jacking slab surface adjacent to the kerb, to prevent concrete spalling during the jacking operations. The kerbs extended from the back of the box casting positions to the jacking slab edge at the interface with the steel pipe pile headwall.

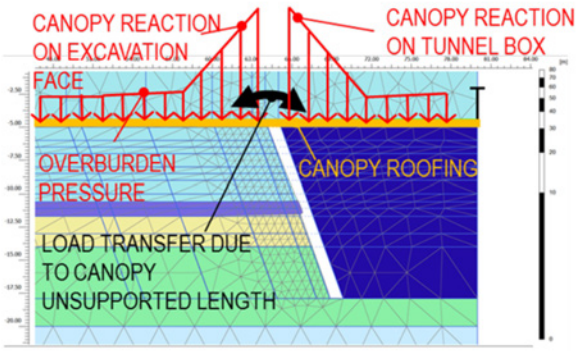

Figure 11: FEM Excavation Analysis (Load Redistribution)

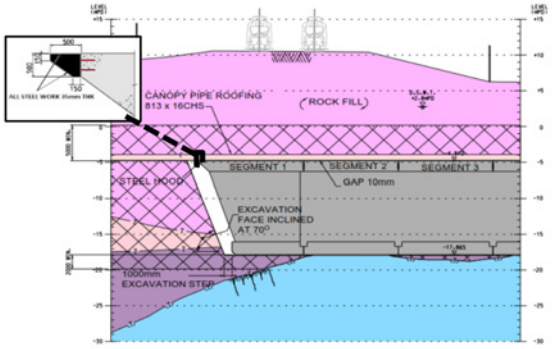

Figure 12: Longitudinal Ground Profile of T002

4.3 Pull Jacking System

The pull jacking system was the first to operate to enable the box jacking works. The pull system applied a load to the base of the box segment, via a re-useable propped cantilever frame at the rear of each segment, which moved the box structure forward. The loads were generated by 800 tonne safe working load VSL strand jacks with 550mm strokes located at the back of each segment in the jacking trenches. The vertical jacking frames were formed from 3 no. lift weight constrained (10 tonnes) fabricated steel box sections and associated steel components (Figure 13, 16 and 17). Prior to the start of the pull system operation the jacking frames were installed at the back of the box segment, and the jacks in the trench were positioned behind the frame.

The jacking frame was detailed as a propped cantilever. The jack loads were applied to the cantilever tip, causing a push-pull effect at the reaction points of the beam (Figure 17). Three rows of stress bars were located at the upper end of the beam. The tension stress bars tied the frame to the box segment walls and the temporary concrete support structure (Figure 17), preventing movement and rotation during the jacking operation. Box T001 required three frames, located at the side walls and centre of the box segment, while box T002 required two frames, located at the side walls only. The pull system operation for each segment was used until the frames reached the end of the jacking trench. At this point they were disassembled and moved to the initial jacking position of the trailing segment, which subsequent segment was advanced using the same procedure.

4.4 Push Jacking System

Once a box segment was jacked to the limit of the jacking trenches, the push jacking system within the intermediate jacking stations (IJS) between segments was utilised to push the unit further inside the AEL embankment. Hydraulic solid ram jacks installed at the interface of the lead two segments in the IJS, were activated to progress the lead box segment forward by a distance equivalent to the stroke length of the jack. The same operation was repeated at the following segment interfaces to close the gap

created as the lead box advances. This process was repeated until the final gap between segments was closed by the pull jack system (which system otherwise acted as a passive restraint at the rear), after which the lead segment was advanced by a further stroke length. The jacks were positioned in recesses formed along the base slab and lower walls of the box segments (Figure 16), located to ensure that the load centre of the applied forces matched the calculated resultant friction force centre. A number of VSL type SPE-1000-200 jacks (1000tonne safe working load each) were required for Box T001 and VSL-SPE-610-75 jacks (600tonne safe jack capacity each) were required for Box T002. Skirt plates across the joints between segments at the rear of each box segment were provided to prevent any ingress of material from the excavation, as the gap between segments opened and closed during the jacking process (Figures 14 and 16). As noted above the resultant pushing force needed to be applied eccentrically in order to offset unbalanced frictions and or to "steer" the box in a particular direction. Therefore, the jacking system required an integrated control and monitoring system to facilitate this. Alignment control of the boxes was enabled by varying the intermediate station jack loads so that the applied jack load resultant centre was offset in the required direction to match the friction restraint force theoretical centre, both horizontally and vertically, until the required alignment trend was observed. Any variation caused in alignment due to unforeseen events was offset by this adjustment to the applied jack load centre to compensate. Thus the boxes were steered within tolerance.

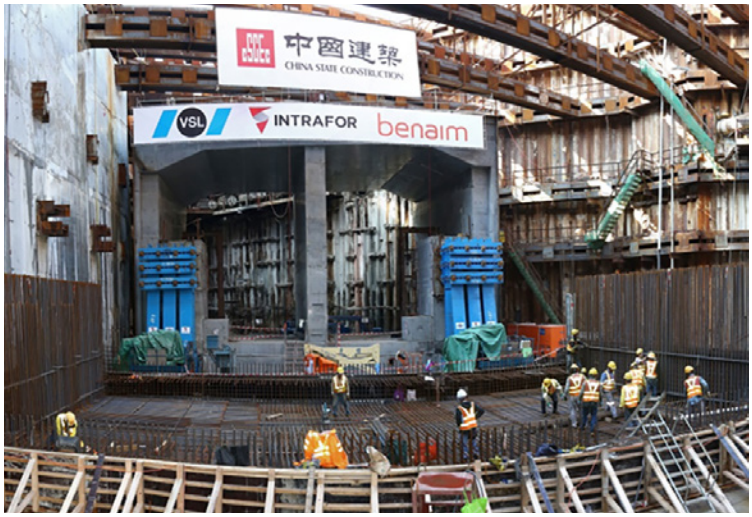

Figure 13: Launching of T002 Leading Segment with Concurrent Construction of Segment 2

Figure 14: Side Wall of T002 Showing Lubrication Channels and Skirt Plates

4.5 Sliding Surface and Lubrication system

In order to minimize the friction and stiction forces on the jacking slab surface, the tunnel segments were precast on greased plywood panels laid on top of the jacking slab.

In addition a lubrication system was designed to 'wet' the outer surfaces of the segments should the soil friction forces rise above the expected jacking forces. To enable this surface cast-in omega channels were provided in the outer walls and top and bottom slab (Figure 14). A bentonite mix was then able to be injected through cast in pipes connected to these surface omega channels, lubricating the contact surfaces between the segments and ground. The lubricating system was a proven method used previously by the parties on the Airport Link Toombul Box Jacking project in Australia. Finally the same injection system pipes and omega channels were used for grouting to stabilise the box in its final position, by filling the surrounding voids.

4.6 Determination of Jacking Load Requirements

The required total jacking force to overcome the friction between the tunnel box and the surrounding interfaces was estimated by carrying out a sensitivity study using upper and lower bounds for the materials present, allowing for with and without the provision of the bentonite lubrication system

that was intended to reduce the friction during jacking. With the adopted approach the expected 'serviceability' friction forces were estimated allowing for a lubrication reduction factor. The design jacking force (see Table 3) was then calculated applying a safety factor to the friction to allow for unforeseen variations, this was then compared with worst case ultimate expectations. The adopted friction coefficients for the interface between ground/tubes and concrete were selected by reference to the Hong Kong GEOGUIDE No.1 (1993), and considered all the different ground strata internal angles of friction (φ')/adhesion values anticipated to be encountered during jacking.

The provided total jacking capacity was significantly higher than the design friction forces to allow for unforeseen geotechnical variations and out of balance forces due to the box skew geometry. In practice, even when ignoring the lubrication, the provided jacking capacity was set above the factored serviceability friction forces and the un-factored ultimate worst case estimate without lubrication to ensure robustness, and to provide margin to ensure the boxes did not become stuck during installation.

Table 3: Estimated Friction Force

Box	Design Friction Force (max FF) [ton]	Strand Jacks [No.]	Ram Jacks [No.]	Total Safe Working Load (SWL) [ton]	SWL/(max FF)
T001 (Pull Jacking System)	8,700	18		14,400	1.65
T001 (Push Jacking System)	19,400		24	24,000	1.25
T002 (Pull Jacking System)	5,900	12		9,600	1.62
T002 (Push Jacking System)	13,100		28	16,800	1.28

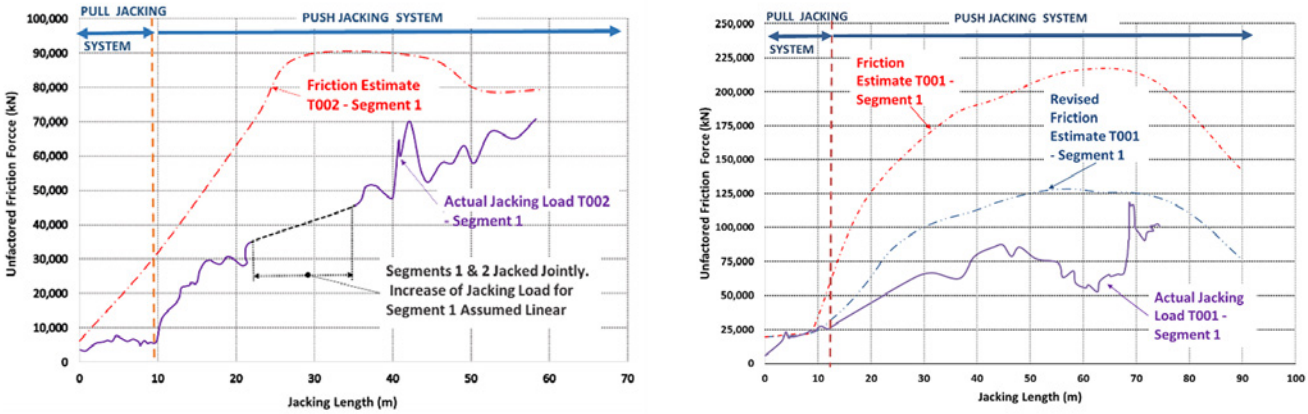

(a) (b)

Figure 15: (a) T002 Segment 1 Original Upper bound Design Friction vs Actual Jacking Load and (b) T001 Segment 1 Original Upper bound Design Friction vs Lower bound Design Friction (adopted after T002 back analysis).

Box T002 was jacked ahead of T001. The monitoring data from the T002 observed jacking loads (Figure 15a) was then used in a back analysis to derive the actual friction developed. The T002 back analysis considered several parameters (including side soil pressures and 3D effects of load distribution) to derive revised strata unit area pressures. These back-analysis results, adjusted for strata and geometry differences, were then used to estimate the most likely jacking load requirements for the installation of the T001 box. A review of these results showed they were similar to the lower bound friction forces originally estimated, so these latter were subsequently adopted for the T002 jack provisions. Figure 15b presents a comparison graph between the T001 lead segment S1 originally estimated upper bound friction force versus the revised T001 S1 lower bound friction forces and shows the actual jacking load measured on site. As can be seen in Figure 15b, the actual jacking loads for the T001 segment were found to be in reasonable agreement with the lower bound predictions.

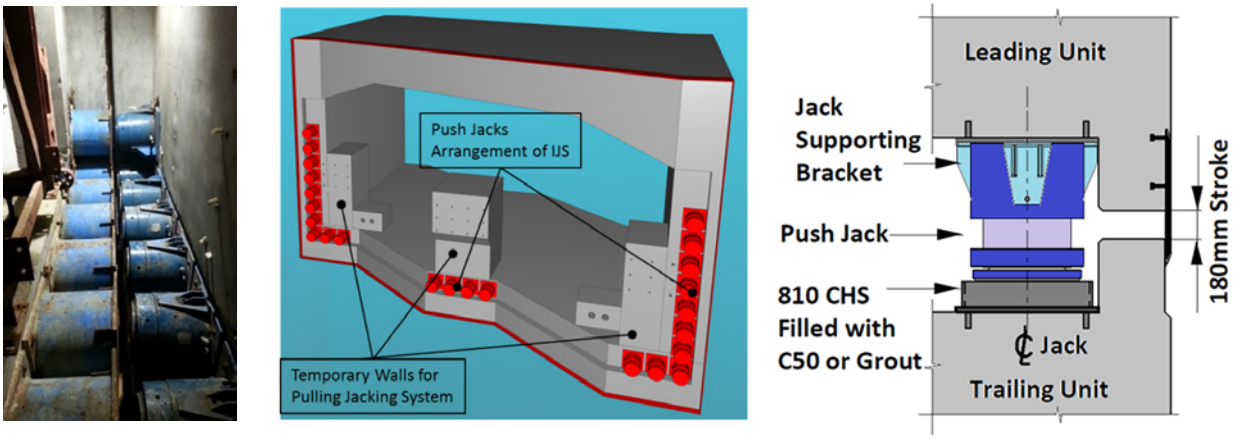

Figure 16: Intermediate Jacking Stations (IJS) with VSL Solid Ram Jacks of up to 1000 ton Safe Working Load

The design load path during jacking was critically reviewed at each generically different position with the emphasis being put on the out of balance friction forces and side pressures that were anticipated to develop due to the box skew. Due to geometrical constraints, each segment while being jacked from the launching shaft, was partially embedded in the ground, with the north wall being almost fully engaged, and the south wall not yet having entered the embankment. Consequently, the resultant friction restraint force was significantly eccentric to the box centreline both horizontally and vertically. Due to this eccentricity, the required jacking force varied between the trenches of each box. Effectively, the segments were jacked primarily by the north and the central jacking trench for T001 and concurrently were "steered" by the south jacking trench. This caused the position of the resultant jacking load centre to coincide with the actual resultant friction force centre, to ensure racking loads did not develop. Notwithstanding that the guide kerbs prevented the segments from deviating from their original position, counterbalancing the out of balance friction forces developed during jacking by varying the applied jacking forces in real-time was expected to be a challenge. This was overcome by the use of a linked hydraulic jack computerised system that allowed the boxes to be 'steered' as alignment monitoring required.

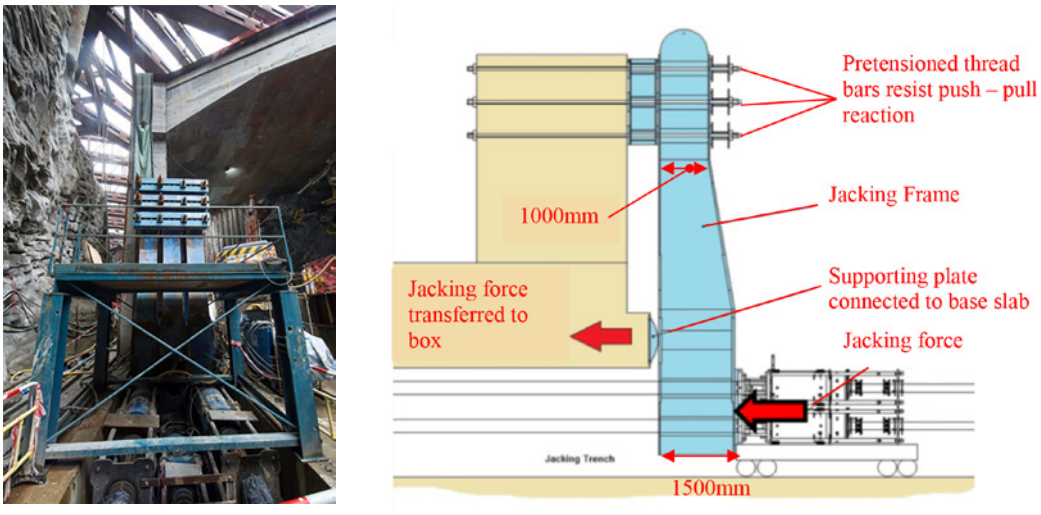

Figure 17: Typical Trench Details with Pull Jacking System Showing 5No. x 800 tonne VSL Strand Jacks.

5 CONCLUSIONS

The Scenic Hill jacked box tunnel section is the first to be built in Hong Kong using jacked box tunnelling techniques. The state of the art ground treatment carried out by Intrafor under the AEL to stabilize and improve the ground properties, and the directional steel pipe installation to form a protective canopy roof, were paramount to ensure that the box jacking works of the two tunnels were carried out safely,

without causing any disruption to the operating Airport Express Line railway. The latter concern being one of the key aspects which led to the adoption of the box jacking method. The skew tunnels were jacked into the ground in segments in a cyclical caterpillar motion, with the use at the outset of a rear mounted pull strand jacking system and subsequently a push jacking system located between the segments at intermediate jacking stations. The construction planning and detailed design particularly addressed the unusual skew spatial constraints of the site. The high overburden pressures resulted in high friction forces and consequently required consideration of high jack loads on the segments. The robust design and the coherent planning of the works ensured that the installation of the T001 and T002 tunnel boxes, were successfully completed within tolerance in May 2017, and as noted above, without having had any effect on the regular operations of the Airport Express Line.

ACKNOWLEDGEMENTS

The authors wish to acknowledge the contribution and support of the project teams shown in Figure 2.

REFERENCES

GEO, 2014. GEO Report No. 298. Ground Control for EPB TBM Tunnelling, HKIE Geotechnical Division Working Group on Cavern and Tunnel Engineering and Geotechnical Engineering Office, Civil Engineering Department, The Government of the HKSAR, Government Publication Centre.

GEO, 1984. Geotechnical Manual for Slopes. Geotechnical Engineering Office, Civil Engineering Department, The Government of the HKSAR, Government Publication Centre.

GEO, 1993. GEOGUIDE 1 – Guide to Retaining Wall Design. Geotechnical Engineering Office, Civil Engineering Department, The Government of the HKSAR, Government Publication Centre.

Rock Condition Evaluation Using Tunnel MWD Data

S. Gao
GEOECO Consultants

K.Y. Chow
CRBC-CEC-KADEN JV

ABSTRACT

Underground drilling rigs are equipped with MWD (Measurements While Drilling) system for monitoring the drilling performance, drilling parameters such as position, drilling rate, thrust force, torque, rotation speed, percussion energy, water feed rate and water feed pressure are logged in centimeter intervals. Parameters such as the penetration rate are mainly mechanical responses to the materials drilled and hence can be correlated with the geological conditions of the drilled areas. Due to the extensive coverage and relative low cost of the MWD data, inferring rock conditions from MWD data could be a supplementary source for underground constructions.

In this paper, an analysis is conducted on a set of MWD data collected from 125 probing holes of a tunnel (which is being under construction at the moment of writing) in Hong Kong. The objective is to validate and explore the possibility of evaluating the weak rock zone using MWD data. The data processing results and the statistical characteristics of MWD data are described, and an interpolation using the MWD data has been conducted. Comparing the site geological records with the interpolation results, it is found that the MWD data can provide a good indication about the weak rock zones in this project and should have a potential to be used in future construction processes.

1 INTRODUCTION

Drill-and-blast and TBM are common means for tunnel driving. Computerized jumbo is extensively used for drill-and-blast tunnel excavation, the drilling positioning, alignment and depth can be accurately adjusted and the drilling cycle can be manually or automatically operated. The jumbo is equipped with MWD system where drilling data are collected in centimeter level. The MWD data is initially recorded for monitoring the efficiency of the drilling process. As the MWD data such as the penetration rates are mainly mechanical responses to material drilled and can be correlated with the geological conditions of the drilled areas, the MWD data have also been applied to evaluate the rock conditions for tunneling and other geotechnical projects.

In HK context, a DPM (Drilling Processing Monitoring) system for charactering the ground conditions has been developed to estimate rock strength, RQD (Rock Quality Designation), rock mass integrity, rock hardness and discontinuities (Tan et al. 2006; Yue, 2014). Lam et al. (2006) conducted an evaluation on the DPM technique and concluded that "apart from ground condition, penetration rate, being the most important parameter for characterisation of ground condition, also depends on other factors including state and construction of drilling equipment, operator skill, groundwater regime and nail length. Penetration rate from the DPM system/technique at its present state has good potential for crude qualitative assessment of the ground intercepts, especially for inferring rock". Barmuta et al.

(2012) reported an effort on detecting faults encountered in the HATS 2A project using MWD data and summarized the following advantages of applying interpretative probing:

1) Eliminating safety hazards related to presence of geologist at drilling location;
2) Obtaining results reliable and superior or equivalent to visual logging;
3) Often eliminating a need of probing as additional activity in the production cycle (grout holes or other technical holes can be used as probes);
4) Easiness to produce various graphic reports.

2 TUNNEL MWD DATA

2.1 Percussion Rotary Drilling

In the drill-and-blast excavation drillings are conducted for various purposes as follows:

1) Probing for information collection
2) Installing temporary support such as rock doweling
3) Loading of explosives
4) Grouting

The commonly used drilling method in the drill-and-blast excavation is the hydraulic percussion-rotation drilling. A typical percussion-rotation drilling sketch (Jimeno et al. 1995) is presented in Figure 1 and the key components are summarized as follows (Zhou, 2017):

1) *Percussion:* To strike the tail end of the rod or bit itself and generate shock wave that are transmitted to the bit, generated stress concentrate at bit tooth and crush rock;
2) *Rotation:* To rotate the rod or hammer so the bit is turned and produce impact on rock in different positions;
3) *Feed force:* To keep the shank in contact with the drill and the drill bit in contact with the rock, so the maximum impact energy is transferred from the piston to rock;
4) *Flushing:* To remove the drilling cuttings from the hole, cooling drill bits, keeping the drill hole wet and reduce abrasions.

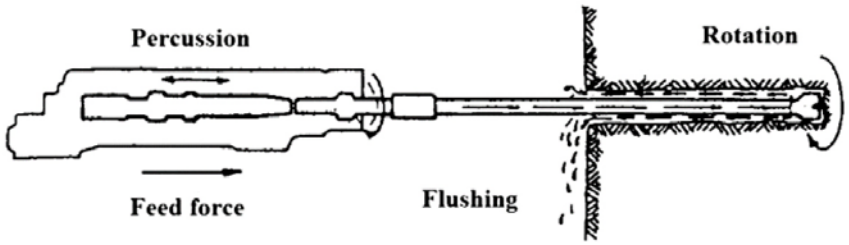

Figure 1: Percussion rotary drilling (Jimeno et al. 1995)

2.2 MWD Data

The drilling parameters such as percussion pressure, rotation pressure, feed pressure, flushing pressure, rotation speed and penetration rate etc. are recorded in a small scale (normally in centimeter scale) by the MWD system. The MWD parameters can be categorized into two groups: independent

parameters and dependent parameters (Peck 1989). The independent parameters are controlled by the drilling operator or the drilling system, and the dependent parameters are the responses to the changes of the rock mass properties and control parameters. In general, the variation range of the dependent parameters is larger comparing to the independent parameters. The parameters commonly used are shown in Table 1.

Table 1: Parameters of MWD data (Peck 1989)

Independent Parameters	Dependent Parameters
Depth	
Time	Penetration Rate
Feed Force	Torque
Rotation Speed	Vibration
Air Pressure	

It needs to note Peck's study was based on data from the rotary drilling of blast holes. Similar assumptions were also adopted by Schunnesson (1997) for percussion rotary drilling, where penetration and rotation pressures were assumed as dependable variable while the rock resistance, hammer pressure, feed pressure and drilling length were treated as independent variables. Meanwhile, drilling controlled by torque has also been observed especially for holes with a short length. The categorization of MWD data should be conducted on a case by case basis.

3 PROJECT INTRODUCTION

3.1 Project Background

The tunnel is a dual two-lane tunnel. The lengths are approximately 744m and 751m for the northbound and southbound tunnel respectively. The maximum excavated span is approximately 15m. The tunnel is within a moderately to slightly decomposed tuff rock mass. Documents show the site is adjacent to a major fault zone in Hong Kong.

MWD data of 125 probing holes from 38 rock face in major portion of the tunnel were collected at various locations for this paper. The locations of these probing holes are presented in Figure 2.

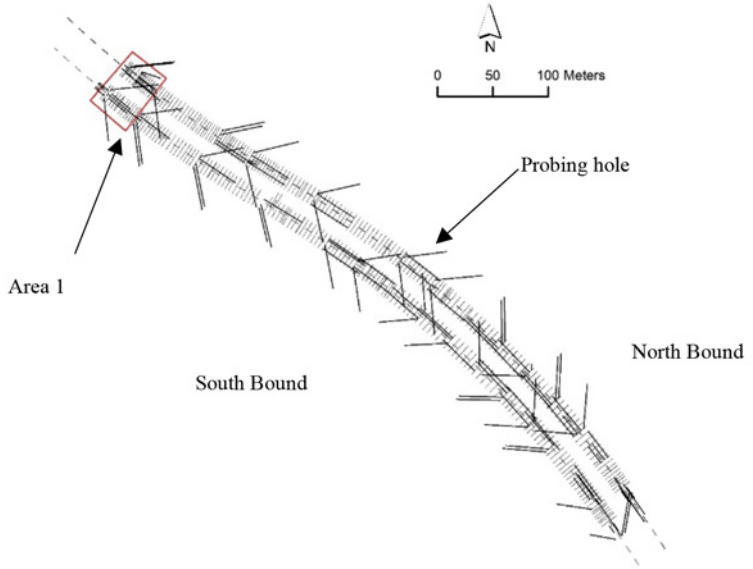

Figure 2: Locations of Probing holes

3.2 Data Filtering

It is unavoidable that noisy data are recorded in the original MWD data. The noisy data are generated by activities such as extension of drilling rods, removing clogging, etc., and should be filtered before further processing to be conducted. Commonly used outliner removing methods includes visual inspection, threshold value and probability method. The visual inspection method may be more reliable but cannot be adopted when the amount of processed data is large. The threshold value method is the most straightforward method and has been used in many projects (Barmuta et al. 2012; Oosterhout 2016). The difficulty for adopting this method lies on choosing the significant threshold values. In probability method the data are checked based on the dataset statistical characteristics. For instance, in the MWD study for the Aitik mine located in the northern part of Sweden, a frequency analysis of the feed force, rotation speed, rotation torque and air pressure has been conducted, the cut off limits were defined as the 99.99% of empirical distribution functions and the values above those limits were filtered out (Ghosh et al. 2015).

In this study, the probability method was adopted and the outliners of the original MWD data were filtered by boxplot measures. Figure 3 refers a schema showing the boxplot components (Ferreira et al, 2016). The outliners are defined as data outside the upper and lower fences. The major advantage of using the boxplot to define the outliner is no distribution assumption required. The abnormal data is defined only based on quantile value and interquartile distance.

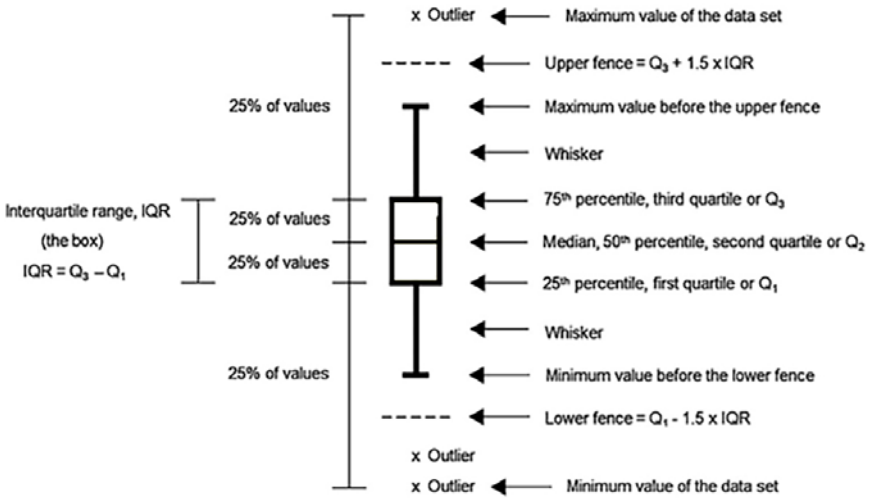

Figure 3: The boxplot components (Ferreira et al. 2016)

The MWD data were recorded at every 2 centimeter drilling depth in this project. For each individual hole, the upper fences and lower fences (Fig.3) were calculated for the recorded penetration rate, feed pressure, flush flow, flush pressure, percussion pressure and rotation pressure respectively. Then the recorded data were further compared with the corresponding fence values and once an outliner were detected, the data for this drilling depth would be all removed from the dataset.

Figure 4 shows the original pressure data and the filtered results for a probing hole at chainage 490.5 of north bound tunnel (NB490.5_2). The major spikes have been removed as shown in Figure 4. There are still some unfiltered data especially for the rotation pressure because the rotation pressure is a dependent parameter and has higher variation. However, in view of the sizes of whole dataset and unfiltered data, the effect of the unfiltered data is considered insignificant.

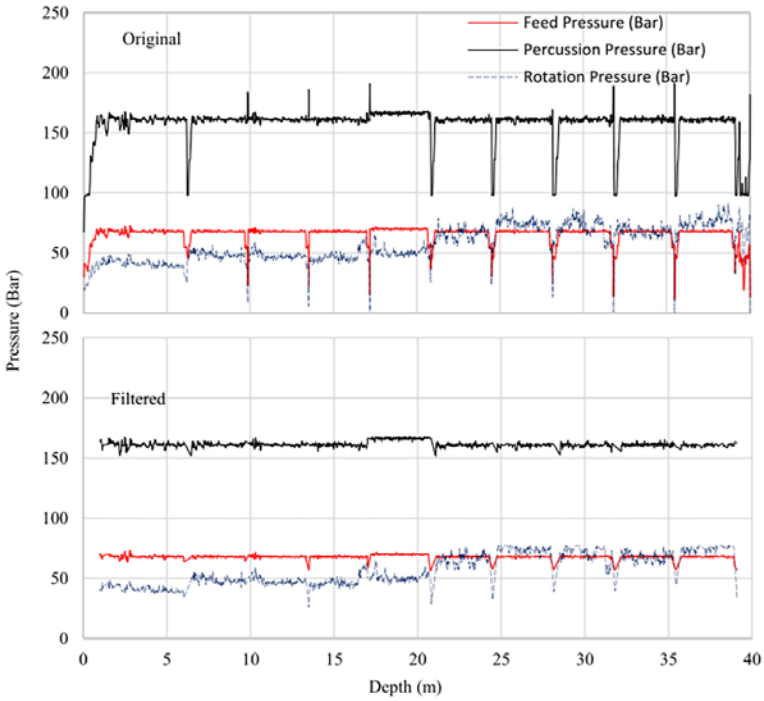

Figure4: Comparison of the original MWD data and filtered results (Hole NB490.5_2)

4 STATISTICAL STUDY OF MWD DATA

4.1 Statistical Characteristics

The MWD data after filtering includes 112,397 spatial datasets for 125 probing holes and there is a specific location and a group of corresponding parameters in each dataset. Figure 5 presents the histograms of the MWD data. For easy comparison, the MWD data has been standardized in a range of 0 to 1. The upper part of Figure 5 shows the histograms for feed pressure, percussion pressure and rotation speed, those histograms show less spread and more than 75% of the data are concentrated in a small range (0.5-0.6 for feed pressure, 0.75-0.85 for percussion pressure, 0.65-0.7 for rotation speed), those parameters are independent parameters mainly changed by the operators. On the other hand, the other parameters on the lower part of Figure 5 show a less concentration and large spread, representing the characteristics of dependent parameters.

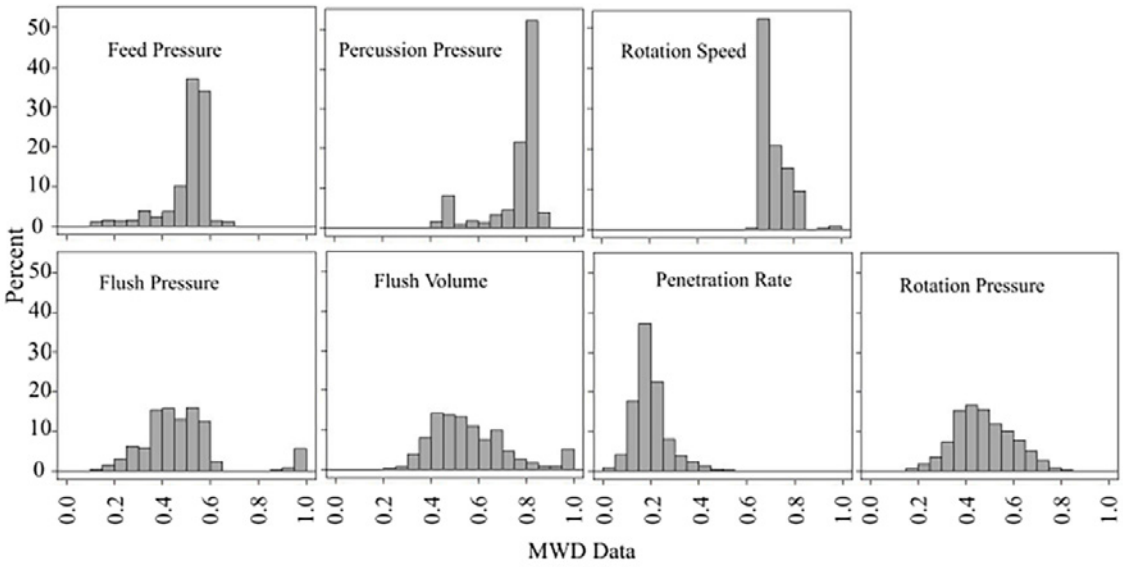

Figure 5: Histogram of MWD data (Total data number 112,397)

4.2 Feed Pressure vs. Percussion Pressure

In practice, the percussion is not totally independent with the feed. In a study on the drilling system behavior for hydraulic in-the-hole (ITH) drilling, Ghosh et al. (2017) summarized that "in modern drilling systems, there is often a correlation between percussion pressure and feed pressure, even though the parameters are independent and are controlled by the rig control system. If feed pressure is reduced, it is important to control the percussion pressure to prevent damage to the drill system". Similar observation was also addressed by Lam et al. (2006) that "for smooth and effective drilling, the thrust needs to be adjusted to suit the percussion pressure, and generally a high percussion pressure requires a high feed pressure and vice versa".

The correlations between feed pressure with percussion pressure were analyzed and the results are presented in Figure 6 below. A scatterplot of the 112,397 pair of data was produced and a correlation between the feed and percussion pressure can be found in the scatter plot, the calculated correlation coefficient of the 112,397 pair of data is 0.8. The correlation coefficient between the feed and percussion pressure were also calculated for each individual probing hole, and the histogram of the correlation coefficients for 125 probing holes is also shown in Figure 6.

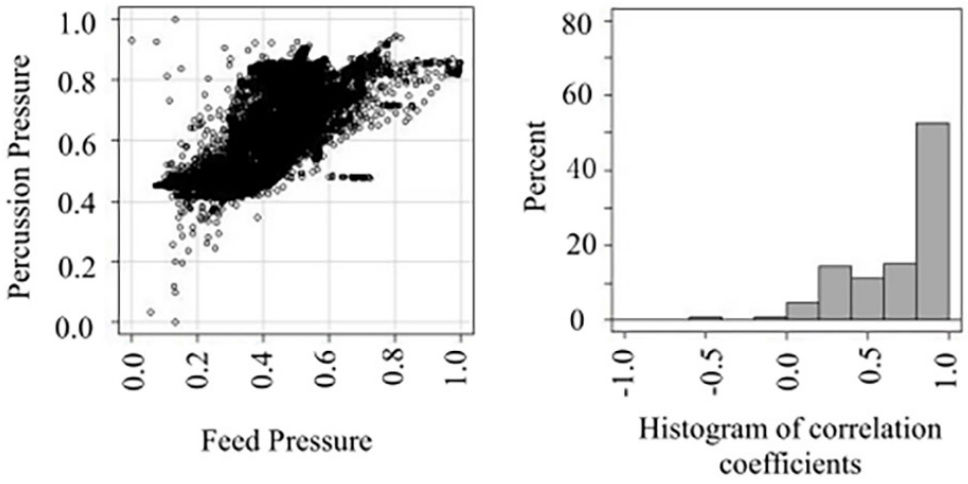

Figure 6: Correlation between feed pressure and percussion pressure

4.3 Adjusted Penetration Rate (APR)

The penetration rate is a dependent parameter and affected by many factors (Lam et al. 2006). To compare data from different drilling holes and evaluate the rock conditions, the major affecting factors other than the rock conditions must be identified and removed. It is rational to assume that if the working parameters were controlled to be constant, the penetration rate will reflect the rock hardness (Zhou et al. 2012). Several adjustment methods have been reported (Zhou et al. 2012, Barmuta et al. 2012, Leung et al. 2015, Junhyeok, 2016) and the method proposed by Junhyeok (2016) was adopted in this study, the APR is defined using following equation:

$$APR = \frac{PR_{obs}}{\frac{FP_{obs}}{FP_{ref}}\sqrt{\frac{RS_{ref}}{RS_{obs}}}} \quad (1)$$

where APR = adjusted penetration rate, PR_{obs} = observed penetration rate
FP_{obs} = oberserved feed pressure, RS_{obs} = observed rotation speed,
FP_{ref} = reference feed pressure, RS_{ref} = refernce roataion speed.

The APR value in equation 1 depends on the reference values chosen and should be treated as a relative index reflecting the variation of rock conditions. Meanwhile, equation 1 is developed for rotary drilling, cautions need to be executed for adopting this method in the percussion-rotatory drilling process. The applicability for tunnel MWD data from percussion rotary drilling should be evaluated before the method is adopted. As there exists a correlation between the percussion pressure with feed pressure in this study (ref. Fig. 6), it is rational to assume that when the effect of the variation of feed pressures is removed by applying equation 1, the majority of effect of the variation of percussion pressure also can be removed.

The adjusted penetration rate can be calculated using equation 1. The reference feed pressure and rotation speed is set as 50 bar and 200 RPM respectively. A comparison of the correlations between the penetration rate with the independent parameters before and after the adjustment has been conducted as following:

1) For each individual probing hole, the correlation coefficients between the *overserved penetration rate* and independent parameters (Feed pressure, Percussion pressure and Rotation speed) were calculated.
2) The histograms of the correlation coefficients from the 125 probing holes were calculated respectively and presented on the upper part of Figure 7.
3) For each individual probing hole, the correlation coefficients between the *adjusted penetration rate* and independent parameters (Feed pressure, Percussion pressure and Rotation speed) were calculated.
4) The histograms of the correlation coefficients from the 125 probing holes were calculated respectively and presented on the lower part of Figure 7.

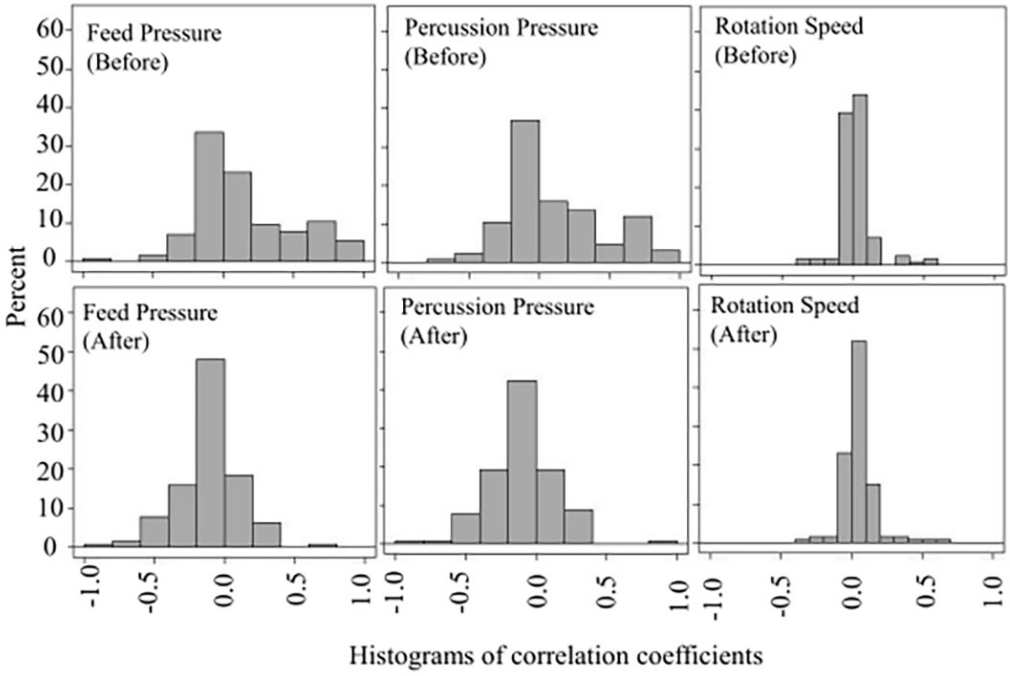

Figure 7: Change of correlation coefficients after the adjustment

As shown in Figure 7, the observed penetration rate is slightly affected with the feed pressure and percussion pressure. However, the existing correlations have been reduced and the histograms of the correlation coefficients are symmetrical around 0 after the adjustment. The results validate the previous assumption that the effect of percussion pressure variation can be removed if the percussion pressure were correlated with the feed pressure, and hence support the application of equation 1 in this study.

5 APPLICATION OF MWD DATA

A detailed study about the APR in a specific area was conducted. This area located at north portal of the tunnel as shown in Area 1 of Figure 2. Total 26 probing holes are inside the area. The APR data in the 26 probing holes were reduced from original 0.02m to 0.5m interval by calculating the moving averages. A 3D interpolation was conducted using Invers Distance Method (IDW) to estimate the APR values in the study domain. The search radius of IDW was set to 6m and the minimum data number for IDW was set to 3.

The interpolated dataset has a mean of 1.52 with a standard deviation (σ) of 0.31. 4 areas with concentration of higher APR values (Mean+1 σ) are presented in Figure 8, and these areas were inferred as weak rock zones. A 3D view of the 4 weak zone from View A (Ref. Fig. 8) is shown in Figure 9. Detailed information about the 4 weak zones is summarized in Table 2 below and the tunnel crown is around 40 mPD.

Table 2: Summary table of weak rock areas

Zone	Plan location	Mean APR of individual zone	Minimum elevation of individual zone (mPD)
A	Ch751-766	2.23	30
B	Ch738-749	2.04	46
C	Ch738-744	1.88	49
D	CH759-764	1.90	35

From the configuration of the 4 weak zones it can be inferred that there may exist a sub-horizontal weak layer (weathered zone) gently dipping towards north-west direction. The weak layer intersects the southbound tunnel at area A and northbound tunnel at area D respectively. In site mapping reports, a zone comprising moderately decomposed tuff with brownish weathered joint infill has been recorded in the study area. Plate 1 shows the rock face conditions at the 4 weak zones, where the weak layer (weathered zone) can be observed especially for the southbound tunnel.

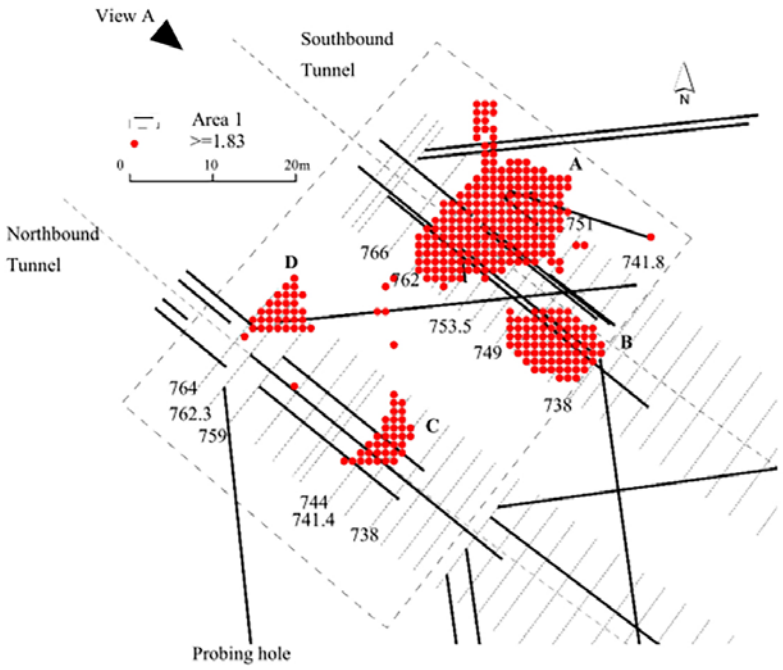

Figure 8: Plan view of 4 weak rock zones

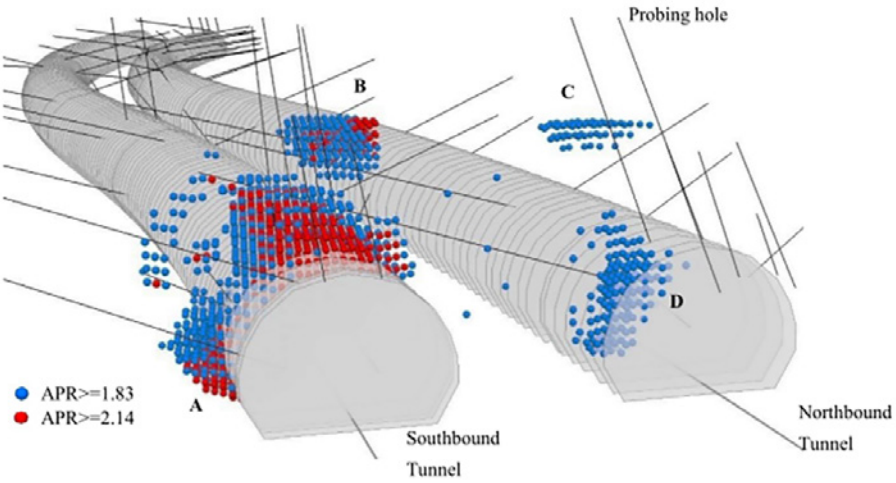

Figure 9: 3D view of 4 weak rock zones (Ref. View A in Fig. 8)

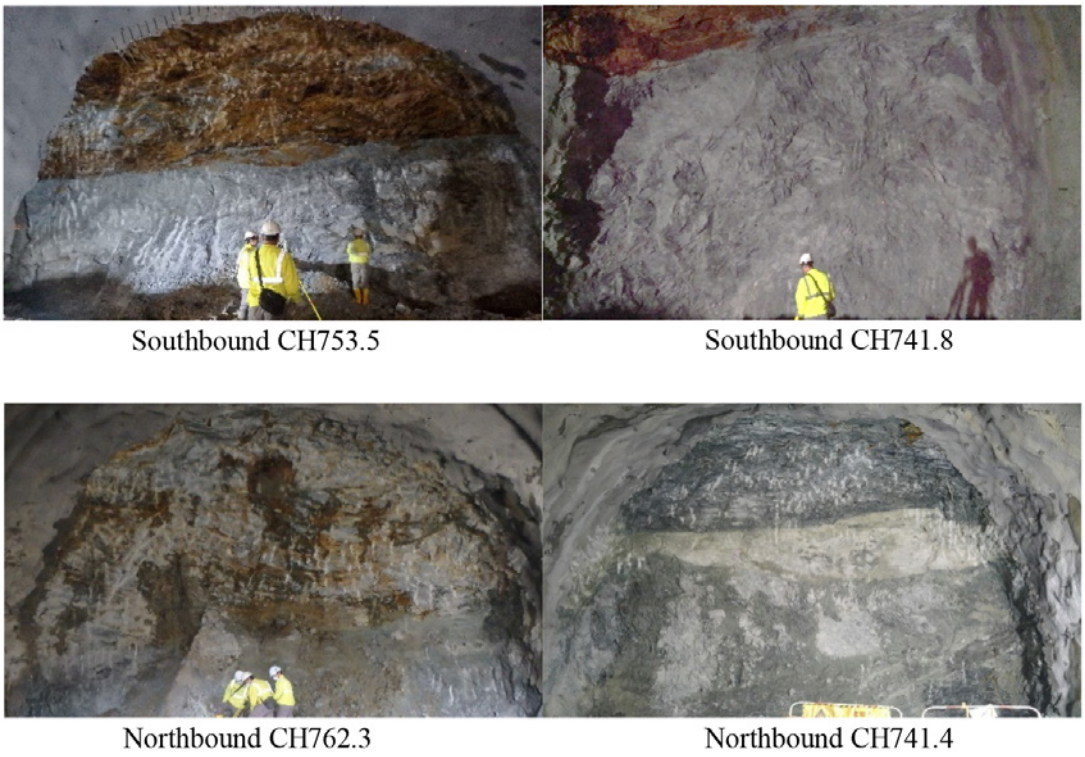

Plate 1: Rock face conditions in the weak rock zones

6 CONCLUSIONS

To improve the understanding to the geological conditions of the tunnel, MWD data need to be converted into geological information through sorting and organizing data. An analysis of MWD data has been conducted and the weak rock zones can be delineated. In this project, the interpolated results are in accord with site records and can be used to explain site observations and validate the design assumptions

The penetration rate is affected by many factors, such as the friction, the wear of the drill bits, ground water conditions, vibration and flushing conditions, those factors are not considered in this paper. Meanwhile, the locations of these data are extracted from the probing reports where a vertical tunnel face was assumed. It is found the effect of omitting above factors is minor for identifying the weak layer in this project. Similar conclusion has been drawn from the HATS 2A study that "from the objective of view, which was detecting the extremely adverse rock condition, these simplification and

assumptions showed to be insignificant" (Barmuta et al. 2012). However, the risk should be aware of and it is prudent to evaluate the error before MWD data interpolation.

There are more than 100 holes drilled in a typical production cycle. Hence huge amount of MWD data can be collected in this tunnel and the data are immediately available without additional cost. In view of the volume of MWD data and the possibility to identify the weak rock zones both in size and volume, the MWD data should be fully explored in the future tunneling works.

REFERENCES

Barmuta P. & Maxwell A. S. (2012) Detecting adverse rock condition ahead of tunnels by interpreting jumbo percussion drill logs, Proceedings of 32nd Annual seminar, Geotechnical division, HKIE, pp.169-175.

Ferreira J.E.V, Pinheiro, M. T. S. and Santos W. R. (2016) Graphical representation of chemical periodicity of main elements through boxplot, Educación Química 2016.

Frequent Drillers Club (2002). Article on Drilling Theory: Principles of Percussive Drilling. Internet website: www.drillersclub.com.

Ghosh R., Schunnesson H., and Gustafson A. (2017) Monitoring of drilling system behaviour for water-powered in-the-hole drilling, Minerals, 7,121.

Ghosh R. (2015) Rock mass characterization using drilling performance monitoring, Lulea University of Technology, Sweden.

Jimeno C. L., Jimeno E. L. & Carcedo J. A. (1995) Drilling and Blasting of Rocks, CRC Press.

Junhyeok P. (2016) Estimation of rock comminution characteristics by using drilling penetration rates. Master Thesis, The University of Arizona.

Lam, J.S & Siu C. K. (2006) Evaluation of application of drilling process monitoring (DPM) technique for soil nailing work, GEO Report No. 189, CEDD, HKSAR.

Leung R. and Scheding S. (2015) Automated coal seam detection using a modulated specific energy measure in a monitor-while-drilling context. International Journal of Rock Mechanics & Mining Sciences, Vol. 75, pp. 196-209.

Oosterhout D. (2016) Use of MWD data for detecting discontinuities, Master thesis, Delft University of Technology.

Peck J. (1989) Performance monitoring of rotary blast hole drills, PhD thesis, McGill University, Montreal, Canada.

Schunnesson, H. (1997) Drill process monitoring in percussive drilling for location of structural features, lithological boundaries and rock properties, and for drill productivity evaluation, Doctoral Thesis, Lulea University of Technology.

Tang Z.Y., Cai, M.F., Yue,Z.Q. Tham L.G. & Lee C.F. (2006) Interface identification of intricate weathered granite ground investigation in HongKong using drilling parameters, Chinese Journal of Rock Mechanics and Engineering, Vol.25 Supp.1.

Yue Z.Q. (2014) Drilling process monitoring for refining and upgrading rock mass quality classification methods, Chinese Journal of Rock Mechanics and Engineering, Vol.33 No.10.

Zhou H., Hatherly P., Monterio S. T., Ramos F., Oppolzer F., Nettleton E. & Scheding S. (2012) Automatic rock recognition from drilling performance data, ICRA 2012 IEEE International Conference.

Zhou D. (2017) Theory and technology of rock excavation of civil engineering, Metallurgical Industrial Press and Springer Science+Business Media Singapore.

A Site Trial of Planting Native Trees on a Soil Cement Fill Slope in Hong Kong

Billy C.H. Hau
The University of Hong Kong, Hong Kong

Jack C.F. Lau
AECOM, Hong Kong

Chester S.C. Leung
Housing Department, Government of the Hong Kong SAR

ABSTRACT

Replacing loose fill by compacted soil cement fill is one of the methods used to improve the safety margin of loose fill slopes in Hong Kong. Very little information on ecological greening on soil cement fill slopes is available in the literature. The objective of this site trial was to identify potential native tree and shrub species that are suitable for soil cement fill slopes. Twenty native woody species were planted on a soil cement fill slope in Shatin in 2015. The results of this field trial in 1.25 year are in line with those in an earlier study in Hong Kong on a soil cement rockfilled embankment in terms of seedling survival and growth rates. Most of the planted species achieved over 50% survival rates some species reaching over 90%. Four species *Cyclobalanopsis myrsinifolia, Syzygium hancei, Viburnum odoratissimum* and *Vitex quinata* achieved excellent survival rates (91-100%) and growth rates (RHI ranging from 0.3-0.8 cm cm^{-1} $year^{-1}$). The performances of the other 16 species are also satisfactory. Longer term monitoring of the planted seedlings in this experiment is recommended to assess the long term sustainability of these native species.

1 INTRODUCTION

Hong Kong is densely populated with a current population of 7.4 million occupying some 1,100 km2 of land (Census and Statistics Department 2018). However, Hong Kong's landscape is rugged with 63% of the total land area steeper than 15° and 30% steeper than 30° (Choi & Cheung 2013). As a result, many man-made slopes have been created in the course of the city's development. About 60,000 man-made slopes, including cut slopes, fill slopes and retaining walls have been registered in Hong Kong (Choi & Cheung 2013). Of these, around 10% are fill slopes created many years ago (Sun 1999; HKIE Geotechnical Division Subcommittee 2003).

At the beginning, loose fill slopes were upgraded by excavation, pit by pit, to a depth of 3 m. Pits are then back-filled with compacted soil (95% relative degree of compaction), soil cement mix (2 to 5%), rockfill or no-fines concrete (GCO 1984; GEO 2011). In recent years, with the advance in soil nailing technology, soil nailing together with concrete grillage beams are increasingly common in slope upgrading works on loose fill slopes (Lee et al. 2001; GEO 2011) but subject to certain qualifying criteria such as the minimum relative degree of compaction of the existing fill shall not be less than 75% (GEO 2008). Yet, excavation and re-compaction of fill materials using soil cement mix is still deployed nowadays.

On the other hand, with an increasing public demand on striking a balance between slope safety and landscape beauty, a lot of of efforts have been put on slope greening since the 1990s (GEO 2000; 2011). In addition, the benefit of green slopes in urban area as a way to promote urban biodiversity has been proposed in recent years (GEO 2011; Environment Bureau 2016). As a result, many field surveys and planting experiments have been conducted respectively to look at what native woody species could regenerate naturally on man-made slopes (Choi & Chau 2004) and what native woody species could be planted on man-made slopes (Hau et al. 2005; GEO 2011; Or et al. 2011). Native tree and shrub species are found to be more beneficial to local biodiversity and could thus enhance species richness of the restored vegetation (Hau & Corlett 2003).

The survival rate of plant species established on a degraded habitat or sites after slope engineering works are governed by multiple biotic and abiotic factors. They generally include physical, chemical, and morphological properties, soil moisture and organic-matter content (Jim 2001). Addition of cementing agent into the soil improves the strength of the soil with porosity of the soil mixture compromised. Reduced availability of pore space in soil would reduce water percolation and infiltration rate and also limit most of the biological activities, including root growth and the water and nutrient uptake processes of the root systems of plants (Mengel & Kirkby 2001). Soil cementation would also elevate the soil pH due to the dissolution of calcareous materials in the cement which may affect plant growth and establishment (Jim 1998; Ivanov & Chu 2008). Soil cement is thus considered a harsh substrate for plant establishment and growth.

In the literature, there is very little information about soil cement fill slope and plant establishment. Kobayashi (1981) suggested that grass and/or tree seeds could be incorporated into the fiber-soil-cement mixture. Yet, germination and establishment performance were not provided. Cecconi et al. (2012) demonstrated that grassy and herbaceous species were able to grow and survive on slopes with slightly cemented soil.

In Hong Kong, Yan and Zhang (2015) reported a field experiment on the soil-water characteristics of a native tree *Schefflera heptaphylla* planted in compacted sandy soil and cemented soil. The results show that the tree survived well in both types of materials in the field but grew better in compacted sandy soil. Fugro (2009) reported a field survey of plants regenerating on nine cement soil fill slopes in Hong Kong. It also reported a nursery planting experiment involving 12 woody plant species planted in soil cement blocks with 3% cement by weight content and 95% relative degree of compaction. The survey result showed that six slopes had excellent to good natural regeneration and three slopes had poor natural regeneration. Certain native tree species such as *Broussonetia papyrifera*; *Macaranga tanarius* var. *tomentosa* and *Mallotus paniculatus* were well established on cement fill slopes. The nursery planting experiment showed that the survival rates in six months were good (>80%) for 10 out of the 12 species. This study was taken further in Fugro (2011) in which a rockfill (Grade 200) embankment with cement fill (2.27% to 6.25% by weight and compacted to 95% relative degree of compaction) as the capping layer (3 m deep) was built in a construction site in Tsing Yi. Fifteen plant species, mainly native shrubs and trees were planted on the embankment for 10 months with irrigation only in the first month to enhance establishment. The survival rate of most species was high (75 – 100%) except the shrub *Ardisia crenata* and there was no significant different between cement content. Whilst many species showed similar growth rate in different cement content, two species (*Ardisia crenata* and *Mallotus panlculatus*) show higher growth rates in 2.27% cement content.

The results of these local studies show that the planted species, mostly native shrubs and trees, were able to survive and grow in cement soil and some native (as well as exotic) plant species were able to colonise cement soil fill slopes. In this field experiment, we aimed at screening more native tree and shrub species that are able to survive and grow well on soil cement fill slopes. We hope to expand the choice of native plant species for ecological restoration on soil cement fill slopes.

2 METHOD

2.1 The study site

The site trial was conducted on a slope feature in a housing development project in Shatin. This is a huge slope on bed rock which is covered with cement fill with an average depth of 2.5 m (Figure 1). The site

Figure 1. The site trial was conducted on the purple areas (left) of the feature in Shatin.

trial area is about 700 m^2. The formation of the soil cement fill slope was commenced in November 2013. The soil cement fill consists of cement, sand and soil in the proportions 1 : 3 : 12 by mass (i.e. cement content 6.25%) and it was compacted to 95% relative degree of compaction by mechanical vibrator with each layer of compaction not more than 300 mm.

2.2 Species selection for the site trial

To identify native tree and shrub species for the current site trial, two reports of the earlier study mentioned above (Fugro 2009; 2011) were reviewed. References were also taken from the latest GEO guidelines on slope greening (GEO 2011) which had summarised previous planting trials on soil cut slopes in Hong Kong. In addition, the eight cement soil slopes surveyed in Fugro (2009) have been re-surveyed in early 2014 with the aim of assessing the long term condition of the plant species on these soil cement slopes. Finally, the performances of trees and shrubs planted in another study on three soil cut slopes (Or et al. 2011) were also reviewed by field surveys in late 2013 which gave a review of the long term performances (almost 10 years) of the planted species. With the results of the literature review and additional field surveys, a list of 41 plant species was generated for this study (Table 1). When this field experiment was started in October 2015, the seedlings of only 11 species were available. Another nine species were selected which enabled us to explore some new species for trying on soil cement slopes (Table 1). All seedlings were sourced from the Nature Tree Nursery of the Kadoorie Farm and Botanic Garden.

2.3 Planting design and monitoring

Thirty-five seedlings of each of the 20 species were planted randomly on two slope panels on the lower part of the slope (Figure 1). Transportation and planting were done by a landscape contractor under the supervision of the research team and in accordance with the General Specification for Civil Engineering Works Vol. 1 (CEDD 2006). Irrigation was only provided in the first month after planting to enhance establishment. No maintenance was provided subsequently throughout the monitoring period. In the nursery, the stem height of each seedling was measured which acted as the baseline for growth rate determination. In addition, a plastic tag with a unique code was tied carefully on each seedling (total 700 seedlings) in the nursery to enable the identification of individuals after they were transplanted in the field.

The seedlings were transplanted from 5 to 16 October 2015. The first field monitoring was conducted on 12 November 2015 to determine the transplantation loss of seedlings. The last field monitoring was conducted in late December 2016 in which stem heights of the surviving seedlings were measured for determining the growth rate (over 1.25 year). For each individual, the increment in stem height

Table 1: Fourty-one species were shortlisted from the literature review as potential species for planting on cement fill slopes. Eleven species (marked by an "#") were available for this experiement and an additional nine species (marked by an "*") were also used making a total of 20 species in this experiment.

Scientific name	Family	Chinese name	Form
Alocasia odora	Araceae	海芋	Herb
Aporusa dioica	Euphorbiaceae	銀柴	Medium Tree
Boehmeria nivea	Urticaceae	苧麻	Shrub
Breynia fruticosa	Euphorbiaceae	黑面神	Shrub
Bridelia tomentosa	Euphorbiaceae	土蜜樹	Small Tree
Broussonetia papyrifera	Moraceae	構樹	Small Tree
Carallia brachiata *	Rhizophoraceae	竹節樹	Small Tree
Celtis sinensis	Ulmaceae	朴樹	Large Tree
Cratoxylum cochinchinense	Clusiaceae	黃牛木	Small Tree
Cyclobalanopsis championii #	Fagaceae	嶺南青岡	Small Tree
Cyclobalanopsis myrsinifolia #	Fagaceae	小葉青岡	Small Tree
Cyclobalanopsis neglecta #	Fagaceae	竹葉青岡	Medium Tree
Daphyniphyllum calycinum *	Daphyniphyllaceae	牛耳楓	Small tree
Desmodium heterocarpon	Fabaceae	假地豆	Shrub
Desmos chinensis	Annonaceae	假鷹爪	Shrub
Diospyros vaccinioides *	Ebenaceae	小果柿	Shrub
Diplospora dubia	Rubiaceae	狗骨柴	Shrub
Elaeocarpus sylvestris *	Elaeocarpaceae	山杜英	Medium Tree
Ficus hispida	Moraceae	對葉榕	Small Tree
Garcinia oblongifolia #	Clusiaceae	嶺南山竹子	Small Tree
Gardenia jasminoides	Rubiaceae	梔子	Shrub
Ilex viridis #	Aquifoliaceae	綠冬青	Small Tree
Lantana camara	Verbenaceae	馬纓丹	Shrub
Ligustrum sinense	Oleaceae	山指甲	Shrub
Lithocarpus glaber *	Fagaceae	柯	Medium Tree
Litsea glutinosa	Lauraceae	潺槁樹	Medium Tree
Litsea rotundifolia var. *oblongifolia* #	Lauraceae	豺皮樟	Shrub
Macaranga tanarius	Euphorbiaceae	血桐	Medium Tree
Machilus chekiangensis *	Lauraceae	浙江潤楠	Large Tree
Mallotus apelta	Euphorbiaceae	白背葉	Small Tree
Mallotus paniculatus	Euphorbiaceae	白楸	Medium Tree
Melastoma malabathricum	Melastomataceae	野牡丹	Shrub
Melastoma sanguineum	Melastomataceae	毛檵	Shrub
Phyllanthus emblica #	Euphorbiaceae	餘甘子	Small Tree
Polyspora axillaris	Theaceae	大頭茶	Small Tree
Psychotria asiatica #	Rubiaceae	九節	Shrub
Pteris vittata	Pteridaceae	蜈蚣草	Fern
Reevesia thyrsoidea	Sterculiaceae	梭羅樹	Small Tree
Rhaphiolepis indica #	Rosaceae	車輪梅	Shrub
Rhododendron simsii	Ericaceae	紅杜鵑	Shrub
Rhododendron sp.	Ericaceae	杜鵑屬	Shrub
Rhodomyrtus tomentosa	Myrtaceae	桃金娘	Shrub
Rhus succedanea #	Anacardiaceae	木蠟樹	Small Tree
Sapium discolor	Euphorbiaceae	山烏桕	Medium Tree
Schefflera heptaphylla #	Araliaceae	鵝掌柴	Medium Tree
Syzygium hancei *	Myrtaceae	韓氏蒲桃(紅鱗蒲桃)	Medium Tree
Trema tomentosa	Ulmaceae	山黃麻	Small Tree
Viburnum odoratissimum *	Caprifoliaceae	珊瑚樹	Medium Tree
Vitex quinata *	Verbenaceae	山牡荊	Small Tree
Zanthoxylum avicennae	Rutaceae	簕欓	Small Tree

(HI) (cm) over the study period (1.25 year) was determined (final stem height minus initial stem height). The growth rate of each species is represented by Relative Height Increment (RHI) in cm cm^{-1} $year^{-1}$ which is determined by (Hoffman & Poorter 2002):

$$RHI = Ln (H_2 - H_1)/Year \quad (1)$$

where H_1 and H_2 are the initial and final stem height in centimeters.

Since seedlings were planted in October at the beginning of the dry season (due to programme problem of the construction project), irrigation was provided by the contractor throughout the 2015/16 dry season according to the General Specification (CEDD 2006).

In this project, we were neither able to secure other soil cement fill slopes as replicates nor any soil cut slopes nearby as controls. Thus, the survival rates of the planted species could only be compared qualitatively with the results of previous studies in Hong Kong (Hau & So 2005; Fugro 2011).

3 RESULTS

3.1 Transplantation loss

The first monitoring on 12 November 2015 showed that transplantation loss of all species except *Cyclobalanopsis neglecta* (37%) was low (Table 2). Ten species have no transplantation loss and the rest of the nine species lost only 1 to 3 seedlings.

3.2 Survival rates

The final seedling survival rates of all species are considered high (71-100%) except *Cyclobalanopsis neglecta* (51%) (Table 2). Eight species achieved a survival rate of over 90% in which *Syzygium hancei* has 100% seedling survival.

3.3 Seedling growth rates

The growth rates of the seedling species varies. *Vitex quinata* has the highest growth rate of 0.81 cm cm^{-1} $year^{-1}$ (Table 2). Nine other species (all trees) have growth rates higher than 0.3 cm cm^{-1} $year^{-1}$. The shrub species *Psychotria asiatica* has the lowest growth rate of only 0.1 cm cm^{-1} $year^{-1}$.

4 DISCUSSIONS

4.1 Transplantation loss

Transplantation loss represents seedling mortality during transplantation (Hau & Corlett 2003) which could be due to a species being particularly sensitive to stress or poor planting treatment and skill of the contractor. The former cause would be reflected by a significantly higher transplantation loss of particular species and the latter would be represented by an overall high mortality rate. The overall transplantation loss is 4% which is comparable to other studies in Hong Kong (Table 3). In general, an overall transplantation loss of 5% or lower is considered acceptable (Hau & Corlett 2003). However, *Cyclobalanopsis neglecta* has an unusually high transplantation loss (37%). This species was planted in quite a few hillside restoration projects (Hau & So 2003) and slope greening projects (Hau et al. 2005) in Hong Kong respectively and such a high transplantation loss is unusual and may be regarded an exceptional case. It was also noted during the field monitoring that a few seedling mortality was due to accidental damage during transplantation (Figure 2). Also, some seedlings planted near the toe of the slope panel were killed by construction activities such as piling of construction materials and waste. Since such mortality is not very severe, it was not treated separately in the transplantation loss and final survival rate computation.

Table 2. Survival and growth rates of the 20 species planted in this experiment in 1.25 year. Transplantation loss was determined one month after planting. The minimum, maximum and mean stem height increment (HI) are stated with Relative Height Increment (RHI) in cm cm^{-1} $year^{-1}$. RHI = Ln (H_2 - H_1)/Year where H_1 and H_2 are the initial and final stem height (Hoffman & Poorter 2002). For all species, 35 seedlings were planted at the beginning.

Species	Transplantation loss		Final seedling survival		Min. HI (cm)	Max. HI (cm)	Mean HI (cm)	Mean RHI
	No.	%	No.	%				
Vitex quinata	1	2.9	33	94.3	1	73	34.3	0.8140
Cyclobalanopsis myrsinifolia	2	5.7	32	91.4	9	71	36.5	0.7181
Viburnum odoratissimum	1	2.9	33	94.3	14.5	73	36.5	0.5399
Phyllanthus emblica	0	0	33	94.3	4	50.5	21.2	0.4081
Elaeocarpus sylvestris	2	5.7	25	71.4	2	32.5	18.7	0.3547
Syzygium hancei	0	0	35	100	10	73	29.3	0.3363
Daphyniphyllum calycinum	0	0	31	88.6	9	39	20.3	0.3302
Cyclobalanopsis championii	1	2.9	28	80	2	37	17.1	0.3209
Cyclobalanopsis neglecta	13	37.1	18	51.4	0	36	18.8	0.3189
Lithocarpus glaber	0	0	31	88.6	4	47	26.4	0.3046
Ilex viridis	0	0	30	85.7	2	46	17.4	0.2777
Carallia brachiata	1	2.9	27	77.1	1	19.5	12.4	0.2708
Schefflera heptaphylla	3	8.6	25	71.4	0	18	7	0.2456
Litsea rotundifolia var. oblongifolia	1	2.9	29	82.9	0	33	6.8	0.2293
Rhaphiolepis indica	0	0	31	88.6	3	56.5	21.6	0.2258
Machilus chekiangensis	0	0	32	91.4	2.5	23.5	10.8	0.2139
Diospyros vaccinioides	0	0	32	91.4	0	30.5	8.4	0.1697
Garcinia oblongifolia	0	0	33	94.3	1	35.5	10.6	0.1576
Rhus succedanea	3	8.6	29	82.9	0.5	31	7.9	0.1329
Psychotria asiatica	0	0	27	77.1	0	18.5	4.3	0.0996

Table 3. Transplantation loss of various field experiments in planting native trees and shrubs in Hong Kong.

Study	Location	Habitat	No. of species planted	Total No. of seedlings planted	Transplantation loss (%)
This study	Shatin	Soil cement fill slope	20	700	4.0
Fugro 2011 (Experiment 1)	Tsing Yi	Soil cement covered rockfill embankment	15	600	1.7
Fugro 2011 (Experiment 2)	Tsing Yi	Soil cement covered rockfill embankment	15	600	4.7
Hau & Corlett 2003	Tai Mo Shan	Hillside grassland	4	1600	2.0

4.2 Survival rates

Despite the fact that soil cement is a harsh substrate for plant establishment, seedling survival rates of most species planted are considered good in comparison with other field planting experiments of native tree and shrub species in Hong Kong (Table 4). For Cyclobalanopsis neglecta, the final survival rate is 51.4%.This is largely due to high transplantation loss (34%). Two species in this site trial were also used in a previous site trial in soil cement slope (Fugro 2011). Both species Psychotria asiatica and Schefflera haptaphylla appear to have lower survival rates than in the previous site trial (Table 4). However, a

Figure 2. Transplantation is a stressful process for tree seedlings (left) especially during the construction stage. Seedlings could be accidentally trampled (middle) and pulled out (left).

Table 4. Final survival rates of seedlings planted in this study in comparison with the same species planted in other studies. It should be noted that the survival rates in Hau et al. (2005) were over a longer period than this study.

Study	This study	Fugro 2011		Hau et al. 2005							
Habitat	Soil cement fill slope	Soil cement rock fill embankment		Soil cut slope	Hillside grassland						
Site	A	B	C	D	E	F	G	H	I	J	K
Species\ Duration (months)	15	10	10	36	24	24	24	24	24	24	24
Carallia brachiata	77										
Cyclobalanopsis championii	80				80			48		40	
Cyclobalanopsis myrsinifolia	91				27					29	
Cyclobalanopsis neglecta	51				43	80	98	90	90	15	49
Daphyniphyllum calycinum	89										
Diospyros vaccinioides	91										
Elaeocarpus sylvestris	71										
Garcinia oblongifolia	94										
Ilex viridis	86										
Lithocarpus glaber	89				18					29	
Litsea rotundifolia var. oblongifolia	83			89							
Machilus chekiangensis	91										68
Phyllanthus emblica	94										
Psychotria asiatica	77	100	100	93							
Rhaphiolepis indica	89	100	100	58							
Rhus succedanea	83										
Schefflera heptaphylla	71	90	95	71	65	59	82		70		
Syzygium hancei	100							97			
Viburnum odoratissimum	94										79
Vitex quinata	94										
Alocasia odora		95	100								
Ardisia crenata		55	25								
Bridelia tomentosa		100	90		90						
Ficus hispida		100	100								
Lantana camara		95	100								
Ligustrum sinense		95	100								
Litsea glutinosa		100	100								
Macaranga tanarius		95	95								
Mallotus panlculatus		75	75								
Melastoma sanguineum		100	90								
Polyspora axillaris		90	90								
Rhodomyrtus tomentosa		100	100								

survival rate of over 70 % in 15 months is satisfactory. It should be noted that for slope greening site trials in Hong Kong involving native tree species, over 50% survival is considered normal (Or et al. 2011).

In conclusion, the results of this site trial are similar to the previous planting experiments by Fugro (2009; 2011) on soil cement fill materials or slopes. Transplantation loss and 15 months seedling survival rates are satisfactory for the 20 species tested.

4.3 Seedling growth rates

Again, despite the fact that soil cement is a harsh substrate for plant growth, the seedling growth rates in this study are rather satisfactory (Table 2). Four species *Cyclobalanopsis myrsinifolia, Syzygium hancei, Viburnum odoratissimum* and *Vitex quinata* has a maximum height increment of over 70cm and a mean height increment of around 30cm (Table 2). In comparison with the site trial on a soil cement fill slope (Fugro 2011) and other field planting experiments on cut slopes and hillside reforestation in Hong Kong (Hau et al. 2005), the growth rates of all 20 species planted are not particularly low (Table 5).

5 CONCLUSIONS

Many loose fill slopes were created in the early development of Hong Kong. To increase the factor of safety by excavation and re-compaction of soil cement fill is still one of the slope upgrading methods. On the other hand, the expectation on slope greening and ecological restoration are rising. A field planting experiment was conducted at a soil cement fill rock slope in Shatin involving 20 native tree and shrub species. The aim was to identify more native woody species that could establish well on soil cement fill slopes. The poor porosity and alkaline nature of soil cement fill are not conducive to plant establishment.

The results of this field planting experiment are in line with those in an earlier study in Hong Kong on a soil cement rockfilled embankment (Fugro 2011) in terms of seedling survival and growth rates. In both studies, most of the planted species achieved over 50% survival rates in around a year with some species reaching over 90%. A 50% survival rate is considered good in hillside restoration in Hong Kong (Hau and Corlett 2003; Hau and So 2003). The growth rates of the 20 species in this experiment are also comparable to those in Fugro (2011) and other field planting experiments in Hong Kong (Hau et al. 2005).

Among the 20 species planted in this experiment, four species *Cyclobalanopsis myrsinifolia, Syzygium hancei, Viburnum odoratissimum* and *Vitex quinata* achieved excellent survival rates (91-100%) and growth rates (RHI ranging from 0.3-0.8 cm cm^{-1} $year^{-1}$). The performances of the other 16 species are also satisfactory.

This field experiment was limited by the availability of replicate sites which is common among contract research study of this kind. As a result, only qualitative interpretation of the results could be made and no statistical comparisons were attempted. Fortunately, there are many previous field planting trials using native tree and shrub species on man-made slopes and natural hillsides in Hong Kong in recent years. These enable the results of this study to be put into the local context of ecological restoration. On the other hand, this study, like in other similar tree planting experiments, was only monitored for slightly more than a year. The results of this study are only applicable to assess the initial seedling establishment. The slope maintenance party is encouraged to keep note of this experimental trial and conduct field assessment of the planted seedlings e.g. every 5 year in order to assess the long term sustainability of the planted tree and shrub species on this soil cement fill slope.

Last but not least, like in previous studies (e.g. Hau & So 2003), this study also shows that good quality seedlings, good transportation and transplanting practices, and site management are essential factors affecting the performance of native tree and shrub seedlings. In this study, the good results are at least partly attributable to the good quality seedlings from Kadoorie Farm and Botanic Garden as well as the project team's supervision on the landscape contractor in seedling transportation and transplant works.

Table 5. Mean Relative Height Increment (RHI cm cm^{-1} $year^{-1}$) of seedlings planted in this study in comparison with the same species planted in other studies. It should be noted that the RHI in Hau et al. (2005) were over a longer period.

Study	This study	Fugro 2011		Hau et al. 2005							
Habitat	Soil cement fill slope	Soil cement rock fill embankment		Soil cut slope	Hillside grassland						
Site	A	B	C	D	E	F	G	H	I	J	K
Species\ Duration (months)	15	10	10	36	24	24	24	24	24	24	24
Carallia brachiata	0.27										
CycloBalanopsis championii	0.32				0.47			0.69		1.14	
Cyclobalanopsis myrisinifolia	0.72				0.66					0.36	
Cyclobalanopsis neglecta	0.32				0.66	0.67	0.64	0.58	0.65	0.52	0.27
Daphniphyllum calycinum	0.33				1.27						0.16
Diospyros vaccinioides	0.17										
Elaeocarpus sylvestris	0.35										
Garcinia oblongifolia	0.16										
Ilex viridis	0.28										
Lithocarpus glaber	0.30				0.55					0.39	
Litsea rotundifolia var. oblongifolia	0.23			0.34							
Machilus chekiangensis	0.21										0.33
Phyllanthus emblica	0.41										
Psychotria asiatica	0.10	0.15	0.08	0.24							
Rhaphiolepis indica	0.23	0.17	0.18	0.15							
Rhus succedanea	0.13										
Schefflera heptaphylla	0.25	0.29	0.24	0.46	0.84	0.52	0.44		0.83		
Syzygium hancei	0.34							0.50			
Viburnum odoratissimum	0.54										0.30
Vitex quinata	0.81										
Alocasia odora		0.55	0.31								
Bridelia tomentosa		0.62	0.56								
Ficus hispida		0.66	0.77								
Lantana camara		1.00	1.15								
Ligustrum sinense		0.67	0.10								
Litsea glutinosa		0.35	0.35								
Macaranga tanarius		0.08	0.08								
Mallotus paniculatus		0.30	0.18		0.39	0.29	0.30		0.26	0.45	0.48
Melastoma sanguineum		0.62	0.22								
Polyspora axillaris		0.22	0.22	0.41	0.69					0.65	
Rhodomyrtus tomentosa		0.50	0.09								

ACKNOWLEDGEMENT

The authors gratefully acknowledge the Director of Housing, the Government of the Hong Kong Special Administrative Region, for permission to publish this paper. Kadoorie Farm and Botanic Garden is also gratefully acknowledged for providing all of the native tree and shrub seedlings at a discounted rate to support local research.

REFERENCES

Census and Statistics Department. 2018. Hong Kong Statistics: Population. Accessed on 14 March 2018. https://www.censtatd.gov.hk/hkstat/sub/so20.jsp

Choi, K.C. & Chau, R.Y.H. 2004. *Identification of Suitable Vegetation Species for Use on Man-made Slopes. SPR 7/2004.* Geotechnical Engineering Office, Civil Engineering Department, The Government of the Hong Kong SAR, 108pp.

Choi, K.Y. & Cheung, R.W.M. 2013. Landslide disaster prevention and mitigation through works in Hong Kong. *Journal of Rock Mechanics and Geotechnical Engineering* 5:354–365.

Cecconi, M., Pane, V., Napoli, P. & Cattoni, E. 2012. Deep roots planting for surface slope protection. *Electronic Journal of Geotechnical Engineering* 17: 2809–2820.

CEDD. 2006. *General Specification for Civil Engineering Works. GS, 2006 edition, Vol. 1.* Civil Engineering and Development Department, Government of the Hong Kong SAR, 469pp.

Environment Bureau. 2016. *Hong Kong Biodiversity Strategy Action Plan 2016-2021*. Hong Kong, the Government of the Hong Kong SAR, 97pp.

Fugro. 2009. *Study on Soil Cement Used in Slope Works.* Study Report, Agreement No. CE 8/2007 (GE) 10-year Extended LPM Project, Phase 7, Package N, Hong Kong Island and the New Territories Landslip Preventive Works on Government Slopes and Related Studies - Investigation, Design and Construction. Fugro (Hong Kong) Limited, Hong Kong.

Fugro. 2011. *Study on Soil Cement Used in Slope Works.* Final Report for Site Trial Planting, Agreement No. CE 8/2007 (GE) 10-year Extended LPM Project, Phase 7, Package N, Hong Kong Island and the New Territories Landslip Preventive Works on Government Slopes and Related Studies - Investigation, Design and Construction. Fugro (Hong Kong) Limited, Hong Kong.

GCO. 1984. *Geotechnical Manual for Slopes. (2nd Edition)*. Geotechnical Control Office (GCO), Civil Engineering Services Department, Hong Kong, 295 pp.

GEO. 2000. *Technical Guidelines on Landscape Treatment and Bio-engineering for Man-made slopes and Retaining Walls. GEO Publication 1/2000*. Geotechnical Engineering Office (GEO), Civil Engineering Department, The Government of the Hong Kong SAR, 146pp.

GEO. 2008. *Guide to Soil Nail Design and Construction. Geoguide 7*. Geotechnical Engineering Office (GEO), Civil Engineering Department, The Government of the Hong Kong SAR.

GEO. 2011. *Technical Guidelines on Landscape Treatment for Slopes. GEO Publication 1/2011*. Geotechnical Engineering Office (GEO), Civil Engineering Department, The Government of the Hong Kong SAR, 217pp.

Hau, B.C.H. & Corlett, R.T. 2003. Factors affecting the early survival and growth of native tree seedlings planted on a degraded hillside grassland in Hong Kong, China. *Restoration Ecology* 11(4): 483–488.

Hau, B.C.H. & So, K.K.Y. 2003. Using native tree species to restore degraded hillsides in Hong Kong, China. Pp. 179-190 in H.C. Sim Editor, S. Appanah Editor & P.B. Durst Editor (ed.), *Bring Back the Forests: Policies and Practices for Degraded Lands and Forests.* FAO, Bangkok, Thailand.

Hau, B.C.H., So, K.K.Y., Choi, K.C. & Chau, R.Y.H. 2005. Using native tree and shrub species for ecological rehabilitation of man-made slopes in Hong Kong. Pp273-286 in *Safe and Green Slopes, Proceedings of the 25th Annual Seminar, Geotechnical Division, Hong Kong Institute of Engineers, 4 May 2005.* Hong Kong.

HKIE Geotechnical Division Subcommittee. 2003. *Soil Nails in Loose Fill Slopes: A Preliminary Study*. Final Report. Hong Kong Institution of Engineers, Hong Kong, 98pp.

Hoffmann, W.A. & Poorter, H. 2002. Avoiding bias in calculations of relative growth rate. *Annals of Botany* 80:37-42.

Ivanov, V. & Chu, J. 2008. Applications of microorganisms to geotechnical engineering for bioclogging and biocementation of soil in situ. *Reviews in Environmental Science and Biotechnology* 7(2): 139–153.

Jim, C.Y. 1998. Soil characteristics and management in an urban park in Hong Kong. *Environmental Management* 22(5): 683–695.

Jim, C.Y. 2001. Ecological and landscape rehabilitation of a quarry site in Hong Kong. *Restoration Ecology* 9(1): 85–94.

Kobayashi, T. 1981. *U.S. Patent No. 4,304,069*. Washington, DC: U.S. Patent and Trademark Office.

Lee, C.F., Law, K.T., Tham, L.G., Yue, Z.Q. & Junaideen, S.M. 2001. Design of a large soil box for studying soil–nail interaction in loose fill. In C.F. Lee Editor, C.K. Lau Editor, C.W.W. Ng Editor, A.K. Kwong Editor, P.L.R. Pang Editor, J.-H. Yin Editor &. Z.Q. Yue Editor (eds.), *Soft Soil Engineering*: 413-418. Routledge, London, 720pp.

Mengel, K. & Kirkby, E.A. 2001. *Principles of Plant Nutrition*. Fifth edition. Kluwer Academic Publishers, Dordrecht, 849pp.

Or, I.O.L., Hau, B.C.H. & Cheung, R.W.M. 2011. Application of native plant species in the landslip preventive measures programme. Pp. 163-169 in *Proceedings of the 31st Annual Seminar, Geotechnical Division, Hong Kong Institute of Engineers, 20 May 2011*. Hong Kong.

Sun, H.W. 1999. *Review of fill slope failures in Hong Kong. GEO Report No. 96*. Geotechnical Engineering Office, Civil Engineering Department, The Government of the Hong Kong SAR, 87pp.

Yan, W.M. & Zhang, G. 2015. Soil-water characteristics of compacted sandy and cemented soils with and without vegetation. Canadian Geotechnical Journal 52: 1331–1344.

Ground Treatment in a Reclaimed Land for Launching of the Subsea Tunnel Boring Machine under the Tuen Mun – Chek Lap Kok Link Project, Hong Kong

A.K.L. Kwong, C.C.W. Ng
AECOM

A. Schwob
Dragages – Bouygues Joint Venture

ABSTRACT

The proposed Tuen Mun – Chek Lap Kok Link (TM-CLKL) project comprises a 9km long dual 2-lane carriageway between Tuen Mun and North Lantau, Hong Kong. The alignment commences at a connection with the North Lantau Highway (NLH) at Tai Ho of Lantau. It heads northwest to the proposed Hong Kong – Zhuhai - Macao Bridge, Hong Kong Boundary Crossing Facilities (HKBCF) near the Hong Kong International Airport (HKIA) at Chek Lap Kok. After landing on the eastern edge of the reclaimed HKBCF, the alignment turns north and heads into a 5km long sub-sea tunnel. After crossing the Urmston Road, the alignment daylights at a new reclamation just east of the Tuen Mun River Trade Terminal (RTT) and then heads eastwards on an elevated structure over Lung Mun Road.

Construction of the sub-sea tunnel across the Urmston Road between Tuen Mun and HKBCF has been carried out by two 14m diameter Tunnel Boring Machines (TBMs). The adoption of TBM completely avoided the impact on the busy Urmston Road during construction and minimized the impacts to the marine habitat of the Chinese White Dolphin, within and near the works site of the project.

The reclaimed land (referred to as the Northern Landfall (NLF)) just east of the Tuen Mun RTT was formed to accommodate the setting up of the launching shaft for the two TBMs, ventilation/retrieval/re-launching shaft, slurry treatment plant, grouting plant and the permanent tunnel ventilation and administration buildings and tunnel portal.

1.2km of vertical seawall, 800m of sloping seawall and approximately 2Mm^3 of fill were used to form the reclamation. Band drain with surcharge was applied to limit the residual settlement and differential settlement of the reclaimed land to less than 500mm and 1 to 300 respectively for a design life of 50 years.

Different ground treatment methods were used between the launching shaft of the TBMs and the ventilation shaft where it was used as the retrieval shaft for the 17.6m diameter TBM for the northbound tunnel. These methods included the formation of a break-in plug at the launching shaft using the method of cutter soil mixing and jet grouting column; formation of jet-grouted walls parallel to both tunnel sidewalls outside the break-in plug at the launching shaft and break-out plug at the ventilation shaft; deep vibro-compaction carried out at the sand fill and surcharging above final formation level to reduce the residual and secondary settlements of the soft marine deposits which remain underneath the reclamation.

All the ground treatment works were completed prior to the launching and driving of the TBMs in the reclaimed area to prevent the loss of confinement pressure during excavation and the risk of blow-out and ground subsidence. The two TBMs (one 17.6m diameter and one 14m diameter) successfully excavated under the reclaimed area without any loss of confining pressure, blow-out or ground subsidence.

1 INTRODUCTION

The proposed Tuen Mun – Chek Lap Kok Link (TM-CLKL) project comprises a 9km long dual 2-lane carriageway between Tuen Mun and North Lantau, Hong Kong. The alignment commences at a connection with the North Lantau Highway (NLH) at Tai Ho of Lantau. It heads northwest on a 1.6km long sea viaduct to the reclaimed Hong Kong – Zhuhai - Macao Bridge, Hong Kong Boundary Crossing Facilities (HKBCF) near the Hong Kong International Airport (HKIA) at Chek Lap Kok. After landing on the eastern edge of the HKBCF, the alignment turns north and heads into a 5km long sub-sea tunnel, which was constructed by large diameter Tunnel Boring Machines, passing under the Urmston Road in the southward direction. After crossing the Urmston Road, the alignment daylights at a reclamation just east of the Tuen Mun River Trade Terminal (RTT) and then heads eastwards on an elevated structure over Lung Mun Road, before joining a proposed toll plaza in Tuen Mun Area 46.

Construction of the sub-sea tunnel across the Urmston Road between HKBCF and Tuen Mun has been carried out by two 14m diameter Tunnel Boring Machines (TBMs). The adoption of TBM completely avoided the impact on the busy Urmston Road during construction and minimized the impacts to the marine habitat of the Chinese White Dolphin, within and near the works site of the project.

As shown in Figure 1, the reclaimed land (referred to as the NLF) just east of the Tuen Mun RTT was formed to accommodate the setting up of the launching shaft for the two TBMs, ventilation/retrieval/re-launching shaft, slurry treatment plant, grouting plant and the permanent tunnel ventilation and administration buildings and tunnel portal.

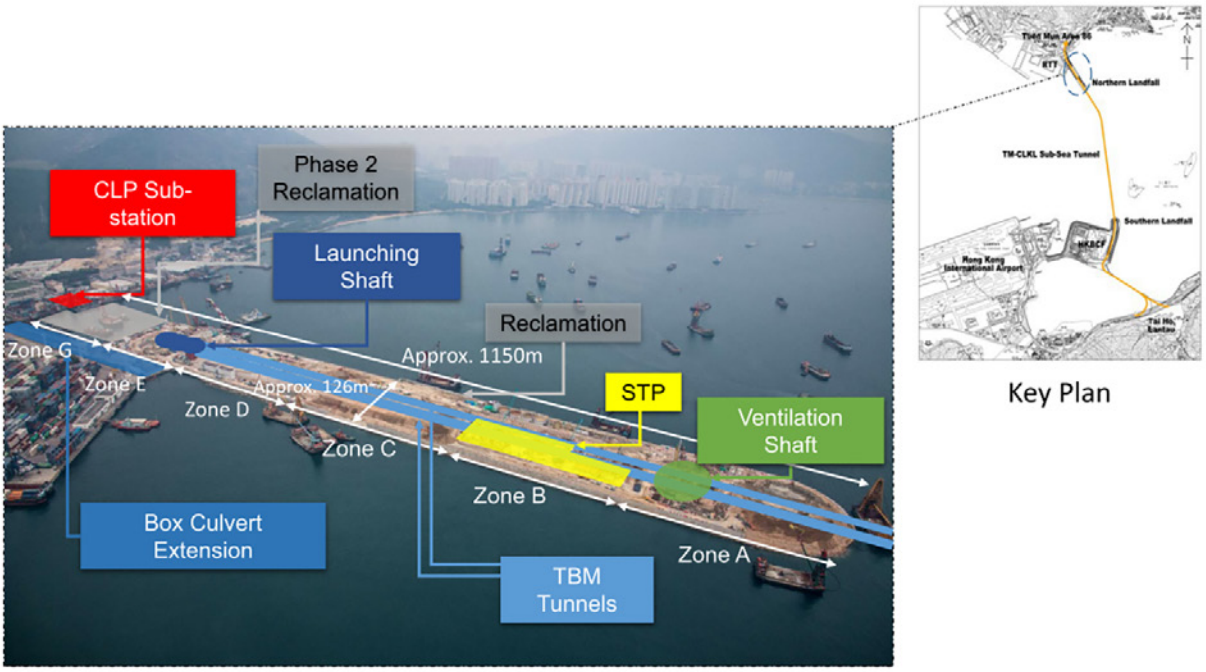

Figure 1 – Site Location Plan and Major Facilities at Northern Landfall

Band drain with surcharge was applied to limit the residual settlement and differential settlement of the reclaimed land to less than 500mm and 1 to 300 respectively for a design life of 50 years.

Different ground treatment methods were used between the launching shaft of the TBMs and the ventilation shaft where it was used as the retrieval shaft for the TBM for the northbound tunnel. These methods included the formation of a break-in plug at the launching shaft using the method of cutter soil mixing and jet grouting column; formation of jet-grouted walls parallel to both tunnel sidewalls outside the break-in plug at the launching shaft and break-out plug at the ventilation shaft; deep vibro-compaction carried out at the sand fill and surcharging above final formation level to reduce the residual and secondary settlements of the soft marine deposits.

1.1 Existing Topography and Bathymetry

The NLF is located at the south-east waters of the existing frontage of the RTT. According to the bathymetric survey results, the existing seabed level around the site generally varies between -5mPD to -13mPD.

1.2 Geological Setting

As shown in Figure 2, the sub-surface profile along the reclamation area consists of a layer of marine deposits overlying a layer of alluvium, which is underlain by completely decomposed rocks. The general description for each material stratum is summarized below.

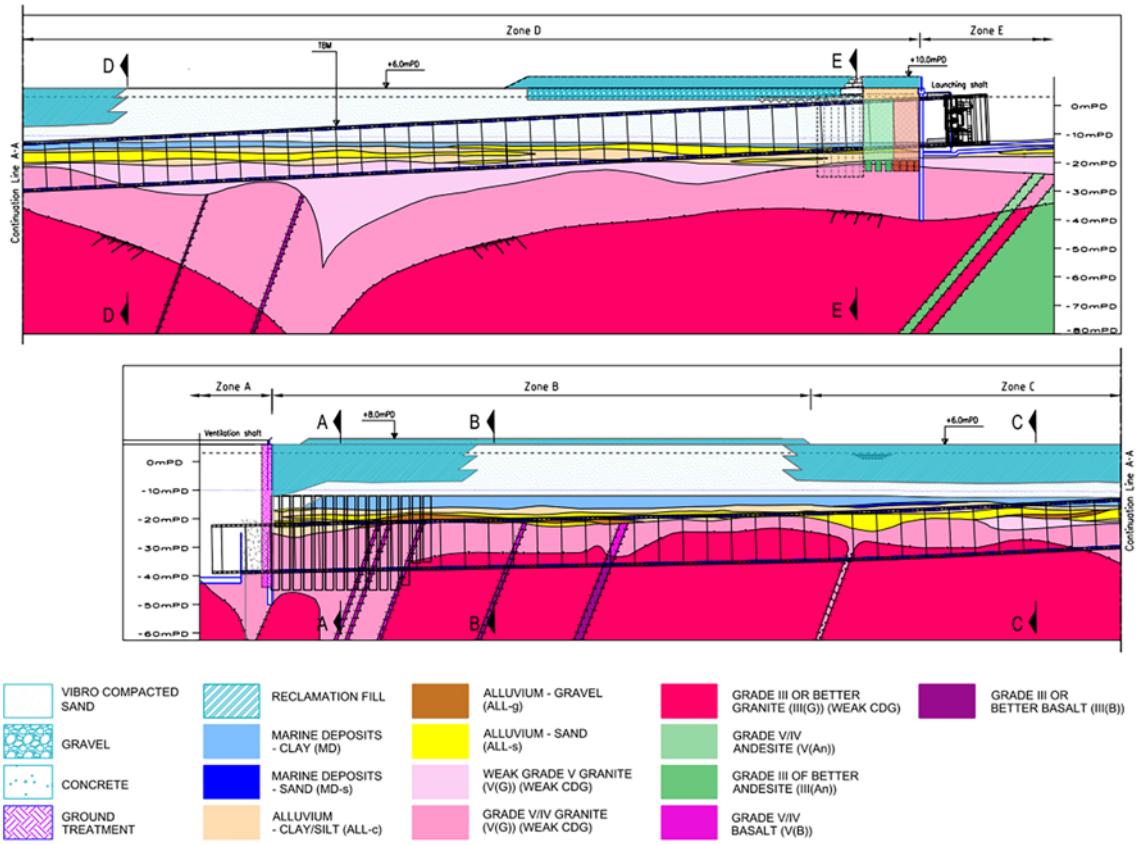

Figure 2 – Sub-surface Geological Profile at Northern Landfall

A layer of marine deposits is encountered at the seabed with thickness varying from 0 to 7.5m. It is predominantly clay, typically described as very soft to firm, grey, slightly sandy, silty clay with occasional shell fragments.

A layer of alluvium, with thickness varying from 0 to 13m, is underlying the marine deposits. The SPT "N" values range from 6 to 90. The alluvium is characterised by inter-bedded clays, silts and sands, which is typically described as firm, grey, sandy silty clay to sandy clayey silt (Alluvial Silt/Clay); and medium dense to very dense, grey to brown, silty, fine to coarse sand with some sub-angular to sub-rounded, fine to coarse gravel of moderately strong quartz (Alluvial Sand).

The saprolitic soils, comprising Grade V to IV materials, are encountered below the stratum of alluvium. Thickness of the saprolite generally varies from approximately 2m to 33m. It is generally extremely weak to very weak, greenish grey, brown or yellowish brown and completely to highly decomposed (firm to very stiff, sandy clayey silt).

Bedrock below the saprolitic soils varying from -5mPD to -55mPD and is about 0 to 45m below seabed. Shallow bedrock level at -5mPD is encountered at the existing sea frontage and then deepened gradually in the seaward direction. The bedrock material is dominated with granite, whereas andesite

is locally encountered at the northern portion. The Granite is moderately strong to strong, pinkish grey, spotted dark green, dappled brown, moderately to slightly decomposed fine to coarse grained granite. Joints are closely to medium spaced, locally very closely and widely spaced, rough stepped and rough planar, occasional rough undulating, extremely narrow to very narrow, iron and manganese stained, occasional kaolin chlorite coated.

From the launching shaft towards the middle of the NLF, excavation mainly occurred in variable thickness of fill, marine deposit and alluvium. Thereafter towards the ventilation shaft, excavation mainly occurred in Grade V to IV materials and bedrock.

2 STAGES OF RECLAMATION AND ACCELERATION OF CONSOLIDATION PROCESS

The TM-CLKL project includes a 16.5ha reclamation beside the existing RTT to accommodate the approach ramps and the north portal for the twin tunnels.

The layout of the NLF reclamation was sub-divided into 3 portions (i.e. Portion N-A through Portion N-C) as shown in Figure 3.

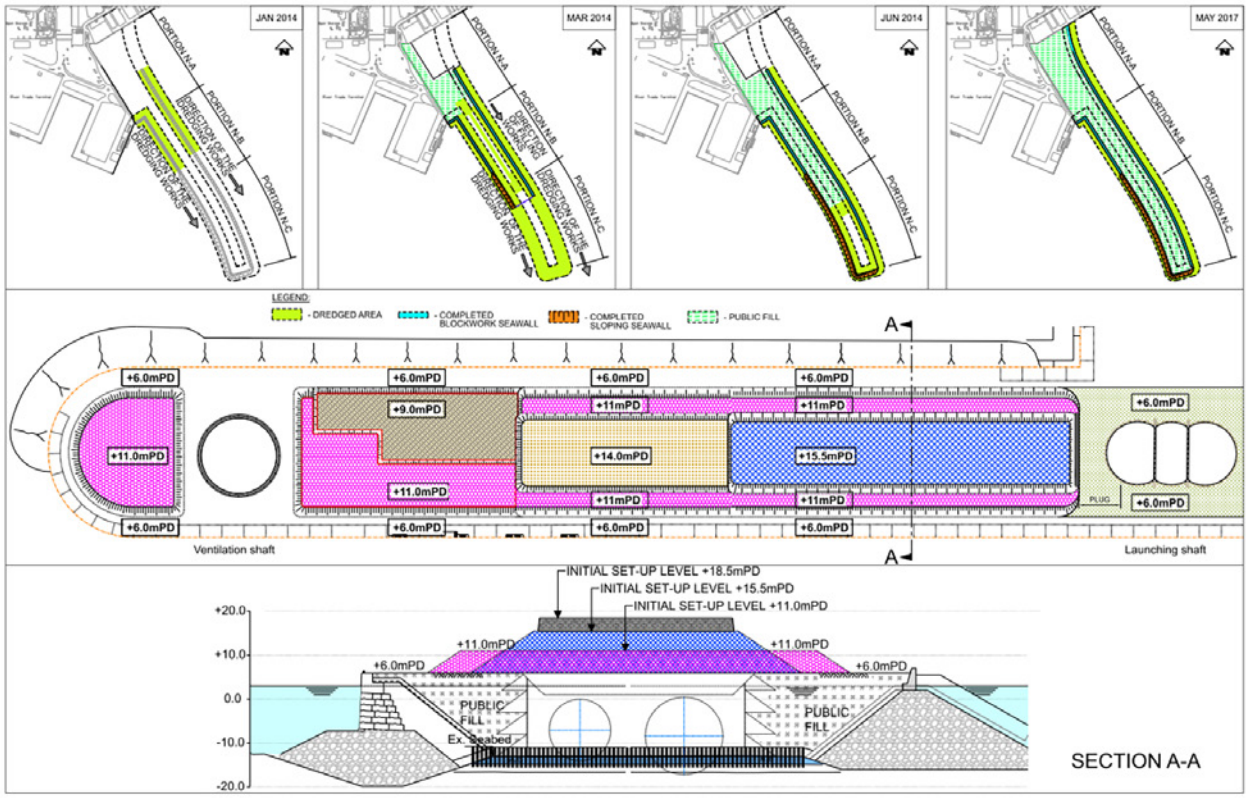

Figure 3 – Progress of Reclamation and Preloading Surcharge Level along the Northern Landfall

The construction of the seawall started at Portion N-A, and progressed generally in the southerly direction towards Portion N-C.

Two types of seawalls were used to surround and retain the reclamation of the NLF. The total length of seawall at the NLF was about 2,055m, comprising approximately 1,214m of vertical blockwork seawalls and 841m of sloping rubble mound seawalls.

Vertical blockwork seawall was adopted along the eastern perimeter of the NLF. The vertical blockwork seawall was formed by stacking of precast concrete blocks founding on the rock fill mound placed above the dredged trench with the in-situ soft marine deposits removed and replaced by granular materials or on the seabed with the in-situ soft marine deposits treated by ground improvement. The blockwork seawall provides a vertical berthing face allowing berthing of vessels at the re-provisioned Government berths and the reserved cargo handling area. Work barges and vessels can make use of the vertical blockwork seawall for berthing during the construction stage.

Sloping rubble mound seawall was adopted along the western and southern perimeter of the NLF. The sloping rubble mound seawall consists a rock fill core covered by layers of rock armour, namely primary armour layer and underlayer, with different weights and sizes for protection and founded either on the dredged trench with the in-situ soft marine deposits removed and filled with granular materials or on the seabed with the in-situ soft marine deposits treated by ground improvement.

The ground level after reclamation is +6.0mPD. Reclamation in the central area circumscribed by the seawalls started once 200m of leading edge was formed above +2.5mPD. As illustrated in Figure 4, the four steps in the reclamation process were the laying of geotextile, the installation of the sand blanket in layers, the band drain installation which was followed by layering with public fill to +2.5mPD to avoid mud waves. Vertical band drains with soil surcharge were used as ground improvement measures to accelerate the consolidation of the marine deposits and underlying alluvial clays and to limit the residual settlement to less than 500mm. Then it was raised to an initial level of +11.0mPD, and surcharged for a period of six months while maintaining design level not lower than +10.0mPD due to settlement.

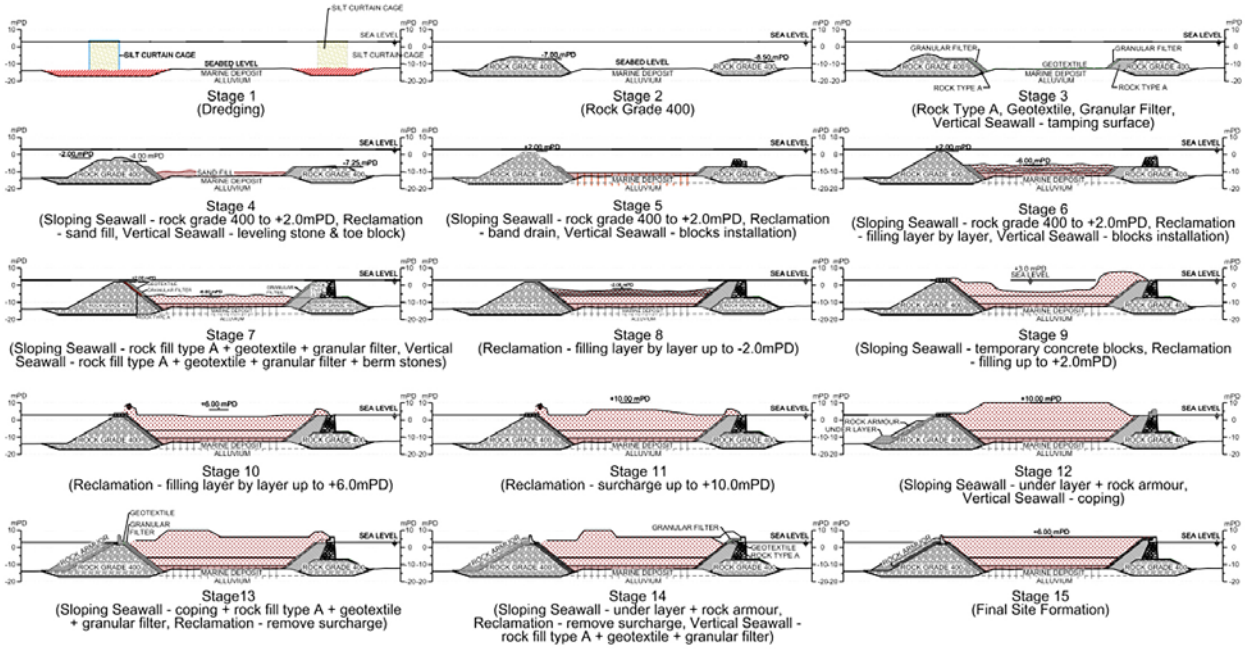

Figure 4 – Stages and Methods of Reclamation

The band drains have penetrated the upper alluvium clay which was targeted to have a gain in undrained shear strength of 25kPa from the original in the temporary condition and 60kPa from the original in the long term.

The spacing of the band drains installed was generally 1.5m c/c but was decreased to 1.2m c/c from the launching shaft towards the middle part of the reclaimed area (Zones C and D of about 400m in Figure 1) in order to accelerate the consolidation of the thicker marine deposits at this location.

Surcharge at Zones C and D were increased from the original surcharge level of +11.0mPD to +15.5mPD for a period of about 3 to 4 months, whereas in some local areas up to +18.5mPD for additional 3 weeks in order to improve the consolidation process by reducing the water content, and hence increasing the strength and decreasing the creep in the marine deposits and therefore minimizing the residual settlement and the associated long term tunnel squat after TBM tunnel construction. Marine deposits have been dredged for facilitating the construction of ventilation shaft. Surcharge near the slurry treatment plant was decreased in height but kept in place for a longer period as far as the construction programme permits.

3 PRIMARY MATERIALS

For reclamation work over soft marine deposits, sand blanket of 1 m to 2 m thick together with a geotextile layer underneath serves to distribute the load of the fill material placed by bottom dumping or end tipping, to prevent generation of mud waves due to slip failures within the soft marine deposits.

For ground treatment works of seawall foundation, sand blanket together with a geotextile layer underneath serves as an initial confinement over the top of very soft marine deposits to improve the strength by consolidation. The sand blanket is also a protective layer to prevent disturbed marine mud from being mixed into the marine environment causing pollution during the ground treatment process.

Public fill comprising of rocks, concrete, asphalt, rubbles, bricks, stones and earth was used as surcharge for preloading to accelerate the consolidation process of the soft marine deposits.

Rock fill was required for construction of vertical and sloping seawall. For vertical seawall, the rock base was made of Grade 400 rock fill and the rock fill of smaller size was used as the rock wedge and granular filter behind seawall. Core of the rubble mound sloping seawall was made of Grade 400 rock fill and the rock fill of smaller size was used as granular filter. Table 1 below shows the total quantity of materials placed in the reclamation at the NLF.

Table 1 – Total Quantities of Materials placed in the Reclamation at the Northern Landfall (excluding Phase 2 Reclamation)

Material	Quantity
Dredging Works	446,000 m^3
Rock Fill Grade 400	986,000 m^3
Seawall Blocks	10,932 nos.
Geotextile Membrane	220,000 m^2
Sand Fill	747,000 m^3
Band Drains	43,600 nos.
Public Fill for Reclamation	852,000 m^3
Public Fill for Surcharge	593,000 m^3

The sloping seawall with rock armour surface was used at the western perimeter and southern tip of the NLF. 4.5 to 5.0 tonne amour rock and 450kg armour rock under layer was used for the sloping seawall of the NLF. The southern tip of the NLF is more exposed than the other area of the reclamation. The curvature of the southern tip with roundhead construction help reduce the interlock between the armour stone. Therefore, larger armour rock of 5.5 to 6.0 tonne and 550kg armour rock under layer was adopted.

4 GROUND TREATMENT FOR TBM BREAK-IN

4.1 TBM Launching Shaft

The launching shaft is located at the permanent tunnel portal location. It forms part of the temporary works for the construction of a 60m long cut and cover tunnel connecting tunnel portal to bored tunnels section. The launching shaft requires 80m long space and 20m free headroom for accommodating the assembly and launching of the TBMs in their minimum configuration for starting excavation. The 3-cell caterpillar shape clears the space from struts, and eases shaft excavation as well as TBM erection.

The main issues with TBM launching are the sudden changes of force applied to the TBM as the head breaks through the shaft front wall and receives the full earth and high water pressure, and the water tightness between the segment lining being installed and the shaft front wall. In order to make a water-tight zone, until the first segments are sealed, ground treatment in the form of a surrounding grout break-in plug of dimensions (25m x 25m x 25m) that withstands the exterior pressure until the segments are sealed onto the shaft front wall was constructed.

In accordance with the requirement stated in Table 1 of Geo Report No. 249, the minimum length of ground treatment for TBM launching shall cover the length of the shield plus the length of two rings.

The dimensions of the ground treatment zone were increased compared to the strict minimum required for break-in based on the analysis of a plastic zone in order to avoid unacceptable deformation due to tunnel excavation at very shallow cover. At the bottom of the ground treatment beneath the opening, water tightness rather than deformation was regarded as the controlling factor of stability requirement.

The factor of safety of grouted soil against shear failure was adopted as 1.5. The unconfined compressive strength was 3MPa and a permeability of 10-7m/s in the ground treatment work was adopted for groundwater inflow control during TBM excavation.

In order to provide a flat area for easier control of the TBM break-in and to minimize the ground treatment works, TBM break-in treatment was divided into two portions as shown in Figure 5. The first portion was located inside the launching shaft in which a concrete block (commonly referred to as tympanum) was provided. The concrete block consisted of a reinforced concrete (RC) shell and a non-reinforced concrete core for the TBMs to excavate through. The length of the concrete block was 5 to 15m. The thickness of the RC shell was 2m. At the connection/interface between the RC shell and the diaphragm wall, water stopper/gasket were provided to ensure water-tightness. The second portion (referred to as break-in plug) was located outside the launching shaft where 20m of ground treatment using cutter soil mixing (CSM) and jet grouting was provided to reduce the permeability of the soil and improve the strength of the ground surrounding the tunnels at shallow cover. The general layout of the TBM break-in treatment is shown in Sections A-A (for water-tightness control) to B-B (for strength control) in Figure 5.

The strength required for the proposed ground treatment work was studied by the use of the finite element computer program Plaxis v.9.02 (BD ref. G0155). By varying different strengths of the ground treatment soil, the maximum deformation of tunnel and ground surface as well as the factor of safety against shear failure could be determined.

4.2 Cutter Soil Mixing (CSM) and Jet Grouting

The function of the CSM panels is to improve the mass strength of the treated ground to provide an adequate margin of safety against instability and deformation, with the added benefit that the high stiffness or the compression modulus of the panels acted to reduce the settlement of the composite ground.

In the CSM method, the soil is pre-mixed with the bentonite slurry during the downward excavation by the rotating cutters and the spoils is moved towards the top of the cutting head. As the machine moves upwards again, it moves the mix from above the cutting head to below it. During this phase a cement binding agent is injected and mixed with the soil. The result is that it creates a grouted panel that is of significantly higher strength and lower compressibility than the surrounding soft sediments.

Bentonite slurry was injected from the very beginning of the drilling, i.e. from the platform level (+3.5mPD to the designated depth of the panel). Then the cutter moves upward while injecting and mixing a pure cement grout. Once achieved the cut-off level (+2mPD) of the panel top, the withdraw phase was completed with a lighter grout.

CSM works were normally carried out from the existing ground level to the designated toe level, but the CSM panels could be terminated when hard materials were encountered and the remaining lower parts would be treated by jet grouting works.

The specifications required the uniaxial compressive strength to be greater than 1.75MPa for jet columns under CSM treatment and 3MPa for the interface between CSM panels and the diaphragm wall.

The CSM plug was further reinforced by the jet grouting columns underneath as shown in Figure 6. Jet grouting works were carried out after completion of CSM works. The designed lap length of CSM panel and jet grout column was a minimum of 200 mm. The top level of jet grouted columns was dependent on the toe level of the related CSM panels.

In general, grouting was carried out from the ground surface. Jet grout technique comprises the fracturing and simultaneous mixing of the soil in-situ with cement grout. Alternatively, the soil can be removed to a certain extent by air-water jetting and simultaneously replaced by grout jetting. The

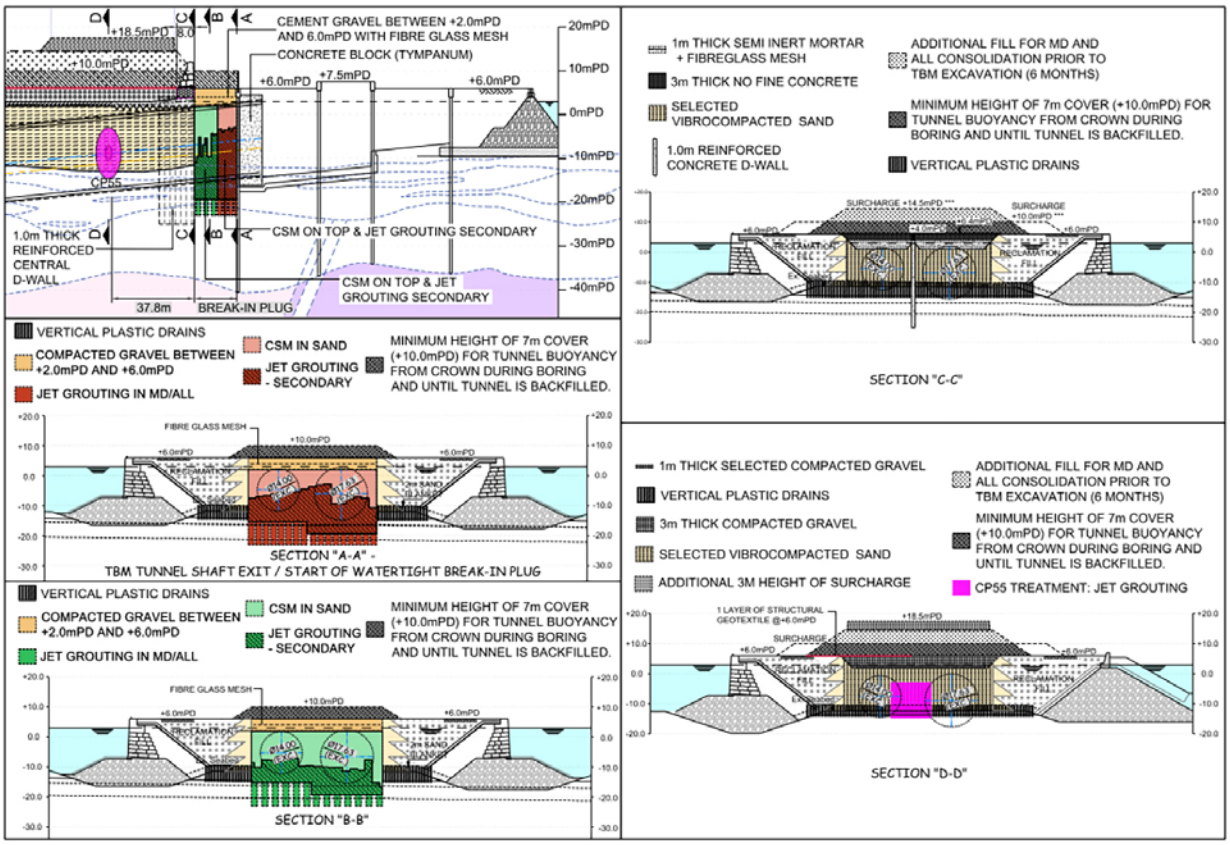

Figure 5 – CSM and Jet Grouting forming the Break-In Plug outside the Launching Shaft

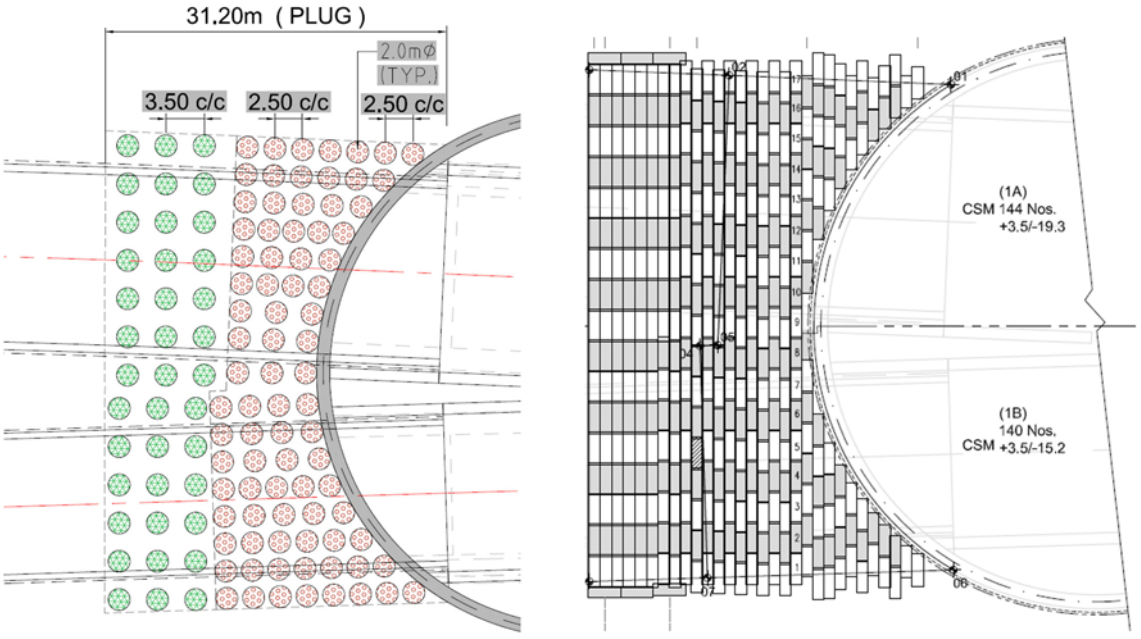

Part Plan 1
(Jet Grout Columns Arrangement)

Part Plan 2
(CSM Arrangement)

Figure 6 – Detailed arrangements of CSM and Jet Grout Columns

sequence of operations consists, generally, of the following main steps: (a) drilling down to the required depth by use of a string of rods fitted at the bottom with a drilling and jetting tool; and (b) grout jetting through radial nozzles located along the jetting tool axis while revolving and drawing up the rod.

The jet grout aims to change the in-situ soil to cemented formation of soil. The permeability of the cemented soil was reduced significantly with mixing of cement grout. The cemented soil generally retains significant cement content (40% – 60%) and gains strength over time. As the jet grouting bond soil particles, the relative strong cemented soil bodies with uniaxial compressive strength typically ranging 2-10MPa was achieved. The grout pattern ensured the overlapping of the grout columns. Deep part of the jet columns aims to reduce residual differential settlements at the transition zone between the bored tunnels and the future cut and cover tunnels to be built in the launching shaft.

4.3 Vibro-Compaction

Vibro-compaction is a deep compaction technique for densifying sandy soils in place by means of an electric vibrating unit. Under the influence of simultaneous vibration and saturation, loose sandy particles are repacked into a more compact state, and lateral confining pressure within the sand mass is increased.

Basically, the plant and equipment consist of 5 machines. The essential machine used in the process is the vibratory probe, which provides the vibration to the in-situ soils. Other include service crane providing the lifting; generator providing electricity power to the probe; air compressor providing air pressure; and high pressure pump providing together an air/water mix to the probe at a high pressure and the service pump to supply water from water sources.

Vibro-compaction works were carried out to enhance the mechanical properties of selected reclamation backfill material within the layout and extent surrounding the twin tube TBM tunnels. The selected backfill material that was used as reclamation fill, after vibro-compaction achieved the design parameters of angle of internal friction $\phi = 36°$ and a soil modulus E' greater than 40MPa to fulfill the design requirements.

Typical triangular grid spacing 3.5m to 3.9m was chosen for carrying out the vibro-compaction.

5 GROUND TREATMENT FOR TBM BREAK-OUT AND LOW CONFINEMENT

The temporary ventilation shaft was a 58.8m internal diameter circular shaft constructed using 1.5m thick diaphragm wall panels which were typically 2.8m wide.

The main purpose of the temporary shaft is to receive the northbound (ML03) large diameter TBM (17.6m diameter) and to modify its shield to a smaller diameter TBM (14m diameter) so that it could be launched again and continued to excavate along the subsea section. The temporary shaft also allows the crossing of the southbound (ML02) TBM (14m diameter) which does not require any change of diameter. There are therefore four TBM openings at the base of the shaft. After TBM operation, the shaft will form part of the temporary works for the construction of the permanent ventilation shaft which connects to the ventilation building.

In the receiving condition, a concrete block inside the retrieval shaft was used. Similar to the concrete block in the launching shaft, the concrete block in the retrieval shaft consisted of a reinforced concrete shell and a non-reinforced concrete core. The thickness of the RC shell was 2 m. The concrete shell was reinforced all around the concrete core (i.e. tunnel opening).

In order to facilitate the northbound TBM break-out operation, the temporary shaft was flooded which ensured balancing of forces when the TBM passed through the shaft D-Wall. After sealing of the segments inside the concrete block, the shaft was dewatered. A steel bell was adopted inside the shaft to balance the pressure and prevent groundwater inflow during the re-launching of the re-configured TBM towards the Southern Landfall. Steel bell was also used for the southbound TBM crossing.

To prevent stress relief (a phenomenon referred to as ovalization) and subsequent extensive lateral expansion of the sidewall of the tunnel when the two tunnels are too close together, 1.2m thick D-wall was formed between the two TBMs as shown in Figure 7 outside the retrieval shaft as part of the temporary design and risk mitigation measures.

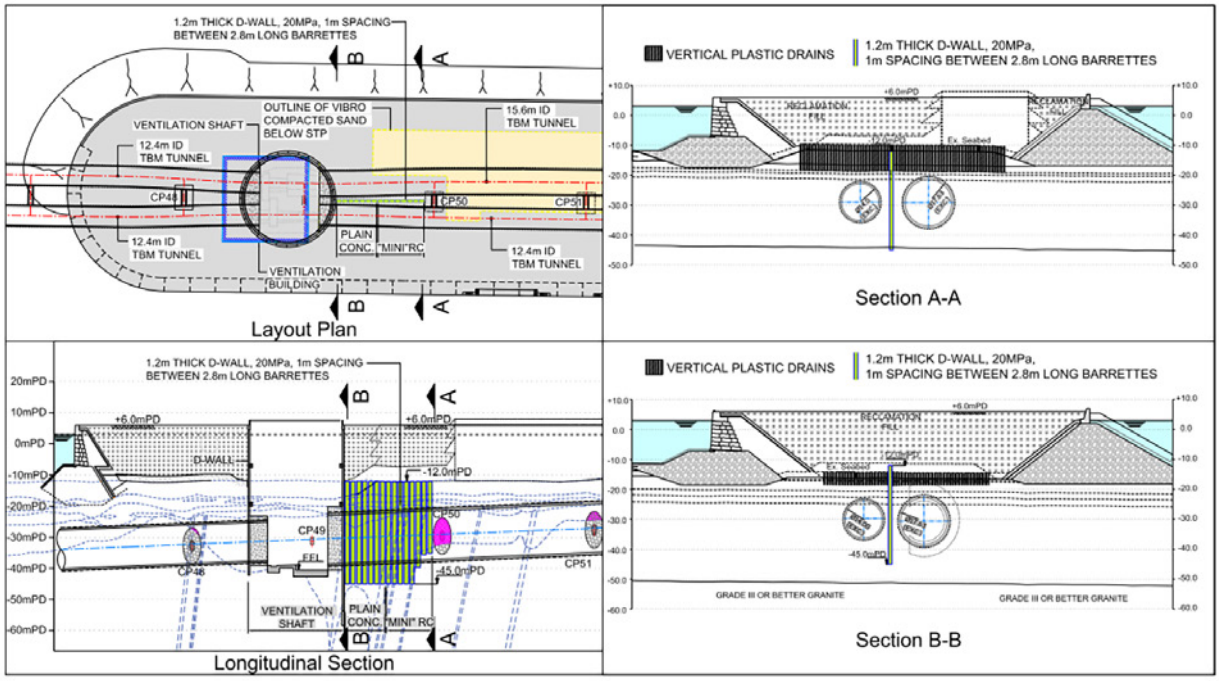

Figure 7 – Partition D-wall at Retrieval Shaft

6 CONCLUSION

Different ground treatment methods were used between the launching shaft of the TBMs and the ventilation shaft which was used as the retrieval shaft for the TBM for the northbound tunnel. These methods included the formation of a break-in plug at the launching shaft using the method of cutter soil mixing and jet grouting column; deep vibro-compaction carried out at the sand fill layer and surcharging above final formation level to reduce the residual and secondary settlements of the soft marine deposits.

All the ground treatment works were completed and the TBMs successfully excavated under the reclaimed area without any loss of confinement pressure, blow-out or ground subsidence.

ACKNOWLEDGEMENTS

The writers are grateful for the support of Highways Department, HKSARG. Their support contributed in expediting the approval process. However, the contents of this paper do not necessarily reflect the views and policies of these supporting organizations, nor does the mention of trade names and commercial products constitute endorsement or recommendation for use.

REFERENCES

AECOM, 2014. Design Verification Report (Ref.B2a-02) for Northern Landfall Reclamation and Seawall Stability. Agreement No. CE 7/2011(HY), Tuen Mun – Chek Lap Kok Link – Design and Construction.

GEO Report No. 249. Ground Control for Slurry TBM Tunnelling. CEDD, Government of the Hong Kong SAR.

Plaxis v.9.02. www.plaxis.nl/.

Cushioning Materials for Reducing Boulder Impact Load on Concrete Barriers

T.L. Lee & H.L. Cheng
C M Wong and Associates Ltd., Hong Kong

A.Y.T. Lam & E.M.Y. Ko
Geotechnical Engineering Office, Civil Engineering and Development Department, the Government of the Hong Kong SAR

ABSTRACT

In Hong Kong, concrete barriers are often employed as mitigation measures to protect building developments and infrastructures, which are subjected to natural terrain landslide hazards. Gabions are commonly installed at the impact face of the concrete barriers to protect and reduce the dynamic impact load from boulders entrained within the landslide debris. This paper describes the large-scale impact tests employed for assessing the cushioning performance of autoclaved aerated concrete blocks and hollow concrete blocks as potential alternative cushioning materials. In the tests, a large concrete sphere impactor was employed to impact different cushioning materials with various thicknesses installed at the impact face of a concrete wall. The cushioning materials were subjected to successive impacts without repair. Measurements of the impact force induced by the impactor on the cushioning layers, the transmitted load acting on the concrete wall and the deformation of the cushioning layers were recorded by accelerometers, load cells, high-speed camera, etc. The results of the tests were compared with test results of similar large-scale impact tests performed on gabion cushioning layer by Ng et al., 2016.

1 INTRODUCTION

1.1 Background

As building developments and infrastructures progress along the urban fringe of Hong Kong, natural terrain landslides could be the potential hazards to such developments (Ho & Roberts 2016). Concrete barrier is a common mitigation measure adopted to protect facilities against natural terrain landslide hazards. They are designed to resist debris flows and boulders, which were entrained to form part of the debris flow. It is shown in previous studies that installation of a cushioning layer in front of a concrete barrier may reduce the boulder impact load (GEO 2012). Under current practice, it is common to employ a 1 m thick gabion layer in front of a concrete barrier for the purpose of protection, minimizing the potential repair works after impact by landslide debris or boulders.

On steep natural terrain, transportation of rock fill for gabion construction could be difficult. This would be reflected in the time and cost for construction and repair of cushioning layers. In view of the above shortcomings of gabion as a cushioning material, other potential alternative cushioning materials, including autoclaved aerated concrete (AAC) blocks and hollow concrete blocks are considered in this paper.

1.2 Previous Studies

In Hong Kong, AAC blocks and hollow concrete blocks were commonly employed for the construction of partition walls. No previous study on the use of AAC block and hollow concrete block as cushioning material has been identified.

Gabion is a commonly used cushioning material for concrete barriers in Hong Kong. Upon impact, a gabion cushioning layer would deform, hence, reducing the load transmitted onto the concrete barrier (GEO 2012). In France, gabion was used as a cushioning layer for reducing impact load from rock fall on protective roof structures for motorways. Large-scale drop tests (Lambert et al. 2009) and large-scale pendulum impact tests (Heymann et al. 2010, 2011; Lambert 2014; Lam 2016; Ng et al. 2016) were performed to study the cushioning performance of gabion.

1.3 Hertz Load

In GEO Report No. 270 "Supplementary Technical Guidance on Design of Rigid Debris-resisting Barriers" (Kwan 2012), a simplified Hertz equation derived based on generalized mechanical properties of boulders and barriers is recommended as follows:

$$F=K_c\ 4{,}000\ v^{1.2}\ r^2 \quad (1)$$

Where r = radius of the boulder (in m) and v = impact velocity (in m/s). A load reduction factor (K_c) with a value of 0.1 is recommended to account for energy loss due to plastic deformation.

2 METHODOLOGY OF LARGE-SCALE IMPACT TESTS

2.1 General

Large-scale impact tests were carried out on AAC blocks and hollow concrete blocks to assess their cushioning performance. In each test, an impactor was set into pendulum motion. Near the lowest point of the pendulum motion, the impactor moved horizontally and impacted on the cushioning layer, which shielded the concrete wall behind. The impactor penetrated into the cushioning layer, then bounced back and forth, and eventually came to rest. The velocity of the impactor at the moment of impact, the deceleration of the impactor during impact, the transmitted load acting on the front face of the concrete wall and the maximum penetration depth at the area of impact were measured.

2.2 Cushioning Materials

In this study, each AAC block and hollow concrete block had dimensions of 0.6m x 0.2m x 0.1m. Based on laboratory measurement, the density of the AAC blocks and the density of the concrete used in the hollow blocks were 805.83kg/m^3 and 2002.76kg/m^3 respectively.

2.3 Impact Test Facility

A large-scale impact test facility occupying an area of 15 m × 6 m was developed for this study (Plate 1). It comprised a concrete sphere, which acted as the impactor, a steel frame which supported the impactor, a reinforced concrete wall and the cushioning material to be tested. The steel frame occupied a plan area of 5 m × 3 m, and has a height of 6 m. The impactor had a diameter of 1.16 m and a mass of 2,000 kg. The impactor was suspended from the steel frame by two steel strand cables attaching to two anchors installed on the impactor. Another anchor installed on the impactor was attached to a lorry crane, which elevated the impactor to a required height.

A release mechanism was employed to release the impactor from the lorry crane. The cushioning layer at the front of the reinforced concrete wall was secured by a steel sections along its periphery to limit lateral displacement. The reinforced concrete wall subjected to the impact tests was 3 m in height, 3 m in width, and 1.5 m in thickness.

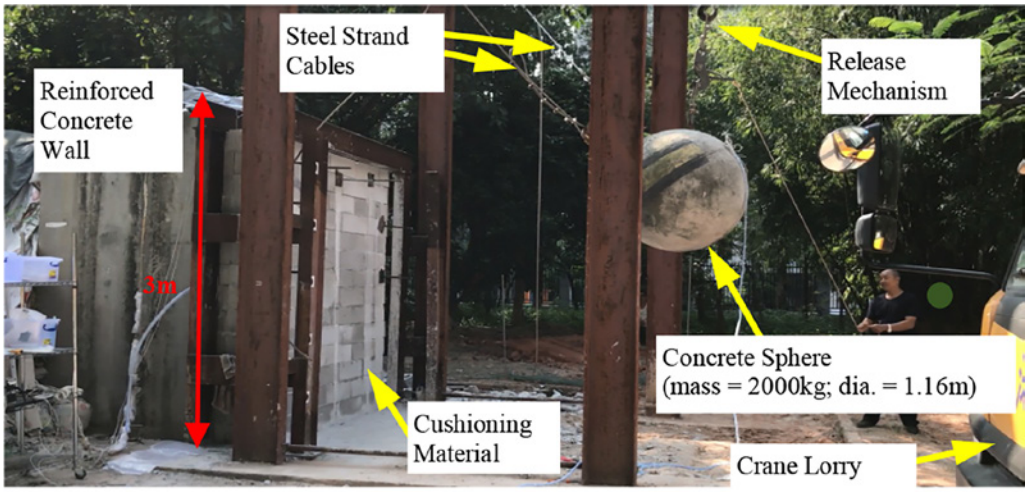

Plate 1: Side view of the large-scale impact test setup

2.4 Instrumentation

Eight load cells with a maximum measuring capacity of 220 kN and an area of 0.15 m x 0.15 m were installed on the reinforced concrete wall. The arrangement of the load cells is shown on Plate 2a. An accelerometer, with a maximum range of 5,000 g, where g is gravitational acceleration and a frequency range of 0.5-10,000 Hz, was installed on the impactor. The accelerometer is shown on Plate 2b. The impact velocity was estimated using a high-speed camera. The high-speed camera can capture up to 200 frames per second (fps). The impacts were also filmed with a video recorder capable of 30 fps.

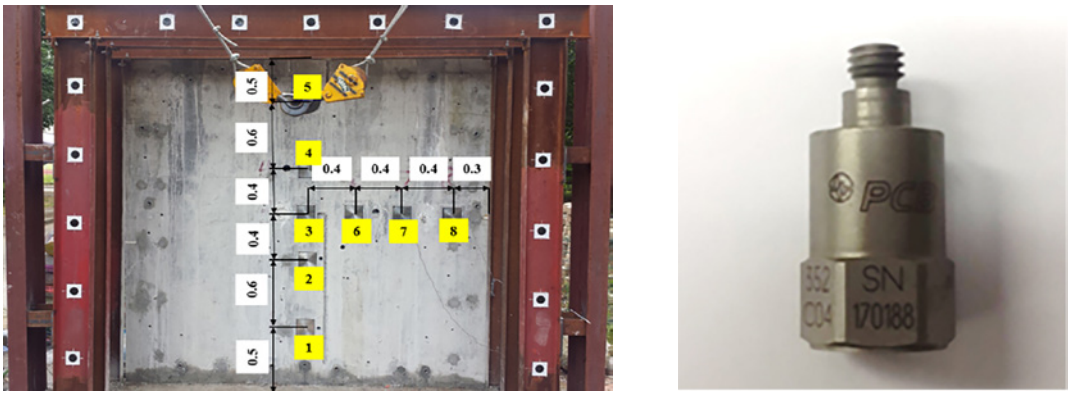

Plate 2: Instrumentation used in the large-scale impact tests. (a) Front view of the concrete wall, showing the distribution of load cells (dimensions in metre); (b) Accelerometer (PCB) installed on the impactor

2.5 Testing Schedule

A total of six large-scale impact tests were carried out in the study, one of which was conducted on hollow concrete blocks while the other five tests were conducted on AAC blocks with various layer thicknesses under an impact energy of 20 kJ or 70 kJ. Table 1 summarizes the details of the six tests.

Table 1: Testing schedule of the large-scale impact tests

Test ID	Cushioning Material	Thickness (mm)	Impact Energy (kJ)	Number of Impacts
HB_400(20)	Hollow Concrete Block	400	20	6
AAC_200(20)	AAC Block	200	20	3
AAC_400(20)	AAC Block	400	20	6
AAC_400(70)	AAC Block	400	70	6
AAC_600(20)	AAC Block	600	20	6
AAC_600(70)	AAC Block	600	70	6

The following data were recorded in each test: (1) cumulated maximum penetration depth into the cushioning layer; (2) time history of acceleration/deceleration of the impactor, measured by the accelerometer; (3) time history of load transmitted to the concrete wall, measured by each load cell; and (4) velocity of the impactor before impact, estimated using the high-speed camera.

3 TEST RESULTS

3.1 Deformation of Cushioning Layers

The deformations of the AAC block and the hollow concrete block cushioning layers (both 400mm in thickness) observed at the first and sixth impacts in the 20 kJ impact tests are shown in Plates 3a, 3b, 3c and 3d. After the first impact, the radii of the impact craters formed on the AAC blocks and the hollow concrete blocks were 0.22m and 0.24m respectively. Minor ring cracks were observed along the rim of the craters in both cushioning layers. After the sixth impact, the radii of the impact craters formed on the AAC blocks and the hollow concrete blocks increased to 0.28m and 0.40m respectively. Both ring cracks and radial cracks were observed around the craters. For the hollow concrete block cushioning layer, blocks within the impact crater had completely collapsed.

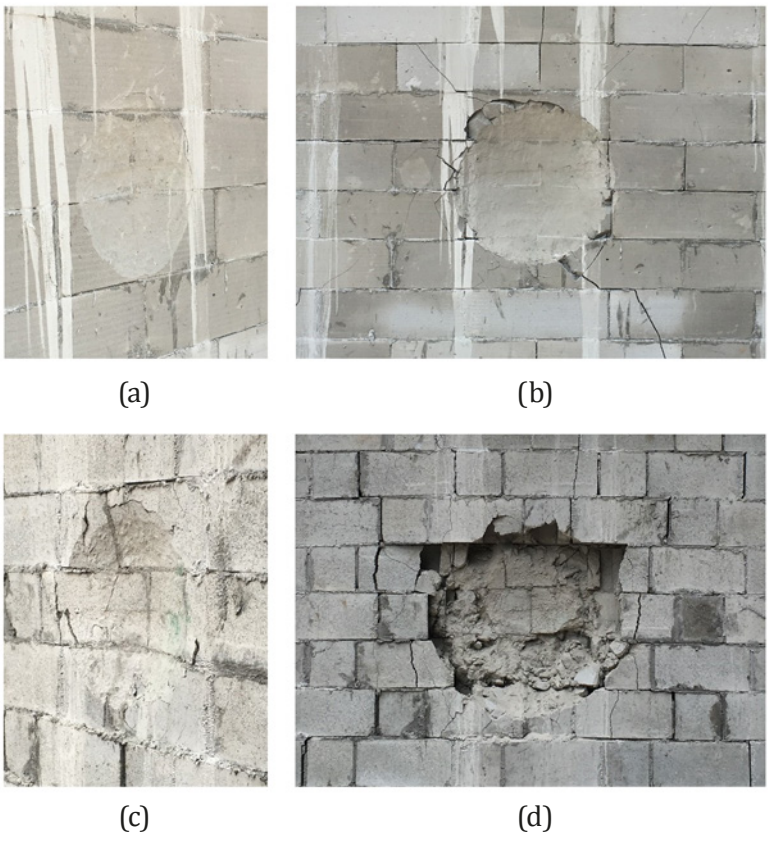

Plate 3: Deformation under impact energy of 20 kJ. (a) First impact of 400mm thick AAC block cushioning layer. (b) Sixth impact of 400mm thick AAC block cushioning layer. (c) First impact of 400mm thick hollow concrete block cushioning layer. (d) Sixth impact of 400mm thick hollow concrete block cushioning layer.

The maximum cumulated penetration depths were recorded near the center of the impact crater after each impact test. Figure 1a and 1b show the maximum cumulated penetration into the AAC block and the hollow block cushioning layers under this study, together with the maximum cumulated penetration into the gabion cushioning layer observed in similar large scale impact tests by Ng et al., 2016. Under an impact energy of 20 kJ, the maximum cumulated penetration into the 200 mm thick AAC block cushioning layer was higher than the 400 mm and 600 mm AAC block cushioning layer.

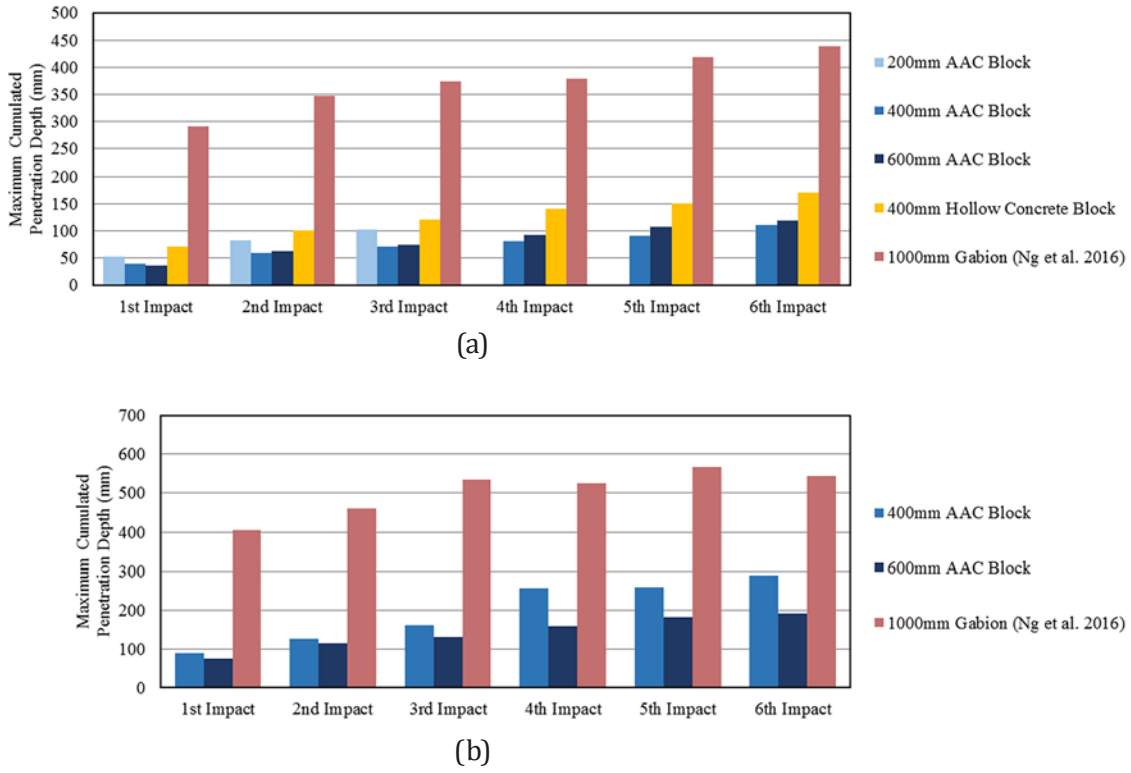

Figure 1: Maximum cumulated penetration depths into cushioning materials of large-scale impact tests; (a) under an impact energy of 20kJ; (b) under an impact energy of 70kJ.

Meanwhile, the maximum cumulated penetration into the 400mm and the 600 mm thick AAC blocks was less than the cumulated penetration into the 400mm thick hollow concrete blocks. In all the impact tests, the maximum cumulated penetration in the gabion cushioning layer was much larger than the penetration observed in the AAC block and the hollow concrete block cushioning layers. This was attributed to the rearrangement of the rock infill inside the gabion when subjected to impact.

3.2 Duration of Impact and Impact Force

The acceleration of the impactor was measured at a frequency of 10,000 Hz by the accelerometer. As the duration of the impact observed in this study was in the range of 0.01-0.03 s, the test data obtained was filtered to a frequency of 1,000 Hz (i.e. equivalent to a time period of 0.001 s, about one-tenth of the measured duration of impact). The filtered acceleration was used to compute the impact force induced by the impactor on the cushioning material.

The time history of impact force (under an impact energy of 20 kJ) for various cushioning materials were plotted in Figure 2. The cumulated loss in momentum of the impactor at time t' is equal to the integral of force with respect to time:

$$P(t') = \int_0^{t'} F(t)\, dt \qquad (2)$$

where P is the cumulated loss in momentum of the impactor, F is the impact force and t is the time after the impact begins. This is equivalent to the total area below each force-time curve.

Figures 2a and 2c show the time history of the successive impacts on the AAC blocks and the hollow concrete blocks of 400 mm in thickness respectively. From the plots, the duration of impact of the two cushioning materials were similar. The duration was about 0.023 s for the first impact and shortened to a range of 0.015 s - 0.02 s under successive impacts. The magnitudes of the impacts were also in similar range, with those of AAC block cushioning layer (about 720 kN at peak) slightly lower than those of hollow concrete block cushioning layer (about 770 kN at peak) at the first impact. The observed decrease in impact duration coupled with an increase in impact force under successive impacts were

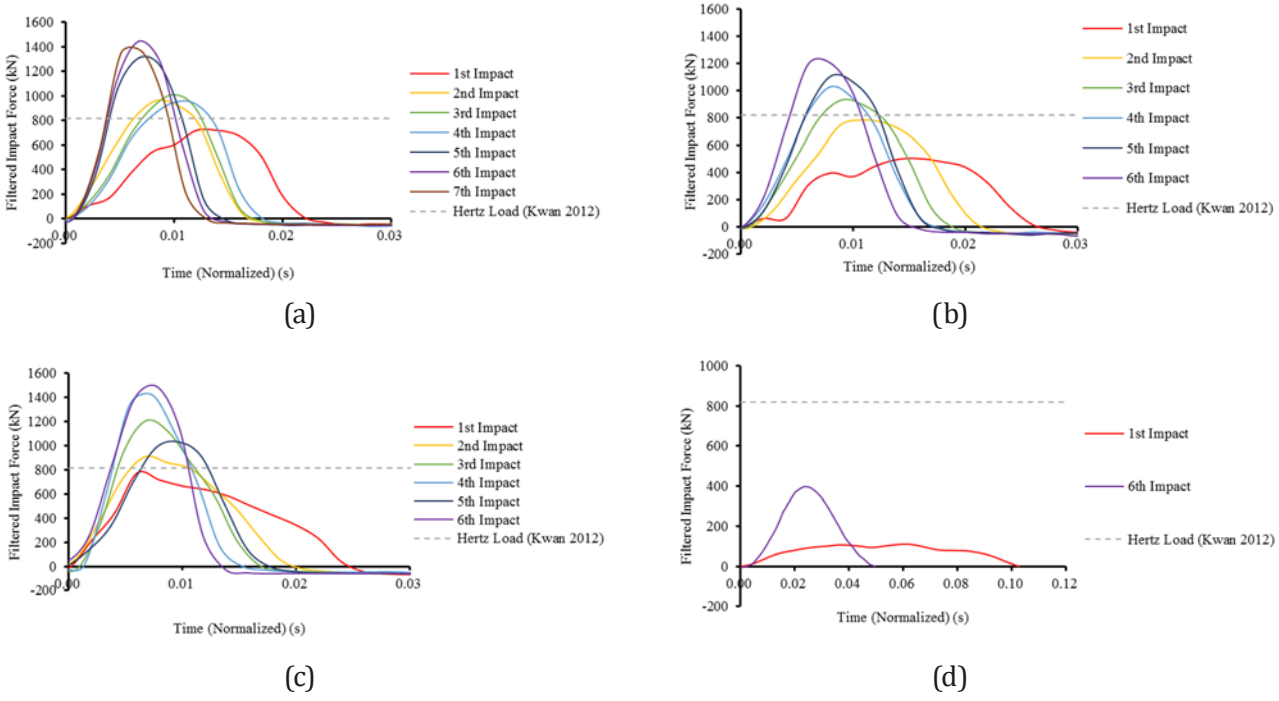

Figure 2: Time history of impact force of large-scale impact tests under an impact energy of 20kJ. (a) 400mm thick AAC block cushioning layer. (b) 600mm thick AAC block cushioning layer. (c) 400mm thick hollow concrete block cushioning layer. (d) 1000mm thick gabion cushioning layer (Ng et al. 2016)

attributed to the plastic deformation of the cushioning material upon impact, resulting in a denser and stiffer material, which was less effective in attenuating impact load.

Figure 2b shows the time history of the successive impacts on the 600 mm thick AAC block cushioning layer. At the first impact, the duration of impact (about 0.026 s) was slightly longer than those observed in the 400 mm AAC blocks (about 0.023s), coupled with a comparatively low peak impact force (about 500 kN). Same patterns were observed under the successive impacts.

Figure 2d shows the time history of the successive impacts on the 1,000 mm thick gabion cushioning layer. At the first impact, the impact duration was about 0.105 s with a peak impact force of about 110 kN. At the sixth impact, the duration was about 0.05 s with a peak impact force of about 400 kN.

In Figure 3, the peak impact forces acting on the AAC blocks and the hollow concrete blocks were compared with the peak impact forces acting on the 1,000 mm thick gabion blocks under an impact energy of 20 kJ (Ng et al. 2016).

From all the impact tests, the observed peak impact forces on gabions were significantly lower than those observed on the AAC blocks and the hollow concrete blocks.

3.3 Translational Kinetic Energy

Ng et al. (2016) defines the translational kinetic energy percentage P_d for large-scale pendulum impact tests as:-

$$P_d = \frac{I_r}{I_t} \times 100\% \quad (3)$$

where I_r is the translational kinetic energy calculated as half the product of the mass of the impactor and the square of the velocity of the impactor and; I_t is the kinetic energy of the impactor before impact.

P_d provides an indication on the rate of energy transferred in the cushioning layer. To compare the rate of energy transfer of AAC block and gabion cushioning layers, a graph of P_d against time was plotted and presented in Figure 4. The velocity of the impactor immediately before impact was estimated by the high speed camera. In the graph, the slope of the steepest part of each curve represents the maximum

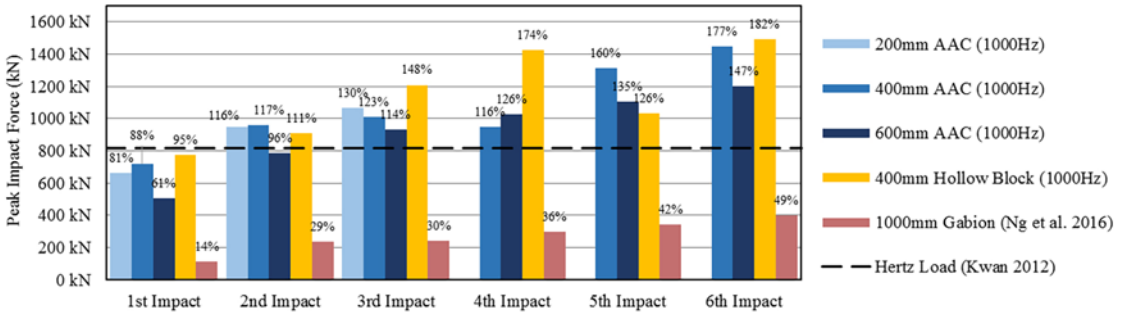

(a)

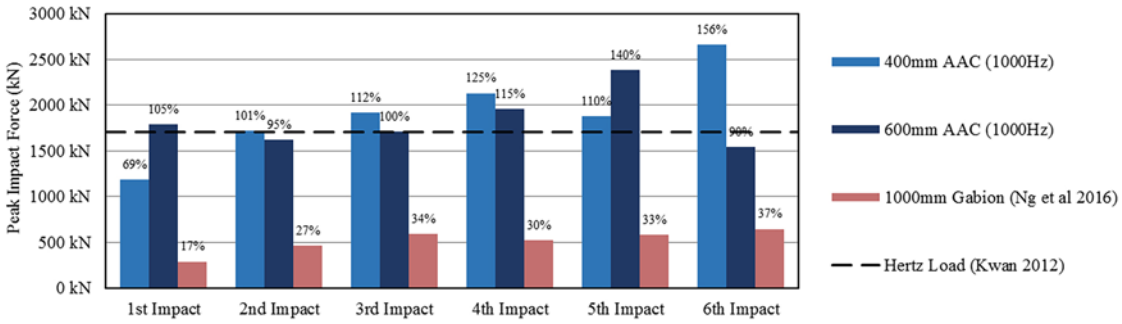

(b)

Figure 3: Peak Impact Force of large-scale impact tests; (a) under impact energy of 20kJ. (b) under impact energy of 70kJ

rate of energy transfer at that impact. It appears that the rate of energy transfer at the sixth impact is significantly higher than the first impact. This is likely due to densification of the cushioning layer with successive impacts. Meanwhile, the rate of energy transfer of both the first and sixth impacts of 600 mm thick AAC block cushioning layer is much higher than that of 1,000 mm thick gabion cushioning layer. In gabions, energy was dissipated by the rearrangement, shearing and crushing of rock infill, and deformation of the wire mesh. In the case of the AAC blocks, energy was dissipated by plastic deformation and crushing of the foamed concrete.

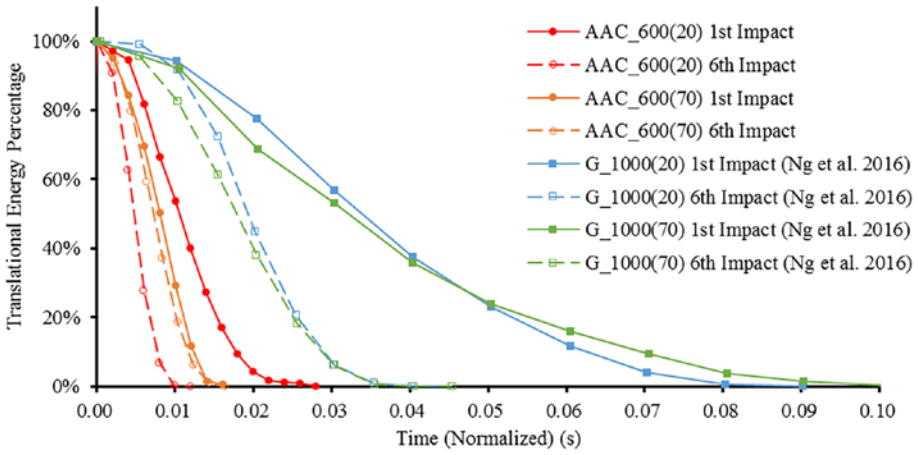

Figure 4: Translational energy percentage of large-scale impact tests on 600 mm thick AAC blocks and 1,000 mm thick gabion

3.4 Transmitted Pressure

The load cells measured the loads transmitted to the reinforced concrete wall at a frequency of 10,000 Hz. The peak transmitted loads under the successive impacts were determined from the time history of the load measurement obtained from the individual load cells. The peak transmitted pressure was calculated by dividing the peak transmitted load by the contact area of the load cell (0.15 m x 0.15 m). From the 20 kJ impact tests on the 600 mm thick AAC block and the 1,000 mm thick gabion cushioning layers, the peak transmitted pressures were plotted in Figure 5.

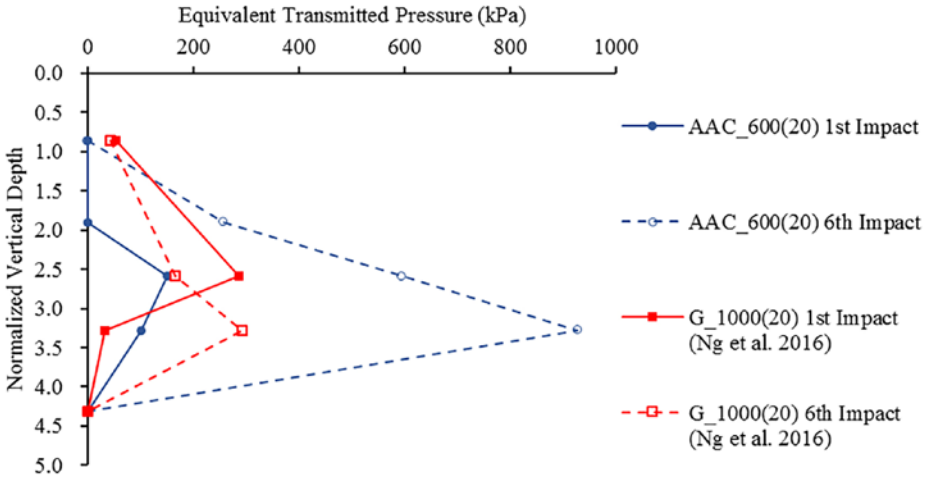

Figure 5: Vertical distribution of peak transmitted pressure acting on the concrete wall under an impact energy of 20kJ

For comparison, the peak transmitted pressures detected by the load cells installed behind the AAC block, the hollow concrete block and the gabion cushioning layers under 20 kJ and 70 kJ large-scale tests were plotted in Figure 6.

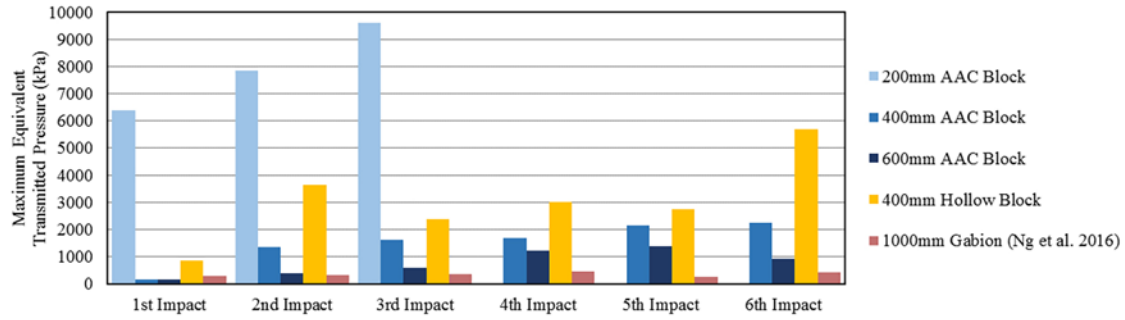

(a)

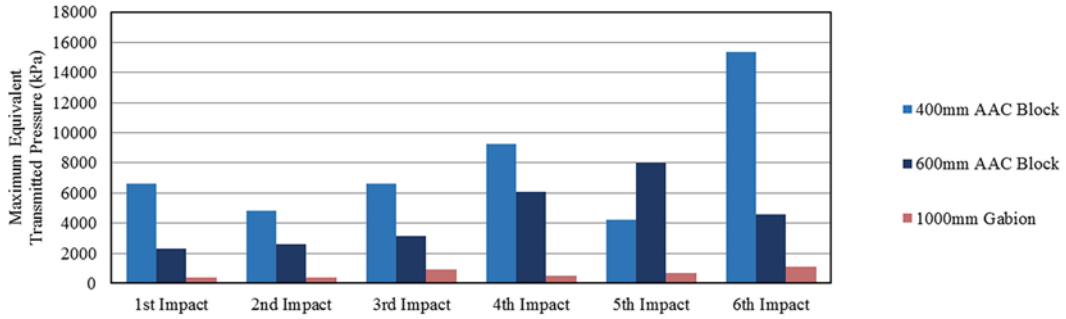

(b)

Figure 6: Peak transmitted pressure detected by the load cells of large-scale impact tests; (a) under 20 kJ impact energy (b) under 70 kJ impact energy

In Figure 6a, under successive impact, the peak transmitted pressures behind the 200 mm thick AAC block cushioning layer were substantially higher than the rest of the cushioning layers, indicating that the 200 mm thick AAC block may not be an appropriate thickness for cushioning layer. As the peak transmitted pressures behind the 400mm thick hollow concrete block cushioning layer were also significantly higher than the peak transmitted pressures behind the 400mm thick AAC block cushioning layer, the hollow concrete blocks may not be as effective as the AAC blocks of the same thickness in reducing impact forces.

For the successive impacts on the AAC block cushioning layers, the transmitted pressure acting on the concrete wall generally reduced with increased AAC block thickness. In the 70kJ impact tests (Figure 6b), the diminished cushioning effect of AAC blocks was observed in the early successive impacts. Considering the relatively high stiffness of the AAC block in comparison with the gabions, it is expected that the diminishing cushioning effect of the gabion would be less prominent.

4 CONCLUSIONS

Based on the large-scale impact tests conducted on the hollow concrete block and the autoclaved aerated concrete (AAC) block cushioning materials, the impact forces induced by the impactor, the cumulated penetration depths into the cushioning layer, and the transmitted pressures acting on the concrete wall were determined. It was acknowledged that the tested cushioning materials served their purpose of protecting the concrete wall from damage, as no cracks or fissures were observed on the concrete wall after the individual impact tests.

The test results also indicate that under successive impacts, the AAC blocks are more effective than the hollow concrete blocks in reducing the transmitted pressures on the concrete wall. It was observed that the transmitted pressures acting on the wall were well below the typical compressive strength of the concrete. If the concrete wall was hit by the impactor without any protection, the impact pressure would have induced indents and cracks on wall surface.

Based on results of the study, the AAC block is considered a suitable alternative cushioning material for concrete barriers, with the advantages of being light weight, ease of handling and installation, lower construction cost, and occupying less space in the barrier for higher retention capacity.

Further studies are recommended to establish suitable design guidelines for the cushioning layers in order to optimize the structural design of reinforced concrete debris-resisting barrier.

ACKNOWLEDGEMENTS

This paper is published with the permission of the Head of the Geotechnical Engineering Office and the Director of Civil Engineering and Development, the Government of the Hong Kong Special Administrative Region.

REFERENCES

Chen J., Wang Q.C., Chen Y.Q. & Li J. 2017. Amending calculation on impact force ob boulders in debris flow based on Hertz theory. *Journal of Harbin Institute of Technology,* 49(2): 124-129.

Goodier, J.N. & Timoshenko, S.P. 1970. *Theory of elasticity:* 383-384. McGraw-Hill Book Company Inc. New York, Toronto, London.

GEO. 1993. *Guide to retaining wall design (Geoguide 1):* 96-97. Geotechnical Engineering Office, Hong Kong.

GEO. 2012. *GEO technical guidance note no. 35 detailing of rigid debris-resisting barriers*. Geotechnical Engineering Office, Hong Kong.

Ho, H.Y. & Roberts K.J. 2016. *Guidelines for natural terrain hazard studies (GEO report no. 138 second edition)*. Geotechnical Engineering Office, Hong Kong.

Hungr, O., Kellerhals, R. & Morgan, C. 1984. Quantitative analysis of debris torrent hazards for design of remedial measures. *Canadian Geotechnical Journal,* 21: 663-677.

Hungr, O., Slaymaker, O. & Zhang, S. 1996. The calculation of impact force of boulders in debris flow. *Debris flow Observation and Research.* Edited by R. Du. Science Press, 6: 67-72

Klingner, R. 2008. Autoclaved aerated concrete. In S. Mindness, *Developments in the formulation and reinforcement of concrete:* 1-42. Woodhead Publishing; Maney Publishing; CRC Press

Kwan, J.S.H. 2012. *Supplementary technical guidance on design of rigid debris-resisting barriers (GEO report no. 270).* Geotechnical Engineering Office, Hong Kong.

Ng C.W.W., Choi C.E., Su A.Y., Kwan J.S.H. & Lam C. 2016. Large-scale successive boulder impacts on a rigid barrier shielded by gabions. *Canadian Geotechnical Journal,* 53: 1688-1699.

Poon, C.S., Yu T.W. & Ng L.H. 2001. *A guide for managing and minimizing building and demolition waste*. Research Centre for Urban Environmental Technology and Management, Faculty of Construction & Land Use, The Hong Kong Polytechnic University.

A Field Trial for Interlocking Pipe Piles

Victor Li
Victor Li & Associates Ltd, Hong Kong

Annie Ho and Charles Lo
China State Construction Engineering Co., Ltd., Hong Kong

ABSTRACT

The paper discusses the problems associated with the current practice for installation of pipe piles in Hong Kong. It presents details of a recently completed field trial in which interlocking pipe piles with sealant in the joints were used to form an embedded wall and the recently developed Spiral Flush drillbit was used for installing the pipe piles. The aim of the trial was to find out if such new techniques and equipment can eliminate or reduce some of the problems in construction of pipe pile wall. The results of the trial confirm that interlocking pipe piles do offer a practical alternative to conventional system of pipe pile wall with grout curtain.

1 INTRODUCTION

In Hong Kong, pipe piles are commonly used as embedded walls for cofferdams in infrastructure projects especially when percussive driving is not feasible due to unsuitable ground conditions (e.g. presence of corestones) or proximity of adjacent sensitive structures prone to damage by construction vibration. When the water table is high, water-tightness of the pipe pile wall is commonly achieved by means of grout curtain installed behind the pipe piles and also the lagging wall above the excavation level (Figure 1).

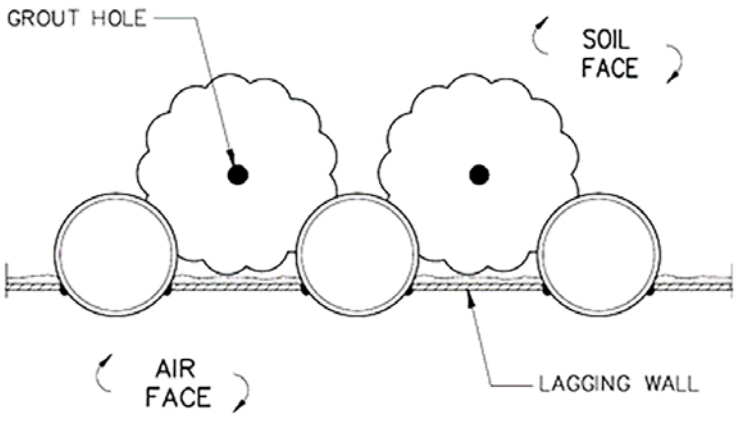

Figure 1: Typical details of pipe pile wall

2 CONSTRUCTION OF PIPE PILE WALL

Sometimes, there are problems associated with the conventional pipe pile wall due to the following causes:

2.1 Effectiveness of grout curtain

The functions of the grout curtain are to provide water-tightness of the cofferdam and enhance the arching effect of soils to maintain temporary stability of the unsupported vertical cutting necessary for installation of the lagging wall. Tube-a-manchette (TAM) grouting is commonly used for the grout curtain. There are often situations where TAM grouting is not effective, such as when clay soil or rockfill is present or when there is a potential for high velocity flow of groundwater (e.g. close to seawall). When TAM grout curtain cannot achieve its intended functions, large inflow of water into the site or excessive oozing of soils through the pipe piles can occur before the lagging wall is installed. Plate 1 shows a photograph of pipe pile cofferdam located close to the seashore. Grouting was not effective at a particular spot between pipe piles with rockfill behind them, leading to uncontrollable inflow of water flooding the site.

Plate 1: Photograph of a flooded cofferdam caused by leakage through pipe piles

There is a similar case history of another site also located close to the shoreline, but the inflow of water was through springheads formed at the base of cofferdam after reaching the final excavation level. The water inflow was initially small and manageable by just a few small pumps. However, more springheads were formed with time. The inflow rate of water in the new springheads gradually increased and finally became too large to be manageable by more and larger pumps. In the event, the contractor vacated the site, allowing the whole cofferdam to be inundated. The rate of rise in water within the cofferdam was recorded during inundation, giving an estimate of 1500m^3/hr at peak flow. It is believed that the TAM grout curtain was not effective at some locations behind the embedded wall, causing subsurface flow of water into the site beneath the final excavation level. The water flow progressively eroded the soils underneath the cofferdam causing soil pipes to be formed and manifested themselves as springheads within the site. With time, the soil pipes might have increased in size and extended laterally to reach the highly permeable fill materials behind the seawall located close to the site. The open sea would then provide a plentiful supply of water for flooding the site.

2.2 Installation of pipe piles

In Hong Kong, pipe piles are usually installed using drillbit operated by compressed air. The required air pressure for operating the drillbit and for flushing the cutting is usually over 10 bars (or 1000 kPa). In the past, the so-called Odex system (which stands for overburden drilling excentric)

is almost exclusively used for installation of pipe piles. The Odex drillbit comprises a pilot bit and an excentric reamer. During the down-stroke mode, the excentric reamer will swing out to drill a hole larger than the external diameter of the pipe pile to enable the pipe pile to advance in phase with the pilot bit. It is not difficult to imagine that the combined effect of the protruded excentric reamer and high air pressure can cause significant overbreak of soils during installation of the pipe pile. A common form of soil overbreak is the formation of an annular void outside the pipe pile. One could often see water and/or air bubble gushing up the void. Worst still, sinkholes may be formed as a result of collapse of large soil cavities formed by soil overbreak. Plates 2 and 3 show a masonry wall with a surface settlement of over 0.5m and an example of a sinkhole respectively, both caused by installation using Odex drilling.

Plate 2: Settlement caused by Odex drilling

Plate 3: Sinkhole caused by Odex drilling

Odex drilling is no longer accepted by the Buildings Department for private development projects. The so-called "concentric method" of drilling is now used as replacement, but the term is not clearly defined. Many vastly different drilling systems are claiming to be employing the "concentric method" of drilling. It is often asserted by contractors or suppliers that the "concentric method" performs better than the Odex method because (a) the drillbit for the "concentric method" will protrude less outside the pipe pile during drilling and (b) the concentric drilling system is designed to allow the majority of exhaust compressed air to safely return to the ground surface through the inside of the pipe pile. Unfortunately, significant ground loss or sinkholes are still observed from time to time and exhaust air is still often seen escaping out of the pipe piles.

The "concentric method" of drilling is still a risky operation although it is better than Odex drilling. The root problem may be attributed to the fact that in most drillbits for the "concentric method" of drilling, the nozzle of the air jet flushing the cuttings is still directed downwards as shown in Figure 2. The vertical air jets with high velocity may cause significant overbreak of soils around the tip of the pipe pile, thereby creating a path for compressed air to escape out of the pipe pile.

Figure 2: Discharge of compressed air in drillbit for "concentric method" of drilling

Plate 4 shows a photograph of a huge raking shore used to support a tilted building. The tilting was apparently caused by the installation of socketed H-piles close to the building, which also employed the "concentric method" of drilling used for installation of steel casing.

Plate 4: A raking shore supporting a tilted building

3 RECENT DEVELOPMENTS IN HONG KONG

There have been recent attempts by local contractors to introduce new techniques or equipment for installation of pipe piles which can hopefully eliminate some of the problems discussed above. Some recent developments are described below.

3.1 Interlocking pipe piles

Interlocking pipe piles are quite common overseas. The O-pile system developed by the PilePro Group in USA is one such system. Interlocking pipe piles have only been used in very few occasions in Hong Kong.

A field trial on installing interlocking 610mm diameter pipe piles using the O-pile system has recently been conducted by China State Construction Engineering Co. Ltd. (CSCE) in 2017 in Hong Kong. The salient features of O-pile system used in the trial include:

- 7 pipe piles were installed to a depth of 24m. The top 5m of soil profile is fill material which is underlain completely decomposed granite with corestones.

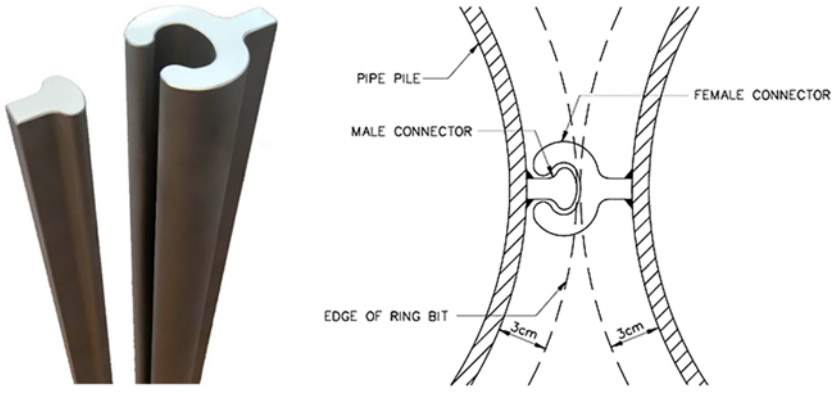

(a) (b)

Figure 3: Connectors for interlocking joint

- The WOM-S type connectors developed by the PilePro Group are used for forming the interlocking joints (Figure 3). The connectors are one of the smallest connectors available in the market but sufficiently strong to withstand the induced stress during installation and to hold the adjacent pipe piles together. The heights of the male and female connector are about 3cm and 6cm respectively.
- The connectors are fixed onto the pipe piles by fillet welds. The connector is initially held in position along the design alignment by intermittent spot welding. To avoid warping of the connector, it is important that fillet welding is carried out on both sides of the connector in phase by two welders.
- To install pipe piles with a male connector, an oversized ring bit needs to be installed at the bottom of the pipe pile to create a larger drillhole to accommodate the connector. Plate 5 shows the ring bit supplied by the Mincon Group used in the trial. The Mincon ring bit is oversized by 3cm and it creates a drillhole large enough to accommodate a 3cm high male connector. For this reason, only male connectors can be used in the first pipe pile to be installed. The ring bit has roller bearings and it can rotate while the pipe pile is held stationary. During excavation, the drillbit will engage the ring bit to rotate in phase when cutting through soils and rocks. Once a pipe pile with male connector(s) is in place, the larger female connector in the next pipe pile will fit onto the male connector as shown in Figure 3(b). Since half of the female connector will be located within the gap already created when installing the pipe pile with male connector(s), a ring bit oversized by 3cm will also be enough for installing the pipe pile with a female connector. The same Mincon ring bit can therefore be used for installing pipe piles with male or female connectors as long as the sequence of pipe pile installation is well planned.

Plate 5: A Mincon ring bit connected to pipe pile

There are limited case studies of interlocking pipes in Hong Kong. Plate 6 shows the O-pile system used for horizontal pipe pile in a tunneling project in Hong Kong.

Plate 6: O-pile system for a tunneling project in HK (Courtesy of Mincon Group)

Plate 7: Interlocking pipe piles for a tunnel connection (Courtesy of GCL)

Other interlocking joints have been used in Hong Kong for installation of pipe piles. Plate 7 shows the interlocking joints used for horizontal pipe piles for forming a tunnel connecting a shopping mall and the Tsim Sha Tsui MTR station and Figure 4 shows a patented system of interlocking joint developed by Gammon Construction Ltd. (GCL), which has been used for the project of Lyric Theatre Complex in West Kowloon Cultural District.

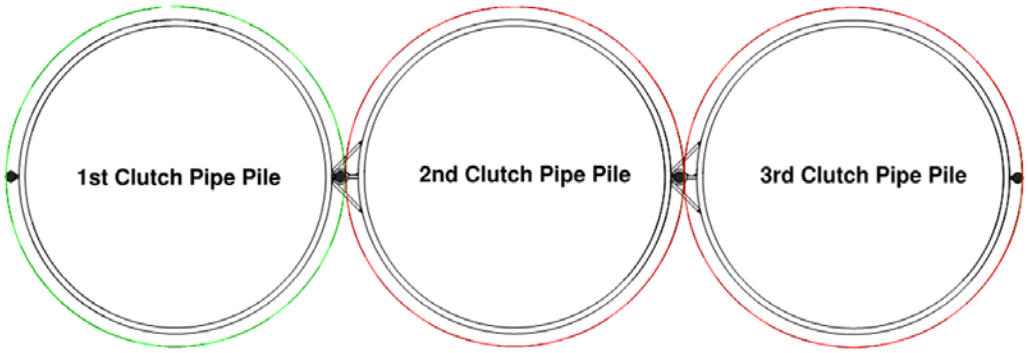

Figure 4: Interlocking joint system developed by GCL (Courtesy of GCL)

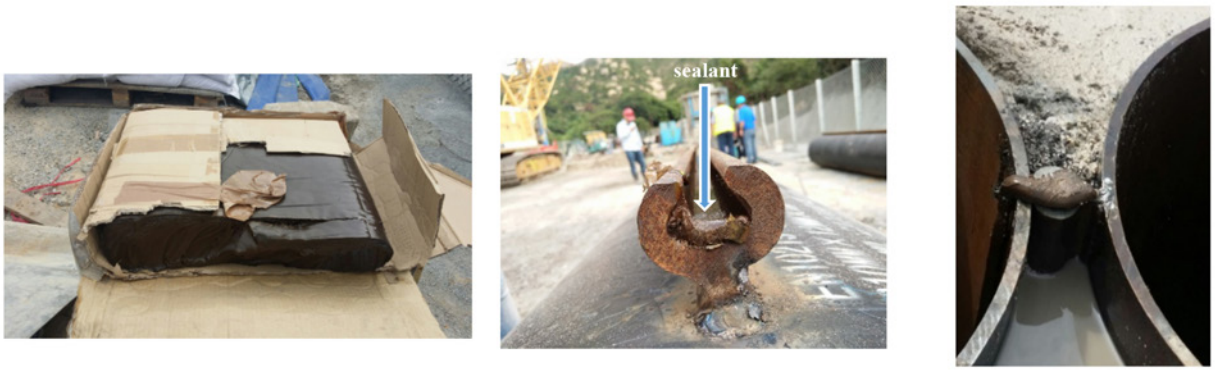

Plate 8: Wadit sealant for improving water-tightness of interlocking joints

3.2 Sealant for interlocking joints

Sealants can be used in the interlocking joint to further improve the water-tightness of pipe piles. In the field trial by CSCE, the sealant product Wadit supplied by the PilePro Group was used. It is a highly plastic material of wood resin with a melting point of about 140oC (Plate 8a). The molten Wadit can be poured into and half-fill the female connector before installing the pipe piles (Plate 8b). After cooling,

the Wadit sealant will adhere strongly to the female connector and tend to stay within it despite large displacement. During installation of pipe piles, the male connector will displace the sealant in the female connector such that the sealant will completely fill up the interlocking joint (Plate 8c).

The Wadit sealant was found to be effective. During the field trial by CSCE, no water seepage through the sealed interlocking joint was observed after the installed pipe piles had been exposed to level below the groundwater table. It is worth mentioning that the use of sealant will not reduce the wall stiffness of pipe piles.

3.3 Choice of drilling system

The choice of drillbit has a significant effect on ground disturbance. The Spiral Flush drillbit (Figure 5) recently developed by the Mincon Group was tested in the field trial by CSCE. This new drillbit possesses some good features. Firstly, the Spiral Flush drillbit is practically flush with the ring bit and this can reduce the risk of soil overbreak and leakage of compressed air out of the pipe pile. Secondly, the nozzle for release of compressed air is placed horizontally and thus has a lower risk of overbreak than a drillbit with vertical nozzles. The horizontal nozzle also makes the exhaust air more likely to return to the ground surface through the inside of the pipe pile. The field trial by CSCE confirms that the Spiral Flush drillbit tends to produce less ground disturbance and leakage of air than other more commonly used drillbits in Hong Kong. However, the rate of rock excavation was found to be slower although more field trials are needed to explore the optimum combination of equipment for gaining the maximum efficiency of the Spiral Flush drillbit.

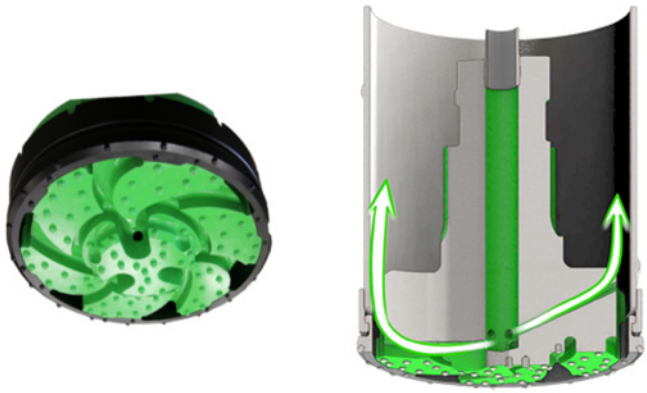

Figure 5: Spiral Flush drillbit

Most drilling systems for installation of pipe piles adopted in Hong Kong use compressed air as the flushing medium for removal of cuttings. To this end, the discharge point of compressed air needs to be at the drillbit. There is therefore an inherent risk that compressed air may leak out of the pipe pile.

A better system is to use water as the flushing medium to remove the cuttings by air-lifting. The discharge point of compressed air for air-lifting needs not be very close to tip of the pipe pile, making leakage of compressed air less likely. Although such systems have been available in the market for some years, they are still not common in Hong Kong because of its higher cost. Figure 6 shows a system developed by HD Engineering Ltd. that uses reverse circulation of water for removal of cuttings and is quite popular in Australia, New Zealand, America and more recently in Singapore. Plate 9 shows the drillbit for this system. In this system, a double-wall drill pipe is used for operating the drilling system. The compressed air is fed into the outer pipe which then removes the cuttings by air-lifting through the inner pipe to a controlled discharge point or a sedimentation tank.

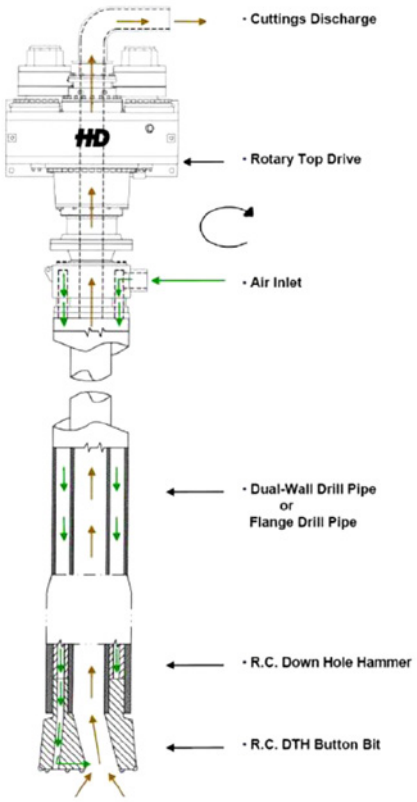

Figure 6: A reverse circulation system for drilling
(Courtesy of HD Engineering Ltd.)

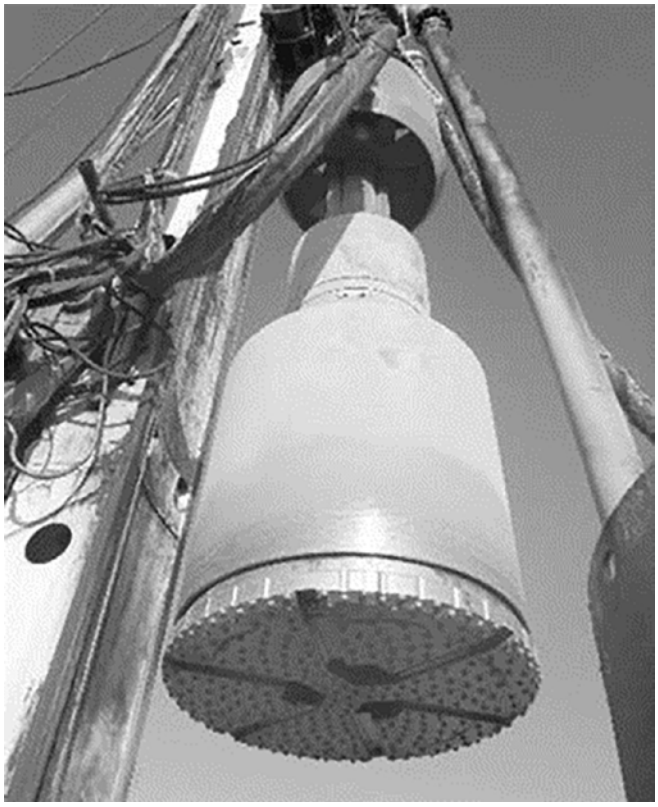

Plate 9: Drillbit for reverse circulation system
(Courtesy of HD Engineering Ltd.)

Figure 7 shows a system named Closed Air Loop Drilling method developed by GCL, which also uses water as the flushing medium. A triple-wall drill pipe is used in this system. Compressed air and water are fed through the triple-wall pipes and the cuttings are removed by air-lifting through the space between the drill pipe and the pipe pile. As the double-wall or triple-wall drill pipe requires more space, the system described in Figures 6 and 7 can only be used for installing larger pipe piles of 610mm or larger in diameter.

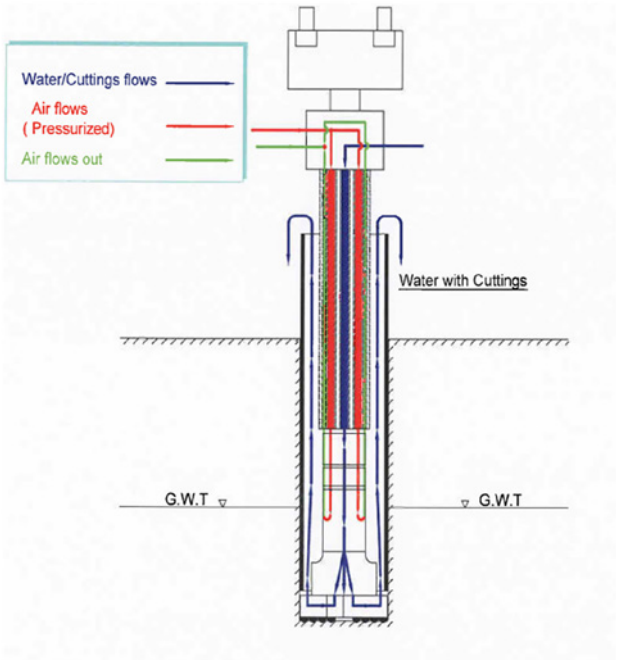

Figure 7: Closed Air Loop Drilling (Courtesy of GSL)

4 EFFECT ON GROUND SETTLEMENT

There is a common perception that significant ground settlement may occur when installing interlocking pipe piles with an oversized ring bit. If one assumes that the closing up of the annular gap is due to movement of the soil profile under constant density, the associated volume change of soils may lead to significant ground settlement around the pipe piles. Experience shows that it is not the case.

It is worth pointing out that a circular drillhole can be quite stable due to arching effect of soil. Lam & Li (2003) reported a case history in which a stable pile bore of 2m in diameter could be formed in a fill layer after extraction of temporary casing for a depth of over 20m. As explained by Lam & Li (2003), a very low radial stress will be sufficient to maintain permanent stability of the drillhole. If this is the case, radial movement of the drillhole will be arrested when there are very loose materials filling up the annular void.

Some observations from the field trial by CSCE are worth noting. As usual, the spoils flushed out of the pipe pile were being continuously deposited around the pipe pile during installation. When the spoils were removed, there was no visible gap observed around the pipe pile installed by the oversized ring bit. There was no difficulty for the pipe pile with a female connector to slide along the male connector of a previously installed pipe pile. It is believed that the loose spoils deposited around the pipe pile will be dragged into the annular void during advance of the pipe pile. The spoils filling up the annular void must be in relatively loose state. Otherwise, it may be difficult to install a pipe pile with female connector.

The field trial by CSCE confirms that the settlement associated with installation of the interlocking pipe piles is not worse than the total settlement associated with the conventional pipe piling works with grout curtain. The induced settlement is short-ranged and becomes negligible at a distance of over 2m from the pipe pile. The most important thing to prevent ground settlement is to minimize the ground loss and sinkhole caused by compressed air leaking out of the pipe piles. The culprit is the inappropriate choice of drilling method and not the oversized ring bit.

5 CONCLUSIONS

Interlocking pipe piles offer a robust type of embedded wall for cofferdams in terms of water tightness and safety during bulk excavation. The use of water sealant can further enhance the water-tightness of the interlocking joints. The effect of ground disturbance can be minimized by using a suitable system of drilling.

Although interlocking pipe piles have been used for a long time in a range of applications overseas, it is still not widely used in Hong Kong due to the higher cost of the equipment and accessories. Interlocking pipe piles are particularly useful for situations when water-tightness cannot be provided by grout curtain (e.g. marine cofferdam) or when the soil conditions will render the grout curtain not effective (e.g. rockfill). The recent field trial conducted by CSCE and some of the projects successfully completed by GCL confirm that it is practical to use interlocking pile piles for construction of cofferdams.

ACKNOWLEDGEMENTS

The authors are grateful to Mr. Jukka Ahonen of Mincon Group and to Mr. Falco Chu of Unicon Ltd. in providing the diagrams and photographs in Figures 2, 3 and 5 and Plate 6 and their technical assistance in conducting the field trial; to Messrs. C.C. Wai, Alan Wan and Samson Lam of Gammon Construction Ltd. for permission to use the photograph in Plate 7 and figures in Figures 4 and 7 and providing technical information of their Closed Air Loop Drilling; and to Mr. C.S. Cheng of HD Engineering Ltd. for providing the information of the reverse circulation system for installation of pipe piles shown in Figure 6 and Plate 9.

REFERENCE

Lam, J. and Li, K.S. (2003). Influence of construction method on shaft friction of bored pile – a case study. Proc. HKIE Geotechnical Division Annual Seminar, 143-152.

Geotechnical Design & Construction Considerations, Gold Line Metro, Doha, Qatar

A.D. Mackay
HSS Integrated, Kuala Lumpur, Malaysia

ABSTRACT

The Gold Line Metro, Doha, Qatar is the largest Doha Metro Contract, totaling US$ 4.5 billion capital cost at project initiation. It is presently due for completion 2019 ahead of the Qatar World Cup, 2022. It comprises a total of 32 kilometre (km) twin bore tunnel drives; 10No. stations with one Emergency Exit Shaft, 20No. subway connections, up to 15m span and totaling 4km length, and 42No. cross passages. The tunnels were driven by six Herenknecht, Earth Pressure Balance (EPB), tunnel boring machines (TBM) and the subways constructed using cut and cover and sequential excavation methods. The paper provides a published overview of the metros constructed in Doha, which at their peak had 36No. on-going Earth Pressure Balance (EPB), TBM drives totaling US$ 36 billion capital cost. An overview of the ground conditions encountered along the Gold Line Metro is provided and the challenges for the TBM tunnel drives and cross passage construction are described, these included the station break in and break-outs, the presence of karstic limestone formation and highly variable groundwater pressures, typically associated with karst formation coinciding with areas of relatively low lying topography.

1 INTRODUCTION

The Doha Metro is scheduled to be in operation towards the end of 2019 with locomotive speeds reaching 100km/h. The metro system will eventually accommodate four lines with an approximate overall length of 300 km and about 100 stations and will include long-distance rail passengers and freight links. The initial Phase 1 of the metro operation includes the Red, Green and Gold Lines, which run from a central interchange located at the Msheireb Station. The tunnels are formed by a total of 21No. Herenknecht TBMs. The Blue Line, Phase 2, which is to be constructed at a later date, will provide a semi-orbital service (Wikipedia 2018). Refer to Figures 1 for the Red, Gold, Green and Blue metro alignments and Figure 2 for the Gold Line alignment and stations.

Figure 1: Metro Locations (Doha)

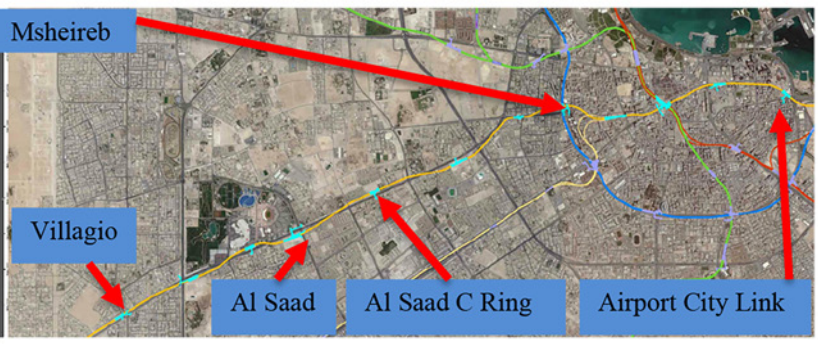

Figure 2: The Gold Line Metro, presenting station locations (blue)

The design and construction of the Gold Line Metro was awarded to a joint venture consortium of Larsen & Toubro, Aktro, Yapi Merkezi, STFA Group and Al Jaber Engineering (ALYSJ JV) during May 2014.

This paper provides a published overview of the ground conditions encountered along the tunnel alignment, comprising the uppermost Simsima Limestone and underlain by the Midris and Rus Formations. The main challenges for the tunnel drives and station break in and break-outs included the presence of karst (cavities) and chert nodules, generally located immediately above the Midris Formation. Highly variable groundwater pressures were typically associated with the karst formations and areas of relatively low lying topography. An overview of the contract team and interfaces and the design and construction approaches for the temporary works, for the TBM drives and cross passages is provided.

2 CONTRACT TEAM AND INTERFACES

To construct the project within the allocated budget and time frame a consistent communication and interface processes with all parties was required. The JV employed 7500 staff mobilized from 35 different nations, with different cultures, approaches & experiences, 450 of these staff had specific tasks and interface requirements identified in the project organization chart and resource documentation. 14No. key personnel, requiring specific qualifications and experience, were allocated in the Employers Requirements as agreed with the Client and the Client's Project Management Consultant (PMC).

Key interfaces outside the JV included the Client (Qatar Rail) and their representative PMC, key stakeholders such as government stakeholders, utility owners (Ashgal) and on-going infrastructure project liaison groups, such as the IDRISS tunnel. The contractor interfacing for other sections of the metro construction involved the Metro Systemwide and the Blue Line Msheireb Station advance works Contractors. Support parties included numerous specialist Sub-contracts and designers. Examples of the key interfaces, reporting structure and consultant and sub-contractor support and lines of communication are provided in Figures 3 and 4.

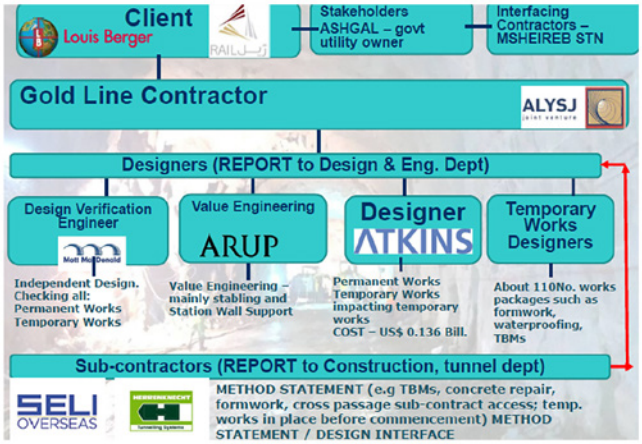

Figure 3: JV Support; designers, contractors and client

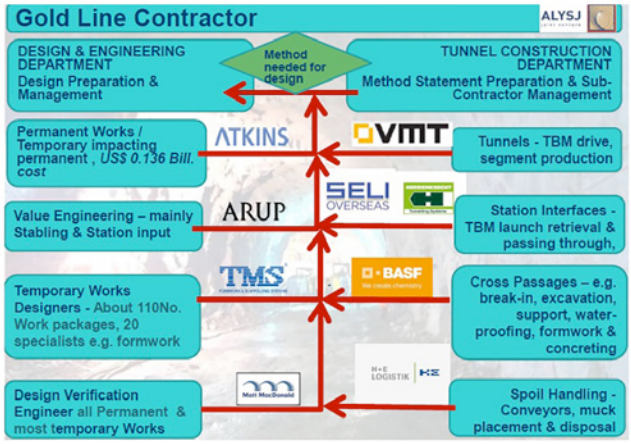

Figure 4: JV Support; designer / contractor interface

3 GROUND CONDITIONS

The Qatar Peninsula is formed from a suite of carbonaceous sedimentary rocks located on the eastern fringes of the Arabian Shelf. The Peninsula was originally formed by an uplift of the marine sediments above sea level during the Oligocene Geological period (34 – 23 Ma, Alsharhan et al, 1994) forming an anticline with an axis trending north to south along the centre of the peninsula. This anticline is referred to as the Qatar Arch (See Figure 5, West et al, 2006). The majority of the Qatar Peninsula is overlain by the Sabkha, evaporite and carbonaceous deposits.

Doha is located on Qatar's eastern coastline of the Qatar Peninsula. The topography is level, rising to 40m above sea level (asl) further inland and influenced by depressions in the ground, such as ephemeral stream courses (Wadis). Refer to Figures 6 and 7 for the topographic elevation, depressions and sinkholes in the Doha vicinity.

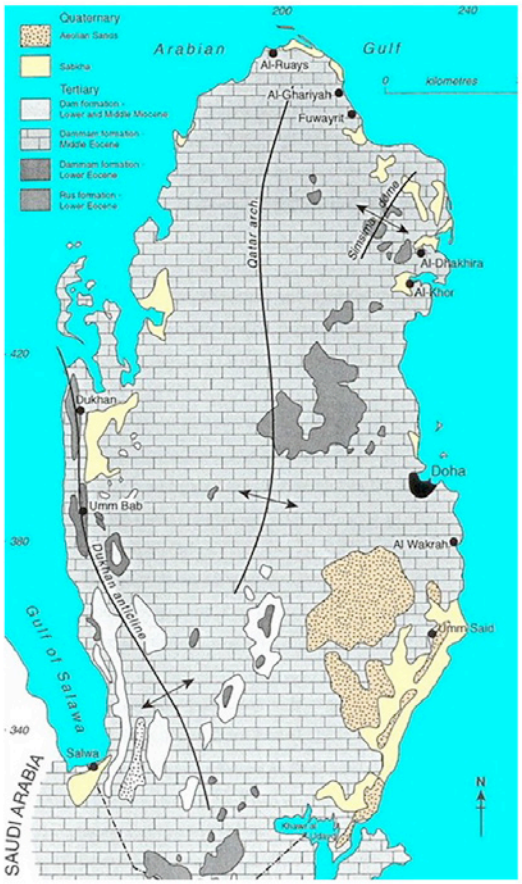

Figure 5: Geology, Doha Peninsula

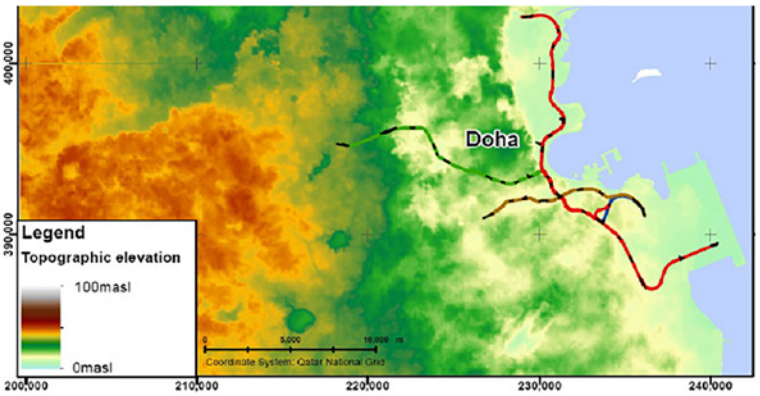

Figure 6: Topographic Elevation, Doha

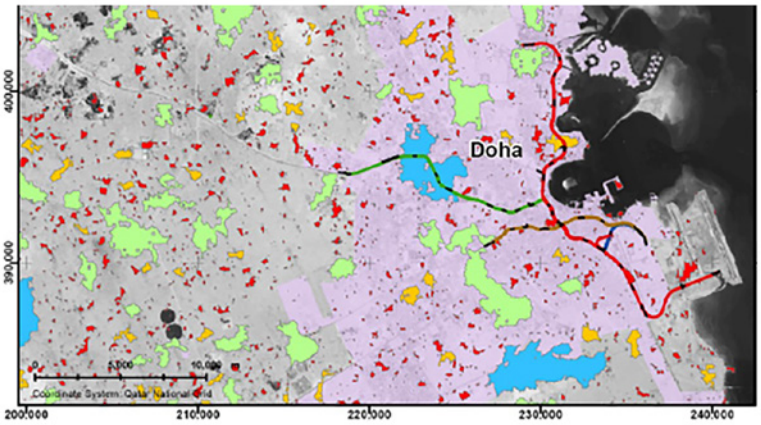

Figure 7: Identified sink-holes and depressions, Doha

As the underlying ground is carbonaceous this typically dissolves over geological time as a result of intermittent rises in surface water level from infrequent, intense rainfall, typical of Qatar's arid climatic conditions. This causes ground-water recharge initiating groundwater flow and dissolution of the ground forming karst (cavities) features. This imposes significant risks for subsurface excavation and tunneling required for the metro construction. Refer to Table 1 for a summary of the ground conditions encountered along the tunnel alignment (Eccleston et al. 1981 & McCulloug 1986) and Figure 8 for geological and hydrogeological processes for karst formation.

Table 1: Geological Units Encountered Along the Alignment

Geological Age	Million Years Ago (Ma)	Formation; Member	Thickness (m)	Description	Tunnel Alignment
Quaternary	0 – 2.58	Overburden	Variable	Sabkha, Residual Soils and Cap-rock	Above
Eocene; Middle	38 – 48	Upper Damman (Simsima Limestone)	<30	Limestone with Siltstone. Towards base, chalky/clayey/ silty matrix	Locally passes through
		Upper Damman (Midris Shale)	0-3	Shale with varying limestone Content; laminated, occasional fissile	
Eocene; Lower	48 – 56	Rus Formation	Variable	chalky limestones with clay/ siltstone layers	Majority pass through

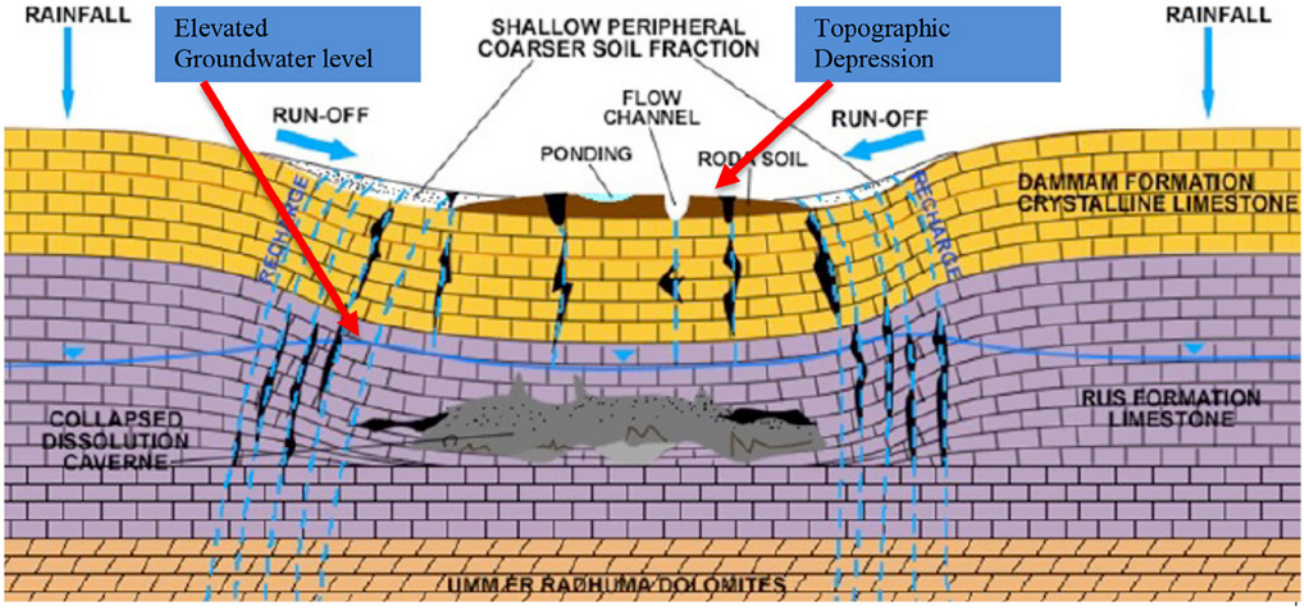

Figure 8 - Idealized karst formation process

The Site Investigation (SI) was carried out in accordance with British Standard (BS) 5930; 1999; described in accordance with QJEG, 1995, classified from I to V with increased weathering intensity. The Mass Quality Designation (MQD), Chan, Y.C, 1994, was used to classify the weathering from the ground investigation (GI) rock cores. Examples of rock core weathering are shown in Figures 9 and 10 and karst observed during the Msheireb Station advance works excavation in Figures 11 and 12.

Figure 9: Competent Simsima Limestone, MQD I

Figure 10: Simsima Limestone, intense karst weathering, MQD V

Figures 11 and 12: Karst identified in the Simsima Limestone, immediately above the Midris Shale boundary

Other risks were identified from potential, localized rises in groundwater levels and resistant precipitate infills following dissolution of the limestone. As the Msheireb Station was located along "Wadi Msheireb", the advance excavation allowed identification of chert bands and increased groundwater levels potentially impacting TBM advancement. In particular the chert bands had nodules rising to Unconfined Compressive Strength (UCS) values up to 200MPa surrounded by rock of 20MPa. The presence of groundwater rises and chert bands, located in Simsima Limestone immediately above Midris Shale are shown in Figures 13 and 14.

Figure 13: karst feature identified in Simsima Limestone

Figure 14: Chert bands in Simsima Limestone

4 TEMPORARY WORKS

Temporary works are defined as "parts of the works that allow or enable construction of, protect, support or provide access to, the permanent works and which might or might not remain in place at the completion of the works" (BS5975: 2008) and typically included crane support, falsework, formwork, slope support, foundations, grouting, retaining structures, trench support and tunnelling. A balance for efficiency and budget is required for all projects to ensure the works do not impact program and cost yet all works need to achieve the minimum safety requirements. The temporary works for the Gold Line were classified in accordance with BS 5975: 2008, ranging from simple (Class 1) to Complex (Class 3) works. Examples are summarized in Table 2 and Figures 15 to 17.

Table 2: Temporary Works Category Classes

1	2	3
Simple; independent check by a Design Team Member	More complex / involved; independent check by an Individual; not in design team	Complex, innovative and sequenced; independent check by Another Organisation

Figure 15: Pad Foundation

Figure 16: Formwork

Figure 17: Cross Passage support frame

To ensure an efficient design and ease of construction generic design, construction and similar plant generic approaches for the works, similar throughout the stations and tunnels were adopted and programmed throughout the project. For each temporary works a process was set up following BS5975: 2008 which continued through the initial design, through checking through the works continuing to dismantling upon completions as presented in Figure 18.

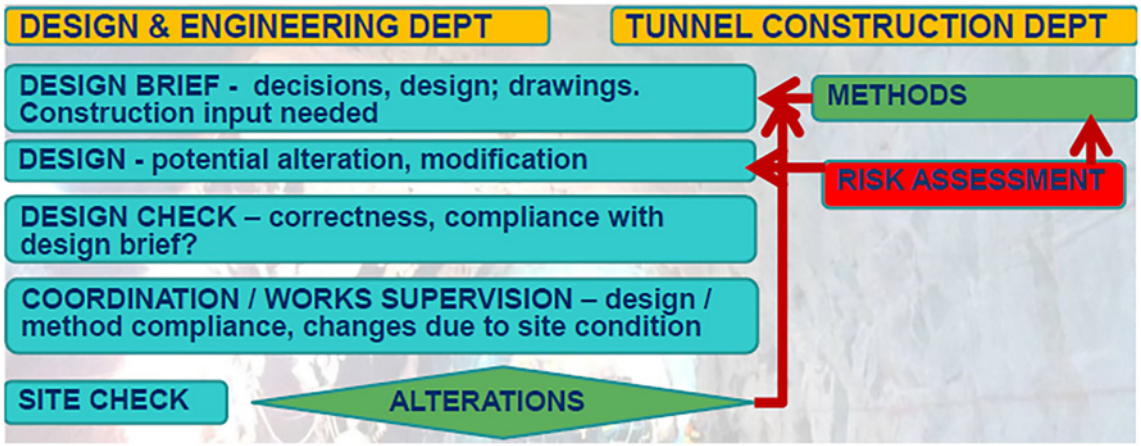

Figure 18: Temporary Works procedure

5 TUNNELING

The tunnels were constructed using six No. Herrenkneckt TBMs with 7.05m cutterhead diameter using EPB support. Two TBM comprised two launches from the Airport City North and four from the Al Saad Station; the TBM retrievals comprised two from the Villagio Station and four from the Msheireb Station as shown in Figure 2. All station excavations were completed prior to the TBM break-in and break-out, allowing the TBMs to be accessed, maintained and refurbished as necessary during the station transfer.

The Herrenkneckt EPB TBM was designed and manufactured to provide soil and earth support during each drive. Refer to the Figures 19 and 20 for an illustration of the face support pressures and the cutter-head.

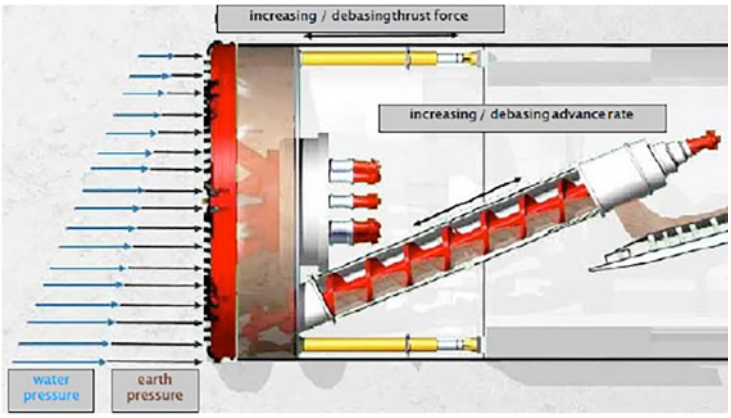

Figure 19: Cross Section of the EPB TBM with water and earth pressure illustrations

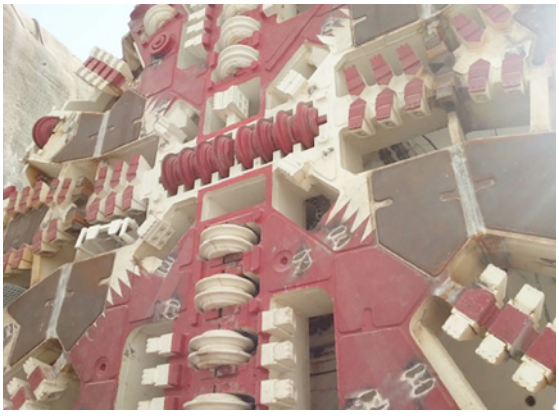

Figure 20: TBM Cutter-head

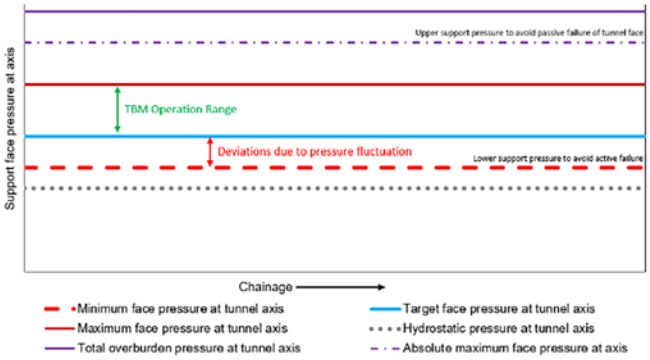

Figure 21: TBM Face Pressure Operational limits

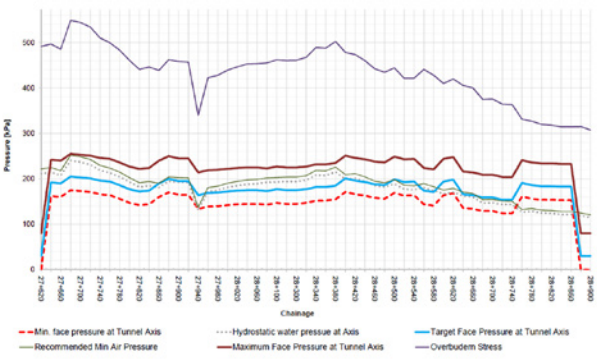

Figure 22: Estimated Face Pressure along the alignment

The face pressure design included maximum and minimum operation pressures, to prevent blow out and collapse and target face pressures, and optimum face pressure operation during advancement (Anagnostou et al, 1996). Refer to Figures 21 and 22 for the operational pressure limits and an example of the face pressure support along a section of the alignment.

Due to the presence of karst an upper water inflow limit of 50m^3 per second was estimated and the EPB support mix adjusted accordingly to accommodate the inflow. Tail grout was used to seal voids between the TBM shield and segments injected through 7No. grout tubes passing through brushes preventing grout blow back into the TBM. The tail grout pressure exceeded the TBM face pressure to ensure the voids were sealed. Despite this groundwater pressure increase often occurred due to the presence of karst adjacent to the tunnel drive and ground fracturing as a result of the TBM drive.

As shown in Figure 18 the face pressure was reduced and increased as the TBM advanced towards and away from the station respectively. To allow these abrupt pressure changes and prevent water inflow to the station the ground was improved by grout injection for a length greater than the TBM shield to ensure the tail grout pressure containment. A bullflex membrane seal with sufficient capacity to contain the maximum water pressure was installed between the TBM shield and the station wall as a precaution. The station water-proof membrane was placed ready to seal the annulus between the segment and station box following TBM launch or retrieval. The TBM was advanced onto and off a cradle and sledge to allow the station transfer. Close coordination was required between the station and tunnel construction teams to ensure the station base slab had sufficient recess to accommodate the TBM shield, cradle, sledge, blind rings required for launch and thrust frame. Refer to the TBM transfer through the Al Saad C-Ring Station in Figures 23 and 24.

Figures 23 and 24: TBM transfer through Al Saad C-Ring

Grout blocks were formed to allow TBM intervention at regular intervals or locations accessible for the grout injection plant. Despite the efforts made the risks identified in the localized rises in groundwater levels; chert bands with abrupt changes in UCS value, clay bands and the karst limestone impacted the TBM cutters. As a result required unplanned, pressurized intervention was required to replace the cutters. The damage typically occurred along the boundary between the Simsima Limestone and Midris Shale. Examples of the damage are presented in Figures 25 to 28.

Figure 25: Cutter breakage (chert bands)

Figure 26: Scraper distortion (chert bands)

Figure 27: Cutter clogging with clay (Midris Shale)

Figure 28: Groundwater pressure increases (Karst)

6 CROSS PASSAGES

Cross passages were located every 0.25km along to allow emergency access to the adjacent tunnel; mechanical, electrical and plumbing (MEP) provision and sump connections at the lowest alignment levels. Access to the adjacent tunnel was required for emergency refuge in accordance with the Employer's Requirements. Cross passage spacing could be relaxed provided access to the ground surface was available, either through stations or emergency escape shafts. The design requirements to determine this spacing depended upon the access space; patronage, such as number of passengers and physical ability; and emergency precaution availability, such as fire ventilation provision. The challenges associated with the cross passage design and construction included a flat 7m wide central span; increased annulus within the fractured ground between the cross passage and the tunnel and due to the variable configuration along the excavation difficulties with waterproofing, formwork and falsework installation. Refer to Figures 29 for the cross passage configuration and Figure 30 for a 3 dimensional (3D) view.

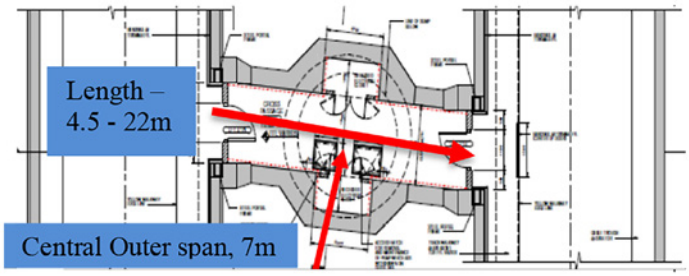

Figure 29: Cross passage configuration

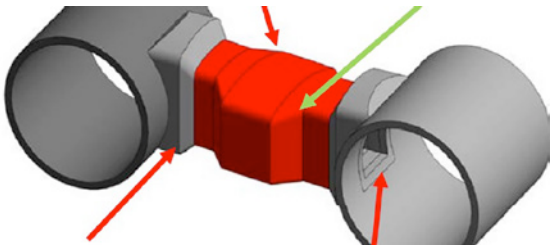

Figure 30: 3D cross passage view

The cross passage excavation was between the nearest adjacent segment openings between the tunnels. As the segment width was 1.5m the maximum offset perpendicular to the tunnel was therefore 0.75m between the edges of the tunnel annuli. As the alignment varied the cross passage length varied accordingly, ranging from 4.5m length to 22m length (See Figure 29).

Grouting was initially carried out. As access to the surface was limited and the ground was intensely fractured following the TBM drive allowing groundwater to flow into the voids around the tunnel, the grout was injected from within the tunnel. This was carried out through the sacrificial lining segments and extended along the excavation length from the initial tunnel drive to limit grout injecting required from the opposite tunnel drive. The grout was carried out in stages with secondary grout carried out for the interface between the cross passage and tunnel and sump excavation. Refer to Figure 31 for the potential water flow around the tunnel annulus, Figure 32 for the inflow during grout injection and Figure 33 for the grout configuration.

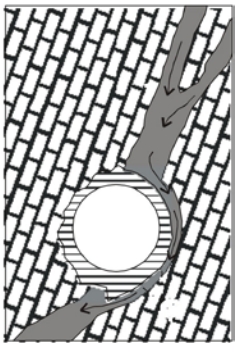

Figures 31 and 32: water inflow

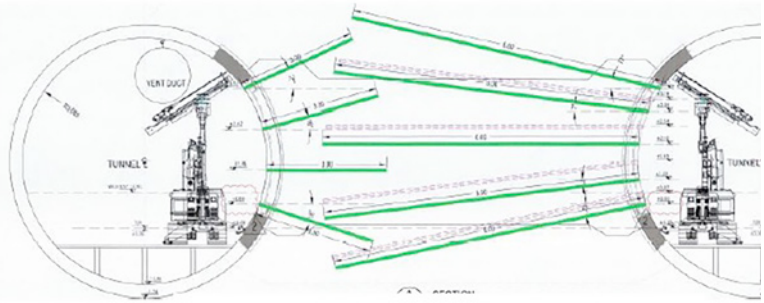

Figures 33: grout hole configuration between tunnels

Following grout injection the sacrificial segments were removed using an industrial chain-saw to dissect each portion. A qualified operator was employed to operate the chain saw and protective chain mail clothing was provided during operation. To ensure sufficient hoop thrust was in place the segment removal and steel frame installation was carried out sequentially with the steel frame later embedded in concrete to form the permanent works. Refer to Figure 34 for the steel frame placement and Figure 35 for the sequential segment removal and steel frame installation.

Figures 34: steel frame

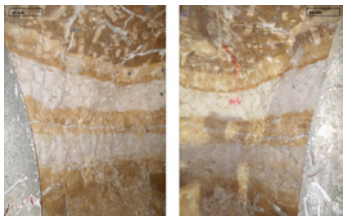

Figures 36: excavation

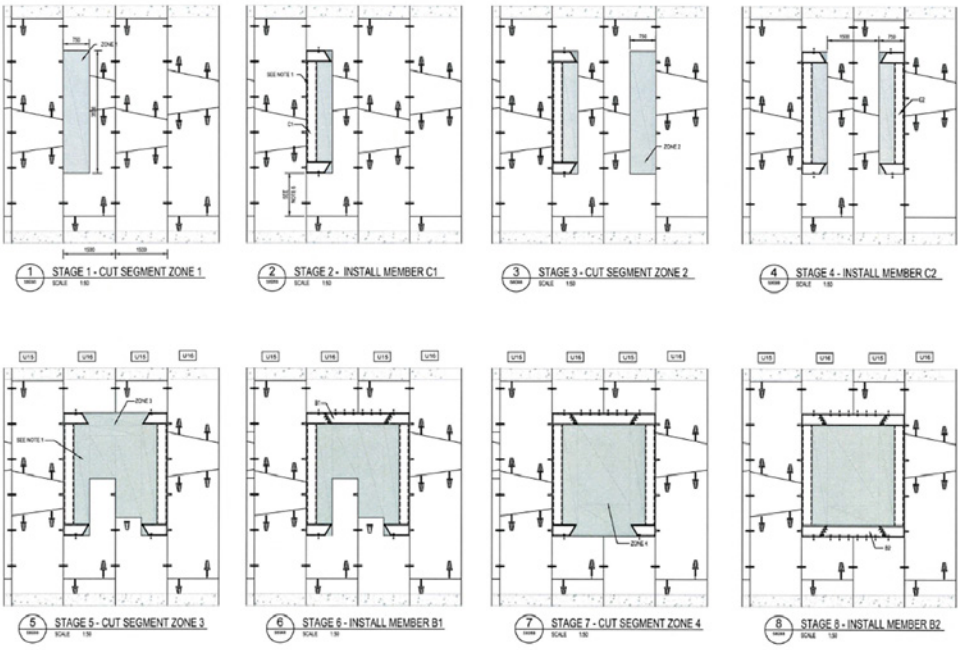

Figures 35: Cross passage steel frame installation sequence

Following the segment removal the excavation progressed in stages, mapped by a qualified, experienced engineering geologist. Upon completion of each excavation stage a decision was taken whether the grout take had been adequate to arrest the groundwater inflow, the temporary support requirement based on Barton et al, 1974 support requirements and whether the excavation could proceed as a full face or heading and bench excavation. Refer to Figure 36 to 38n for the excavation mapping and sequencing.

Prior to the formwork installation a waterproofing membrane was installed. A rigorous sub-contract procurement process was set up to ensure the nominated sub-contractor had sufficient technical ability and could carry out the works within time and budget. As spray-on lining membrane could not be installed in accordance with the Employers Requirements major temporary works were needed for scaffold erection and frame loading to allow the membrane installation and joining in the required installation sequence. Refer to Figure 39 and 40 for the membrane installation.

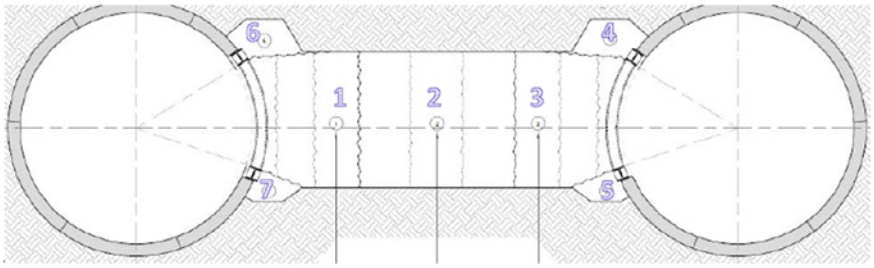

Figures 37: Cross Passage excavation sequence

Figures 38: Central span excavation

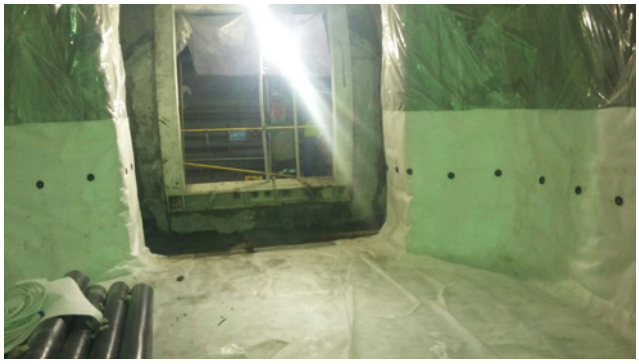

Figures 39 and 40: Waterproofing membrane scaffold erection and placement

Upon completion of the excavation formwork was installed to commence concrete pouring. This was carried out in stages, initially to form the sidewalls followed by the crown placement. As the interface between the tunnels and cross passage and the central span and connecting passages varied to different angles flexible lengths and joints were required between the formwork panels (refer to Figure 41).

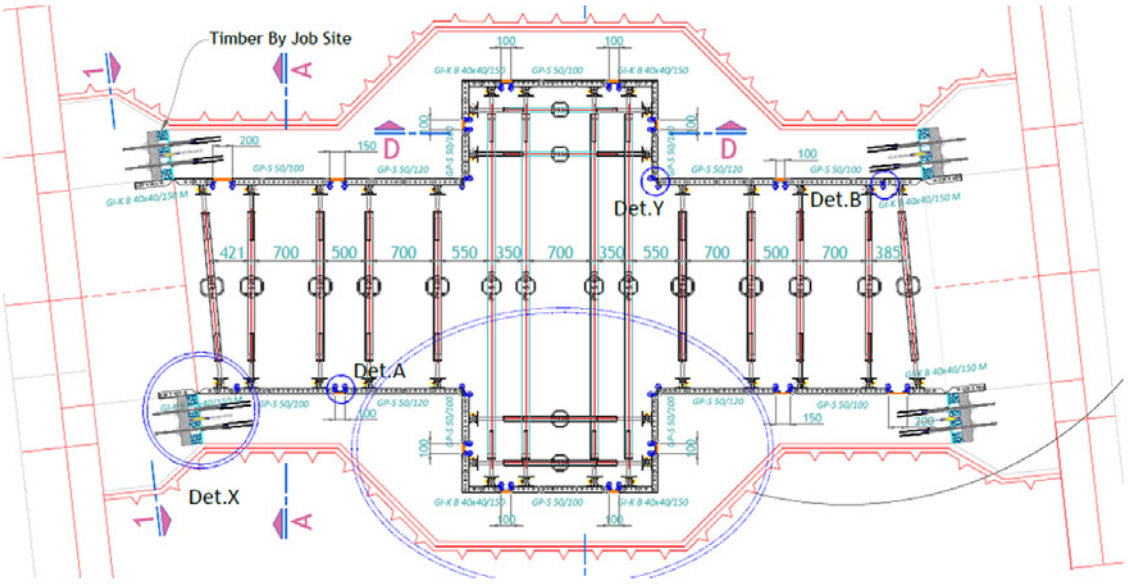

Figures 41: Cross Passage flexible formwork installation

7 CONCLUSIONS

At US$ 4.5 billion capital cost, the Gold Line Metro is the largest of the four metro lines presently being constructed to complete the Doha Metro in advance of the 2022 Qatar World Cup. The challenges have included the interfaces between individuals from a range of nationalities forming the JV and the

external stakeholders, designers and sub-contractors. The design and construction challenges involved the stations and escape shafts, mined subways and cross passages and effective temporary works implementation to allow the project to progress efficiently and safely.

ACKNOWLEDGEMENTS

Any opinions expressed in this paper are those solely of the authors and not of any other party. The author was employed as the Engineering Manager for the ALYSJ Joint Venture Contractor from 2015 to 2016.

REFERENCES

Anagnostou, G and Kovari, K (1996). Face Stability in Slurry and EPB Shield Tunneling, Tunnels and Tunneling. December, 1996.

Alsharhan, A. S. and A. E. M. Nairn (1994). "Geology and hydrocarbon habitat in the Arabian Basin: the Mesozoic of the State of Qatar." Geologie en Mesezoic" 72: 265-294.

Barton, N., Lien, R. & Lunde, J. (1974). Engineering classification of rock masses for the design of tunnel support. Rock Mechanics, vol. 6, pp. 189–236.

British Standard Institution (BSI, 1999). Code of Practice for Site Investigations, BS 5930.

British Standard Institution (BSI, 2008). Code of practice for temporary works procedures and the permissible stress design of falsework, BS 5975:2008+A1:2011.

Chan, YC (1994). Classification and Zoning of Marble Sites (GEO Report No. 29). Geotechnical Engineering Office, Hong Kong.

Eccleston, B.L and Pike J.G. (1981). The Water Resources of Qatar and their development. Technical Report No. 5, Water Resources and Agricultural Development Project (FAO Funds-in-Trust). Doha. Ministry of Industry and Agriculture.

McCullough, R.C. (1986). Rus Formation facies distribution and geologic model of near-surface sediments in Qatar. Geologic Report 86005, Western Arabian Gulf Group. ARAMCO.

West, I. and West, T (2006). Simplified geological map of the Qatar Peninsula, modified after UNDP, 1978 and Al-Yousef (2003).

Wikipedia, 2018: https://en.wikipedia.org/wiki/Doha_Metro

Quarterly Journal of Engineering Geology (QJEG), 1995, Description and classification of weathered rocks for engineering purposes. 28(3), 207-242.

Numerical Analysis of Unforeseen Geological Conditions in a Tunnel

Geoffrey Pook & Anthea H.Y. Seto
Meinhardt Infrastructure and Environment Ltd.

Wang Yanhua
China Road and Bridge Corporation

ABSTRACT

Tunnel works are associated with the inherent risks posed by unforeseen ground conditions. Despite advancement in excavation and construction methods to enhance safety and improve efficiency, uncertainty caused by limited ground investigation or complex geology and hydrogeology remain. The demand for robust, safe and cost-effective support to safeguard the excavation and secure the programme is also increasing. Overcoming problems associated with unforeseen geological conditions, such as deep weathering profiles and structural instabilities, as well as the adequacy of the support types and installation methods, can greatly influence the success of a tunnel works project. .

Numerical analysis through the use of 2D Finite Element Method (FEM) is a proven technique to enhance the confidence of proposed support as well as modelling the performance of ground conditions. This paper discusses the application of FEM from probing, tunnel face mapping and monitoring data to overcome the challenges posed by unforeseen geological conditions. The actual condition of the tunnel during construction is also compared to empirical assessment during design stage. This approach demonstrates the importance of updating the ground model with temporary support design when the ground condition deviates from the assumed parameters to enable engineers and geologists to enhance the reliability of temporary support.

1 INTRODUCTION

1.1 Site Description

Two 1-way vehicular underpasses (tunnels) were constructed underneath a local hill. The underpasses are approximately 744m and 751m long for the northbound and southbound tunnels respectively with associated seven cross passages. The maximum tunnel span is approximately 15m for the main tunnel. The North and South portals are expected to be in mixed ground conditions while the central portion of the underpass is expected to be in rock. The excavation adopted top heading and bench excavation using drill and break for the initial mixed ground portions and drill and blast for rock portions with rock cover of at least half the maximum tunnel span (Figure 1).

The tunnel is located beneath natural hillside and is bound by roads to the south and northeast. The natural hill slope rises from approximately +36mPD in the south portal up to a high point of +167mPD near cross passage 2 and cross passage 3 and falling down to +50mPD near the north. The tunnel invert is situated between +30 and +20 mPD.

Superficial deposits consist predominantly of Quaternary debris flow deposits which are generally

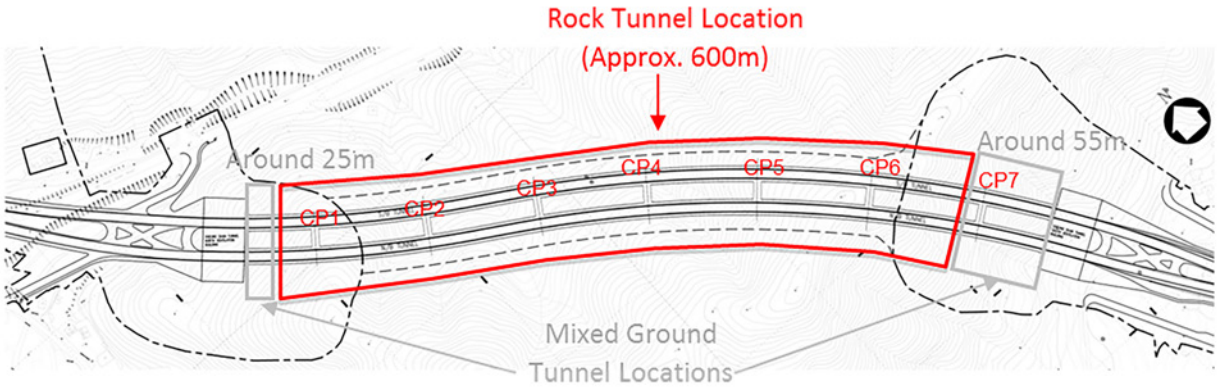

Figure 1 – General layout of the tunnel

encountered with thicknesses less than 2.0m. They can be found on hill slopes and large fans downslope which are mainly composed of sandy silt to silty sand with fine to coarse gravel sized tuff fragments. The solid geology of the site area consists of fine to coarse ash tuff. The area is lithologically uniform, largely featureless coarse ash crystal tuff with intermittent eutaxitic vitric tuff and impersistent layers of volcaniclastic sediments. Meta-andesite has been recorded near the north portal. Evidence of mafic dykes and quartzphyric rhyolite intrusion have also been recorded. The engineering rockhead, which is defined as Grade III or better Rock with Total Core Recovery (TCR) greater than 75%, based on the Geotechnical Baseline Report, along both underpasses ranges from +27mPD to +125mPD (Figure 2). The GI data indicates that the underpass is within a moderately to slightly decomposed tuff rock mass with greater than 8.5m cover above the excavation crown.

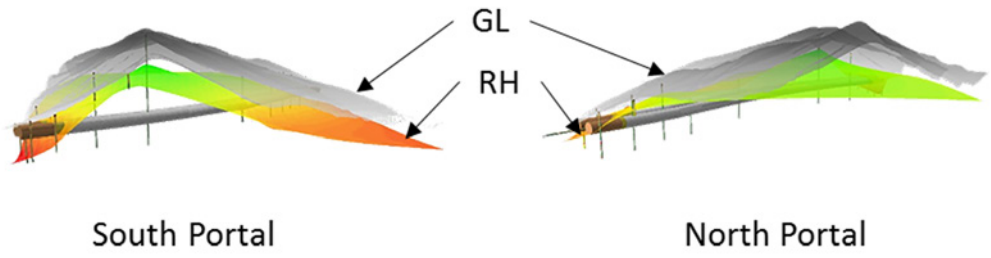

Figure 2 – Topography and inferred rockhead of the tunnel alignment

The rockhead in the tuff is generally shallow with approximately 15m of saprolitic zone below the ground surface as confirmed by the GI. However, the tuff weathers along weaker seams, likely formed due to heterogeneous rock conditions or joints/planes of weakness, which extended to depths within or below the tunnel alignment. Due to the occurrence of these local weakness zones with the potential for variable geology (hydrothermal alteration or tuffaceous sedimentary rock), the rock cover was verified by check probing as part of the excavation programme. The rockhead is established for assessment of the general geological condition of the tunnel pass alignment and tentative extent of the mixed ground tunnel portion. The site area is affected by major structural features such as northeast-trending faults, shear zones and fold axes with minor influence from northwest- and east-trending faults. Evidence of faulting has been identified during the GI as fault gouges and breccia concentrated within the vicinity of the north portal. Based on the GI records and correlations of the cataclasites, several local faults can be inferred to strike in a northwest – southeast direction, sub-parallel to the northbound tunnel to the northeast. Zones of cataclastic metamorphism and hydrothermal alteration associated with the faulting are generally expressed as quartz veins, mylonized tuff, meta-andesite and meta-tuff. The majority of the hydrothermal alteration incidences are concentrated within the vicinity of the north portal. The hydrogeological conditions along the entire tunnel alignment are rather favourable for this project, with minimal seepage and groundwater ingress.

1.2 Rock Mass Classification Systems

Rock mass classification systems are the recognized method for qualitatively describing a rock mass for use in the design of underground excavations. These systems classify the rock mass surrounding the tunnel based on various parameters. Two of the most widely used systems (Barton and Bieniawski, 2008) are Rock Mass Rating System (RMR) (Bieniawski, 1984, 1989) and the Norwegian Geotechnical Institute's (NGI) Rock Mass Quality of the "Q-system" (Barton et al., 1974) as updated by Grimstad and Barton (1993) and NGI (2015). The Q-system was used to assess the rock mass quality of the entire length of the rock portion for both tunnels and cross passages whilst the RMR was adopted to assess the unsupported length and stand-up time of the excavations (Romana, 2014). The Q-system is based on six parameters that quantitatively describe three aspects of the rock mass as follows:

- Rock block size (RQD/J_n)
- Joint shear strength (J_r/J_a)
- Confining stress (J_w/SRF)

These classification methods are built on successive research into empirical data of many cases around the world (Barton, 2002; Barton and Grimstad, 2014a, 2014b). They provide a platform for the evaluation of the stability of the surrounding rock mass. The limitations of these methods are that they cannot, by their very nature, provide quantitative assessment of stress or instability conditions within the surrounding rock mass (Palmström and Broch, 2006).

In order to model the change in strength parameters for different Q values, the rock material followed a Generalized Hoek-Brown failure criterion (Hoek, 1990), where the Geological Strength Index (GSI) and GSIr (residual) values were used. The GSI and GSIr values were obtained using the RMR relationship in Equations 1 and 2; and verified with the RQD and joint conditions from GI:

GSI=RMR-5	(Barton, 2014a)	Eq. (1)
GSIr=GSIexp × (–0.0134 × GSI)	(Cai et al., 2007)	Eq. (2)

1.3 Tunnel Support Design Approach

The temporary support design for the rock tunnel for both north and southbound passageways and associated cross passages adopted the following primary assumptions:

- The temporary support consisted of plain (P1) or steel fibre reinforced (S1) shotcrete based on in-situ geotechnical and ground conditions. Untensioned rock bolts or friction bolts alone or in combination with shotcrete were also considered either in feature or pattern configuration. Spiles were used to limit overbreak in cross passage construction. Glass fibre reinforced polymer bolts replaced steel bolt supports where the main tunnel wall coincides with cross passage face. This enabled more efficient removal of main tunnel temporary support as cross passage excavation was undertaken.
- The temporary lining was designed to provide support to the excavated ground and to facilitate the safe development of the full tunnel span either full face or phased.
- The temporary lining was designed for a variety of load and rock cover conditions including the most conservative.
- An influence zone was identified at the intersections of the main tunnel and cross passage where the Q-values were reduced by adopting 3 times J_n value. This was implemented for a total length of 18m, representing 3 times the span of the cross passage, along both north and southbound tunnels. For conservative purposes the full width of the main tunnel was included within this influence zone.

The design procedure adopted a range of different design approaches in order to validate the proposed support recommendations and likely failure mechanisms, thus providing confidence that the proposed recommendations are appropriate. The initial empirical analysis based on Barton et al. (1974) was followed by a series of verification stages including: key block analysis based on an assessment

of site specific joint orientations; and numerical analysis of stress and displacement of the rock mass. Q values were obtained for every core run of each borehole and horizontal directional corehole along the tunnel alignment. A ground model was developed to divide up the alignment into regions of similar rock mass types. These types formed the basis for the empirical support design in which each region of the tunnel alignment can be assessed for temporary support requirements in accordance with the Q chart. Due to the anticipated homogeneous rock type along the tunnel alignment no divisions were made based on the predominant geological strata.

2 METHODOLOGY

2.1 Numerical Analysis

Empirical methods and numerical analysis are two of the main methods to analyse the stability of the tunnel and surrounding rock mass. The finite element method offers the ability to measure the displacement of the surrounding rock mass during and after the tunnel is excavated. It also allows the assessment of the plastic zone extent, stress distribution as well as assessing the effects to the proposed supports on stress strain diagrams. This quantitative evaluation of the surrounding rock mass is dependent on the accuracy of the ground model and the suitability of the input parameters. The aim of the finite element method is to verify the empirically evaluated support design. The initial ground support designs were verified using finite element numerical models in the FEM software module RS2. Numerical modelling allows the interaction of the ground and temporary support to be assessed in more detail allowing the impact of issues such as construction sequence and in-situ stress to be assessed. The numerical modelling work can also verify the rock loading for temporary lining design.

To simulate the tunnelling sequence, the rock mass in the tunnel is substituted by computing the ground stress balance and, during subsequent computations, reducing the reverse stress on the excavation to simulate the stress release during tunnelling. The numerical analyses using RS2 are carried out to verify the adequacy of the proposed temporary support based on Q-system. GSI values are obtained from RMR values, calculated using the GI (GEO, 2018; Palmström, 2005), and verified by the RQD and joint condition (Hoek et al. 2013) of the GI data to produce a generalized Hoek-Brown failure criterion to represent the intact rock mass. Joint networks, obtained from the ground investigation data analysis are added to simulate a discontinuous rock mass. The temporary support, consisting of shotcrete lining and pattern dowels, is modelled in the program while displacements at the crown, wall and invert are then produced for sections of the tunnel representing the Q classes. Forces and moments exerted on the lining are also obtained.

2.2 Empirical Design

The rock portion of the main tunnel and cross passages was designed to be excavated by drill and blast method, with an anticipated Q-value greater than 0.15. The design criteria considered a potential weak zone within the tunnel with D/2 rock cover. During rock excavation the exposed ground profile was mapped and stabilized by a temporary support system consisting of rock bolts and shotcrete designed in accordance with the Norwegian Geotechnical Institute (NGI) Q-system of rock mass classification (NGI, 2015). The anticipated Q range for the tunnel based on the Geotechnical Engineering Report and the available data is shown in Table 1.

Table 1 – Percentage of estimated Q values for tunnel alignment

Q>10	10>Q>5	5>Q>1	1>Q>0.3	0.3>Q>0.1	Q<0.1
1.1%	8.2%	56.9%	17.5%	9.0%	7.3%

2.3 Excavation Data

Additional GI was carried out during construction at both portals. This was assessed along with the mapping and probing records to refine the ground model (Figure 3 and 4). It was noted that the presence

of sub-horizontal joints at the crown as well as significant weathered seams within the tunnel face was potentially problematic for the current design.

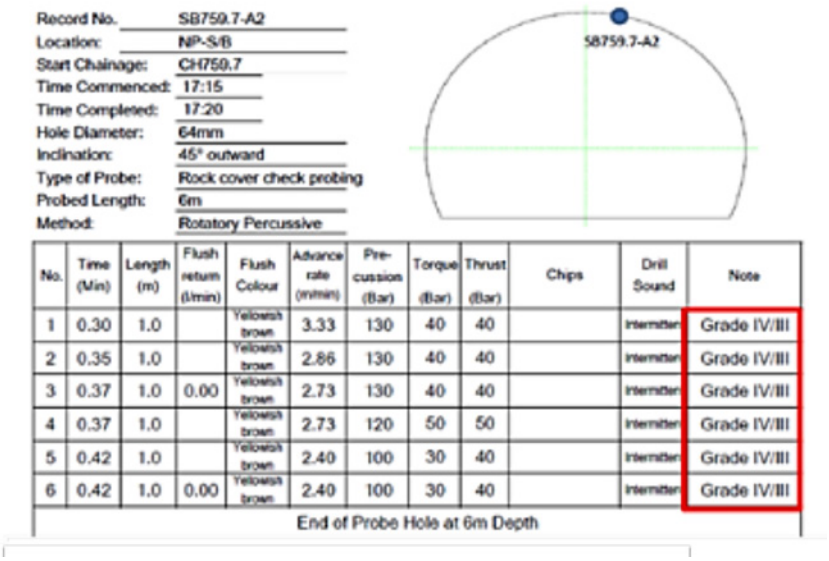

Record No.	SB759.7-A2
Location:	NP-S/B
Start Chainage:	CH759.7
Time Commenced:	17:15
Time Completed:	17:20
Hole Diameter:	64mm
Inclination:	45° outward
Type of Probe:	Rock cover check probing
Probed Length:	6m
Method:	Rotatory Percussive

No.	Time (Min)	Length (m)	Flush return (l/min)	Flush Colour	Advance rate (m/min)	Pre-cussion (Bar)	Torque (Bar)	Thrust (Bar)	Chips	Drill Sound	Note
1	0.30	1.0		Yellowish brown	3.33	130	40	40		Intermitter	Grade IV/III
2	0.35	1.0		Yellowish brown	2.86	130	40	40		Intermitter	Grade IV/III
3	0.37	1.0	0.00	Yellowish brown	2.73	130	40	40		Intermitter	Grade IV/III
4	0.37	1.0		Yellowish brown	2.73	120	50	50		Intermitter	Grade IV/III
5	0.42	1.0		Yellowish brown	2.40	100	30	40		Intermitter	Grade IV/III
6	0.42	1.0	0.00	Yellowish brown	2.40	100	30	40		Intermitter	Grade IV/III
End of Probe Hole at 6m Depth											

Figure 3 – Probing records indicating Grade III/IV material from North Portal South Bound Tunnel at CH759

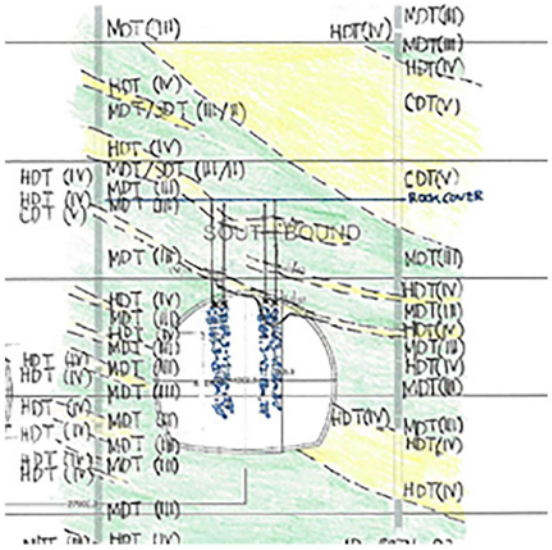

Figure 4 – Interpretation of GI and probing records from South Portal South Bound Tunnel at approximately CH200

2.4 Encountered Geology

The encountered geological condition indicated closely-spaced (<200mm), daylighting sub-horizontal joints against the tunnel drive (recorded as J1 (45/305) in mapping reports and through site inspection (Figure 5). The major joint (40-65/305-315) was identified during mapping of both mixed ground and rock tunnel portion within the southbound tunnel at north portal. The joint is persistent within the tunnel and is recorded from ~CH790 to ~CH740.

The orientation of the major joint set is in an unfavourable condition of driving against dip as excavation proceeds from North Portal. The Q system classification does not specifically account for joint orientation within the determination of temporary support classes and therefore the observational

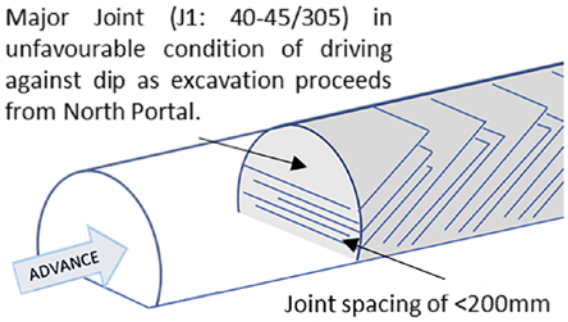

Figure 5 – Assessment of the jointing from North Portal

approach is required to mitigate against the effects of the adverse jointing. A weathered zone is apparent within the tunnel alignment which consists of moderately decomposed tuff with brownish silty clay weathered joint infill. The zone is dipping gently against the tunnel advance. Highly decomposed tuff was also encountered on the left hand side of the crown. Sharp contacts are identified at the tunnel crown which delineates a potential geological feature that has been preferentially weathered to a moderately weak rock mass. Probing records indicated weathered materials up to 5 to 6m thick are present immediately above the crown (Figure 6).

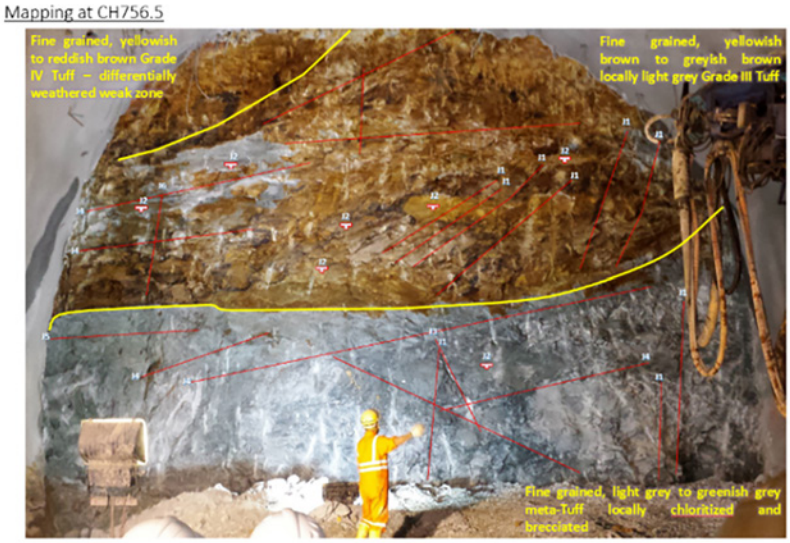

Figure 6 – Condition of tunnel face at CH756.5 showing a differentially weathered weak zone clearly defined and locally chloritized and brecciated tuff

Based on these observations it was inferred that gently dipping weathered zones were present above the tunnel crown whist minor weathered seams intersected with the tunnel faces. The persistence of the weathered zone based on rock mass assessment and core loss encountered in drillhole records suggested a thickness of approximately 10m. This preferential weathering is likely a result of regional metamorphism where bands of slightly metamorphosed tuff are comparatively less resistant to weathering.

3 COMPARISON OF ACTUAL TUNNEL CONDITION WITH EMPIRICAL DESIGN ANALYSIS

3.1 Empirical Approach

The results of the verification by numerical analysis of the empirical approach indicated a robust temporary support method had been adopted based on the initial ground model. Expected displacements are shown in Table 2.

Table 2 – Estimated displacements for original design cases

Support Type	Case	Q	GSI	GSI_r	Max Total Displacement of Model (mm)
1 – High Rock Cover	II	Q = 3.9	62	27	8.4
	VI	Q = 0.15	31	20	51.4
1 – Low Rock Cover	II	Q = 3.9	62	27	2.8
	VI	Q = 0.15	31	20	10.9
1b – Weak Rock Face Condition	VII	Q = 0.02 (at face)	26	18	46.6

The revised and updated ground model using probing and mapping data obtained during excavation prompted verification of the ground model to ensure the proposed support would be adequate and feasible. The site condition of the tunnel face, including minor instabilities, indicated additional support measures would be required. This prompted the use of a revised design to cater for the encountered geological condition of the tunnel. The original support classes were amended for various conditions, including the presence of sub-horizontal joints at the crown, for implementation of the revised design.

In light of the unforeseen ground situation, general design amendments were implemented to cater for the occurrence of the following localized disturbed zones: sub-horizontal joints at tunnel crown and unfavourable joint spacing (< 0.2m).

Based on the GI available at the time of the original temporary support design and an understanding of the regional geological context of the site, it was not anticipated that sub-horizontal joints intersecting the tunnel crown and joints of spacing < 0.2m would be encountered to such an extent. These zones present diverse concerns for both the excavation and support stability of the rock tunnel portion. Sub-horizontal joints at the crown resulted in excessive overbreak in the immediate aftermath of excavation (Figure 7). Joints with an unfavourable joint spacing of 0.2m or below have necessitated the alteration of the support types as it has been found that in some cases the fractured nature of the rock mass can induce overbreak. Based on the specific concerns presented by these zones further design analysis was conducted to assess the actual tunnel conditions in response to the proposed revised temporary support.

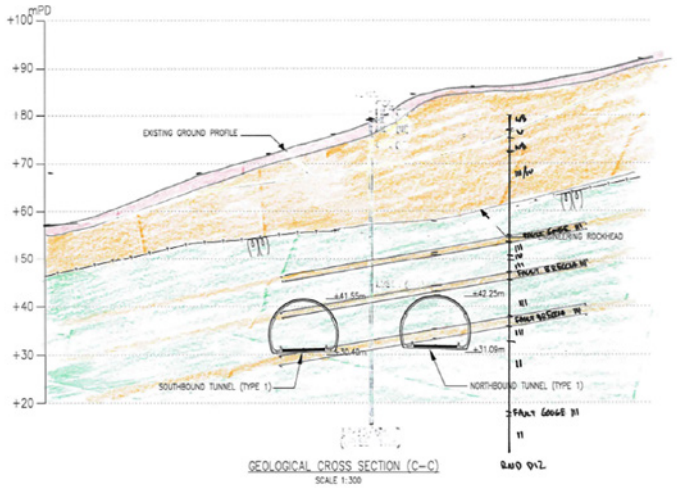

Figure 7 – Interpretation of weak zones with sub-horizontal joints at CH585-610 in the North Bound Tunnel

3.2 Numerical Analysis for Technical Queries

The revised design was verified through FEM based on a ground model created using data obtained through excavation. Two additional support designs were adopted: 400mm shotcrete and 150mm shotcrete and forward bolts. The details of these designs and the conditions for their use based on the FEM assessment are shown in Table 3. The designs were verified to cater for specific mapped conditions to ensure the unfavourable joint arrangements did not exceed the allowable displacements.

Table 3 – Revised design options based on technical queries

Q Value <= 0.06	Sub-horizontal joint near tunnel crown	Unfavourable Joint Spacing <= 0.2m	Prescriptive Design
Yes	–	–	Steel Ribs as per Original Design
No	–	Yes	400mm Steel Fibre shotcrete (12MPa) + Forward Dowels (if Sub Horizontal Joint exist)
No	Yes	No	Pattern Dowels as per Original Design + min. 150mm Polypropylene or Steel Fibre Shotcrete + Forward Dowels

The following assumptions were made during the verification of the modified design:

- Highest ground level/lowest rock head for applicable location adopted
- Rock mass properties for surrounding rock is based on Q from GI and mapping using average values and considering low parameters as the rock was not excavated (e.g. SRF 2.5)
- Intact rock assumed as 100 RQD with Young's Modulus 23500MPa
- Joints are added manually or as a joint network with joint parameters derived using intact rock strength and lowest applicable Q to calculate joint stiffness and shear
- Shotcrete with steel fibre used with compressive strength of 12MPa and Young's Modulus 20210MPa
- Bolt spacing as wide as applicable for the Q value
- Relaxation of 20% used to model some ground movement but conservatively model high pressure on the lining

The unfavourable nature of the jointing, with regards to both joint spacing and location, provided heterogeneous conditions not catered for in the original design. Additional design models (Figure 8 and Figure 9) were produced for the typical and worst case potential scenarios, with regards to overburden, and numerical analysis was run using an analytical approach to determine the level of support required to prevent excessive displacement of the tunnel and loading on the temporary support. The support options consisted of shotcrete, systematic pattern bolts and forward bolts.

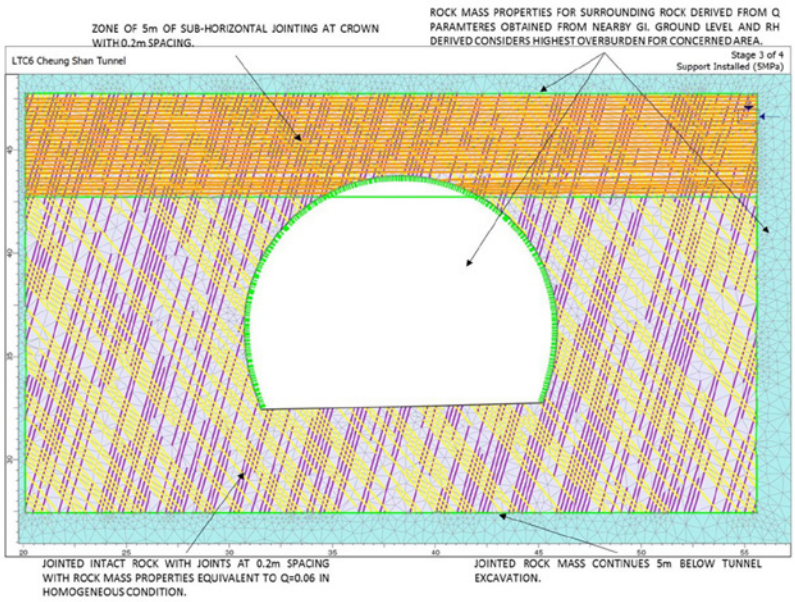

Figure 8 – Ground model for 400mm shotcrete design

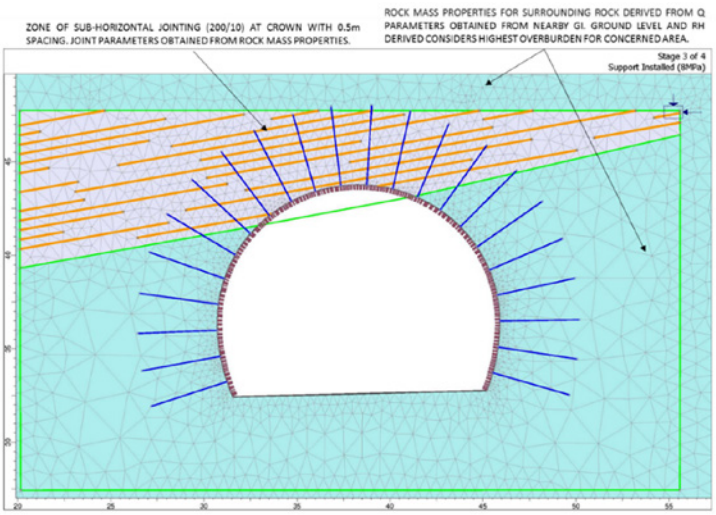

Figure 9 – Ground model for 150mm shotcrete design with shotcrete liner and pattern rock bolts

3.3 Comparison between Anticipated and Mapped Q

The anticipated Q based on the site-specific borehole records from the design stage, and mapped Q from the construction stage for both northbound and southbound tunnels were compared and are shown in Figure 10. The data suggested that in most of the rock portion areas along the tunnel, between cross passage 2 and cross passage 6, both anticipated Q and mapped Q were closely correlated. In contrast, the mapped Q was found to be lower than the anticipated Q towards the interface between rock and mixed ground portions.

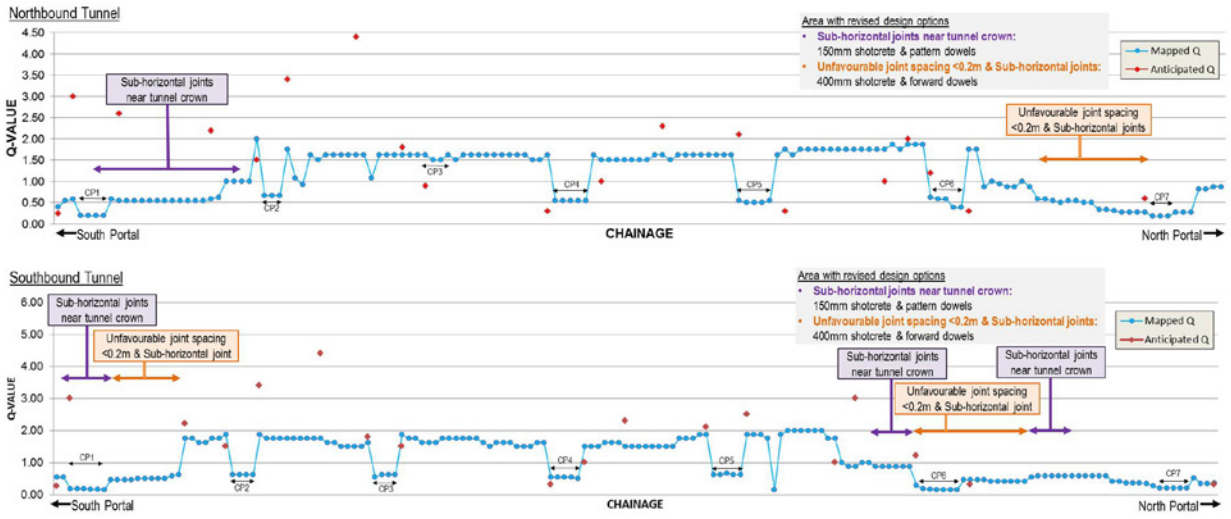

Figure 10 – Comparison between anticipated Q and mapped Q for both northbound and southbound tunnels

Faces where mapped Q was lower than anticipated Q were often correlated with sub-horizontal joints near the tunnel crown and unfavourable joint spacing <0.2m indicating a deeper weathering profile in these portions. Although the mapped Q was similar to that anticipated for the middle portion of the tunnel alignments, the Q value does not reflect the unfavourable nature of joint conditions. The revised design as of the technical queries was successfully installed in those areas where unforeseen ground conditions were encountered. The FEM numerical analysis provided verification of the revised design based on the as mapped ground conditions to model the ground reaction and performance of the support.

4 CONCLUSION

The demand for safe, robust and cost-effective temporary support to safeguard the excavation and secure the programme is always increasing. Overcoming the constraints and problems associated with unforeseen geological conditions, such as deep weathering profiles and structural instabilities can greatly influence the success of a tunnel works project. This paper has presented the significance of updating the ground model and design assumptions of a drill and blast rock tunnel in order to cater for the encountered ground conditions. The following are the salient points to take away from this paper.

1. The initial ground model is constantly updated and reviewed based on the available data. An observational approach can be adopted with assurances that the actual ground conditions remain within the margins of the anticipated ground model conditions.
2. The revised design, based on data obtained during excavation, was modelled to demonstrate the reaction of the support measures to mitigate those areas where the ground conditions were significantly different from the anticipated original design.
3. The use of FEM numerical analysis, in this case RS2, demonstrates the programme's applicability to verify the revised design and the success of the design amendments resulted in the continued excavation on the original scheduled programme.
4. An observational approach to design checking by updating the ground model with monitoring data and ground conditions and verification stages in FEM can provide further fine tuning of the design to secure the programme and avoid costly robust support.

REFERENCES & BIBLIOGRAPHY

Barton, N., R. Lien and J. Lunde 1974. Engineering classification of rock masses for the design of tunnel support. *Rock Mechanics and Rock Engineering, 6(4):* 189-236.

Barton, N. 2002. Some new Q-value correlations to assist in site characterization and tunnel design. *International Journal of Rock Mechanics & Mining Sciences,* 39: 185-216.

Barton, N. and Bieniawski, Z. T. 2008. "RMR and Q – Setting records straight". *Tunnels and Tunneling International:* 26-29.

Barton, N. and Grimstad, E. 2014a. Forty Years with the Q-System in Norway and Abroad *Fjellsprengningteknikk Bergmekanikk/Geoteknikk:* 4.1-4.25

Barton, N. and Grimstad, E. 2014b. *An Illustrated Guide to the Q-System following Forty years use in Tunnelling.* www.nickbarton.com: 44

Bieniawski, Z. T. 1984. *Rock Mechanics in Mining and Tunneling.* A A Balkema

Bieniawski, Z. T. 1989. *Engineering rock mass classifications*. Wiley.

Cai, M., Kaiser, P. K., Tasaka, Y. and Minami, M. 2007. Determination of residual strength parameters of jointed rock masses using the GSI system. *International Journal of Rock Mechanics and Mining Sciences, 23(2):* 247-265.

Geotechnical Engineering Office 1983 Geoguide 1 *Guide to Retaining Wall Design. 2nd Ed.:* GEO

Geotechnical Engineering Office 2018 Geoguide 4 *Guide to Cavern Engineering 2nd Ed.:* GEO

Grimstad, E. and Barton, N. 1993. *Updating the Q-System for NMT. In Kompen, Opsahl & Berg (ed.), Proceedings of International Symp. Sprayed Concrete - modern use of wet mix sprayed concrete for underground support, Fagernes.* Oslo, 1993. Norwegian Concrete Association.

Hoek, E. 1990. Estimating Mohr-Coulomb friction and cohesion values from the Hoek-Brown failure criterion. *Intnl. J. Rock Mech. & Mining Sci. & Geomechanics Abstracts,* 12(3): 227-229.

Hoek, E. 2007. *Practical Rock Engineering.* Rocscience.

Hoek, E., Carter, T. G. and Diederichs, M. S. 2013. Quantification of the Geological Strength Index Chart. *47th US Rock Mechanics/Geomechanics Symposium, San Francisco, CA, USA, June 2013*. American Rock Mechanics Association

Jethwa, J. L., Dube, A. K., Singh, B. Singh, Bhawani Singh and Mithal, R. S. 1982. Evaluation of classification system for tunnels in non-squeezing ground conditions. In W. Wittke (ed.) *Proceedings of ISRM Symp. Rock Mechanics: Caverns and Pressure Shafts Rotterdam, 1982.* A.A. Balkema.

John, M. and Mattle, B. 2003. Shotcrete lining design: factors of influence. *Proc. of RETC*.

Materials and Structures 2003. Test and design methods for steel fibre reinforced concrete. *Materiaux et Constructions,* 36: 560-567

Norwegian Geological Institute 2015. *Using the Q System – Rock mass classification and support design.* NGI

Norwegian Tunnelling Society 2014. *Norwegian Tunnelling Technology – Publication No. 23.* Helli.

Palmström, A. 2005. Measurements of and Correlations between Block Size and Rock Quality Designation (RQD)". *Tunnels and Underground Space Technology,* 20(4): 362-377.

Palmström, A and Broch, E 2006. "Use and Misuse of Rock Mass Classification Systems with Particular Reference to the Q-System". *Tunnels and Underground Space Technology,* 21: 575-593.

Romana, M. 2014. Update of 1989 Bieniawski's RMR guidelines for tunnel excavation. In L. R. Alejano, A. Perucho, C Olalla & R. Jimenez (ed.) *Rock Engineering and Rock Mechanics: Structures in and on Rock Masses Proceedings of EUROCK 2014, ISRM European Regional Symposium, Vigo, 26-28 May 2014*. CRC Press.

Numerical Modelling of Cement-treated Soil Columns

A.L. Saw & C. Shi
Golder Associates (HK) Limited, Hong Kong

ABSTRACT

Cement-treated soil columns have been used in the embankment construction to enhance the stability and reduce settlement. It is well documented that cement-treated soil is a brittle material and any bending/tension induced micro-cracks tend to propagate, causing failure of the whole column. How to model cement-treated soil columns in a finite element analysis remains a key issue to the successful design of the improved ground. In this study, three common modelling approaches (viz. composite block, composite strip walls and individual columns) to simulate cement-treated soil columns are discussed. These methods have been exercised to simulate the construction of a typical embankment over cement-treated soil columns using finite element software PLAXIS 2D and PLAXIS 3D. Moreover, the effectiveness of individual columns and conjoined columns (wall panel) in resisting bending failure are discussed. Analysis results show that the composite block model predicts an unrealistically high Factor of Safety. While the apparent FoS calculated from strength reduction method in PLAXIS cannot really capture the bending failure of the columns. One possible solution to eliminate the bending induced tension cracks is to conjoin those single columns to form a continuous wall panel forcing columns to work under shearing.

1 INTRODUCTION

In-situ soil mixture with cement binder has been a widely used stabilization technique in the reclamation works and the construction of embankments in soft ground. There are few mechanical techniques to mix cement with the in-situ soil such as jet grouting, deep mixing and cutter soil mixing. Compared with other conventional soil improvement methods (viz. PVD, vacuum preloading), the cement-treated soil columns have the advantages such as a fast strength and stiffness gain within a short period. The cement-treated soil columns have been successfully applied to a variety of on-land and offshore projects all over the world.

Despite cement-treated soil columns have gained a popularity in soft ground improvement, there is a large degree of uncertainty as to how to model the columns using the available commercial finite element softwares such as PLAXIS. In this study, we modelled an embankment supported by cement-treated columns with different area replacement ratios using PLAXIS 2D and PLAXIS 3D. Three common modelling approaches (viz. composite block, composite strip walls and individual columns) are exercised to investigate the external stability of the embankment and their predicted failure mechanisms are compared. Moreover, the possible solution to resist the bending failure of the columns is explored.

2 MECHANICAL BEHAVIOURS OF CEMENT-TREATED SOIL

It is essential for designers to have basic understanding of the mechanical behaviours of cement-treated soil so that its field performance can be estimated during design stage. For the past three decades, substantial efforts have been made in laboratory studies to understand the properties of cement-treated soil. The factors that influence the strength and stress-strain characteristics were identified. The

characterization of the properties of cement-treated soil has often been presented in terms of strength, deformation and modulus. In many studies, it has been revealed that the soil becomes brittle by adding small amount of cement. The material stress reaches peak under a smaller strain and then decreases abruptly to smaller post-peak value.

2.1 Compressive Strength

In the past studies, compressive characteristic of cement-treated soil has been measured through unconfined compression test (UCT), consolidated isotropic undrained test (CIU) and consolidated isotropic drained test (CID). From the UCT results, ductile behaviour is manifest for very low cement content. Conversely, the cement-treated soil becomes more brittle at higher cement content. According to Chin (2006)'s laboratory results on cement-treated Singapore marine clay, the CIU test shows that the difference in deviatoric stress increases significantly with increase in curing stress and resulting in the material turning brittle (see Figure 1a). The curing stress is isotropically loaded stress applied on the specimen during curing period. Comparison of stress-strain behaviour from both CIU and UCT tests is shown in Figure 1b, the maximum deviatoric stress is identical to each other but the post-peak behaviour varies.

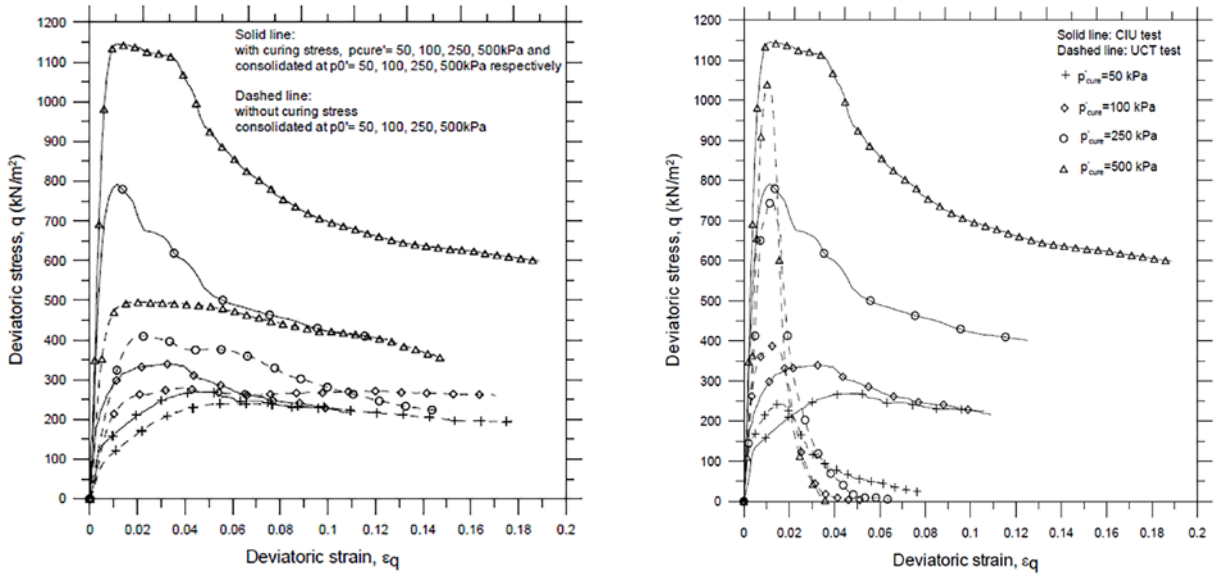

Figure 1: Comparison of cement-treated Singapore marine clay stress-strain curves: (Left) with and without curing stress; (Right) CIU and UCT test (after Chin, 2006)

2.2 Tensile Strength

As discussed, addition of cement helps to improve the compressibility and strength of in-situ weak soil. Conversely, it results in a brittle material that is weak in tension. Conventional uniaxial tension test is the direct approach that is most appropriate to obtain the stress-strain relationship of the cement-treated soil under tension. However, the execution of this test is very challenging and very limited data are available so far. Split tension test is often preferred as it is easier to perform and the results are more consistent (Porbaha et al., 2000). Very often, the tensile strength σ_t is correlated to the key parameter unconfined compressive strength q_u as illustrated in Table 1. Nevertheless, these empirical correlations should be applied with care, as they differ from soil to soil.

Owing to split test being an indirect tensile strength test, it provides no possibility of strain measurement according to Das and Dass (1995). As such, Namikawa (2006) and Saw (2014) conducted three-point bending notched beam test by using fracture energy concept to study the post-peak tensile behaviour of cement-treated Toyoura sand and cement-treated Singapore marine clay, respectively. Their studies show that softening occurs after the material reaches peak stress. This might alarm the current design approach of assuming the ultimate tensile strength maintains after reaches peak.

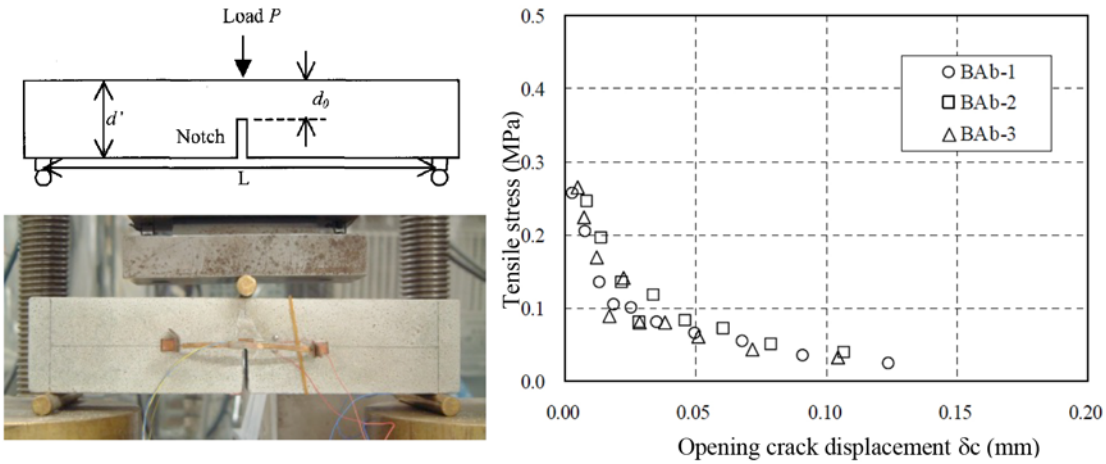

Figure 2: Tension-softening study on cement-treated Toyoura sand by Namikawa (2006)

Table 1: Summary of some published $\sigma_t - q_u$ relationships of cement-treated soil

Reference	Relationship
Porbaha et al., 2000	$\sigma_t = 0.1 - 0.15\ q_u$
Saitoh et al., 1996	$\sigma_t = 0.1 - 0.3\ q_u$
Tanaka and Terashi, 1986	$\sigma_t = 0.15\ q_u$
Xiao, 2009	$\sigma_t = 0.127\ q_u$

Literature shows that cement-treated soil columns can exhibit strain softening behaviours when subjected to compression and tension. The brittleness must be carefully tackled during numerical modelling for a safe design. Any bending/tension induced micro-cracks tend to propagate, causing failure of the whole columns.

3 NUMERICAL MODELLING OF CEMENT-TREATED SOIL COLUMNS

The weighted average simulation (WAS) method has been the most common way to model cement-treated columns. WAS adopts the averaged mechanical properties between the treated and the untreated soils based on the area replacement ratio of the ground. The composite soil properties can be derived from the below formula.

$$P_{com} = a_p \times P_{col} + (1 - a_p) \times P_{soil} \quad (1)$$

where P_{com} is the composite property (i.e. strength/stiffness), P_{soil} and P_{col} is the property of in-situ soil and treated soil column, respectively; a_p denotes the area replacement ratio.

Another method is real allocation simulation (RAS), which utilizes 3D models to simulate each individual treated soil column to further understand the underlying mechanism.

In this study, a typical embankment seating on cement-treated soil columns is envisaged. The columns are simulated using both the WAS and RAS methods to demonstrate the rational way of modelling cement-treated columns.

3.1 Geometry of the Embankment

Figure 3a shows the elevation view of the embankment. The height of the embankment is 10m and the slope gradient is 1:3 (V:H). The soft clay has a total thickness of 15m and the ground is improved by cement-treated soil columns. The plan view of the columns is exhibited in Figure 3b. Each column has a dimeter and a c/c spacing of 1m and 2.8m, respectively, equivalent to an area replacement ratio of about 10%. The area replacement ratio has also been revised to 20% and 30% for parametric analyses.

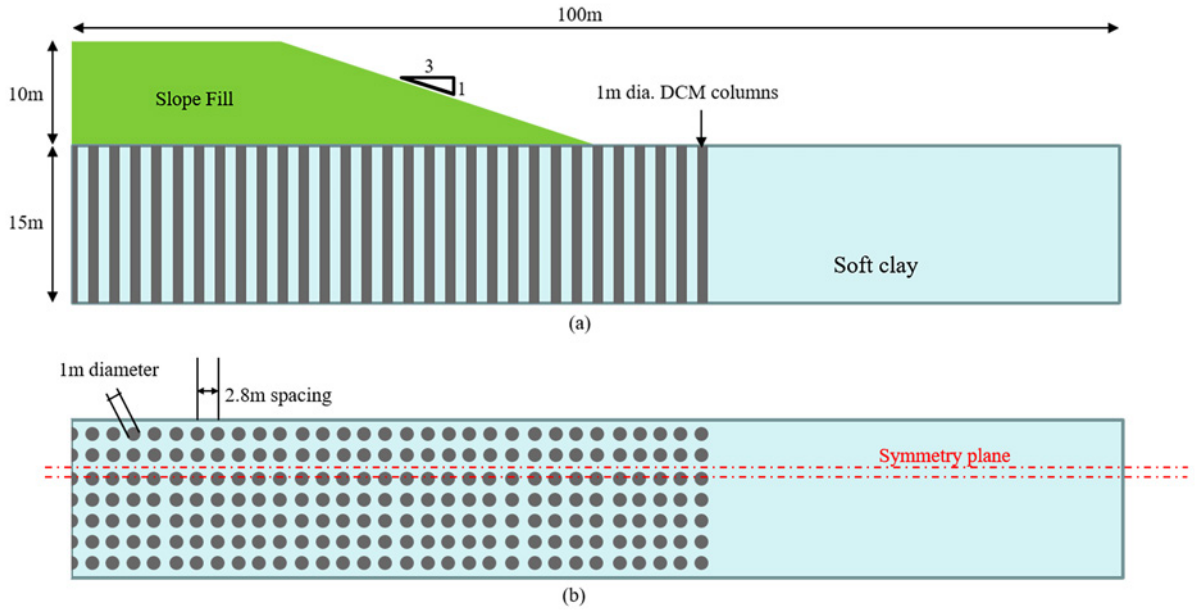

Figure 3: Geometry of the embankment: (a) Elevation view; (b) Plan view

3.2 Input Soil Properties

The input soil parameters for the numerical analysis are tabulated in Table 2. Linearly elastic-perfectly plastic model, Mohr-Coulomb failure criterion is adopted. The design undrained shear strength (C_u) of the column is taken to be 400kPa. Note that the C_u value for cement treated columns in Table 1 has to be revised proportionally with the replacement ratio if WAS method is adopted. For example, if the a_p = 10%, the C_u value for composite columns is 40kPa, ignoring the untreated in-situ soil for simplicity.

Table 2: Input Soil Parameters

Soil	Drainage	Density, γ (kN/m^3)	Friction Angle, ϕ (degree)	Cohesion, C_{ref} (kPa)	Cohesion, C_{inc} (kPa/m)	Reference Young's Modulus at top of soil layer, E_{ref} (MPa)	Increment of Young's Modulus with depth, E_{inc} (MPa/m)
Fill	Drained	19	33	20*	–	50	–
Soft Clay	Undrained (B)	16	0	5	1	2	0.35
Treated Column	Non-porous	16	0	400	–	117	–
*The cohesion is assigned to the fill material to prevent the occurrence of shallow slope failure.							

3.3 Ground Water level

The initial ground water table is assumed to be 6.5m above the top level of soft clay and the level remains constant throughout the construction.

3.4 Modelling of Cement-Treated Soil Columns

Both WAS and RAS approaches have been used to model the cement-treated soil columns and the modelling details are summarized in Table 3. The cement-treated soil columns are treated as non-porous Mohr-Coulomb material with tension capacity = 0kPa. The external stability is calculated using the strength (Phi/C) reduction approach in PLAXIS, in which the soil strength parameters are successively reduced in each step along the failure surface. In this type of calculation, the incremental multiplier Msf

is used to specify the increment of the strength reduction of the calculation step. Once failure occurs, the factor of safety is given as

$$\text{FoS} = \text{Available Strength} / \text{Strength at Failure} = \sum \text{Msf} \quad (2)$$

The finite element models for cement-treated columns with 10% replacement ratio is shown in Figure 4. The same process has been repeated for columns with the replacement ratio of 20% and 30% for parametric study. In total, three series of analysis are carried out in this study.

Table 3: Numerical Modelling of Cement-treated Soil Columns

Model	Derivation of material strength and stiffness
Plaxis 2D plane strain: Composite block (WAS)	a) Treated zone modelled as a single composite block b) Composite strength and stiffness based on area replacement ratio
Plaxis 2D plane strain: Composite strip walls (WAS)	a) Treated zone modelled as composite strip walls b) Composite strength and stiffness based on area replacement ratio
Plaxis 3D: Individual columns (RAS)	a) Treated columns modelled as individual 3D columns b) Actual strength and stiffness of treated soil and untreated soil

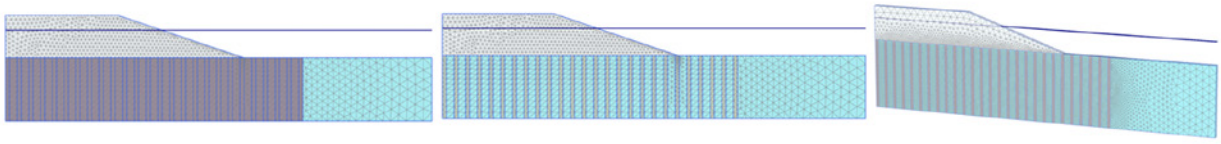

(a) (b) (c)

Figure 4: Finite element models: (a) Composite block; (b) Composite strip walls; (c) Individual columns

3.5 Analysis Results

Figure 5 shows the calculated Factor of Safety (FoS) for the embankment with 10% area replacement ratio of cement-treated soil columns. The composite block method predicts a FoS of 1.7. The slip surface cuts through the whole composite block. In comparison, both the strip walls and individual columns give a lower FoS of about 1.3 and the slip surfaces are much shallower, i.e. upper part of cement-treated soil columns.

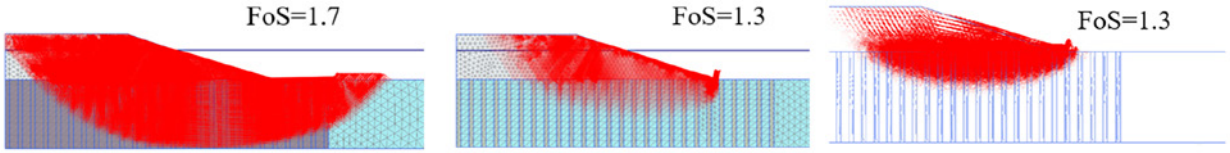

(a) (b) (c)

Figure 5: Predicted FoS for columns with 10% replacement ratio: (a) Composite block; (b) Composite strip walls; (c) Individual columns

Table 4 compares the results from the three series of numerical analyses. Irrespective of the replacement ratios, the composite block model predicts slip surface cutting through the whole composite block thus yielding an unrealistically high FoS. The predicted FoS from the 3D columns model is close to that of the composite strip walls model with a negligible difference. Generally, the predicted FoS from the individual columns in PLAXIS 3D should be considered as the most representative value as it models the actual column geometry and relative location.

Table 4: Summary of Predicted External Stability

Methodology	Factor of Safety		
	10% replacement ratio	20% replacement ratio	30% replacement ratio
2D plane strain: Composite block (WAS)	1.7	3.1	3.4
2D plane strain: Composite strip walls (WAS)	1.3	1.9	2.4
3D: Individual columns (RAS)	1.3	1.9	2.5

However, the above slip surface analysis only fulfils the external stability check. Kitazume (2008) in his centrifuge studies had illustrated that the cement-treated soil columns could fail in bending when used as foundation system for an embankment. Fliz et al. (2012) also suggested to carry out internal stability checks to ensure the overall safety.

4 DISCUSSIONS

As mentioned, the above estimated FoS from the Phi/C reduction method in PLAXIS is calculated by iteratively reducing the cohesion and friction angle of soils/columns until the ultimate equilibrium is obtained. However, it is worth noting that the brittleness of cement-treated soil column has not been taken into consideration.

If carefully examine the deformed mesh plot of cement-treated columns with 10% area replacement ratio after constructing the embankment (shown in Figure 6), two distinct deformation zones can be observed, namely shear zone and bending zone. Cement-treated soil columns in the bending zone are subjected to bending, generating lots of tension failure (presented by tension points) close to the embankment toe. The failure mode fits well with the failure mechanism proposed by Kivelo (1998) and centrifuge tests result carried out by Kitazume (2008), see Figure 7.

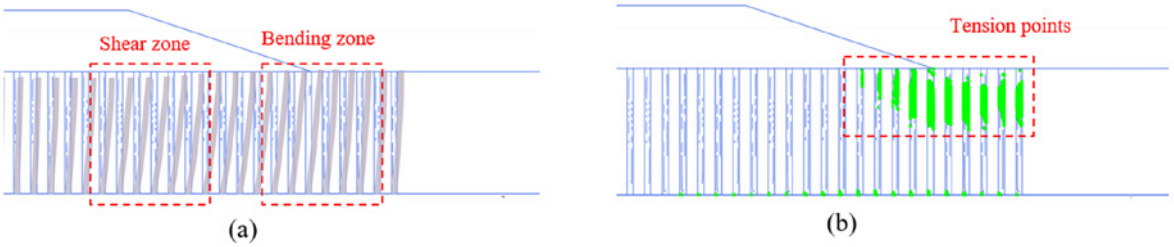

Figure 6: Performance of cement-treated soil columns with 10% area replacement ratio in PLAXIS 3D: (a) Deformed mesh; (b) Tension points

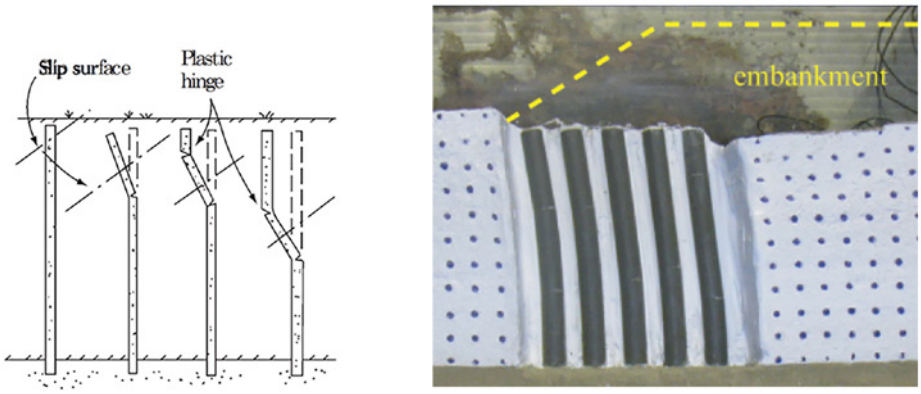

Figure 7: Potential failure modes of single columns: (Left) suggested by Kivelo (1998); (Right) centrifuge test result by Kitazume (2008)

By default, we have set the tension cut-off value of all the cement-treated soil columns to be zero, which means the tension capacity is capped at zero value. Some people would attempt to deduce tension failure from positive vertical stress within cement-treated soil columns shown in the output result, which may miss the full tension failure extent as tension occurs both horizontally and vertically. The tension points in Figure 6 mainly concentrate on the cement-treated soil columns below the slope toe due to bending effect. In reality, if any bending or tension induced micro-cracks occur within columns, the crack would propagate quickly and cause the total failure of the column. Once failed, the columns cannot provide any shearing resistance. Thus, the apparent FoS generated from Phi/C reduction in Plaxis could be misleading.

To simulate the bending capacity of the cement-treated soil columns which is often correlated as 0.15qu, some designers simply assign the input parameter $C_u = 0.15q_u$ to cement-treated columns. Obviously, they may have mistook the shearing and bending failures. As shown in Figure 6, those tension points are generated by bending rather than shearing. By adopting a lower shear strength ($C_u = 0.15q_u$) to cement-treated columns, excessive columns are required to maintain the stability of the embankment while the extent of tension points may have merely been reduced but the underlying mechanism is not well understood. Another approach is to relax the tension cut-off restriction and assign an alternative tension capacity (i.e. $0.1q_u$). It is conceivable that the extent of tension points can be reduced but cannot be eliminated as the columns are still subject to bending.

Despite above mentioned approaches to capture the potential bending failure of cement-treated soil columns, the linearly elastic-perfectly plastic model, Mohr-Coulomb failure criterion cannot address the bending failure as it assumes no softening effect (viz. crack propagation).

To design for a safe system, there are two possible options to minimize the cement-treated columns subjected to bending mode failure. The first option is to design the embankment geometry by reducing the slope gradient or introducing a wide berm in between the slopes. Sometimes, this can hardly be achieved due to site constraint or tight construction period. The other option is to conjoin those individual cement-treated soil columns forming a wall panel and thus eliminating the bending failure mode. Figure 8 exhibits the deformation mesh and tension points after conjoining columns to form a shear wall panel below the slope toe. It is clearly shown that the tension failures due to bending have been eliminated. The wall panel works as a shear resisted element, which helps utilize the enhanced shearing capacity of the cement-treated columns.

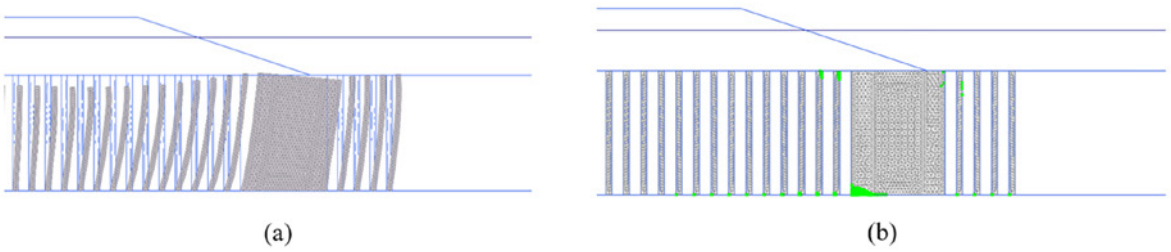

Figure 8: Performance of shear wall panel in PLAXIS 3D: (a) Deformed mesh; (b) Tension points

5 CONCLUSION

In this study, the three common ways of modelling cement-treated soil columns in PLAXIS are discussed. These methods are exercised to simulate the construction of a typical embankment over cement-treated soil columns in soft ground. The failure modes of the embankment under different scenarios are compared and the sensible approaches to reduce/prevent the occurrence of columns fail in bending are discussed. The analysis results show that the composite block method predicts an unrealistically high FoS. While the current modelling techniques cannot really capture the bending failure of the columns. The most effective way to prohibit the propagation of tension points is to conjoin single columns to form a continuous shear panel, forcing columns to work under shearing.

REFERENCES

Chin, K. G. 2006. *Constitutive behavior of cement treated marine clay*. Ph.D, National University of Singapore.

Das, B. M. and Dass, R. N. 1995. Lightly cemented sand in tension and compression. *Geotechnical and Geological Engineering,* 13, 169-177.

Kitazume, M. 2008. Stability of group column type DM improved ground under embankment loading behavior of sheet pile quay wall. *Report of the Port and Airport Research Institute,* 47:1.

Kivelo, M. 1998. *Stabilization of embankments on soft soil with lime/cement columns*. Ph.D, Royal Institute of Technology.

Namikawa, T. and Koseki, J. 2006. Experimental determination of softening relations for cement-treated sand. *Soils and Foundations,* 46(4): 491-504.

Porbaha, A., Shibuya, S. and Kishida, T. 2000. State of the art in deep mixing technology. Part III: geomaterial characterization. *Ground Improvement,* 4(3), 91-110.

Saitoh, S., Suzuki ,Y., Nishioka, S. and Okumura, R. 1996. *Required strength of cement improved ground.* Balkema.

Saw, A. L. 2014. *Characterization and modeling of cement-treated soil column used as cantilever earth retaining structure*. Ph.D, National University of Singapore.

Tanaka, H. and Terashi, M. 1986. Engineering properties of treated soil by DMM in field. *Report of Port and Harbour Research Institute*. (Japanese).

Xiao, H. W. 2009. *Yielding and failure of cement treated soil*. Ph.D, National University of Singapore.

Slope Restoration and Topographical Monitoring for Heritage Preservation of Gediminas Hill and Castle Tower in Lithuania

Šarūnas Skuodis[1] & P.L. Ng[1,2*]

[1]*Department of Reinforced Concrete Structures and Geotechnics, Vilnius Gediminas Technical University, Vilnius, Lithuania*

[2]*Department of Civil Engineering, The University of Hong Kong, Hong Kong, China*

ABSTRACT

Gediminas Hill and Gediminas Castle Tower at the centre part of Vilnius are highly important architectural monument which is symbolic of Lithuania. According to official documentary records, the Gediminas Castle was first mentioned in year 1323. Due to natural (glacial geology and hydrogeology) and anthropogenic (artificial activities and warfare) reasons, the slopes of Gediminas Hill have been associated with geotechnical risks. There have been recorded occurrences of landslides date back to early XIV century, until recently a shallow landslide happened in 2016. This paper consolidates an archival study of the geological and hydrogeological conditions of the Gediminas Hill and castle site, with particular emphasis on the stability of the slope and castle. To preserve the important heritage of Lithuania, a combination of engineering measures for slope restoration and protection are being implemented. Extensive instrumentation and monitoring as well as topographical monitoring and digitalization are conducted. Details of these works are reported in this paper.

1 INTRODUCTION

The Gediminas Hill and Upper Castle along the outskirt of Neris and Vilnelė rivers valleys and their slopes extending from the confluence of rivers with other hills, are belonging to the territory of State Cultural Reserve of the Vilnius Castles (Morkūnaitė et al. 2015). The cultural reserve was established in 1997 and it is highly important historic monument of Lithuania (Skuodis et al. 2017). Gediminas Castle Tower is the remaining part of the Upper Castle in Vilnius, and is an UNESCO (United Nations Educational, Scientific and Cultural Organization) listed heritage (Figure 1). The castle is connected to the foot of Gediminas Hill by a footpath as well as a passenger funicular. Gediminas hill formation began with the retreat of glaciers out of Lithuanian territory 18–22 thousands years ago (Baubinienė et al. 2015).

According to official documentary records, first of all wooden fortifications were built (Rackevičius 2010) by Grand Duke of Lithuania Gediminas in 1323 (Semaškaitė 2005). The first brick castle was completed in 1409 by Grand Duke Vytautas. First record about slopes landslide dates back to about 1396, where it was reported that the soil landslide did a lot of damage, including destroying Manvydas mansion (Balinskis 2007). The next huge landslide record was found in 1547 occurring in the eastern part of Gediminas Hill during winter time (Ragauskienė 2005). This landslide also did a lot of damage to surrounding buildings and retaining wall. Since 1794, Russian artillery units were located on Gediminas Hill and in the Upper Castle. According to Russian State military history archive, slopes

stability problems of Gediminas Hill were reported in 1816, 1817, as well as large-scale landslides in 1843, 1845 and 1846. Two main reasons of these landslides were: increased water level of Neris river by 5 m and inclement weather conditions with huge amount of rainfall. Later, there were also reports about slopes instability in 1930-1938 (Figure 2, left side). However, due to historical reasons (such as warfare), primitive measures such as filling additional layer of soil onto the eroded parts of slope rather than proper engineering measures were applied to Gediminas Hill slopes.

Figure 1: Gediminas Hill and Castle Tower (https://www.pinterest.com/pin/514677063656144453/)

Figure 2: Gediminas Hill slopes instability: on the left had in period of 1930-1938 and on the right hand in period of 2004 and 2008 (Photos from Lithuanian National Culture Heritage Centre archive)

After Lithuania has become an independent country from the Soviet Union in 1991, the geotechnical issues of the Gediminas Hill were visited in more detail. Due to natural and anthropogenic reasons, slope instability problem still existed. In recent years, shallow landslide appeared at the eastern side slope in 2004 and recurred in 2008 (Mikulėnas et al. 2017) (Figure 2, right side). One of the latest recorded landslides occurred in spring 2016, at the northern part of Gediminas Hill (Skuodis et al. 2017). This paper explains the reasons of the occurred landslides with reference to archival data of geological and hydrogeological conditions, describes the engineering measures implemented for slope restoration and protection, and discusses the instrumentation and monitoring as well as topographical monitoring and digitalization works carried out.

2 GEOLOGICAL AND HYDROGEOLOGICAL CONDITIONS

2.1 Engineering geological conditions

In Lithuania, the inventory of geological investigations contains records from XIX century onwards (Česnulevičius et al. 2011). During the engineering geological investigations of Gediminas Hill, since 1955 up to now, a total of 431 boreholes were bored. Only three deep boreholes were bored from the hilltop with a depth of 35–45 m, whereas others boreholes were up to 4–10 m of depth (Drumsta et al. 2010). One of the first geological cross-section was prepared (Figure 3, left side) during archeologic investigations by Holubovičienė and Holubovičius (1940). Up to this moment, 620 boreholes on Gediminas Hill were recorded in total, including registered and unregistered geological investigations. Based on a very big amount of geological information in the archives and additional investigations, Guobytė (2008) prepared an updated Gediminas Hill geological conditions cross-section (Figure 3, right side).

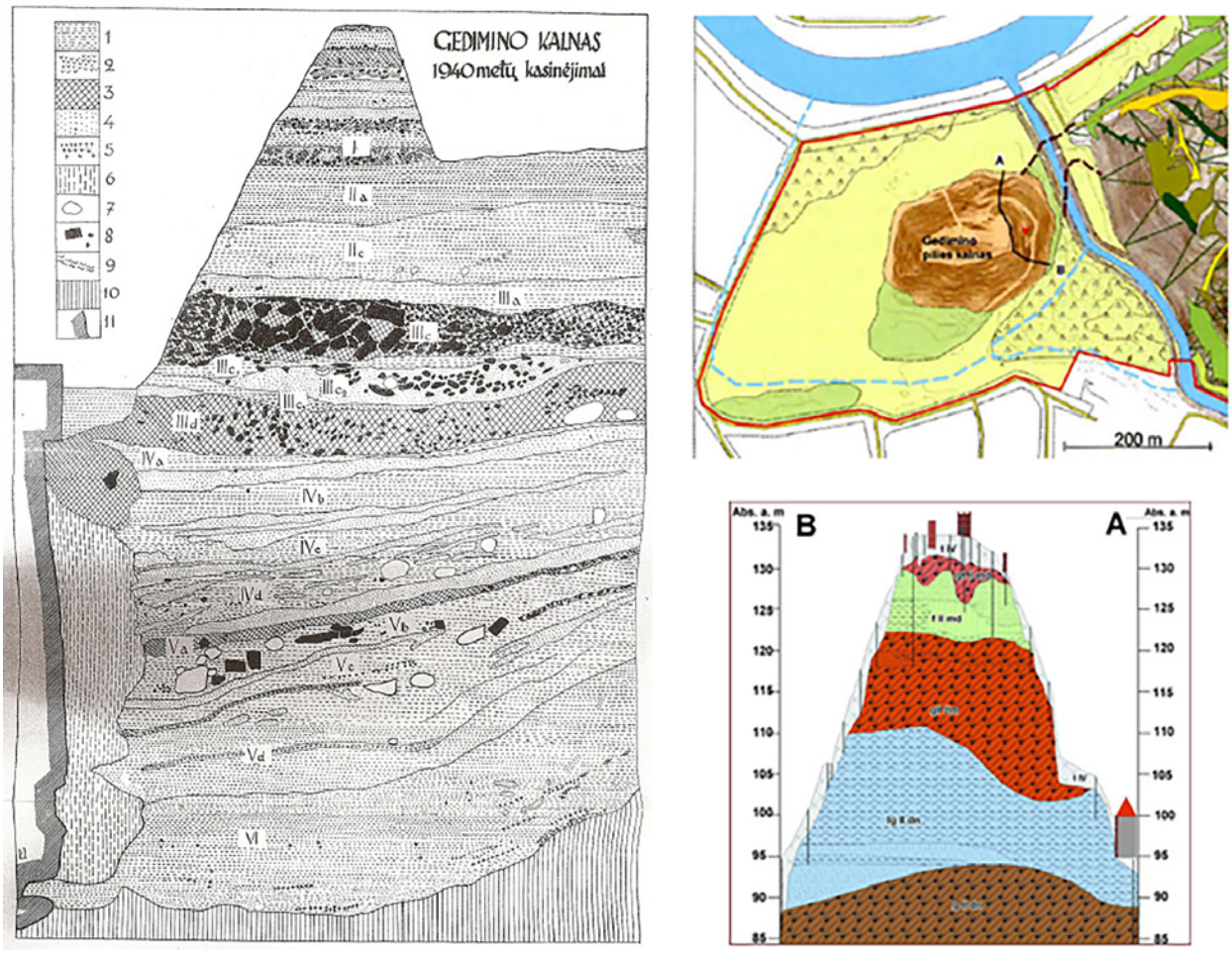

Figure 3: Gediminas Hill geological cross-sections: on the left hand – record in 1940; on the right hand – record in 2008

The height of the Hill is nearly 48 m, measured from the architectural ground level of Cathedral Square (Gaigalas 1983; Gadeikis et al. 2016). The soil mass of Gediminas Hill and bed of Neris and Vilnelė rivers (Baubinienė et al. 2015) consist of the grey, very stiff morainic deposits, such as glacial till and other mixtures of fine and coarse soils. Formations of this layer were dated ~400,000 years ago during the middle Pleistocene ice age – Dainava ice age (gIIdn). The bottom part of Gediminas Hill (thickness of the stratum is 10–20 m) consists from very dense greenish-grey proglacial lake sediments to fine and silty sand (lgIIdn). In the middle part of Gediminas Hill (thickness of the stratum is 10–15 m) is predominantly brown stiff morainic deposits, such as till stratified with sand interlayers and lenses.

The upper part of the Gediminas Hill consists of fliuvioglacial deposits, which was deposited during the middle Pleistocene ice age – Medininkai ice age (fIImd), about 175–130 thousands years ago (thickness of the stratum is 6–8 m). This stratum consists of dense fine sand with silty sand interlayers (Mikulėnas et al. 2017). The fliuvioglacial stratum is overlain by terminal morainic deposits of middle Pleistocene Medininkai ice age (gtIImd). The deposits consist of thin layers (from 0.5–1.0 m to 3.0–5.0 m of thickness) of firm and stiff brown till, with interlayers and lenses of sand (Skuodis et al. 2017). Holocene age artificial deposit (tIV) is mostly obtained in the upper part of the Gediminas Hill. The thickness of the layer is 4–5 m (Skridlaitė et al. 2015). The slopes of the Gediminas Hill are covered by diluvium and artificial deposits (Mikšys et al. 2002). The thickness of layer is very uneven, on the hillside it is from 0.0 to 1.0 m or little more, whereas at the bottom of the slope it is up to several metres. More detailed engineering geological conditions are described by Skuodis et al. (2017).

2.2 Hydrogeological conditions

The hydrogeological conditions of Gediminas Hill mostly depend on the amount of precipitation and melting snow. Part of precipitation water seeps through the artificial deposits (tIV), morainic deposits (gtIImd) and fliuvioglacial sand (fIImd) to reach the stratum of Žemaitija (Samogitia) morainic deposits (Skuodis et al. 2017). The surface of this moraine deposits is uneven and has inclined aquifers in the centre of Gediminas Hill. There were occasions of groundwater discharges from the east slope and formed the spring (Figure 4). Due to this phenomenon, two landslides occurred in 2004 and 2008 (Čyžienė et al. 2012) at the eastern part of Gediminas Hill (Figure 2, right side). Furthermore, the surface of stratum of Žemaitija morainic deposits has inclination to the north direction (Figure 3), where a few locations of groundwater discharges have been observed (Figure 4).

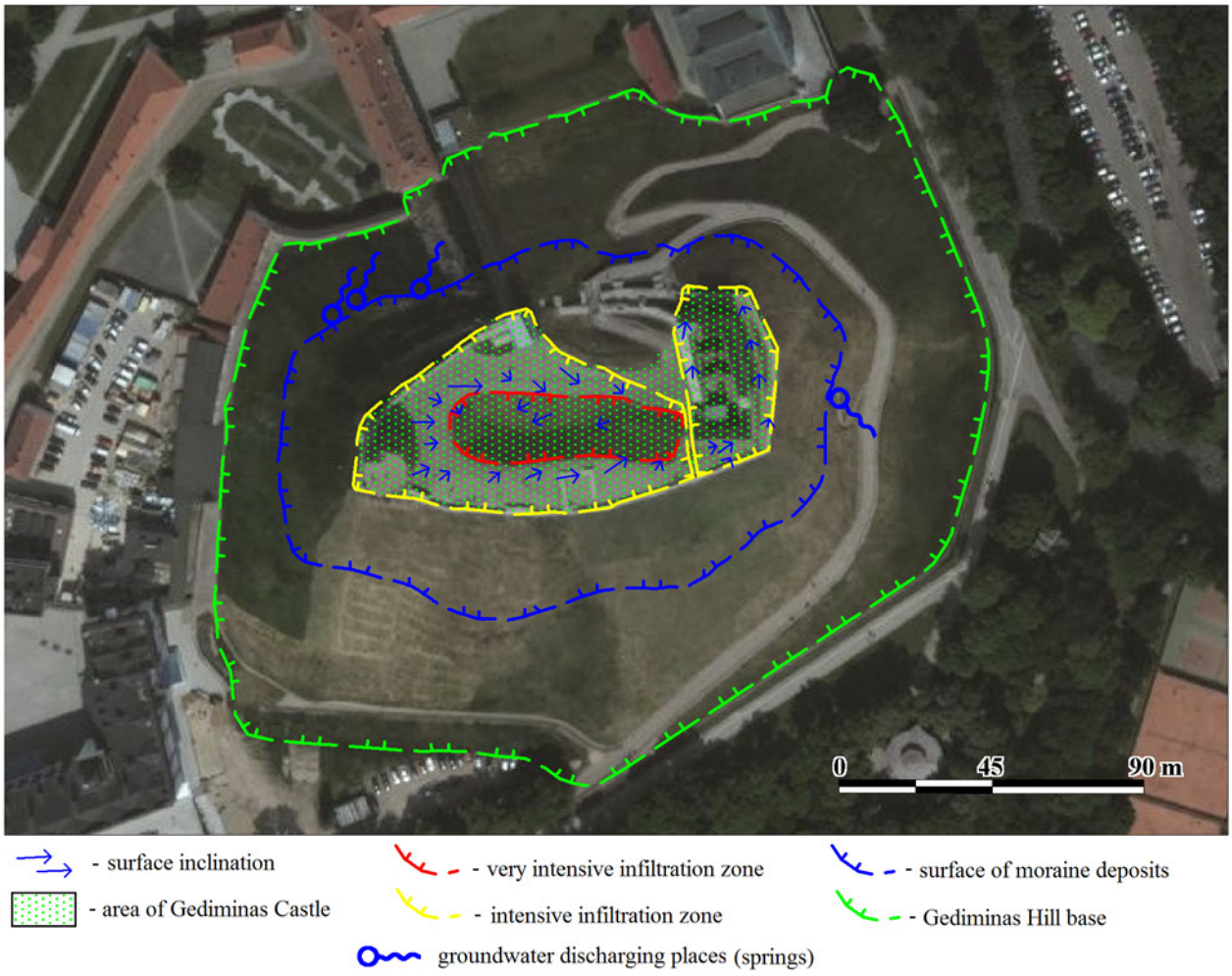

Figure 4: Gediminas Hill groundwater discharging locations (Grota 2016)

According to meteorological data, the average annual precipitation of Vilnius city is 550-670 mm. The amount of precipitation value is not the same for different months and can be ranging from 15-30 up to 80-110 mm per month. The precipitation was in correlation with the groundwater discharge quantity from the springs at the northern and eastern slopes. In accordance with the intensity of water infiltrations, the Gediminas Hill area could be divided into 3 zones (Table 1).

Due to the geological and hydrogeological conditions of Gediminas Hill, the groundwater can be obtained in two levels. The higher groundwater level was identified at 14-15 m of depth from the hilltop, and the lower groundwater level was identified at 40-45 m of depth from the hilltop (Figure 5).

Table 1: Evaluation of water infiltration and discharging

Zone	Area (m^2)	Precipitation (m^3)		Possible infiltration and discharge (m^3)	
		per year	per day	per year	per day
Very intensive infiltration	1180	791	35	396	18
Intensive infiltration	4100	2747	123	824	37
Low infiltration	9100	6097	273	610	27
In total:	14380	9635	431	1830	82

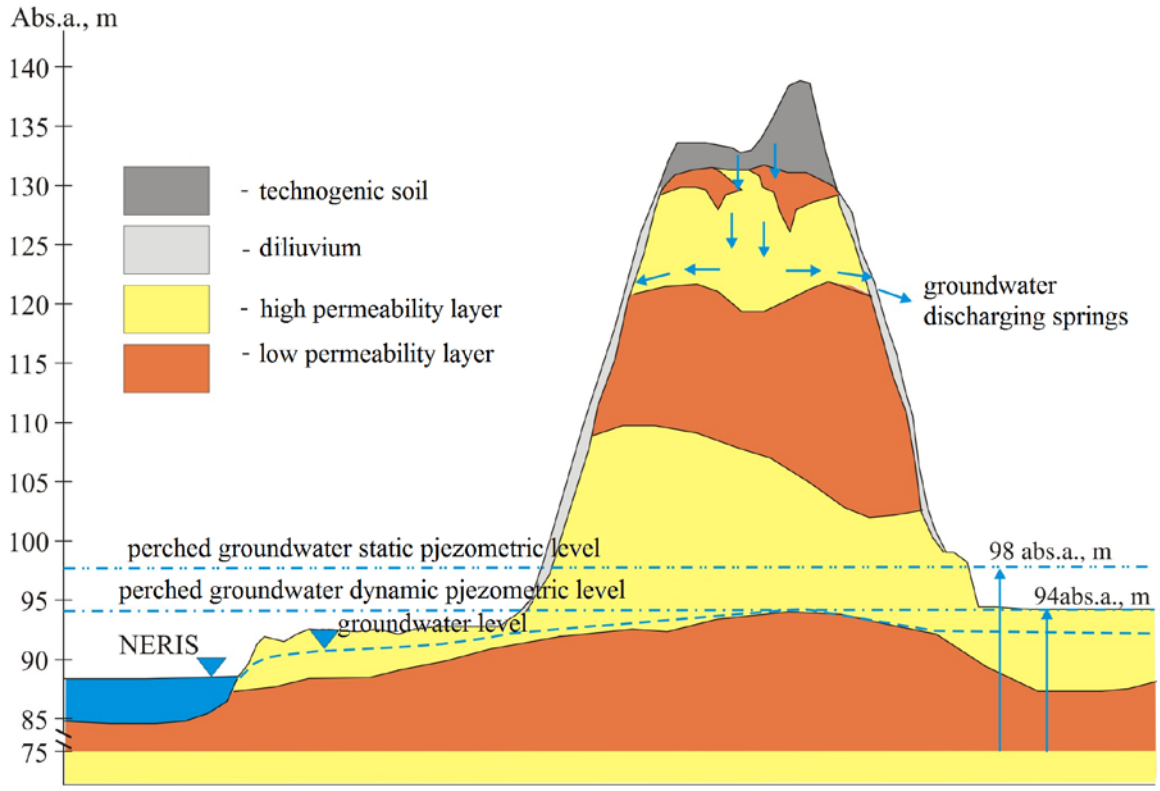

Figure 5: Gediminas Hill hydrogeological cross-section

3 METEOROLOGICAL CONDITIONS

Gediminas Hill is located in south eastern highlands area of Vilnius territory. According to the data from the meteorological station close to Gediminas Hill, the yearly average temperature is 6.1-6.7°C (lowest recorded temperature -37.2°C, highest recorded temperature 35.4°C), annual precipitation is 610-690 mm (average 658 mm/year), period with snow coverage is 90-105 days (maximum recorded thickness of snow 52 cm) and duration of sun shine is 1690-1770 hour/year (Lithuaniae Academia Scientiarum 2016). To reflect the meteorological conditions in recent years, the average monthly temperature and precipitation from 2013 till 2017 are plotted in Figure 6 and Figure 7.

In relation to the shallow landslide occurred in spring 2016, it is observed that the highest temperature and the largest amount of precipitation were recorded in February 2016, comparing with data in year 2013 through 2017. The comparatively high temperature according to Lithuanian climate zone and large amount of rainfall (usually it is snowing in February) were among the main reasons to adversely affect the slopes stability of Gediminas Hill.

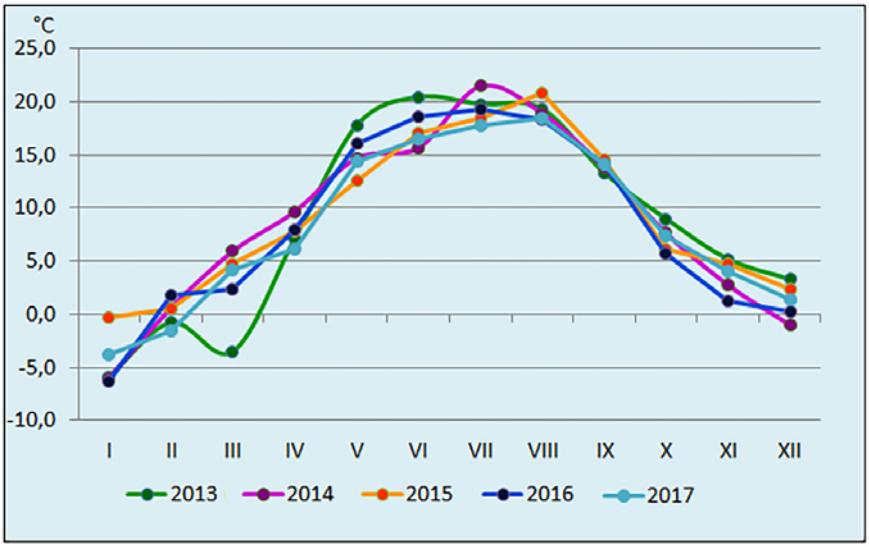

Figure 6: Average month temperature from year 2013 to 2017
(http://www.hkk.gf.vu.lt/vu_ms/duomenu-suvestine/)

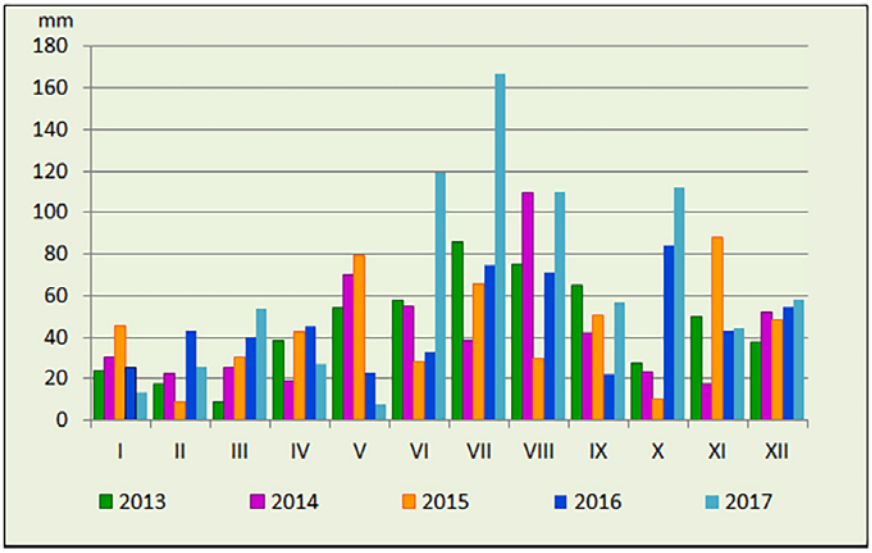

Figure 7. Average precipitation quantity from year 2013 to 2017
(http://www.hkk.gf.vu.lt/vu_ms/duomenu-suvestine/)

4 ROLE OF TREE VEGETATION IN THE STABILITY AND PROTECTION OF GEDIMINAS HILL SLOPES

According to historical records, Gediminas Upper Castle on top of Gediminas Hill was built for defence purposes. To ensure effective military defence, the presence of trees on the slopes was considered undesirable (Figure 8, left side). Until the modern age, trees started to grow in the middle of XIX century, and circa 500 trees was planted by inhabitants on the slopes in 1955. Up to 2011, there were trees reaching even 30 m in height (Figure 8, middle). To restore the historical view of Gediminas Hill, the trees were cut and fell in 2011 (Figure 8, right side).

Figure 8: On the left hand – view of Gediminas Hill in 1795 (https://www.pinterest.com/pin/108438303506360568/); in the middle – view of Gediminas Hill from 1955 till 2011 (https://www.15min.lt/naujiena/aktualu/lietuva/retinami-gedimino-kalno-medziai-56-178622); on the right hand – view of Gediminas Hill after tree-cutting in 2011 (http://www.vilnius.lt/index.php?1098836875)

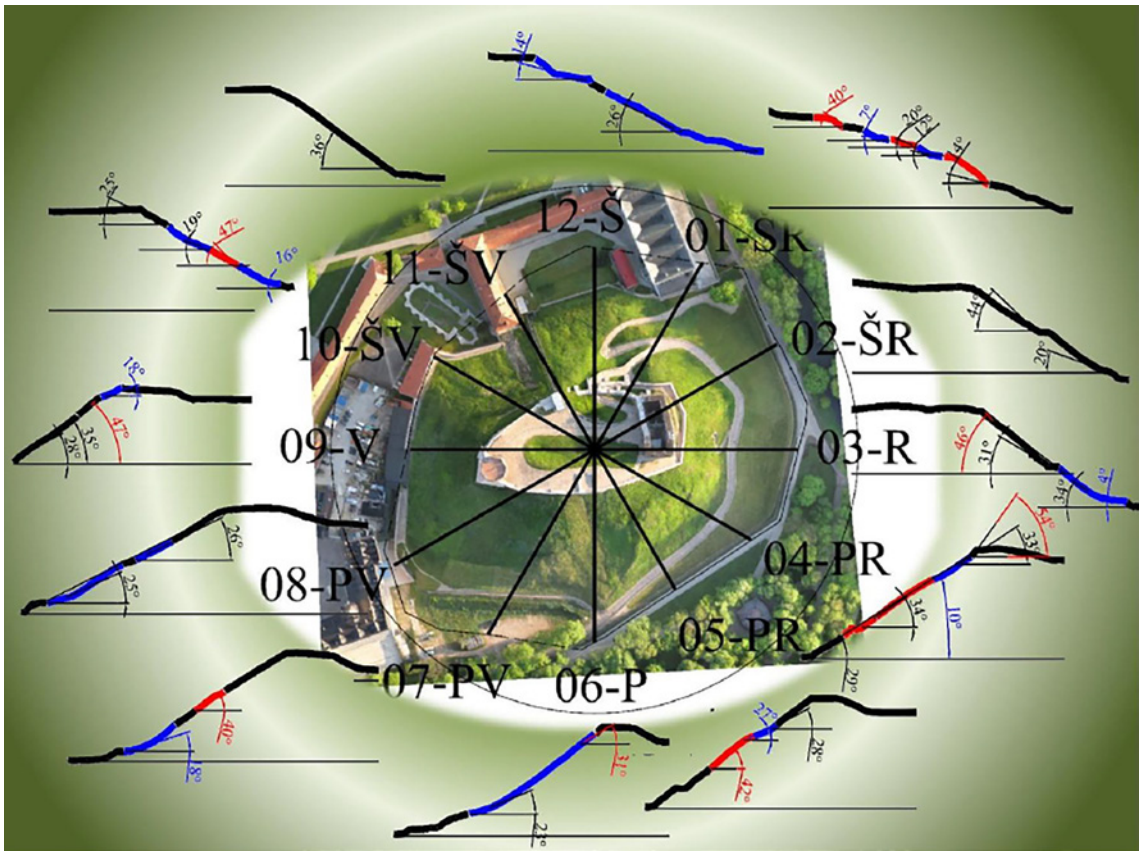

Figure 9: Gediminas Hill slopes inclination (Lithuaniae Academia Scientiarum 2016)

Vegetation, primarily woody plants, helps to prevent soil erosion and movement, particularly shallow sliding in slopes (as happened in 2016 at Gediminas Hill). The presence of woody vegetation may affect the balance of forces in a slope in a number of ways, including: root reinforcement, soil moisture modification, buttressing and arching, surcharge, root wedging and windthrowing. Woody vegetation growing on slopes reinforces soils and enhances stability, conversely its removal weakens soils and destabilises slopes. Knowing that the slopes of Gediminas Hill have inclination from 37° to 43° and in a few parts up to 54° (Figure 9), trees felling on steep slopes would result in subsequent destruction of stabilising root system and contribute to the occurrence of shallow landslides (Figure 10).

The decision to cut the trees on Gediminas Hill in 2011 was based solely on the consideration to restore the historical view of slopes. With reference to Figure 10, the trees on slopes can contribute to the stability by their surcharge due to self-weight, lowering the water table, exerting root cohesion, and decreasing soil cracking. At 1 year after trees removal, the water table would become higher while part of the root cohesion would remain. After 5 years of trees removal, the adverse effects on slope stability

would become apparent due to the absence of surcharge, high water table level, loss of root cohesion, and increased soil cracking. This would increase the likelihood of shallow landslide. Eventually, such incident happened in 2016 (exactly after 5 years).

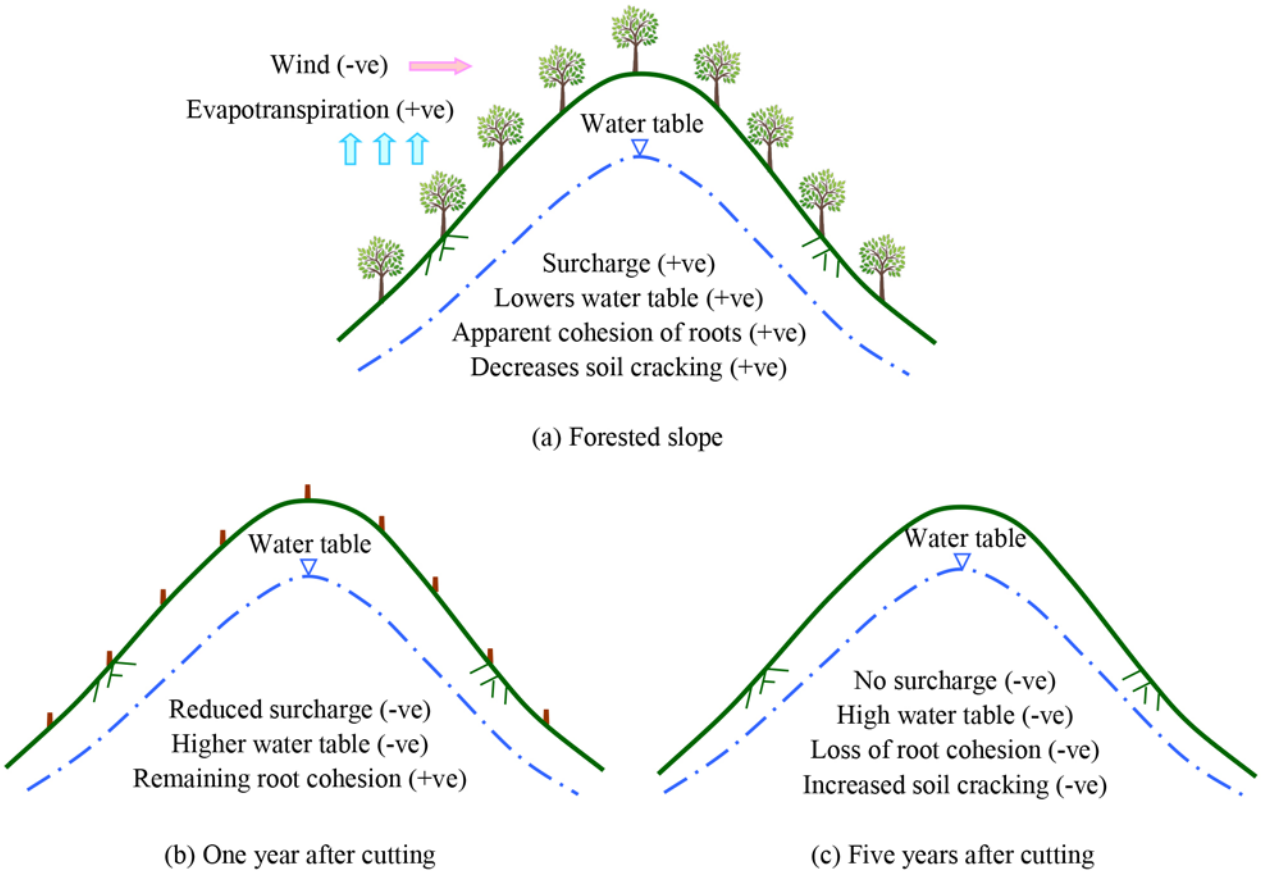

Figure 10: Consequences of trees removal on slope stability

5 TOPOGRAPHICAL MONITORING

Gediminas Hill slope instability incident occurred in 2016 spring, when 30 m^3 debris slide down from the north part of slope close to the existing funicular (Figure 11). The government immediately organized a 2.5-D scanning of Gediminas Hill (Figure 12). Unmanned aerial vehicle (UAV) with programmatic remote control system was employed. It is capable of transmitting signals to and receiving signals from the satellite positioning systems for real-time kinematic control. Special permission for the usage of UAV was obtained due to military restriction of the surveying area. The UAV was equipped with specific photogrammetric software based on LIDAR (light detection and ranging) surveying technique. The camera and software are capable of automatic scanning and recording to produce 2.5-D digital image of the topography. The scanning procedures provided a basis to determine the area of landslide (351 m^2) and to check the deformation of the rest of slopes. It revealed the possibility of ensuing landslide in close vicinity with an affected area of 867 m^2. In addition to topographical monitoring, extensive instrumentation has been applied to Gediminas Hill slopes. For example, survey prisms, inclinometer, and movement sensors were installed over the proximity of landslide area, in addition to a computerised automatic data acquisition and alarming system. Automated measurements have been conducted on an hourly basis throughout 24-hour per day, whereas manual measurements have been conducted at least daily with increased frequencies upon changes in weather conditions and any necessary event. Any excessive movement due to slope instability would trigger the alarm for immediate actions. An emergency action plan has been formulated to ensure timely and appropriate measures to be taken.

According to the findings from topographical monitoring, the landslide volume was 31 m^3. Compared to the totally removed soil volume from the landslide area of circa 30 m3 (Lithuaniae Academia Scientiarum 2016), this proves the precision of the topographical monitoring works. The occurred landslide was shallow with maximum depth of 0.6-0.8 m, and did not encroach into the natural soil layers. In the assessment and mitigation of future risk of landslides, it was accepted to remove the unstable soil from the zones 2 and 3 depicted in Figure 11 and to launch the slopes restoration project to improve the stability. Since Gediminas Hill is included in Lithuanian cultural heritage and is under UNESCO protection, the restoration works are associated with substantial national and public interest and should be coordinated with various stakeholders, including government authorities, archaeologist and institutions. During the coordination process, there was occurrence of shallow landslide in zones 2 and 3 (Figure 11) subsequently on 10th of October 2016. This landslide involved sliding of 140 m^3 of soil.

Figure 11: Landslide area in spring 2016 (Lithuaniae Academia Scientiarum 2016):
1 – landslide area (351 m^2); 2 – slope deformations and possible ensuing landslide area (222 m^2);
3 – slope deformations and possible ensuing landslide area (645 m^2).

Figure 12: Gediminas Hill topographical monitoring (Lithuaniae Academia Scientiarum 2016):
on the left hand – digital topography scheme; on the right hand – digital surface (2.5-D view)

6 GEDIMINAS HILL NORTH PART SLOPES RESTORATION

Gediminas Hill north part slopes restoration project covered an area of approximately 3780 m^2. The works included removal of the technogenic and diluvium soil from the slopes, which was filled during the time of World War I and II. A large part of the additional soil layer was filled by German army, when they dug an escaping tunnel from Gediminas Castle in 1944 and all dug-out soil was layered directly onto the slopes. The tunnel was of width 1.6 m and height 2 m, and the entrance portal was at a depth of 25 m from the hilltop. The tunnel had 2 exits where one led to Cathedral Square of Vilnius through a length of approximately 88 m, and the other led to the north part of Gediminas Hill slope (where the landslide occurred) through a length of approximately 79 m. After removing the landslide soil, gabion wall with dolomite fill was installed. The gabions were additionally reinforced with geogrids. Table 2 lists the main geological layers properties (density ρ, unit weight γ, water content W, degree of saturation S_r, void ratio e, plasticity index I_P, liquid limit index I_L, cohesion c, angle of internal friction ϕ, Young's (deformation) modulus E_{oed}, cone resistance q_c) applied in the design of Gediminas Hill north part slopes stabilisation (http://atviras.vilnius.lt/gedimino-kalnas).

Schematic representation of Gediminas Hill north part slope stabilisation works is shown in Figure 13 (http://atviras.vilnius.lt/gedimino-kalnas). The slope stability is enhanced by the installation of gabions wall. Each gabion wall unit is of 3 m length, 2 m width and 1 m height. Depending on the slope inclination and location, the calculated safety factor against slope instability varied from 1.55 to 2.10. Figure 14 depicts the execution of gabion wall installation. The filling material of gabions wall imitates the high permeability technogenic layer, which ensures drainage of infiltrated precipitations from the Gediminas Hill slope surface. After installation, the gabion wall will be covered with: a) geomat which is made from a three-dimensional matrix of UV-resistant, non-degradable synthetic fibres, heat-weld bonded where they cross, extruded onto a double twisted steel woven mesh; b) coir blankets which consist of 100% untreated coir stitched on one or two sides with polypropylene (PP) or jute netting (PP or jute/cotton thread is used for the stitching with 100% soil coverage) for protection of finished slope surface.

Table 2: Main physical and mechanical properties of Gediminas Hill north part slope geological layers

Geological layer No.	Soil description	ρ, Mg/m^3	γ, kN/m^3	W, %	S_r	e	I_P	I_L	c, kPa	ϕ, °	E_{oed}, MPa	q_c, MPa
11	Medium coarse sand	1.68	16.48	0.12	0.50	0.65	–	–	9	35.0	25	–
12	Fine sand	1.73	16.97	0.15	0.64	0.62	–	–	11	34.0	23	–
13	Morainic clay loam	2.21	21.68	0.12	0.91	0.35	0.075	–0.16	54	29.2	25	–
15	Silty sand	1.87	18.34	0.11	0.52	0.57	–	–	12	41.0	35	–
16	Sandy loam	1.95	19.13	0.17	0.86	0.55	0.060	–0.69	20	28.1	40	–
17	Clay loam	1.97	19.33	0.21	0.92	0.62	0.090	0.14	29	24.9	35	–
23	Morainic clay loam	2.25	22.07	0.12	0.92	0.36	0.240	0.14	105	31.4	35	18
24	Fine sand	1.71	16.78	0.21	0.96	0.58	–	–	20	35.9	30	–
26	Silty sand	1.97	19.33	0.24	1.00	0.62	–	–	22	30.5	45	15
27	Sandy loam	1.89	18.54	0.25	0.97	0.69	0.070	0.25	25	24.2	30	12
28	Clay loam	2.01	19.72	0.27	0.97	0.75	0.120	0.35	35	26.1	25	14

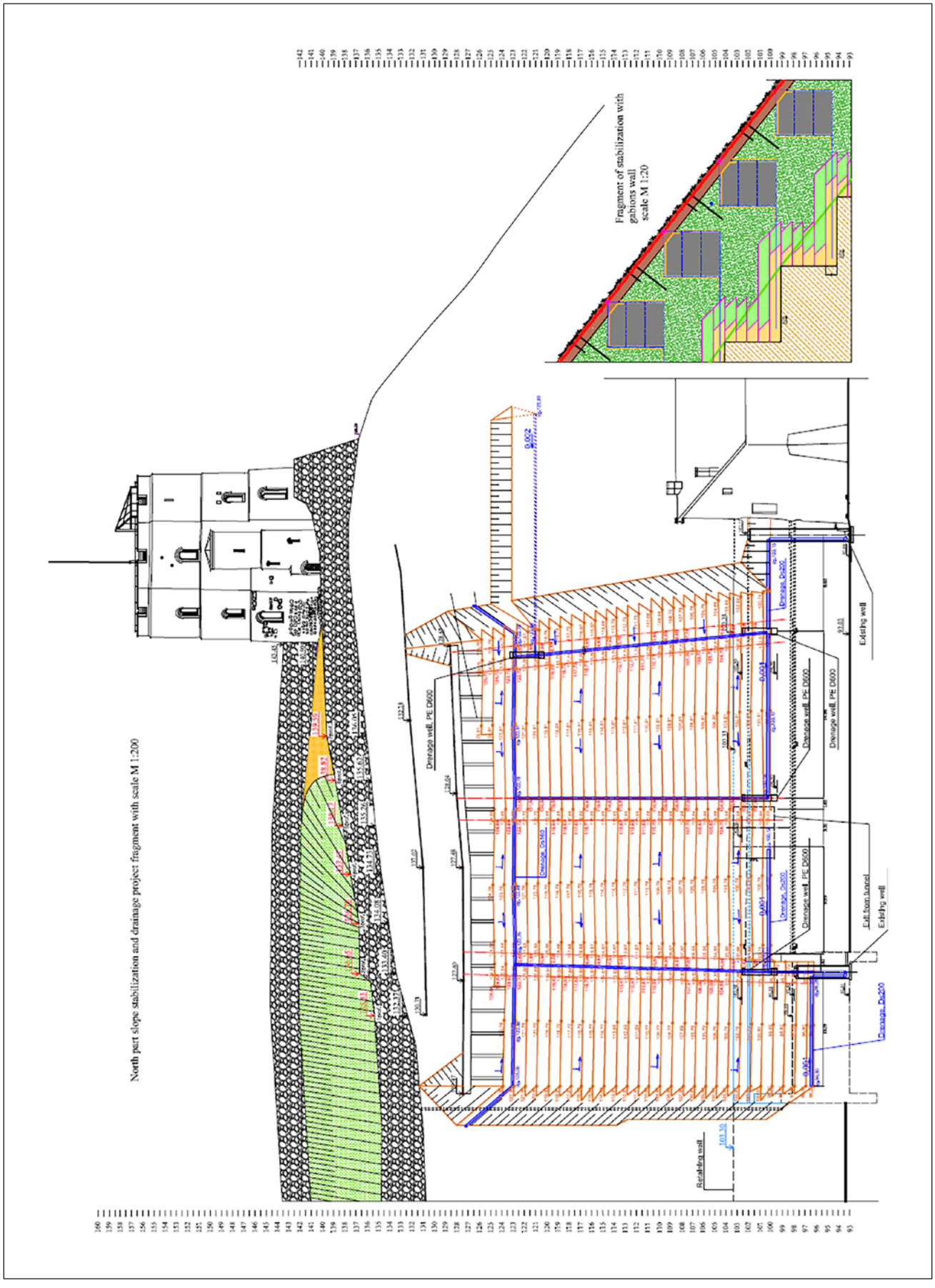

Figure 13: Schematic representation of Gediminas Hill north part slope stabilisation project

Figure 14: Gediminas Hill north part slope stabilisation with gabions wall installation

7 CONCLUSIONS

Owing to both natural (glacial geology and hydrogeology) and anthropogenic (artificial activities and warfare) reasons, the slopes of Gediminas Hill in Vilnius have manifested instability problems and shallow landslides have occurred in the past. The various factors associated with the recent landslide have been highlighted and explained in this paper. To preserve Gediminas Hill and Gediminas Castle Tower which are highly important cultural heritage of Lithuania, a combination of engineering measures for slope restoration and protection have been implemented. At the same time, topographical monitoring and digitalization have been conducted using unmanned aerial vehicle and advanced surveying technology, in addition to extensive instrumentation and monitoring. The slope stability is improved by removal of surface layer of filled soil and installation of gabion wall with desirable drainage property of fill material and surface protection by geomat and coir blankets.

REFERENCES

Balinskis, M. 2007. Vilniaus miesto istorija, Vilnius: Mintis, p. 165.

Baubinienė, A.; Morkūnaitė, R.; Bauža, D.; Vaitkevičius G.; Petrošius, R. 2015. Aspects and methods in reconstructing the medieval terrain and deposits in Vilnius, *Quarternary International* 386: 83–88.

Česnulevičius, A., Švedas, K., Morkūnaitė, R., Paškauskas, S., Pukelytė, V., Vekeriotienė, I., Karmazienė, D., 2011. Lithuania's geomorphology development in the 20th century in the context of global ideas. *Baltica,* Vol. 24, Special Issue - Geosciences in Lithuania: challenges and perspectives, 19–22.

Čyžienė, J.; Minkevičius, V.; Mikulėnas, V.; Satkūnas, J. 2012. *Geohazard description for Vilnius.* PanGeo D7.1.28

Drumsta, V.; Trumpis, G.; Grigonienė, L. 2010. *Gedimino kalno ir Aukštutinės pilies Vilniuje, (unikalus kodas 141) atliktų geologinių ir hidrogeologinių tyrimų archyvinės medžiagos sąranka, analizė ir išvados.* V. Į. Lietuvos paminklai. 34 p.

Gadeikis, S.; Dundulis, K.; Daukšytė, A.; Gadeikytė, S. 2016. The Cathedral of Vilnius: problems and features of natural conditions, in *13th Baltic Sea Geotechnical Conference,* 22–24 September 2016, Vilnius, Lithuania. (https://doi.org/10.3846/13bsgc.2016.001)

Gaigalas, A. 1983. Vilniaus pilies kalno sluoksniai, *Mūsų gamta* 8: 6–7.

Grota 2016. *Gedimino kalno hidrogeologinės situacijos įvertinimas ir rekomendacijos jo šlaitų stabilumui gerinti,*11 p.

Guobytė, R. 2008. Vilniaus pilių teritorijos egzotiškasis reljefas ir gelmių sandara, *Lietuvos pilys* 3: 34–35.

Holubovičienė, E., Holubovičius, V. 1940. Gedimino kalno Vilniuje 1940 metų kasinėjimų pranešimas.

Lithuaniae Academia Scientiarum 2016. Gedimino pilies kalno šlaitų būklės ir jų tvarkymo programos vertinimo ataskaita.

Mikulėnas, V., Minkevičius, V., Satkūnas, J. 2017. Gediminas's Castle Hill (in Vilnius) case: Slopes failure through historical times until present. *Advancing Culture of Living with Landslides*.

Mikšys, R.B., Marcinkevičius, V., Mikulėnas, V. 2002. Human factors in landsliding processes of Lithuania. *In: Landslides: Proceedings of the First European Conference on Landslides,* Prague, Czech Republic, June 24–26, 2002. A. A. Balkema Publishers, Lisse, Abingdon, Exton (PA), Tokyo, 251–254 p.

Morkūnaitė, R.; Baubinienė, A.; Vaitkevičius, G. 2015. Geographical–historical interpretation of natural conditions in the reconstruction of Vilnius city formation and development, *Geologijos akiračiai* 3: 15–22.

Rackevičius, G. 2010. LDK valdovų rūmų ir Vilniaus pilies teritorijos tyrimai 2002-2009 metais. *Lietuvos pilys,* 5(2009): 164–182.

Ragasukienė 2005. *Vilniaus Žemutinė pilis XIV a. –XIX a. pradžioje. 2002–2004 m. Istorinių šaltinių paieškos,* Vilnius.

Semaškaitė, I. 2005. Lietuvos pilys ir dvarai. *Vilnius: Algimantas*.

Skridlaitė, G., Guobytė, R., Satkūnas, J. 2015. The forts and castle mounds in Lithuania: interaction between geodiversity and human-shaped landscape. *Geophysical Research Abstracts*.

Skuodis, Š., Kelevišius, K., Žaržojus, G. 2017. Vibrations measurement of the funicular generated vibrations on Gediminas Hill north part slope. *10th International Conference "Environmental Engineering"*, 27-28 April 2017, Vilnius Gediminas Technical University, Lithuania. Vilnius: VGTU Press, 2017, p. 1-8.

Webpage: *Atviras Vilnius: Gedimino kalnas* (http://atviras.vilnius.lt/gedimino-kalnas) (accessed in 2018 01 17).

Webpage: *Pinterest.com: Gediminas Castle, Vilnius* (https://www.pinterest.com/pin/514677063656144453/) (accessed in 2018 01 15).

Webpage: *Pinterest.com: View of Gediminas Hill (1795) from west side* (https://www.pinterest.com/pin/108438303506360568/) (accessed in 2018 01 15).

Webpage: *Vilniaus Universiteto Hidrologijos ir Klimatologijos Katedra: Duomenų suvestinė* (http://www.hkk.gf.vu.lt/vu_ms/duomenu-suvestine/) (accessed in 2018 01 15).

A Case Study On the Application of Multiple Regression Analysis to Predict the Overbreak of a Weak Rock Tunnel

Arthur K.O. So, Joe C.H. Ng, Nickman K.W. Fong and Simon K.C. Lam
Meinhardt Infrastructure and Environment Limited

Wang Yanhua
China Road and Bridge Corporation

ABSTRACT

The research on the prediction of overbreak is very limited. It involves very complex mechanism and is considered largely controlled by the geological factors and blasting factors; generally increasing as the rock mass quality decreases and the blasting parameters increase. In this paper, 221 blasts of a tunnel in very poor to poor rock are reviewed. The lumped geological factor Q-value and some blasting parameters including the powder factor, maximum charge per delay, explosive per pull length and explosive in perimeter hole are analyzed. The data distributions are found to be very scatter, likely because the contributing parameters are many and are inter-related, and the trends of overbreak therefore appear not distinct. Linear regression analysis of individual controlling parameter shows that the overbreak generally increases slightly as the blasting parameter decreases except in very poor rock. This trend is different to the findings of other researchers and may be due to the local collapse of overhang loose fragmented rock in very poor rock leading to some large overbreaks. Based on these findings and information that is readily obtained in most blasting works, and using multiple regression analysis and a predictor to capture the unusual overbreaks in the previous blasting round, a simple predictive equation can be obtained to determine the overbreak of a poor volcanic tuff tunnel.

Keywords: Drill and Blast Tunnel, Overbreak, Geological and Blasting Factors, Rock Mass Quality, Q-System, Powder Factor, Maximum Charge per Delay, Multiple Regression Analysi

1 INTRODUCTION

Drill and blast is a commonly used method in mining, quarrying and civil engineering such as tunnel, dam and road construction. It is a controlled use of many different varieties of explosives of different compositions and performance properties to break up rock for excavation. Before the advent of the tunnel boring machines in 1960s, the drill and blast method is the only way to excavate long tunnels through hard rock where digging is not possible. Despite the tunnel boring machine has the advantages of quicker advancement in favourable ground, less impact to the environment and less overbreak to the designed profile, the drill and blast method is still widely used because of its low investment cost, high adaptability to very varied ground condition, and large flexibility to deal with different shapes and sizes of openings. However, the drill and blast method will inevitably damage the surrounding rock mass due to the formation of a network of fine cracks which may lead to safety and stability concerns.

According to some researchers (e.g. Singh, S. and Lamond, R.D. 1994, Verma, H.K. et. al. 2016), the rock mass damage zone surrounding an underground opening can be distinguished into an over-break zone (or failed zone), a damaged zone and a disturbed zone. As shown in Figure 1, the over-break zone represents the zone beyond the minimum excavation line of the designed periphery from where the rock blocks/slabs detached from the rock mass. It is a measure of the difference between the designed profile and the after blast profile. The damaged zone is a zone of fine networks of micro-cracks and fractures induced by the blasting and excavation process. It is characterized by the deterioration in the mechanical and physical properties and the increase in the transmissivity properties. The disturbed zone is a zone in the rock mass immediately beyond the damaged zone where the changes in the rock mass properties are insignificant and reversible. This zone is dominated by the changes in the stresses and hydraulic permeability. As the over-break and damaged zones have significant impact on the project cost, construction period, safety and performance of the underground opening, prediction of their extents prior to the construction becomes important. In this paper, the prediction of the overbreak zone in relation to the local practice is examined.

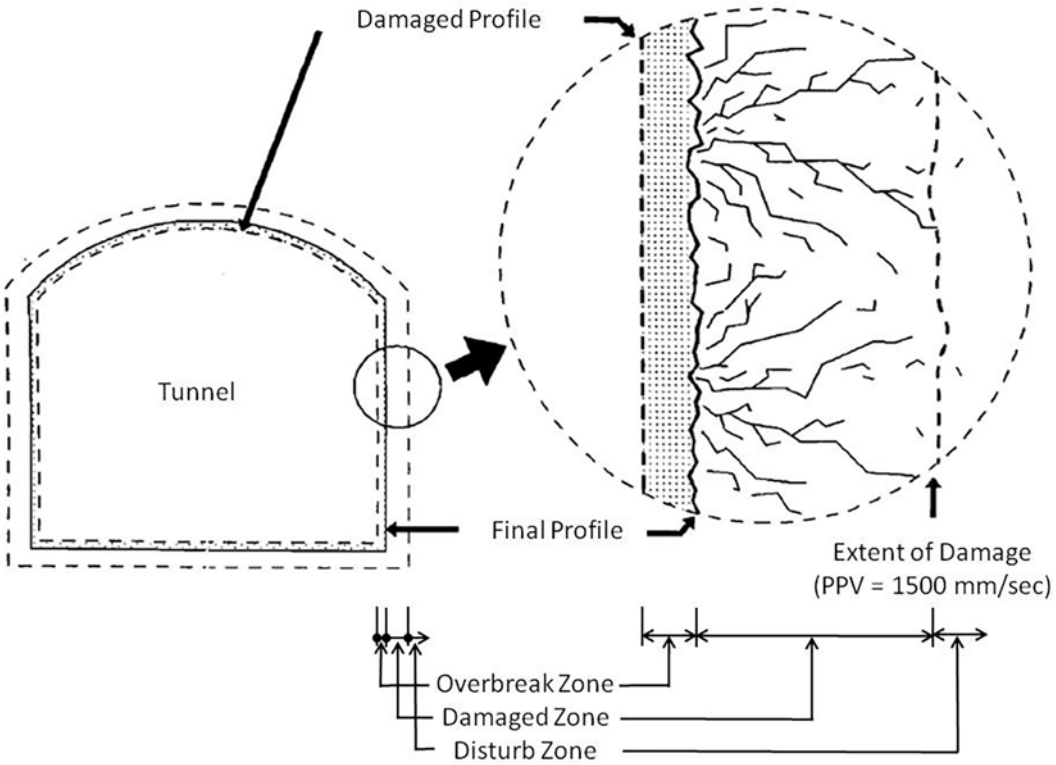

Figure 1 – Schematic Representation of Extent of Rock Mass Damage Zone

2 Prediction of the Overbreak

Overbreak is commonly expressed in term of thickness/distance (Singh, S.P. 1994, Jang, H. and Topal, E. 2013) or percentage (Ibarra, J.A. et al. 1996, Murthy, V.M.S.R. et al. 2003, Verma, H.K. et al. 2016) of rock that is removed from the periphery of an opening beyond the planned limit. It can be influenced by two major groups of factors; namely, the geological parameters and the blasting parameters (Ibarra, J.A. et al. 1996, Mahrab, M.A. et al. 1997, Mandal, S. et al. 2008, Jang, H. and Topal, E. 2013, Verma, H.K. et al. 2016, Mottahedi, A. et al. 2017). Of the geological parameters, jointing is the major factor influencing the overbreak. Other factors including the joint orientation, spacing (i.e. block size) and filling (or alteration), intact strength of the rock and in-situ ground stress conditions also contribute. They are the intrinsic properties of the rock mass and are "unchangeable" factors. The blasting parameters include the explosive type and powder factor, charge concentration, delay timing, perimeter blasthole pattern, drilling deviation, blasthole length and diameter, large hole cut etc. They are the result of the blasting

design aiming to reduce the overbreak and to limit the vibration effects to the surrounding environment and are therefore "changeable" factors. Over the past decades, many controlled blasting techniques / methods such as line drilling, trim (cushion) blasting, smooth (contour or perimeter) blasting, pre-splitting, selecting and employing various parameters of blast design, using modern technology such as precise timing delays, varied density of explosives product by using bulk explosives; muffle blasting are also used. Because of the large number of these variants, there are no efficient and precise methods to predict the overbreak. The predictions of overbreak by some previous researchers are abstracted in Table 1.

Researchers	Methodology	Major Findings/Research Results
Singh, S.P. (1994)	Considering the tensile strength (Ts) and elastic modulus (E) of rock are the two major parameters to determine the critical particle velocity (Vd) at which the damage occurs. The location where Vd will occur is determined using a predictive model developed from the blast vibration monitoring readings.	V_d (mm) = V_pT_s/E where V_d = the critical particle velocity V_p = longitudinal wave velocity T_s = tensile strength of the rock E = Elastic modulus of the rock For the test site, V_d was found in the range of 1500-2000mm/s with an average of 1750mm/s.
Ibarra, J.A. et al. (1996)	Q-factor is considered to give the closet correlation between the rock mass characteristics and overbreak. Perimeter Powder Factor (PPF) is taken as a lumped blasting design parameter. They are used to predict the overbreak using multiple regression analysis.	Overbreak (%) = -0.12 + 15.07 PPF – 2.55 log(Q) where PPF = perimeter powder factor
Innaurato, N et al. (1998)	Rock Mass Rating (RMR) is considered in describing the rock mass characteristics because it is widely used in tunnel design. Based on the research data of 17 tunnels from others, graphical plots are presented to verify the effect of RMR to the blasting quality.	1. Large ratio of length of half casts of holes present in the contour after blasting to the total length of contoured boreholes (HCF) reduces with the overbreak. 2. There is no distinct trend between the ratio of theoretical pull of the round (η) and RMR, nor between the powder factor RMR and RMR, possibly the specific consumption of explosives (c) is dependent, to a great extent, on the tunnel section.
Murthy, V.M.S.R. et al. (2003)	Existing PPV based damage estimation models by other researchers are reviewed. It is considered that before the rock fails as overbreak, it must pass through two stages; namely, the blast-induced crack growth and the crack widening due to expanding gas, and these two threshold levels are needed to identify. Based on the vibration monitoring of trial blasts, the maximum charge per delay and measured overbreak are statistically analyzed.	Overbreak (%) = $0.2867\ X^{1.999}$ where X is the maximum charge per delay in kg
Schmitz, R.M. et al. (2006)	Digitised geomechanical data such as the RMR, stratigraphy, lithology and discontinuity spacing and disgitised geodetric overbreak data are superimposed.	1. There is no straightforward relationship between the overbreak and the rock mechanical data. 2. Overbreak is related to the RMR, and more in detail to the discontinuity spacing and orientation of the discontinuity with respect to the tunnel and gravity.

Jang, H. and Topal, E. (2013)	Geological and blasting factors are considered as two principal groups influencing overbreak. Overbreak prediction models relating to the RMR and RMR criteria are developed using linear multiple regression analysis, nonlinear multiple regression analysis and artificial neural network.	1. Overbreak (centimeter) = 54.825 + $0.114S_c$ + 0.338RQD – $0.910J_s$ + $0.883J_w$ – 2. 0.785RMR Overbreak (centimeter) = 53.607 – 3. $1.210J_a$ – $1.919J_s$ Overbreak (centimeter) = 3.457 – 0.072[quadratic]J_s + $272.58/J_a$ where S_c = unconfined strength of rock J_s = joint spacing J_a = joint state
Sun, S. et al. (2013)	Combined Wavelet Neural Network Method and Statistics Theory.	An artificial neural network (ANN) is proposed which is a soft computing method that is motivated by the human brain process. It is made up of three components; namely, the network architecture, learning algorithm, and transfer function.
Barton, N.R. and Grimstad, E. (2014)	Q-value is considered more advantages than RMR or GSI because it resembles a logarithmic scale of quality with its six orders of magnitude from approximately 10^{-3} to 10^{3}. Using an unusual combination of Q-parameters, the overbreak facilitating ratio = joint set (J_n)/joint roughness (J_r) to predict the overbreak.	Overbreak is extremely likely to occur if the most frequent value of the ratio J_n/J_r > = 6.
Verma, H.K. et al. (2016)	Q-factor is considered as the preferred method of classification of rock mass for civil construction such as tunnels. Based on the field data, overbreak is related to the specific charge (q), maximum charge per delay (W), perimeter charge factor (q_p), advancement factor (A_f) and confinement factor (C_f) using multi-linear regression analysis.	1. Overbreak (%) = 6.52 (q_p/A_f) + 0.78 2. Overbreak (%) = 0.64 (100 C_f/Q) + 7.51 3. Overbreak (%) = 0.854 $q/Q^{0.15}$ (Wd/a + $3.89q_p/A_f$) + 0.69 where q = specific charge W = maximum charge per delay q_p = perimeter charge factor A_f = advancement factor = pull (l) / hole depth (d) C_f = confinement factor = hole depth (d) / cross sectional area of tunnel (a)
Mottahedi, A. et al. (2017)	Geological and blasting parameters are as two major factors influencing overbreak. Based on past researchers and collected data, overbreak is predicted using multiple linear regression analysis, multiple non-linear regression analysis, artificial neural network, fuzzy logic model, ANFIS and SVM.	Like the ANN, a multi-layer perceptron (MLP) neural network approach is proposed.

Table 1 – Predictions of Overbreak

3 The Tunnel Site

In this paper, the tunnel site being studied is in the New Territories in Hong Kong. As shown in Figure 2, it consists of about 0.75km long twin tunnels underneath a natural hill. The natural hill slope of the area rises from about +36mPD in the south up to the highest point of +167mPD at the summit and falls to +50mPD in the north. Each tunnel is about 15.0-15.6m excavation span and 11.2-13.4m excavation height, and with 7 cross passenger crossings each of 7.1-8.1m excavation span and 4.8- 7.9m excavation height.

Prior to the construction, 20 vertical, 4 inclined and 2 horizontal drillholes were sunk. Figure 3 and Figure 4 are the 3D geological model and geological profiles along the tunnel alignment. They show that the surface is a layer of superficial deposits, underlain by the completely to highly decomposed tuff, then a matrix of soil containing corestones / boulders of moderately decomposed tuff or better and finally moderately to slightly decomposed tuff. Televiewers indicates that there are 4 major joint sets at different dip angles and dip directions; namely, at 38°/336° (dip angle/dip direction), 86°/172°, 78°/121°

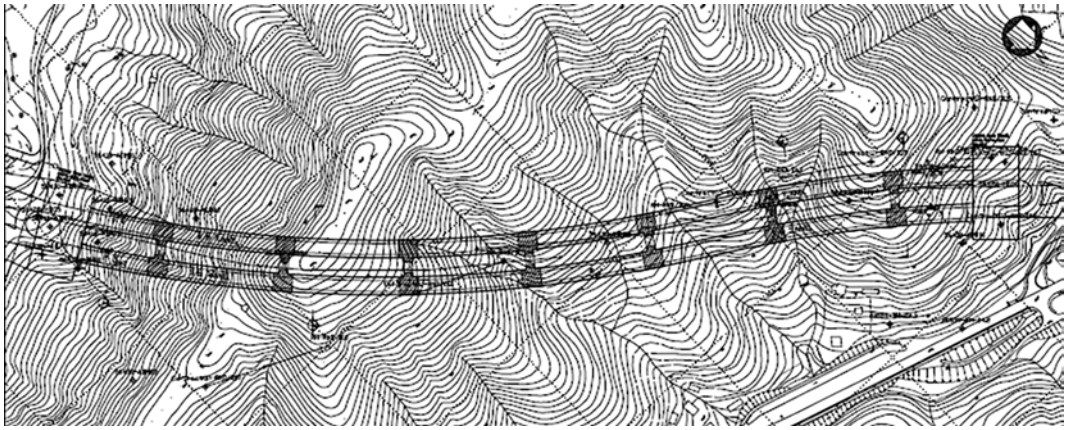

Figure 2 – The Tunnel Site

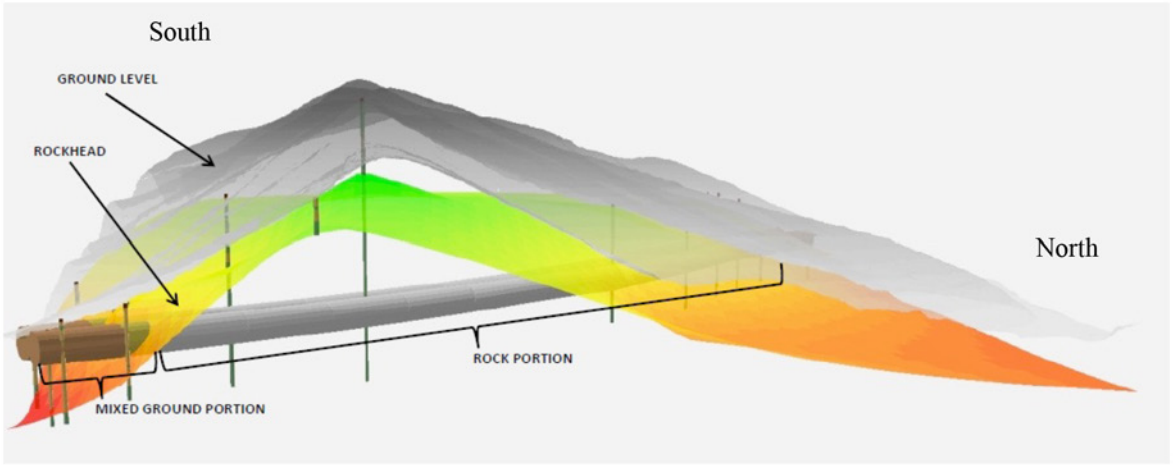

Figure 3 – 3D Geological Model

and 24°/263°. The north and south portals are found to be in a mixed ground while the central portion is in rock. Rock mass parameters are then assessed using the empirical NGI Tunneling Quality Index (Q-System) (Barton, N.R. et al. 1974). Table 2 is a summary of the distribution of the Q-values. It indicates that the majority of the rock mass quality to be blasted is from very poor to poor rock with about 10% being fair or better rock. Drill and blast method was adopted to excavate the rock portion of the main tunnel and cross passage with anticipated Q-value greater than 0.15.

Rock Classes (The Q-Support Chart by Grimstad, E. and Barton, N.R. 1997)					
F	E		D	C	B
Extremely Poor	Very Poor		Poor	Fair	Good
$Q \leq 0.1$	$0.1 < Q \leq 0.3$	$0.3 < Q \leq 1$	$1 < Q \leq 5$	$5 < Q \leq 10$	$Q > 10$
7.3%	9.0%	17.5%	56.9%	8.2%	1.1%

Table 2 – Summary of Distribution of Q-Values for the Entire Rock Portion

Since blasting requires the storage, transport and use of commercial explosives, it has to be subject to local regulations to ensure its safe implementation. According to the Practice Notes for Authorized Persons, Registered Structural Engineers and Registered Geotechnical Engineers PNAP APP-72 in the control of blasting, at the proposed areas of blasting, the locations of all sensitive receivers including streets, structures, foundations, railways, public utilities, water mains, drains, sewers, gas mains and other services, geotechnical features such as slopes, retaining walls, boulders, tunnels, caverns etc. that

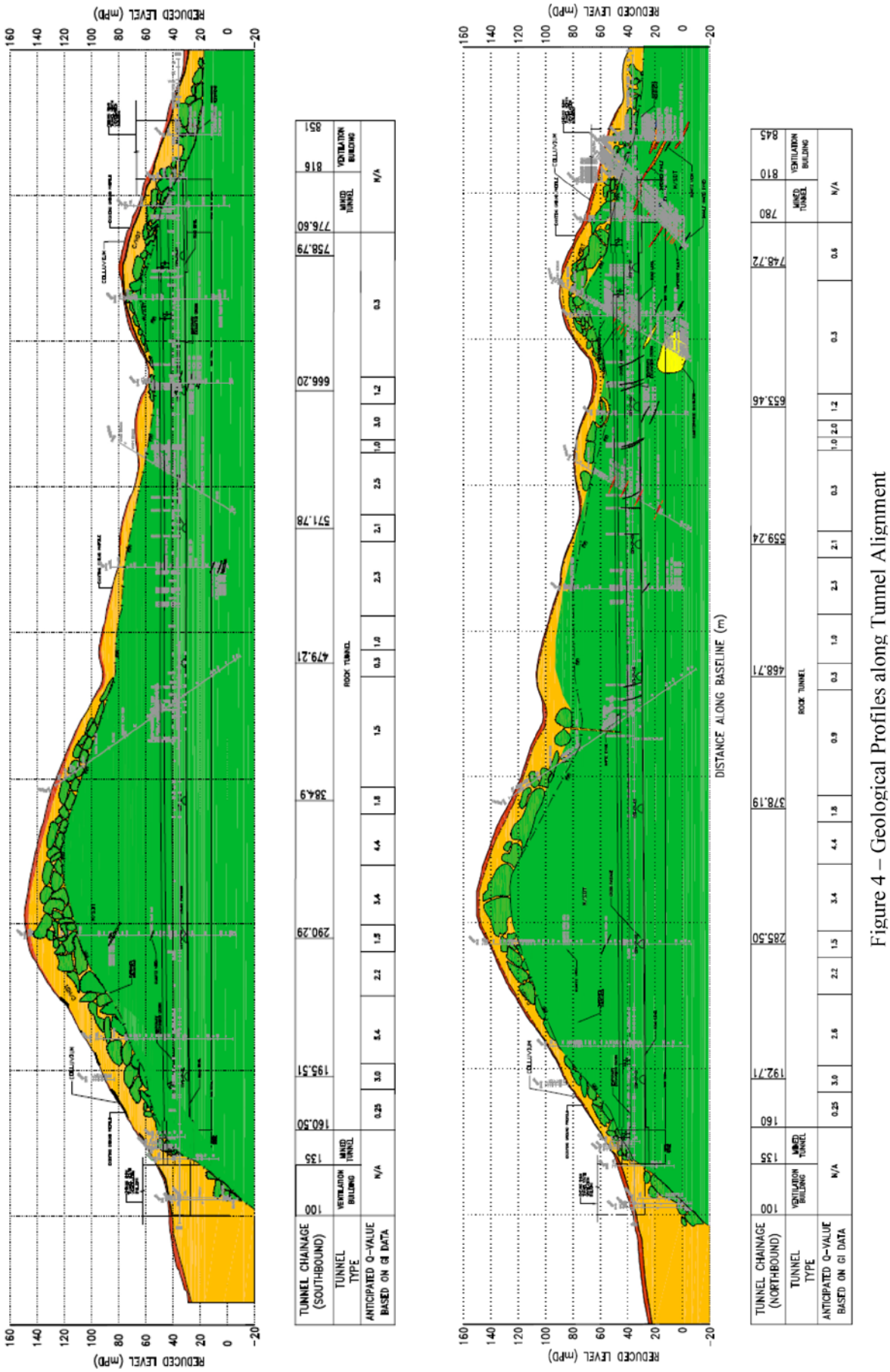

Figure 4 – Geological Profiles along Tunnel Alignment

may be damaged or destabilized by the proposed blasting works were indentified and clearly indicated in the site plans. A blast design was submitted for approval by various government authorities to demonstrate that the blasting works could be safely carried out and the proposed limits and any other constraints could be satisfied. Typical blasting design and blasthole arrangement of the main tunnel are given in Table 3 and Figure 5 respectively. The effect of blasting to the adjacent sensitive receivers and features was monitored and reviewed during the course of blasting. Mapping was carried out after the exposed surface was mechanically scaled, mucked out and surveyed.

In the following section, the overbreak of the main tunnel is reviewed. Based on the information collected from the 221 blasts, the geological factors and blasting factors are analyzed. Of the geological factors, only the lumped rock mass characteristics are considered because jointing is the major factor influencing overbreak and is readily interpreted from the borelogs before the blasting. Other factors such as the joint orientation, spacing and filling contribute but most of the data can only be obtained from mapping after the blasting. According to Ibarra, J.A. et al. (1996), the Q-system appears to give the closest correlation with the overbreak (and underbreak) among the three commonly used rock mass classifications. For the blasting factors, the powder factor and drill factor are considered because they are the major indicators of the overall economy of blasting and permit easy comparison among blast patterns. The effect of delay blasting as a controlled blasting technique to overbreak is also reviewed.

Blasting Parameters		
Typical Cross Section (Surface Face Area)	129.8 m^2	
Rock Volume	389.4 m^3	
Rock Mass	1,012.3 ton	
Burden (Average)	0.9 m	
Spacing (Average)	1.0 m	
Relief Hole Diameter & Number (Uncharged)	102.0 mm	3 no.
Perimeter/Contour Hole Diameter & Number (Charged)	45.0 mm	40 no.
Easer (Production) Hole Diameter & Number (Charged)	45.0 mm	130 no.
Bottom/Lifter Hole Diameter & Number (Charged)	45.0 mm	18 no.
Cut Hole Diameter & Number (Charged)	45.0 mm	6 no.
Total Charged Hole		194 no.
Allowable Charge Weight per Delay	7.07 kg	
Drilling (Pull) Length	3.0 m	
Production Charge Length	2.4 m	
Stemming Length	0.9 m	
Powder Factor	1.0 kg/m^3	

Table 3 – Typical Blasting Design for Main Tunnel

4 Results and Findings

Figure 6 is a linear regression analysis of the Q-factor with overbreak. It shows that the data distribution is very scatter and the overbreak appears to decrease slightly when the rock quality increases and with an average overbreak of about 9%. This trend of decrease is less obvious than that obtained by Ibarra, J.A. et al. (1996) for very poor to fair rock quality with Q between 0.1 and 10. Furthermore, 6 large overbreaks (18-22%) are found in the very poor rock zone possibly due to the collapse of some overhang loose fragmented rocks. This is similar to the findings of Schmitz R.M. et al. (2006) in relating overbreak to RMR when RMR is less than 20. This may be explainable from the overbreak-facilitating ratio Jn/Jr given by Barton N.R. and Grimstad E. (2014) that "overbreak is extremely likely to occur despite a contractor's effort with careful blasting if most frequent value of the ratio Jn/Jr > 6". Overbreak in very

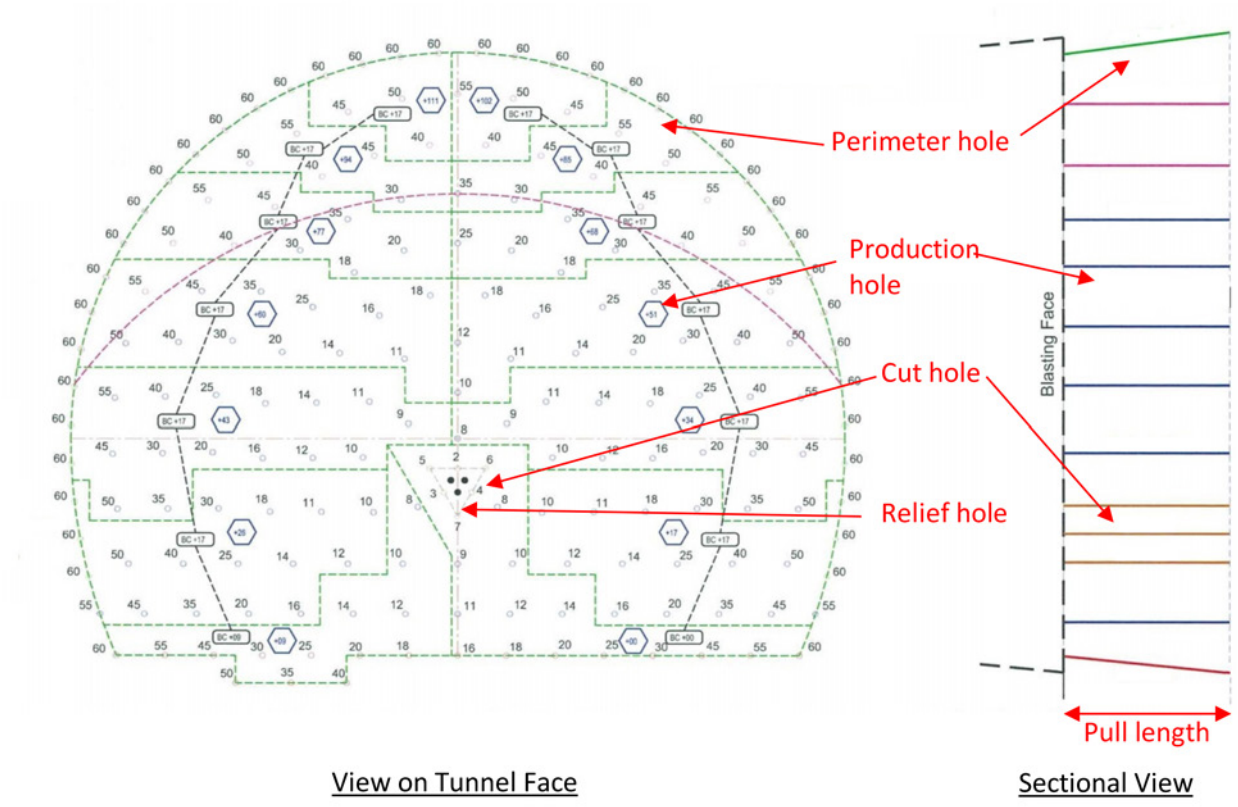

Figure 5 – Typical Blasting Design and Blasthole Arrangement in Main Tunnel

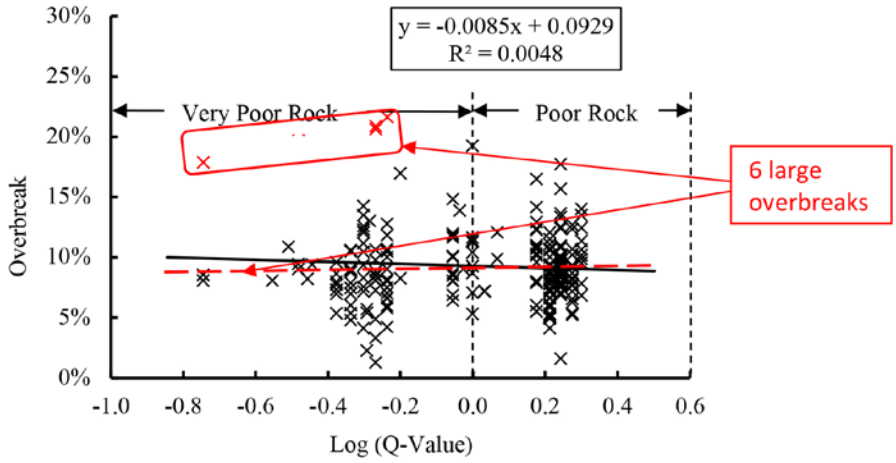

Figure 6 – Effect of Geological Parameters

poor to poor rock is expected to increase as the rock quality decreases due to collapses of overhang loose fragmented rocks but can be exceedingly large in the very poor to poor rock of which Jn/Jr is normally large.

Figure 7 shows the linear regression analysis of some major blasting parameters; namely, (a) powder factor, (b) maximum charge per delay (MIC), (c) explosive per pull length and (d) explosive in perimeter hole. Likewise, the data distributions are very scatter and all trends appear to show that the overbreak decreases slightly when these blasting parameters increase with an average overbreak of about 9%. These findings are different from other researchers as they reported that the overbreak will increase with an increase in the perimeter powder factor (Ibarra, J.A. et al. 1996 Verma, H.K. et al. 2016)),

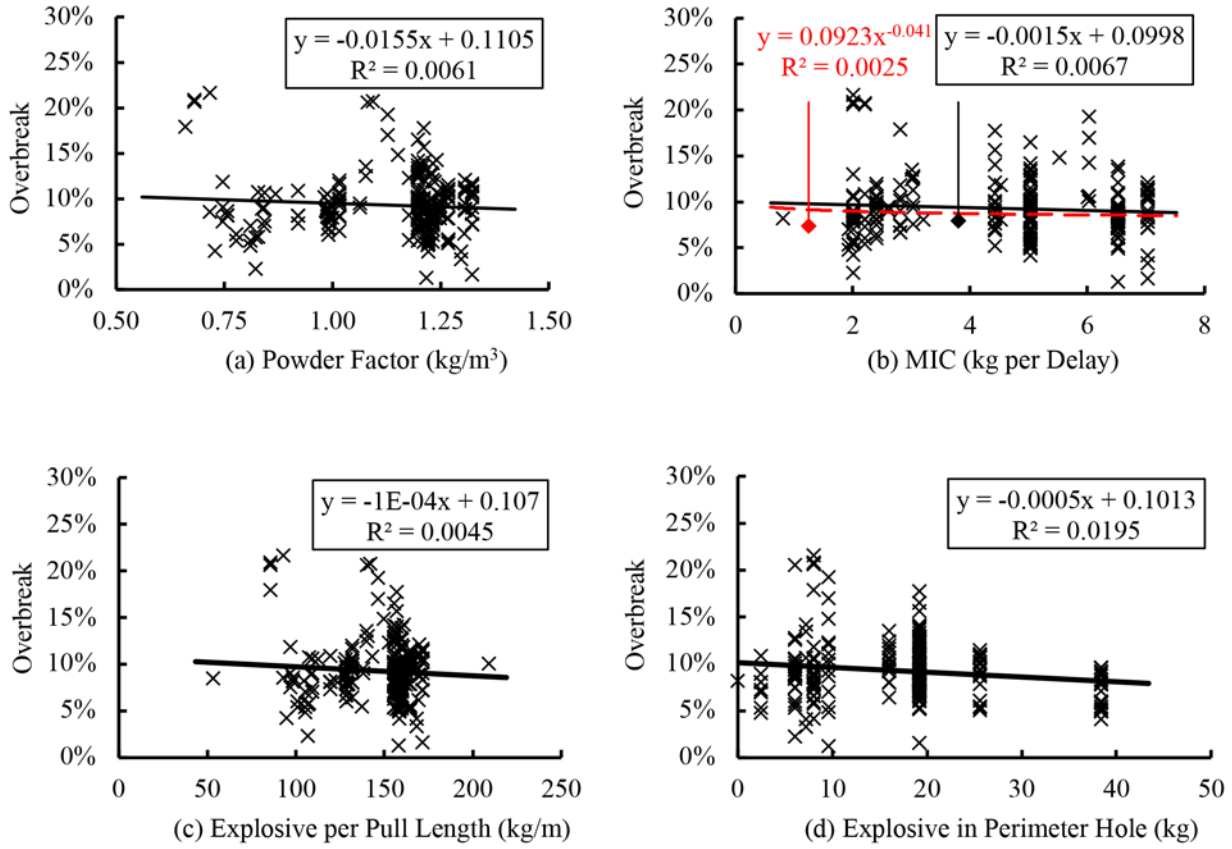

Figure 7 – Effect of Blasting Parameters

maximum charge per delay (Murthy, V.M.S.R. et al. 2003 Verma, H.K. et al. 2016), unconfined strength of rock, RQD and joint spacing (Jang, H. and Topal, E. 2013). The reverse in the blasting behaviour may be the result of some exceedingly large overbreak occurred in the very poor to poor rock of which J_n/J_r is normally large.

The multiple effects of the geological factors and blasting factors are reviewed. Figure 8 shows the linear regression analysis of different blasting parameters for various bands of rock mass quality. The data distributions are very scatter and all trends appear to show that the overbreak decreases slightly as the blasting parameters increase which are similar to the trends in Figure 7 except the powder factor, maximum charge per delay and explosive per pull length in very poor rock with log(Q) < 0.3 (Figure 8(a)-8(c)), and the explosive in perimeter hole in very poor rock with log(Q) < 0.6 (Figure 8(d)). Similar to Figure 7, the reverse in the general blasting behaviour may be the result of some exceedingly large overbreak occurred in the very poor to poor rock of which J_n/J_r is normally large. However, the bands of rock mass quality show that the overbreak increases with an increase in Q-value which is reverse to the trend in Figure 6 and the findings of Ibarra, J.A. et al. (1996). The possible explanation may be due to the intervention of the blasting factors as shown in Figure 7.

Based on these 221 blast data and multiple regression analysis, a predictive equation is obtained as follows:

Overbreak (%) = - 0.0155 * log(Q) + 0.0745 * powder factor - 0.0059 * MIC + 0.0003 * Explosive per pull length - 0.0006 * Explosive in perimeter hole [1]

The predictability of this proposed equation is reviewed. Figure 9 shows that it tends to under-predict the overbreak by about 12% with low sensitivity as the predictions are at a narrow range of 6% to 12% only which is not much better than the findings in Figures 6 and 7 using linear regression analysis to individual parameter. Although most of the predictions (68%) are within 30% of the confidence levels, the equation seems not meaningful because the predicted value is close to the average measured values. It appears unable to capture the effect of controlling parameters to the large or small overbreaks.

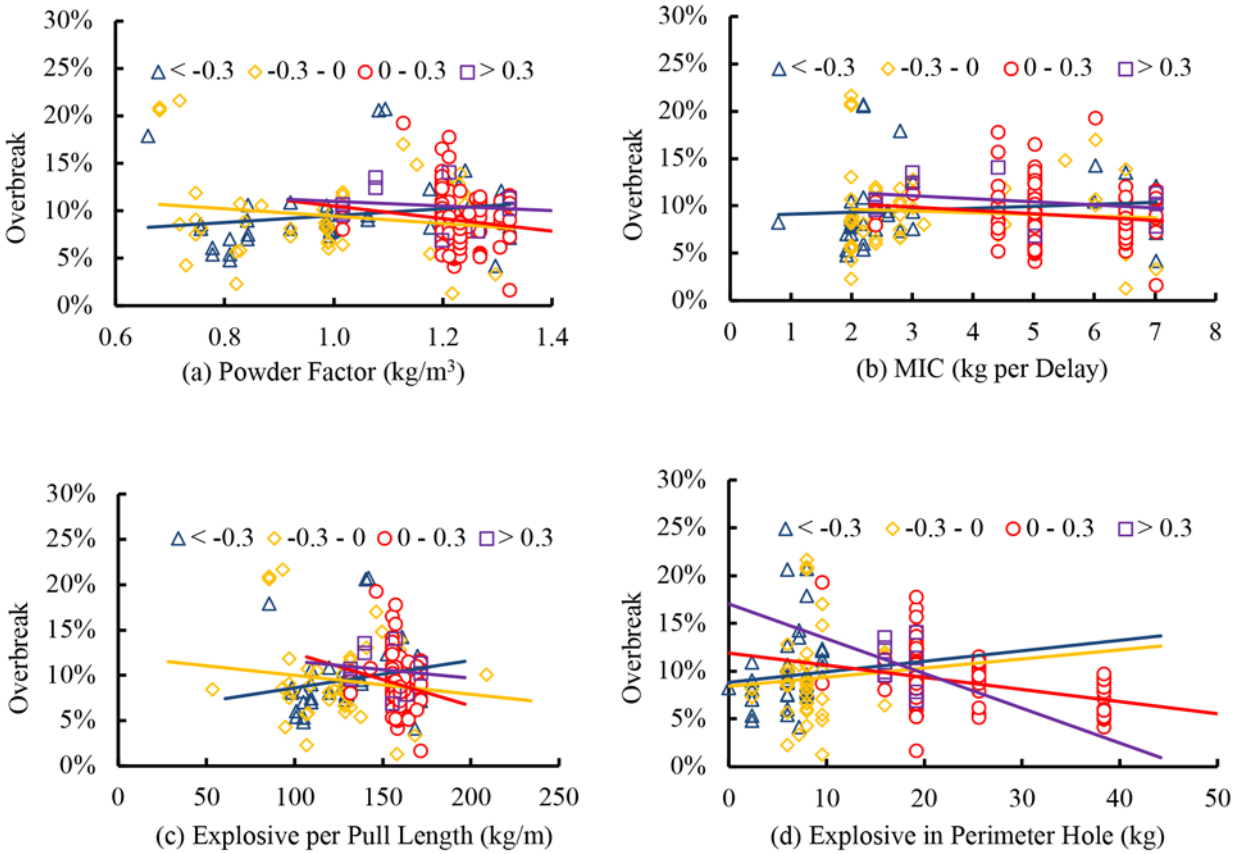

Figure 8 – Multiple Effect of Geological and Blasting Parameters

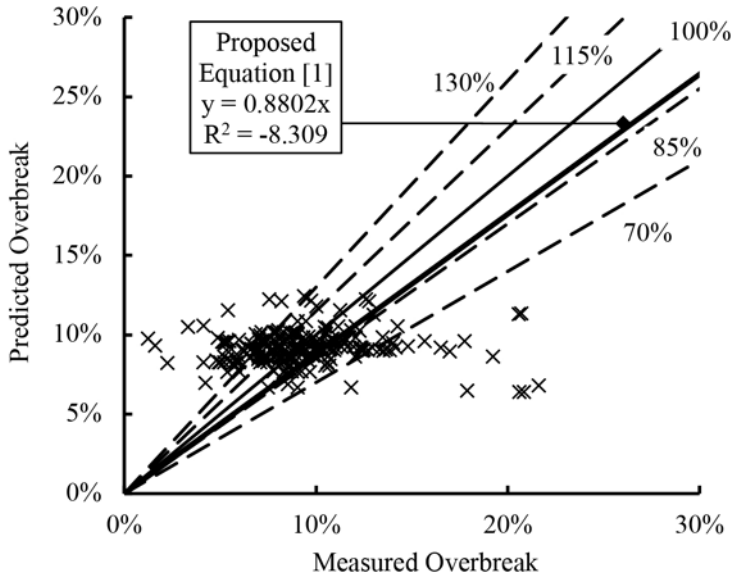

Figure 9 – Predictability of the Proposed Equation [1]

However, if the trend of the measured overbreaks is reviewed, it was found that large overbreaks mainly occurred in several continuous blasting rounds only as shown in Figure 10.

Further examination of these blasting rounds with unusual large overbreaks found that very poor rocks with unfavourable geological conditions were actually encountered at some localized areas, resulting in much larger overbreaks, while in other areas the overbreaks are generally smaller. Considering the condition of rock is likely similar between continuous blasting rounds except when

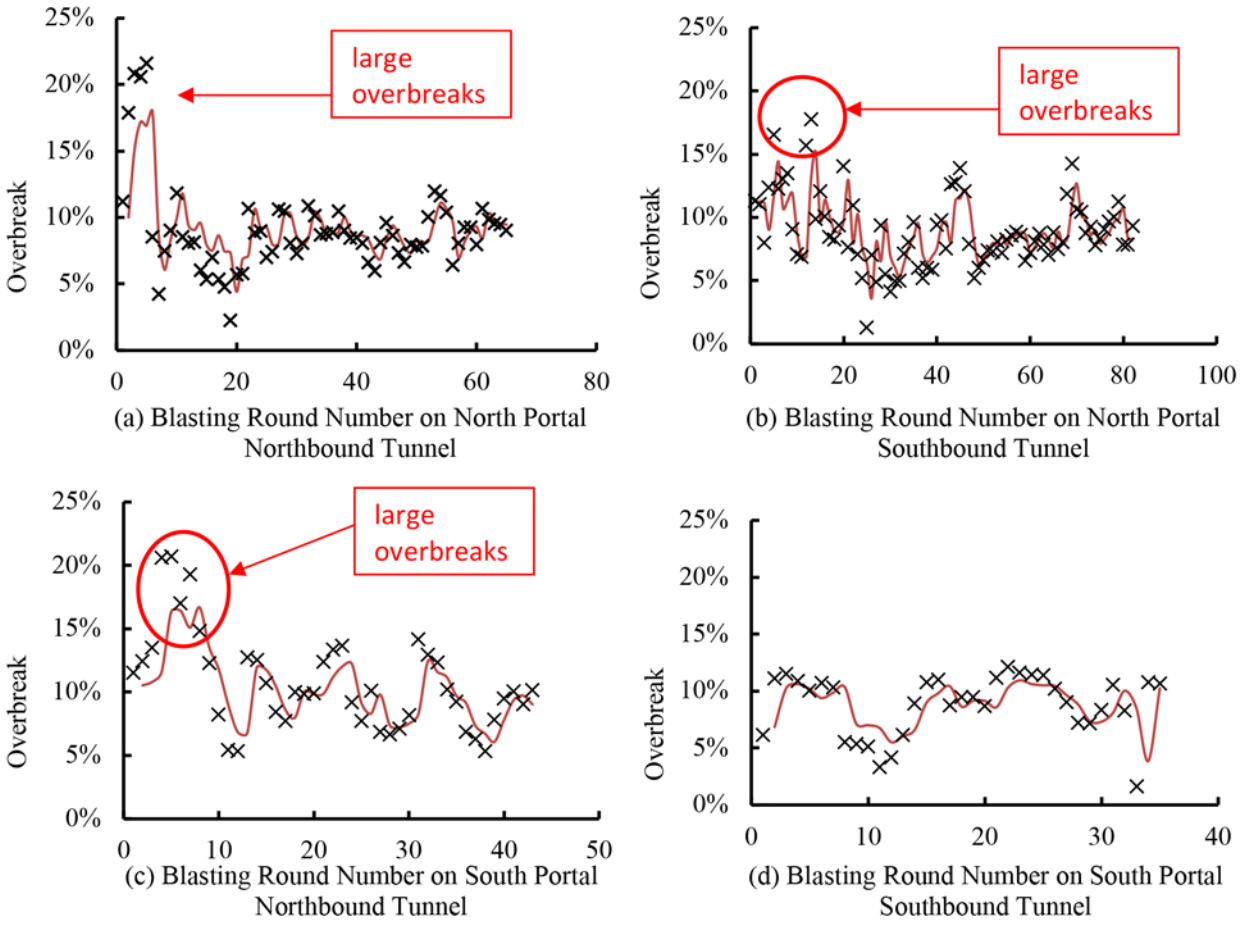

Figure 10 – Measured Overbreaks along the Tunnel with Prediction Curves

localized weak zone is encountered, the extent of overbreak shall be similar under the same set of blasting parameters. Similar to the concept of the artificial neural network approach (Sun, S. et al. 2013, Mottahedi, A. et al. 2017), an additional predictor is therefore introduced aiming to capture the unusual overbreaks in the previous blasting round. Using multiple regression analysis again, a revised predictive equation is obtained as follows:

Overbreak (%) = - 0.0077 * log(Q) + 0.0127 * powder factor - 0.0018 * MIC + 0.0002 * Explosive per pull length - 0.0001 * Explosive in perimeter hole + 0.6960 * Measured overbreak in previous round [2]

The predictability of the revised equation is then reviewed. Figure 11 shows that it has improved the prediction as it has covered a wider range of overbreaks and most of the predictions (96%) are within 30% of the confidence levels, but it still tends to under-predict the overbreaks by about 7%.

5 Conclusions

Previous researchers have shown that overbreak in a drill and blast tunnel generally increases as the rock mass quality decreases and the blasting parameters increase. However, in very poor to poor rock, the data distributions are found to be very scatter and the trends of behavior are not obvious. Linear regression analysis of individual parameters appears to show that the overbreak decreases slightly when these blasting parameters increase which is reverse to the findings of other researchers. Further linear regression analysis distinguishing various bands of rock mass quality shows that the overbreak decreases slightly as the blasting parameters increase except the powder factor, maximum charge per delay and explosive per pull length in very poor rock when log(Q) < 0.3, and the explosive in perimeter

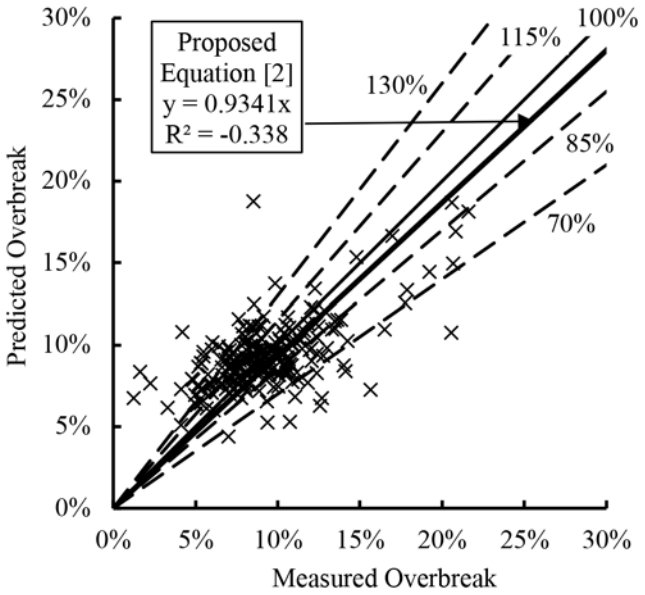

Figure 11 – Predictability of the Proposed Equation [2]

hole in very poor rock when log(Q) < 0.6. The reverse in trend in the general blasting behaviour may be due to the collapse of overhang loose fragmented rock in very poor rock leading to larger overbreak. Based on these findings and information that is readily obtained in most blasting works, and using multiple regression analysis and a predictor to capture the unusual overbreaks in the previous blasting round, a simple predictive equation can be obtained to determine the overbreak of a poor volcanic tuff tunnel.

REFERENCES

Barton, N.R, Lien, R. and Lunde, J. (1974), "Engineering Classification of Rock Masses for the Design of Tunnel Support", Rock Mechanics, Vol. 6, No. 4, pp. 189-236.

Barton, N.R. and Grimstad, G.E. (2014), "Q-System Application in NMT and NATM and the Consequences of Overbreak", 7th International Symposium on Prayed Concrete – Modern Use of Wet Mix Sprayed Concrete for Undeground Support, Sandefjord, Norway, 16-19 June 2014.

Grimstad, E. and Barton, N.R. (1993), "Updating of the Q-system for NMT", International Symposium on Sprayed Concrete. Fagernes, Proceedings, pp. 46-66.

Ibarra, J.A., Maerz, N.H. and Franklin, J.A. (1996), "Overbreak and Underbreak in Underground Openings Part 2: Causes and Implications", Geotechnical and Geological Engineering, 1996, Vol. 14 pp. 325-340.

Innaurato, N., Mancini, R. and Cardu, M. (1998), "On the Influence of Rock Mass Quality on the Quality of Blasting Work in Tunnel Driving", Tunnelling and Underground Space Technology, Vol. 13, No. 11, pp. 81-89.

Jang, H. and Topal, E. (2013), "Optimizing Overbreak Prediction based on Geological Parameters comparing Multiple Regression Analysis and Artificial Neural Network", Tunnelling and Underground Space Technology, Vol. 38, pp. 161-169.

Mottahedi, A., Sereshki, F. and Ataei, M. (2017), "Development of Overbreak Prediction Models in Drill and Blast Tunnelling using Soft Computing Methods", Engineering with Computers, Published online on 26 April 2017, Springer-Verlag London.

Murthy, V.M.S.R., Dey, K. and Raitani, R. (2003), "Prediction of Overbreak in Underground Tunnel Blasting - A Case Study", Journal of Canadian Tunneling, 2003, pp. 109-115.

Schmitz, R.M., Viroux, S, Charlier, R. and Hick, S. (2006), "The Role of Rock Mechnaics in Analysing Overbreak: Application to the Soumagne Tunnel", EUROCK 2006 - Multiphysics Coupling and Long Term Behaviour in Rock Mechanics, Van Cotthem, Charlier, Thimus and Tshibangu Ed., Taylor and Francis Group, London, ISBN 0415410010, pp. 631-636.

Singh, S.P. and Lamond, R.D. (1994), "Investigation of Blast Damage and Underground Stability", 12th Conference on Ground Control in Mining, Proceedings, pp. 366-372.

Verma, H.K., Dwivedi, R.D., Roy, P.P., Singh, P.K. (2016), "Cause, Impact and Control of Overbreak in Underground Excavations", Recent Advances in Rock Engineering, Atlantis Press. Pp29-34.

Slope Failures Along Joint Planes in Mudstones

L.W. Wong & K.L. Pak
SMEC Asia Ltd, Hong Kong

ABSTRACT

Four case histories on slope failures in mudstones have been reviewed. The slopes are 5 m to 12 m in height with the slope inclinations ranging from 10°o to 40°. The slip surfaces are along joint planes approximately parallel to the existing ground profiles. Results of back-analyses shows that the shear strengths of moderately weathered to slightly weathered mudstones mobilized along the joints have the residual effective friction angle about 14° with zero cohesion at the effective normal stresses ranging from 25 kPa to 150 kPa.

1 INTRODUCTION

During construction of the road widening works for an existing highway in northern Borneo, several slope failures occurred at the partially excavated slopes. The cut slopes are 5 m to 12 m in height formed in mélange dominated with mudstone. Two of the failed slopes slid along joint planes in mudstones. In order to study the failure mechanism along the joints, four case histories on slope failures in mudstones have been collected for critical review. Case 1 is located in the Toukoshan Formation in northern Taiwan. Case 2 to Case 4 are located in the Garinono Formation in northern Borneo.

The geological conditions of the rock formations have the key role on development of joints and mobilization of the residual strengths along the discontinuities. Both Taiwan and Borneo are located in seismic active regions with presence of tectonic structures. There are occurrence of earthquakes with Magnitudes over 6 in Richter scale associated with the active faults. As a result, horizontal compression has produced compressive strains in the rock mass. Unloading due to removal of the lateral supports by excavation causes development of the stress relief joints in the ground. On the other hand, the shear strengths along the joints would reduce from the intact strength to a softened condition and could be even mobilized to the residual condition.

Slope stability analysis on the 4 case histories using the limiting equilibrium method have been conducted. The shear strengths mobilized along the joints in mudstones are back-estimated from the failure cases. The orientation of the joint planes developed are related to the original ground profiles existed prior to excavation.

2 SHEAR STRENGTHS OF MUDSTONES

2.1 Degree of Weathering

The slightly weathered mudstones encountered in the project sites for Case 1 to Case 4 have the uniaxial compressive strengths ranging from 0.1 MPa to 0.9 MPa. According to the criteria recommended by BS 5930, the mudstone materials are extremely weak to very weak. The mudstones are classified according the degree of weathering into completely weathered mudstone (Ms-V), highly weathered mudstone (Ms-IV), moderately weathered mudstone (Ms-III) and slightly weathered mudstone (Ms-II). In general, the Grade I and Grade II rocks preserve the greyish colour. The Grade IV to Grade VI mudstones are

discoloured to yellowish and brownish. The Grade III mudstone is the transition material in grey and brown.

The various degrees of weathering of mudstones are related to the N values of the standard penetration tests. The N values are extrapolated to 300 mm as suggested by Stroud (1974). The Grade V mudstones have the N values ranging from 10 to 20. The Grade IV mudstones have the N values ranging from 20 to 40. The Grade III mudstone have the N values ranging from 35 to 50. The Grade II mudstones have the N values ranging from 50 to over 150.

2.2 Intact Mudstone Materials

Intact specimens of mudstones of various degrees of weathering have been recovered from the boreholes in the project sites for Case 2 and Case 3. These specimens are located at the depths between 1.5 m and 3.5 m. Multi-stage triaxial consolidated undrained compression tests with pore pressure measurement (CIU') were conducted. Ten, four and two numbers of specimens of completely weathered, highly weathered and moderately to slightly weathered mudstones respectively were collected for testing. The effective shear strength envelopes for these intact mudstone materials are presented in Figures 1 to 3 and summarized in Table 1.

The shear strengths of the intact completely weathered mudstones appears to be stress-dependent. At the effective normal stress up to 200 kPa, the effective friction angles determined by regression analysis range from 28.3° to 18.4° with zero effective cohesion intercept.

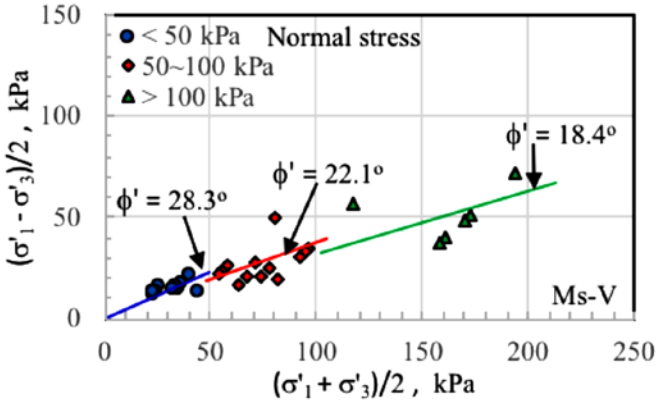

Figure 1: Effective shear strength for completely weathered mudstone.

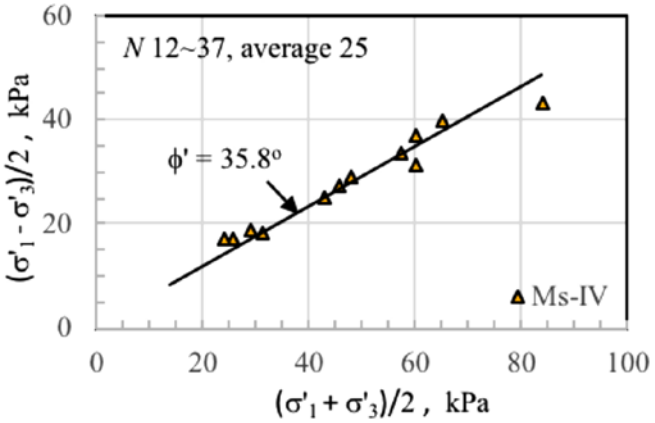

Figure 2: Effective shear strength for highly weathered mudstone.

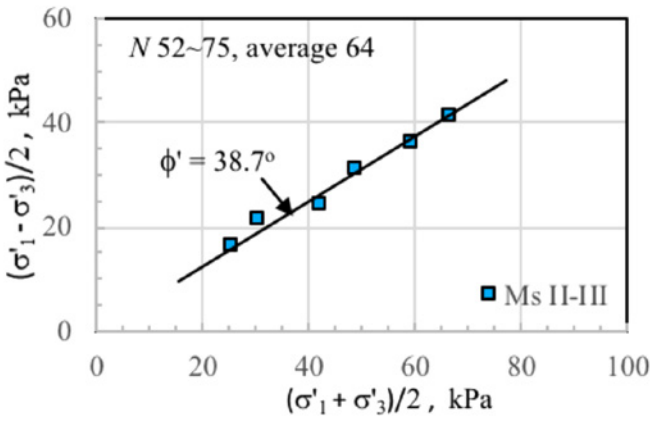

Figure 3: Effective shear strength for slightly weathered mudstone

Table 1: Shear strengths of intact mudstone materials determined by CIU' tests

Rock type	N value		Effective normal stress σ'_n, kPa	Effective cohesion c', kPa	Effective friction angle ϕ', degree
	Range	Average			
Completely weathered mudstone	7 ~ 20	14	< 50	0	28.3
			50~100	0	22.1
			100~200	0	18.4
Highly weathered mudstone	12 ~37	25	20~100	0	35.8
Moderately to slightly weathered mudstone	52 ~ 75	64	20~100	0	38.7

2.3 Shear Strengths of Mudstones Along Discontinuities

Slope failures in clastic sedimentary rocks have been experienced in Malaysia. Raj (2004) reminded that in hilly terrain discontinuities developed due to stress relief or unloading shall be considered in cut slopes design. The shear strengths along the joints or the bedding planes in mudstones could be determined by conducting direct shear tests on specimens of mudstones and by back-analyzing on slope failure case histories.

Wong and Murrells (2004) reported the direct shear test results conducted in mudstones collected from the Cholan and the Toukoshan Formations in northern Taiwan. The peak and the residual shear strengths obtained by direct shear tests conducted on saw-cut specimens have the average peak and residual effective friction angles $\phi'_p = 27.0°$ and $\phi'_r = 16.2°$ respectively with zero cohesion intercept.

Barry (1990) reported the direct shear test results of mudstones of the Garinono Formation in northern Borneo. The tests were conducted on compacted mudstone specimens with re-shearing process. The peak and the residual shear strength have the average effective friction angles $\phi'_p = 29.3°$ and $\phi'_r = 14.0o$ respectively with zero cohesion.

The direct shear test results on mudstones for the above 2 case histories are summarized in Table 2. The exhibition of the peak and the residual strengths shows that mudstones have the strain-softening characteristics. The shear strengths are strain-dependent with the post-peak strengths significantly lower than the peak strength.

Table 2: Shear strengths of mudstone determined by direct shear tests

Case no.	Rock Formation	Effective normal stress σ'_n, kPa	Peak effective friction angle, ϕ'_p, degree		Residual effective friction angle, ϕ'_r, degree		Reference
			Range	Average	Range	Average	
1	Toukoshan	40 ~ 480	32~ 21	27.0	–	16.2	Wong & Murrells 2004
2	Garinono	60 ~ 215	32 ~ 28	29.3	12 ~ 16	14.0	Barry 1990

3 SLOPE FAILURE CASE 1

The slope failure Case 1 reported by Wong & Murrells (2004) is located in the Toukoshan Formation that belongs to the Late Pliocene and Pleistocene Epoch in northern Taiwan. A north-south trending thrust fault of 20 km in length is located in close vicinity of this project site. Wong (2010) reported the ratio of horizontal stress to vertical stress for this project site based on results of pressuremeter tests. Twenty-seven pressuremeter tests were conducted in 9 boreholes in the Toukoshan Formation and in the Cholan Formation. The horizontal in-situ stresses of the ground are determined by the radial cavity pressures measured at the initial radial strains of the borehole walls. The average ratio of effective horizontal stress to effective vertical stress for the rock mass is 1.0, which is associated with the tectonic activities in the region.

The slope for Case 1 is 12 m in height. The slope surface has the dip direction of 110° and the slope angle of 34°. The upper slope of 7 m in height was in terrace deposits underlain un-conformably by the

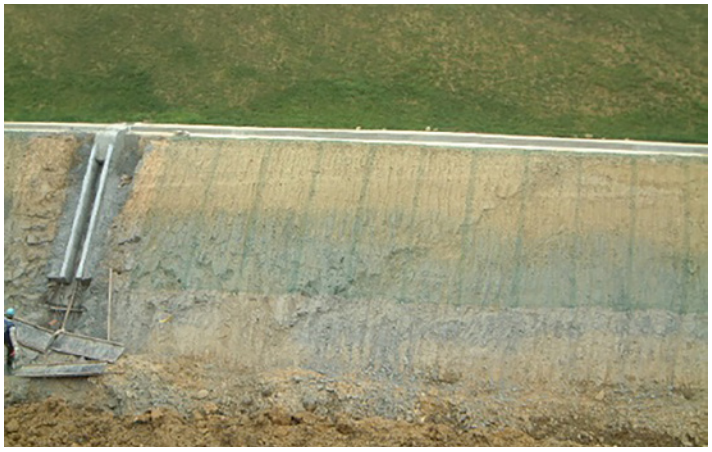

Figure 4: Pre-failure slope at Case 1 showing the joint plane intersecting the slope surface

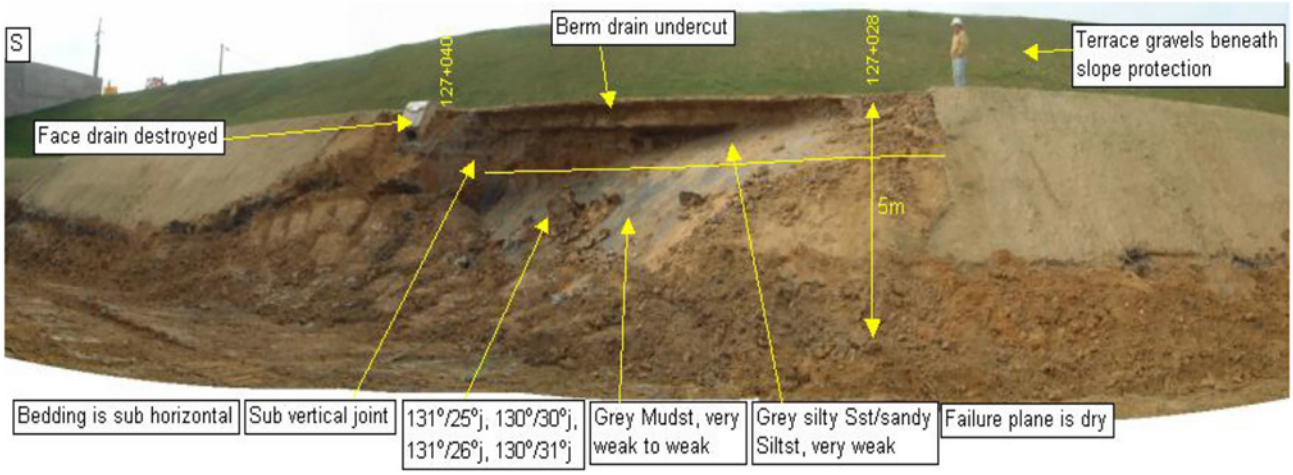

Figure 5: Post-failure slip surface along a joint plane in moderately weathered mudstone for Case 1

Toukoshan Formation. The lower slope of 5 m in height encountered moderately weathered sandstone and mudstone strata that have the bedding planes dipping at about 3°. The boundary between the terrace deposits and the sandstone and mudstone strata is located at mid-height of the slope, where a berm of 2.5 m width and a drainage channel was constructed. The groundwater level was located at the toe level of the slope.

As shown in Figure 4, a joint plane day-lighting at the lower slope was visible on the pre-failure slope surface. This joint plane could not be identified prior to excavation. Failure occurred at the lower slope during excavation for the drainage channel along the toe in February 2003. As depicted in Figure 5, the slip surface slid along a joint plane in mudstone that has the dip direction of 130o and the dip angles ranging from 25° to 31°, with an average of 28°. There was no rainfall on the preceding days and no sign of seepage was observed on the exposed slip surface. The drainage channel along the berm remains intact and watertight after the slope failure.

Excavation for the step channel of about 0.5 m depth triggered the slope failure as the side friction at the south side of the sliding block was removed. The direction of the landslip is taken as 120°, which is the bisector between the dip direction of the slope surface of 110o and that for the joint plane of 130°. The apparent dip angle along the landslip direction of 120° is 27.5°.

Adopting the groundwater level located below the slip surface and zero cohesion, the mobilized effective friction angle, ϕ'_m, along the joint plane in mudstone is equal to the apparent dip angle of 27.5° of the joint plane. The mobilized shear strength along the joint is close to the average ϕ'_p value of 27.0° obtained by direct shear test that summarized in Table 2. Review on this case history suggests that the slip surface in mudstone is likely a stress relief joint, which is developed by unloading due to excavation.

4 SLOPE FAILURE CASE 2

The slope failure Case 2 reported by Barry (1990) is located in north Borneo. The project site is underlain by weak rock strata of the Garinono Formation that belong to the Middle Miocene Epoch. The melange encountered at this slope is mainly composed of mudstones embedded with sandstone fragments and boulders with the size ranging from 50 mm to 5m. The failure occurred in 1987 when a slope of 5 m in height with the inclination of 18.4° was cut to form a new road. The original ground profile has the inclination about 10°.

The unstable area was 12 m maximum in height. Its lengths along the cross-section and along the longitudinal directions of the new road are 70 m and 35 m respectively. Tension cracks at the crest of the sliding block were first identified in October 1987. Further major movements occurred in November 1987. Surface movement markers installed in January 1988 recorded the rate of horizontal movement as high as 400 mm/month in February 1988. The movement rates gradually reduced from 220 mm/month in March to 130 mm/month in May 1988. The total horizontal movement for the period between January and May 1988 was about 850 mm.

Two inclinometers were installed in the unstable area in February 1988. Monitoring on these inclinometers shows that the slip surface was located at the depths of 4 m and 8 m at inclinometers no. 204 and 203 respectively. Figure 6 shows the cross-section of the slope. Using various groundwater levels, Barry (1990) estimated the shear strengths of mudstones along a circular slip surface. For the groundwater levels located at 3 m and 4 m below the original ground surface, the back-calculated effective friction angle ϕ' are 14.5° and 12.5° respectively. The range of the back-analyzed ϕ' values is consistent with the residual friction angle ϕ'_r ranging from 12° to 16° obtained from direct shear tests conducted on compacted re-sheared specimens of mudstone.

The authors re-analyzed this case history by adopting the non-circular slip surface. It is considered that the slip surface between inclinometers no. 203 and 204 is along a joint plane having the inclination about 18°. The intact shear strengths with the effective friction angles of 35.8° and 38.7° for highly weathered and for slightly weathered mudstones respectively are adopted in the stability analysis. The Morgenstern & Price's (1965) limiting equilibrium method is adopted in the slope stability analysis.

The mobilized effective friction angles, ϕ'_m, along the joint plane in Case 2 obtained by back-analysis range from 14° to 11° for the groundwater levels located at 3 m and at 4 m depths respectively. The inclination of the slip surface along the joint plane is 18°, which is parallel to the design cut slope profile of 18.4°. It is noted that the unloading portion for forming the new road is only 20 m in width and 5 m in height. Due to strain-softening characteristics of the mudstone material, the localized slip surface along the joint could gradually propagate from the toe toward uphill. The stress relief joint is then fully developed with the retrogressive type failure mechanism.

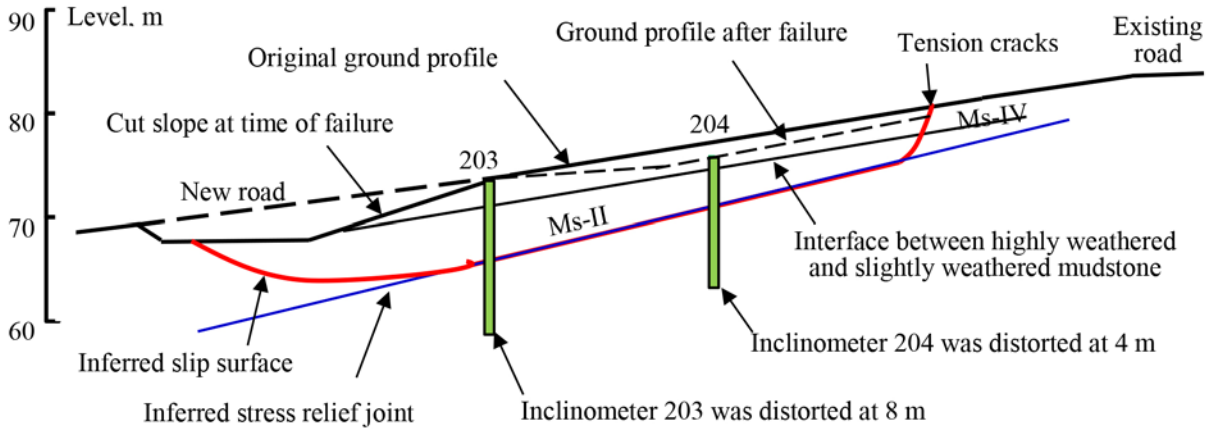

Figure 6. Cross-section of the landslip Case 2 modified from Barry (1990)

5 SLOPE FAILURE CASE 3

The slope failure Case 3 is another cut slope located in the Garinono Formation in northern Borneo. According to the Mineral & Geoscience Malaysia (2015), the east-northeast trending active Tabin Thrust Fault of 80 km in length is distanced 90 km southwest from the slope at Case 3. An earthquake of Magnitude 5.2, generated by a north-northeast trending normal fault, occurred on 14 December 1998. The epicenter of this earthquake is located at 8 km east of the site for Case 3. Yan (2011) reported that the ground in this region is subject to horizontal compressions along the northwest-southeast and along the east-west directions.

The east facing slope for Case 3 has the design inclination of 34o. Slope failure occurred in early December 2017. As shown in Figure 7, the failed slope is 17 m maximum in height and 70 m in length along the longitudinal direction. The rocks exposed on the slope surface is melange, which comprises mudstones embedded with angular sandstone fragments of 50 mm to 300 mm in size. The side view in Figure 8 shows that the sliding block of mudstone had the horizontal and the vertical movements about 1 m and 0.4 m respectively. The sliding block remains intact after slope failure. Figure 9 shows the cross-sections for the pre-failure and the post-failure slopes.

Figure 7: Front view of slope failure in highly and slightly weathered mudstone at Case 3

Figure 8: Side view of slope failure in highly and slightly weathered mudstones at Case 3

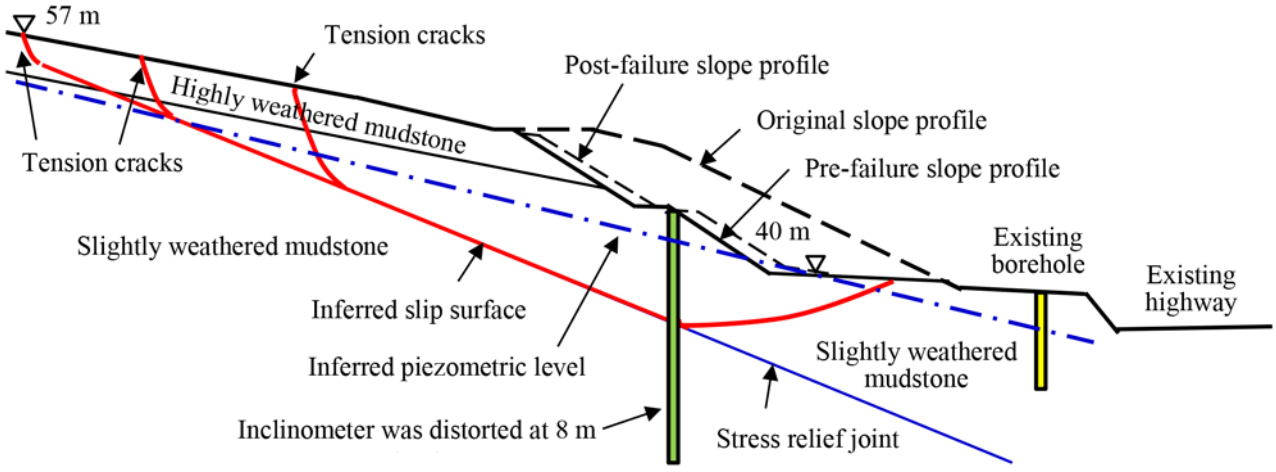

Figure 9: Failure conditions of the slope at Case 3

The platform behind the crest of the cut slope is a plantation area for palm trees. Three rows of tension cracks, which are 1.2 m maximum in depth and about 0.4 m in width, were developed as distant as 30 m behind the crest of the cut slope. The yellowish brown highly weathered mudstone mantle about 3 m in thickness is observed at the upper portion of the slope. The lower portion of the slope is

in greyish slightly weathered mudstone. No bedding plane in the mudstone stratum is observed. The slightly weathered mudstone located at the toe of the slope was sheared off with the polished plane observed on the shearing surface.

There was no sign of seepage at the toe of the slope at time of site inspection in mid-December. An existing borehole is located at 20 m from the toe of the sliding block. The groundwater level recorded in that borehole on the following day of drilling completion was located at about 3 m depth. Based on the dry conditions observed along the toe the sliding block and at the tension cracks, it is inferred that the piezometric level is 3 m below the existing ground profile along the uppermost tension cracks. An inclinometer of 18 m in length was installed on the berm at the level 45 m in late December. On the fourth day after the inclinometer casings were installed, the access tubes were distorted at 8 m depth.

It is inferred that the slip surface located at 8 m depth is a stress relief joint with an inclination about 23.5°, which is parallel to the original slope profile. Back-analysis is conducted to assess the shear strengths mobilized along the joint plane. The shear strengths for the intact highly weathered and slightly weathered mudstones having the effective friction angles of 35.8° and 38.7° respectively are adopted. Assuming the factor of safety at time of failure equal to unity and with zero cohesion intercept, the mobilized effective friction angle, ϕ'_m, of mudstone along the stress relief joint determined by back-calculation is 14°. This ϕ'_m value is consistent with the average residual friction angle ϕ_r' of 14° determined by direct shear tests that summarized in Table 2. Sensitivity studies using a piezometric level 2 m lower than that indicated in Figure 9 is conducted. The ϕ'_m value of 10° along the stress relief joint would then be obtained.

6 SLOPE FAILURE CASE 4

The slope failure at Case 4 is located in melange of the Garinono Formation. This slope is located at 6 km south of the project site for Case 3. The west facing slope is 9 m in height with a berm of 2.5 m in width. The upper and the lower slopes have the inclination of 34° and 41° respectively. As depicted in Figure 10, reddish brown completely weathered mudstone and yellowish brown highly weathered mudstone are encountered at the upper slope. Greyish moderately weathered mudstone is encountered at the lower slope. Angular sandstone fragments and boulders ranging from 50 mm to 1 m in size are observed at the slope surface.

The slope failure for Case 4 occurred in December 2017. As shown in Figure 11, the sliding block of mudstone was separated from the berm drain, which remains intact with a span length about 6 m. The horizontal and the vertical movements for the sliding block are approximately 0.6 m and 0.3 m respectively. The guiding frame for slope trimming mounted on the sliding block remained in vertical position, indicating the occurrence of a translational slide along a joint plane. Should a rotational slide occur along a circular slip surface, that guiding frame would have been tilted. Figure 12 presents the cross-section along the slope of Case 4. The boundaries of the mudstones of various degrees of weathering are inferred from the existing borehole located at 8 m from the toe of the slope and from the geological profile mapped on the exposed slope surface. The weathering fronts of the completely weathered and highly weathered mudstones are approximately parallel to the original ground profile.

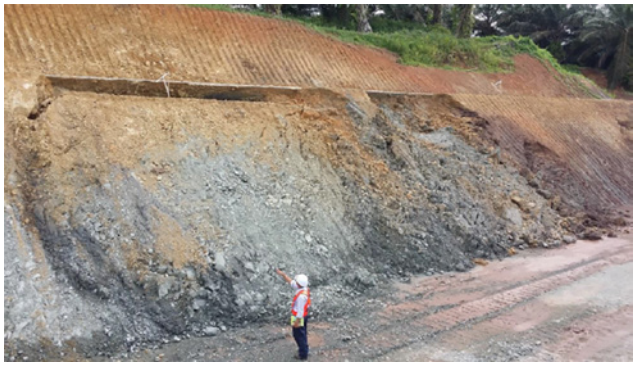

Figure 10: Front view of slope failure in slightly weathered mudstone for Case 4

Figure 11: Side view of the slope failure at Case 4. The guiding frame on the sliding block is vertical.

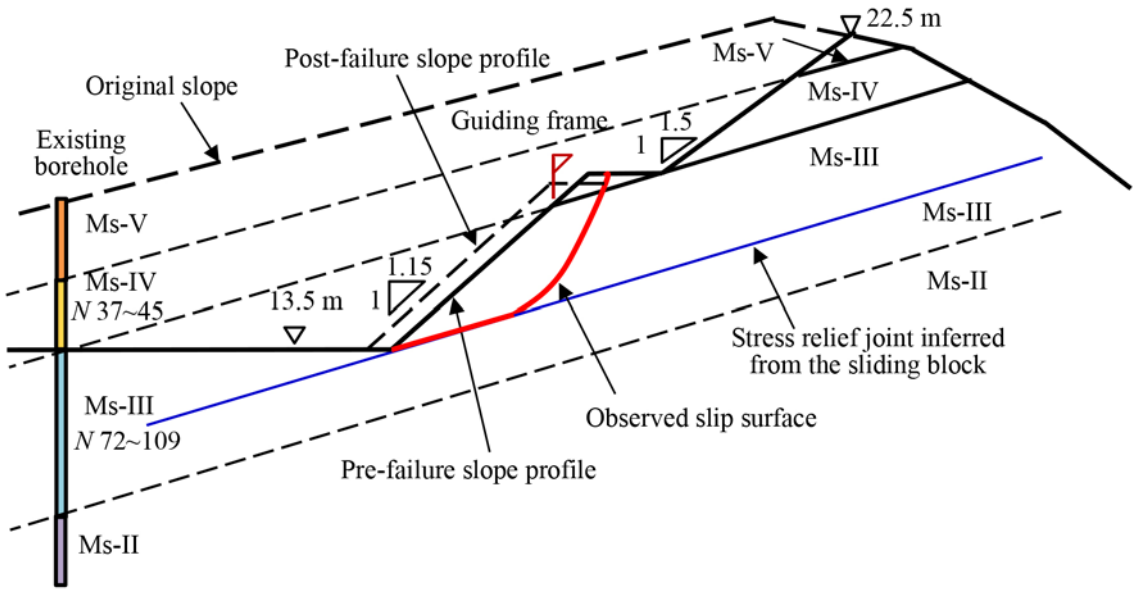

Figure 12: Cross-section along slope failure for Case 4

At time of inspection in December the berm drain remained intact and watertight. There is no sign of seepage in the tension cracks along the crest or along the toe of the failed slope. It is inferred that the groundwater level is located below the slip surface. The shear strength for the intact slightly weathered mudstone having the set of parameter of c' = 0 and ϕ' = 38.7° and the presence of a stress relief joint having the inclination parallel with the original slope profile of 17.5° are adopted in the stability analysis. Based on results of back-analyses, the mobilized effective friction angle, ϕ'_m, for moderately weathered mudstone along the joint plane is 24o with zero cohesion intercept. This ϕ'_m value is slightly lower than the average ϕ'_p value of 29.3° obtained by direct shear test that summarized in Table 2. Secondary failure at the slope of 9 m overall in height occurred in January 2018 due to collapsing of the unsupported surface drains and rainfall infiltration. Post-failure mapping on the slip surface could not be conducted.

7 VARIATION OF SHEAR STRENGTHS

The shear strengths actually mobilized along the joint planes in moderately weathered and slightly weathered mudstones obtained by back-analyses for Case 1 to Case 4 are summarized in Table 3, showing that the mobilized effective friction angles, ϕ'_m , vary from 27.5° to 12.5°. The mobilized effective friction angles are presented in Figure 13. The limited number of case histories show that the shear strengths of mudstones along the joint planes have various degree of mobilization to the residual strength, which is defined as $(\tan \phi'_m - \tan \phi'_r)/(\tan \phi'_p - \tan \phi'_r)$.

Table 3: Mobilization of residual shear strengths of mudstones along joints planes

Case no.	Rock Formation	Rock type	Effective friction angle, degree			Degree of mobilization to residual strength $(\tan \phi'_m - \tan \phi'_r)/(\tan \phi'_p - \tan \phi'_r)$, %
			Peak ϕ'_p	Residual ϕ'_r	Mobilized ϕ'_m	
1	Toukoshan	Ms-III	27.0	16.2	27.5	0
2	Garinono	Ms-II	29.3	14.0	12.5 to 14.5	100
3	Garinono	Ms-II	29.3	14.0	14.0	100
4	Garinono	Ms-III	29.3	14.0	24.0	37

Table 3 shows that the degree of mobilization to residual condition for Case 2 and Case 3 is 100 %, indicating that the residual shear strengths along the joint planes in slightly weathered mudstone is fully mobilized. Such mobilization of residual strength is common for re-activated landslips, where

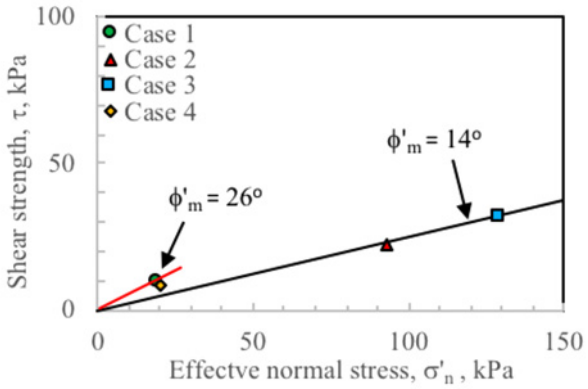

Figure 13: Mobilized shear strength envelope for mudstones along joint planes obtained by back-analysis

displacements had already occurred along the slip surfaces. However, these 2 cases are first-time slides in new slopes. The horizontal movements are as large as 1m occurred after failure. It is likely that excavation for the new slopes removed the lateral support of the rock mass. The horizontal compression strains caused by tectonic activities was released and the rock mass behind the cut slopes expanded due to unloading of the in-situ horizontal forces. Stress relief joints were developed in the slopes. The residual strengths along the joint planes were then gradually mobilized.

For Case 1 the ϕ'_m value of 27.5° is virtually the average ϕ'_p value of 27.0° obtained from direct shear tests. The degree of mobilization to the residual condition is zero. Since the joint plane is dipping at 27.5° along the slip direction, very minimal mobilization to the residual shear strength along the slip surface would be required to initiate the slope failure. The ϕ'_p value would be an upper bound for mobilization to the residual condition.

For Case 4, the ϕ'_m value of 24.0° is slightly less than the ϕ'_p value of 29.3° and the degree of mobilization is 37%. It could be interpreted that 37% of the length along the joint plane in mudstone was mobilized to the residual strength with the ϕ'_r value of 14.0°, and the remaining 63% of the joint plane has the ϕ'_p value of 29.3°. The ϕ'_m value of 24.0° could be regarded as an average along the entire joint plane. The ϕ'_p value obtained by direct shear tests could be the upper bound value for mobilization to the residual condition along the joint.

It is noted that Case 1 to Case 4 are first-time slides occurred shortly after excavation of the new slopes. Pre-existing slip surfaces are not expected in these slopes. The ϕ'_m value as large as the ϕ'_p value would be expected. Based on review of extensive case histories on long-term stability of stiff clay and clay shale slopes, Mesri and Shahien (2003) pointed out that part of the slip surfaces for first-time slope failures may be at the residual condition. Either the residual condition already exists or it develops by progressive deformation along the discontinuities. When shearing strain is localized in weak planes, rather small displacements will cause the clay particles to reach the residual condition.

8 CONCLUSIONS

Four case histories on slope failures along joint planes in mudstones have been collected for critical studies. The triaxial compression test and the direct shear test results conducted on mudstone specimens are reviewed. Based on the results of back-analyses on the slope failure cases, the following concluding remarks could be drawn:

(1) The direct shear test results show that the shear strengths of mudstones are strain-dependent. The peak and the residual strengths for moderately weathered to slightly weathered mudstones along the joint planes obtained from saw-cut core specimens have the average effective friction angles of 27.0° and 16.2° respectively with zero cohesion.

(2) The residual effective shear strength of slightly weathered mudstone mobilized along the joint planes has the effective friction angle about 14° with zero cohesion at the effective normal stresses ranging from 25 kPa to 150 kPa.

(3) The peak effective shear strengths for mudstones along the joint planes determined by direct shear tests could be the upper bound for mobilization to the residual condition.

(4) The stress relief joints with the inclinations approximately parallel to the original slope profiles could be developed in the cut slopes especially in region with tectonic activities.

More case histories on slope failures in mudstone shall be collected to assess the degree of mobilization to the residual condition. The stress relief joints in mudstone is one of the discontinuities in the rock mass. Its likely occurrence shall be considered in slopes design.

ACKNOWLEDGEMENTS

The authors wish to express their sincere thanks to Borneo Highway PDP Sdn Bhd for granting permission for publishing the laboratory testing data presented in this paper.

REFERENCES

Barry, A.J. 1990. A Cut Slope Failure in the Garinono Formation of Sabah, *10th Southeast Asian Geotechnical Conference*, Taipei, May: 381-384.

British Standard Institution 1981. *Code of Practice for Site Investigation.* BS5930:1981, British Standard Institution, London.

Mesri, G. and Shahien, M. 2003. Residual Shear Strength Mobilized in First-Time Slope Failures. *Journal of Geotechnical and Geoenvironmental Engineering,* Vol. 129, No. 1, January 2003: 12-31.

Mineral & Geoscience Malaysia 2015. *Geological Map of Sabah,* 4th Edition, 2015, Published by the Director of Mineral & Geoscience Malaysia.

Morgenstern N.R. and Price V.E.1965. The Analysis of the Stability of General Slip Surfaces, *Geotechnique,* Volume 15, Issue 1, March 1965: 79-93.

Raj, J.K. 2004. Failure at Slope cuts in Clastic Sedimentary Bedrock in Malaysia, Geological Society of Malaysia, *Bulletin 48,* June 2004: 25-29.

Stroud, M.A. 1974. The Standard Penetration Test in Sensitive Clays and Soft Rock. *Proceedings of the 1st European Seminar on Penetration Testing.* Stockholm 2(2): 366-375.

Wong, L.W. and Murrells, C. 2004. Stability of Slopes along Discontinuities in Sandstone and Mudstone, *Proceedings, 15th Southeast Asian Geotechnical Conference,* November, Bangkok, Volume 1: 317-342.

Wong, L.W. 2010. In-situ Measurement of Shear Modulus of Weak Rocks. *Proceedings, 17th Southeast Asian Geotechnical Conference,* Taipei, May: 141-144.

Yan, S.W. 2011. Geological Assessment of the Earthquake Sources and Hazard in Malaysia, *Technical Seminar on Earthquake,* Department of Mineral & Geoscience Malaysia, 20 December 2011.

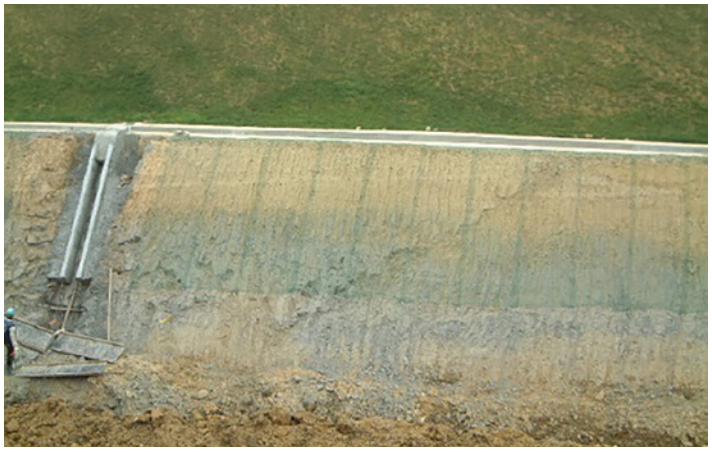

Figure 4: Pre-failure slope at Case 1 showing the joint plane intersecting the slope surface

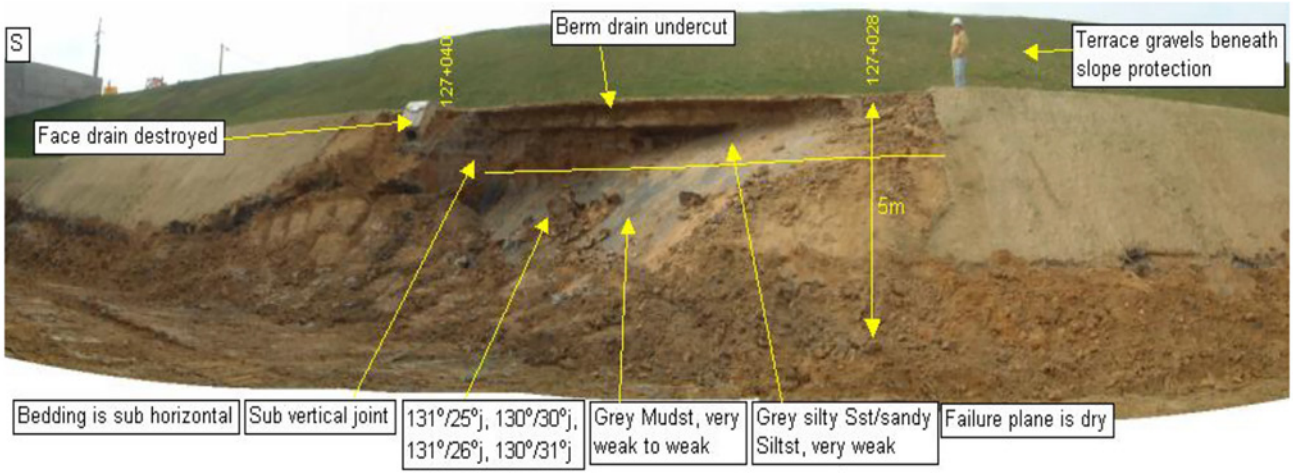

Figure 5: Post-failure slip surface along a joint plane in moderately weathered mudstone for Case 1

Toukoshan Formation. The lower slope of 5 m in height encountered moderately weathered sandstone and mudstone strata that have the bedding planes dipping at about 3°. The boundary between the terrace deposits and the sandstone and mudstone strata is located at mid-height of the slope, where a berm of 2.5 m width and a drainage channel was constructed. The groundwater level was located at the toe level of the slope.

As shown in Figure 4, a joint plane day-lighting at the lower slope was visible on the pre-failure slope surface. This joint plane could not be identified prior to excavation. Failure occurred at the lower slope during excavation for the drainage channel along the toe in February 2003. As depicted in Figure 5, the slip surface slid along a joint plane in mudstone that has the dip direction of 130o and the dip angles ranging from 25° to 31°, with an average of 28°. There was no rainfall on the preceding days and no sign of seepage was observed on the exposed slip surface. The drainage channel along the berm remains intact and watertight after the slope failure.

Excavation for the step channel of about 0.5 m depth triggered the slope failure as the side friction at the south side of the sliding block was removed. The direction of the landslip is taken as 120°, which is the bisector between the dip direction of the slope surface of 110o and that for the joint plane of 130°. The apparent dip angle along the landslip direction of 120° is 27.5°.

Adopting the groundwater level located below the slip surface and zero cohesion, the mobilized effective friction angle, ϕ'_m, along the joint plane in mudstone is equal to the apparent dip angle of 27.5° of the joint plane. The mobilized shear strength along the joint is close to the average ϕ'_p value of 27.0° obtained by direct shear test that summarized in Table 2. Review on this case history suggests that the slip surface in mudstone is likely a stress relief joint, which is developed by unloading due to excavation.

4 SLOPE FAILURE CASE 2

The slope failure Case 2 reported by Barry (1990) is located in north Borneo. The project site is underlain by weak rock strata of the Garinono Formation that belong to the Middle Miocene Epoch. The melange encountered at this slope is mainly composed of mudstones embedded with sandstone fragments and boulders with the size ranging from 50 mm to 5m. The failure occurred in 1987 when a slope of 5 m in height with the inclination of 18.4° was cut to form a new road. The original ground profile has the inclination about 10°.

The unstable area was 12 m maximum in height. Its lengths along the cross-section and along the longitudinal directions of the new road are 70 m and 35 m respectively. Tension cracks at the crest of the sliding block were first identified in October 1987. Further major movements occurred in November 1987. Surface movement markers installed in January 1988 recorded the rate of horizontal movement as high as 400 mm/month in February 1988. The movement rates gradually reduced from 220 mm/month in March to 130 mm/month in May 1988. The total horizontal movement for the period between January and May 1988 was about 850 mm.

Two inclinometers were installed in the unstable area in February 1988. Monitoring on these inclinometers shows that the slip surface was located at the depths of 4 m and 8 m at inclinometers no. 204 and 203 respectively. Figure 6 shows the cross-section of the slope. Using various groundwater levels, Barry (1990) estimated the shear strengths of mudstones along a circular slip surface. For the groundwater levels located at 3 m and 4 m below the original ground surface, the back-calculated effective friction angle ϕ' are 14.5° and 12.5° respectively. The range of the back-analyzed ϕ' values is consistent with the residual friction angle ϕ'_r ranging from 12° to 16° obtained from direct shear tests conducted on compacted re-sheared specimens of mudstone.

The authors re-analyzed this case history by adopting the non-circular slip surface. It is considered that the slip surface between inclinometers no. 203 and 204 is along a joint plane having the inclination about 18°. The intact shear strengths with the effective friction angles of 35.8° and 38.7° for highly weathered and for slightly weathered mudstones respectively are adopted in the stability analysis. The Morgenstern & Price's (1965) limiting equilibrium method is adopted in the slope stability analysis.

The mobilized effective friction angles, ϕ'_m, along the joint plane in Case 2 obtained by back-analysis range from 14° to 11° for the groundwater levels located at 3 m and at 4 m depths respectively. The inclination of the slip surface along the joint plane is 18°, which is parallel to the design cut slope profile of 18.4°. It is noted that the unloading portion for forming the new road is only 20 m in width and 5 m in height. Due to strain-softening characteristics of the mudstone material, the localized slip surface along the joint could gradually propagate from the toe toward uphill. The stress relief joint is then fully developed with the retrogressive type failure mechanism.

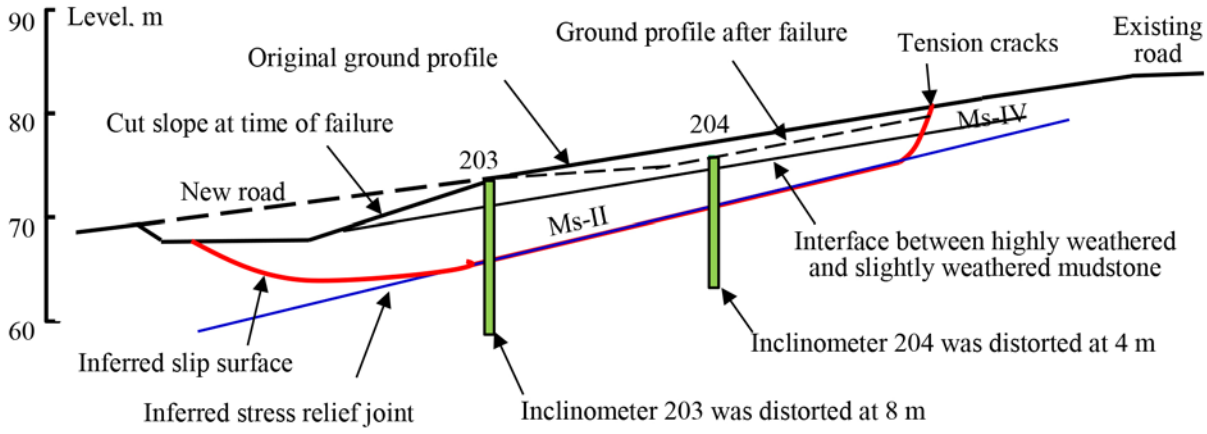

Figure 6. Cross-section of the landslip Case 2 modified from Barry (1990)

5 SLOPE FAILURE CASE 3

The slope failure Case 3 is another cut slope located in the Garinono Formation in northern Borneo. According to the Mineral & Geoscience Malaysia (2015), the east-northeast trending active Tabin Thrust Fault of 80 km in length is distanced 90 km southwest from the slope at Case 3. An earthquake of Magnitude 5.2, generated by a north-northeast trending normal fault, occurred on 14 December 1998. The epicenter of this earthquake is located at 8 km east of the site for Case 3. Yan (2011) reported that the ground in this region is subject to horizontal compressions along the northwest-southeast and along the east-west directions.

The east facing slope for Case 3 has the design inclination of 34o. Slope failure occurred in early December 2017. As shown in Figure 7, the failed slope is 17 m maximum in height and 70 m in length along the longitudinal direction. The rocks exposed on the slope surface is melange, which comprises mudstones embedded with angular sandstone fragments of 50 mm to 300 mm in size. The side view in Figure 8 shows that the sliding block of mudstone had the horizontal and the vertical movements about 1 m and 0.4 m respectively. The sliding block remains intact after slope failure. Figure 9 shows the cross-sections for the pre-failure and the post-failure slopes.

Figure 7: Front view of slope failure in highly and slightly weathered mudstone at Case 3

Figure 8: Side view of slope failure in highly and slightly weathered mudstones at Case 3

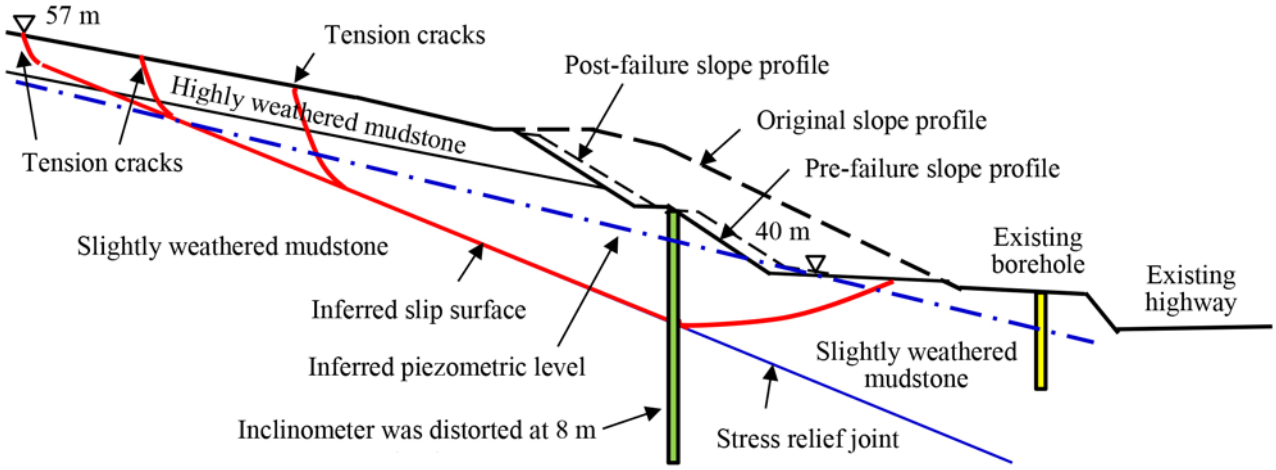

Figure 9: Failure conditions of the slope at Case 3

The platform behind the crest of the cut slope is a plantation area for palm trees. Three rows of tension cracks, which are 1.2 m maximum in depth and about 0.4 m in width, were developed as distant as 30 m behind the crest of the cut slope. The yellowish brown highly weathered mudstone mantle about 3 m in thickness is observed at the upper portion of the slope. The lower portion of the slope is

in greyish slightly weathered mudstone. No bedding plane in the mudstone stratum is observed. The slightly weathered mudstone located at the toe of the slope was sheared off with the polished plane observed on the shearing surface.

There was no sign of seepage at the toe of the slope at time of site inspection in mid-December. An existing borehole is located at 20 m from the toe of the sliding block. The groundwater level recorded in that borehole on the following day of drilling completion was located at about 3 m depth. Based on the dry conditions observed along the toe the sliding block and at the tension cracks, it is inferred that the piezometric level is 3 m below the existing ground profile along the uppermost tension cracks. An inclinometer of 18 m in length was installed on the berm at the level 45 m in late December. On the fourth day after the inclinometer casings were installed, the access tubes were distorted at 8 m depth.

It is inferred that the slip surface located at 8 m depth is a stress relief joint with an inclination about 23.5°, which is parallel to the original slope profile. Back-analysis is conducted to assess the shear strengths mobilized along the joint plane. The shear strengths for the intact highly weathered and slightly weathered mudstones having the effective friction angles of 35.8° and 38.7° respectively are adopted. Assuming the factor of safety at time of failure equal to unity and with zero cohesion intercept, the mobilized effective friction angle, ϕ'_m, of mudstone along the stress relief joint determined by back-calculation is 14°. This ϕ'_m value is consistent with the average residual friction angle ϕ_r' of 14° determined by direct shear tests that summarized in Table 2. Sensitivity studies using a piezometric level 2 m lower than that indicated in Figure 9 is conducted. The ϕ'_m value of 10° along the stress relief joint would then be obtained.

6 SLOPE FAILURE CASE 4

The slope failure at Case 4 is located in melange of the Garinono Formation. This slope is located at 6 km south of the project site for Case 3. The west facing slope is 9 m in height with a berm of 2.5 m in width. The upper and the lower slopes have the inclination of 34° and 41° respectively. As depicted in Figure 10, reddish brown completely weathered mudstone and yellowish brown highly weathered mudstone are encountered at the upper slope. Greyish moderately weathered mudstone is encountered at the lower slope. Angular sandstone fragments and boulders ranging from 50 mm to 1 m in size are observed at the slope surface.

The slope failure for Case 4 occurred in December 2017. As shown in Figure 11, the sliding block of mudstone was separated from the berm drain, which remains intact with a span length about 6 m. The horizontal and the vertical movements for the sliding block are approximately 0.6 m and 0.3 m respectively. The guiding frame for slope trimming mounted on the sliding block remained in vertical position, indicating the occurrence of a translational slide along a joint plane. Should a rotational slide occur along a circular slip surface, that guiding frame would have been tilted. Figure 12 presents the cross-section along the slope of Case 4. The boundaries of the mudstones of various degrees of weathering are inferred from the existing borehole located at 8 m from the toe of the slope and from the geological profile mapped on the exposed slope surface. The weathering fronts of the completely weathered and highly weathered mudstones are approximately parallel to the original ground profile.

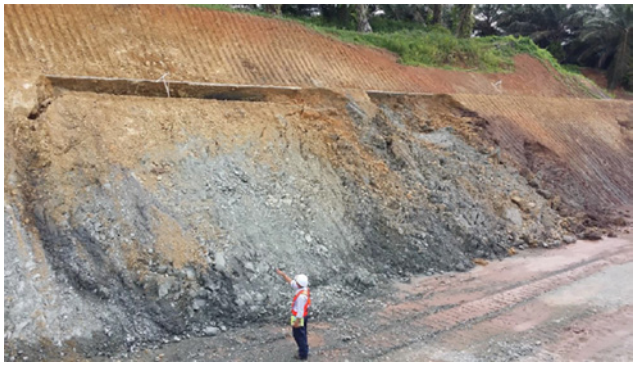

Figure 10: Front view of slope failure in slightly weathered mudstone for Case 4

Figure 11: Side view of the slope failure at Case 4. The guiding frame on the sliding block is vertical.

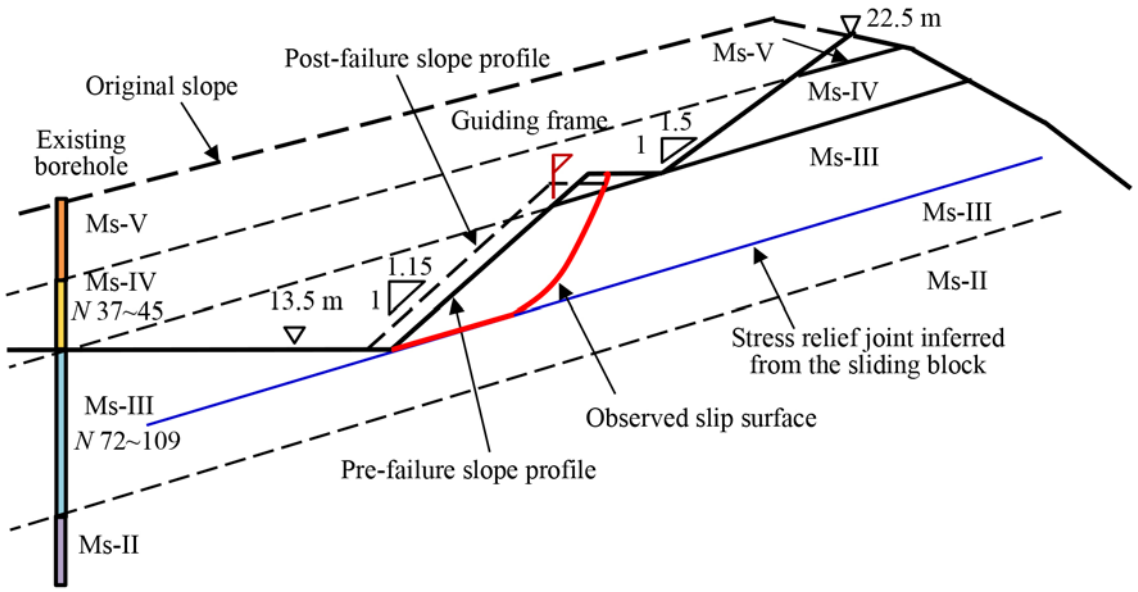

Figure 12: Cross-section along slope failure for Case 4

At time of inspection in December the berm drain remained intact and watertight. There is no sign of seepage in the tension cracks along the crest or along the toe of the failed slope. It is inferred that the groundwater level is located below the slip surface. The shear strength for the intact slightly weathered mudstone having the set of parameter of c' = 0 and ϕ' = 38.7° and the presence of a stress relief joint having the inclination parallel with the original slope profile of 17.5° are adopted in the stability analysis. Based on results of back-analyses, the mobilized effective friction angle, ϕ'_m, for moderately weathered mudstone along the joint plane is 24o with zero cohesion intercept. This ϕ'_m value is slightly lower than the average ϕ'_p value of 29.3° obtained by direct shear test that summarized in Table 2. Secondary failure at the slope of 9 m overall in height occurred in January 2018 due to collapsing of the unsupported surface drains and rainfall infiltration. Post-failure mapping on the slip surface could not be conducted.

7 VARIATION OF SHEAR STRENGTHS

The shear strengths actually mobilized along the joint planes in moderately weathered and slightly weathered mudstones obtained by back-analyses for Case 1 to Case 4 are summarized in Table 3, showing that the mobilized effective friction angles, ϕ'_m , vary from 27.5° to 12.5°. The mobilized effective friction angles are presented in Figure 13. The limited number of case histories show that the shear strengths of mudstones along the joint planes have various degree of mobilization to the residual strength, which is defined as $(\tan \phi'_m - \tan \phi'_r)/(\tan \phi'_p - \tan \phi'_r)$.

Table 3: Mobilization of residual shear strengths of mudstones along joints planes

Case no.	Rock Formation	Rock type	Effective friction angle, degree			Degree of mobilization to residual strength $(\tan \phi'_m - \tan \phi'_r)/(\tan \phi'_p - \tan \phi'_r)$, %
			Peak ϕ'_p	Residual ϕ'_r	Mobilized ϕ'_m	
1	Toukoshan	Ms-III	27.0	16.2	27.5	0
2	Garinono	Ms-II	29.3	14.0	12.5 to 14.5	100
3	Garinono	Ms-II	29.3	14.0	14.0	100
4	Garinono	Ms-III	29.3	14.0	24.0	37

Table 3 shows that the degree of mobilization to residual condition for Case 2 and Case 3 is 100 %, indicating that the residual shear strengths along the joint planes in slightly weathered mudstone is fully mobilized. Such mobilization of residual strength is common for re-activated landslips, where

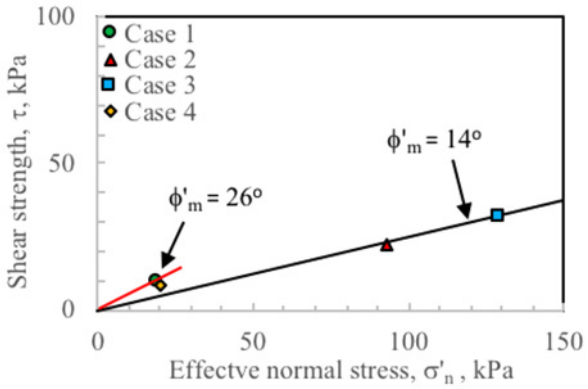

Figure 13: Mobilized shear strength envelope for mudstones along joint planes obtained by back-analysis

displacements had already occurred along the slip surfaces. However, these 2 cases are first-time slides in new slopes. The horizontal movements are as large as 1m occurred after failure. It is likely that excavation for the new slopes removed the lateral support of the rock mass. The horizontal compression strains caused by tectonic activities was released and the rock mass behind the cut slopes expanded due to unloading of the in-situ horizontal forces. Stress relief joints were developed in the slopes. The residual strengths along the joint planes were then gradually mobilized.

For Case 1 the ϕ'_m value of 27.5° is virtually the average ϕ'_p value of 27.0° obtained from direct shear tests. The degree of mobilization to the residual condition is zero. Since the joint plane is dipping at 27.5° along the slip direction, very minimal mobilization to the residual shear strength along the slip surface would be required to initiate the slope failure. The ϕ'_p value would be an upper bound for mobilization to the residual condition.

For Case 4, the ϕ'_m value of 24.0° is slightly less than the ϕ'_p value of 29.3° and the degree of mobilization is 37%. It could be interpreted that 37% of the length along the joint plane in mudstone was mobilized to the residual strength with the ϕ'_r value of 14.0°, and the remaining 63% of the joint plane has the ϕ'_p value of 29.3°. The ϕ'_m value of 24.0° could be regarded as an average along the entire joint plane. The ϕ'_p value obtained by direct shear tests could be the upper bound value for mobilization to the residual condition along the joint.

It is noted that Case 1 to Case 4 are first-time slides occurred shortly after excavation of the new slopes. Pre-existing slip surfaces are not expected in these slopes. The ϕ'_m value as large as the ϕ'_p value would be expected. Based on review of extensive case histories on long-term stability of stiff clay and clay shale slopes, Mesri and Shahien (2003) pointed out that part of the slip surfaces for first-time slope failures may be at the residual condition. Either the residual condition already exists or it develops by progressive deformation along the discontinuities. When shearing strain is localized in weak planes, rather small displacements will cause the clay particles to reach the residual condition.

8 CONCLUSIONS

Four case histories on slope failures along joint planes in mudstones have been collected for critical studies. The triaxial compression test and the direct shear test results conducted on mudstone specimens are reviewed. Based on the results of back-analyses on the slope failure cases, the following concluding remarks could be drawn:

(1) The direct shear test results show that the shear strengths of mudstones are strain-dependent. The peak and the residual strengths for moderately weathered to slightly weathered mudstones along the joint planes obtained from saw-cut core specimens have the average effective friction angles of 27.0° and 16.2° respectively with zero cohesion.

(2) The residual effective shear strength of slightly weathered mudstone mobilized along the joint planes has the effective friction angle about 14° with zero cohesion at the effective normal stresses ranging from 25 kPa to 150 kPa.

(3) The peak effective shear strengths for mudstones along the joint planes determined by direct shear tests could be the upper bound for mobilization to the residual condition.

(4) The stress relief joints with the inclinations approximately parallel to the original slope profiles could be developed in the cut slopes especially in region with tectonic activities.

More case histories on slope failures in mudstone shall be collected to assess the degree of mobilization to the residual condition. The stress relief joints in mudstone is one of the discontinuities in the rock mass. Its likely occurrence shall be considered in slopes design.

ACKNOWLEDGEMENTS

The authors wish to express their sincere thanks to Borneo Highway PDP Sdn Bhd for granting permission for publishing the laboratory testing data presented in this paper.

REFERENCES

Barry, A.J. 1990. A Cut Slope Failure in the Garinono Formation of Sabah, *10th Southeast Asian Geotechnical Conference*, Taipei, May: 381-384.

British Standard Institution 1981. *Code of Practice for Site Investigation.* BS5930:1981, British Standard Institution, London.

Mesri, G. and Shahien, M. 2003. Residual Shear Strength Mobilized in First-Time Slope Failures. *Journal of Geotechnical and Geoenvironmental Engineering,* Vol. 129, No. 1, January 2003: 12-31.

Mineral & Geoscience Malaysia 2015. *Geological Map of Sabah,* 4th Edition, 2015, Published by the Director of Mineral & Geoscience Malaysia.

Morgenstern N.R. and Price V.E.1965. The Analysis of the Stability of General Slip Surfaces, *Geotechnique,* Volume 15, Issue 1, March 1965: 79-93.

Raj, J.K. 2004. Failure at Slope cuts in Clastic Sedimentary Bedrock in Malaysia, Geological Society of Malaysia, *Bulletin 48,* June 2004: 25-29.

Stroud, M.A. 1974. The Standard Penetration Test in Sensitive Clays and Soft Rock. *Proceedings of the 1st European Seminar on Penetration Testing.* Stockholm 2(2): 366-375.

Wong, L.W. and Murrells, C. 2004. Stability of Slopes along Discontinuities in Sandstone and Mudstone, *Proceedings, 15th Southeast Asian Geotechnical Conference,* November, Bangkok, Volume 1: 317-342.

Wong, L.W. 2010. In-situ Measurement of Shear Modulus of Weak Rocks. *Proceedings, 17th Southeast Asian Geotechnical Conference,* Taipei, May: 141-144.

Yan, S.W. 2011. Geological Assessment of the Earthquake Sources and Hazard in Malaysia, *Technical Seminar on Earthquake,* Department of Mineral & Geoscience Malaysia, 20 December 2011.